Hemodynamics of aortic valve stenoses

Araz R. Kivi

School of Mechanical Engineering

The University of Adelaide

Adelaide, Australia

A thesis submitted in fulfilment of the requirements

for the degree of Ph.D. in Mechanical Engineering

June 2021

Abstract

The aortic valve of a human heart is located between the left ventricle and the aorta. Its function is to open during the systole, allowing the blood to flow to the aorta in order to feed the organs and close during the diastole, preventing blood flow back into the left ventricle. Disease can lead to dysfunctionalities of the aortic valve and affect its performance. Calcific aortic valve disease (CAVD) is one of the most common valvular heart diseases which causes malfunctioning of the aortic valve leading to stroke, aortic aneurysm, heart attack and failure over time. Over the past few decades, researchers have investigated the effects of stenosis of the aortic valve on its hemodynamics and performance using in-vitro and in-vivo experiments, as well as numerical models.

In-vitro experimentation and in-vivo measurements are broadly used for the investigation of the effect of aortic valve stenosis on the hemodynamics in the aortic root and the performance of the aortic valve. Numerical methods also play an important role in the modelling of the stenosis of the aortic valve and have obtained considerable attention in biomechanics application due to their very cost effective nature. Significant developments have been made in modelling the stenosis of the aortic valve and the effects on its hemodynamics and malfunctioning, however, the influence of vortex structures in the sinus on the aortic root and the coronary artery hemodynamics, as well as the performance of the valve and its correlation with the development of CAVD, are still unknown.

The aim of this thesis is to develop an understanding of the flow behaviour inside the sinus cavity of the aortic valve in order to predict the shear stress distribution on the aortic valve leaflets and its correlation with CAVD. This aim has been achieved by answering the following research questions: (i) how stenosis of the aortic valve affects the aortic root and coronary artery hemodynamics; (ii) how the geometrical parameters of the aortic valve, such as the locations of the coronary artery ostia and the shape of the sinuses, influences the sinus hemodynamics, especially vortex structures within the sinuses; (iii) what are the effects of coronary artery stenosis on the shear stress distribution on the aortic valve leaflets; (iv) how vortex structures in the sinuses can change the wall shear stress distribution on the leaflets and its correlation with CAVD. In order to answer all of the above-mentioned questions and achieve the main objective of the project, the following tasks have been defined:

- A brief overview of cardiovascular heart diseases with a focus on valvular heart diseases, and various techniques frequently used for diagnostics and treatment of stenosis of the aortic valve has been provided.
- A comprehensive review of different techniques used for modelling aortic valve stenosis has been provided with a focus on the numerical Fluid-Structure Interaction (FSI) method and its advantages in modelling.
- Two dimensional models of a healthy and a stenosed aortic valve have been extracted from the 2D echocardiography images available in the literature and developed in ANSYS- Fluent software.

- Dynamic motion simulation of the aortic valve leaflets have been used to investigate the effects of stenosis of the aortic valve on the sinus vortex structures, coronary artery hemodynamics, wall shear stress on the leaflets and its correlation with CAVD.
- A unique test rig has been designed, fabricated, and used for validation of the transvalvular pressure gradient and flow rate profile of the aortic valve. The test rig experimentally replicates the left ventricle of the heart and is capable of producing the heart beat flow conditions of different patients. The flow rate profile of the aortic valve and the pressure difference through the aortic valve are measured and compared with the simulated results.

The developed model is capable of mimicking the dynamic motion of the aortic valve leaflets and predicting the wall shear stress distribution on the leaflets, which is associated with CAVD. The most important findings of the project showed that the wall shear stress distribution on the leaflets is highly dependent on the geometrical parameters of the aortic valve, such as the locations of the coronary artery ostia, as well as the shape of the sinuses. For example, an aortic valve with proximal coronary artery ostia experiences lower ranges of wall shear stress distribution on the leaflets. This means that a healthy valve with proximal coronary artery ostia are more prone to calcification over time in comparison with a healthy valve with distal and middle coronary artery ostia. Furthermore, the results demonstrated that a severely calcified aortic valve exhibits a lower range of wall shear stress distribution on the leaflets with higher probability of having smaller wall shear stress on the leaflets compared to a healthy valve.

Declaration

I certify that this work contains no material which has been accepted for the award of any other degree or diploma in my name in any university or other tertiary institution and to the best of my knowledge and belief, contains no material previously published or written by another person, except where due reference has been made in the text. In addition, I certify that no part of this work will, in the future, be used in a submission in my name, for any other degree or diploma in any university or other tertiary institution without the prior approval of the University of Adelaide and where applicable, any partner institution responsible for the joint-award of this degree.

I acknowledge that the copyright of published works contained within this thesis resides with the copyright holder(s) of those works.

I also permit the digital version of my thesis to be made available on the web, via the University's digital research repository, the Library Search and also through web search engines, unless permission has been granted by the University to restrict access for a period of time.

I acknowledge the support I have received for my research through the provision of an Australian Government Research Training Program Scholarship.

Araz R. Kivi

Acknowledgments

First of all, I would like to thank my supervisors Professor Maziar Arjomandi, Professor Benjamin Cazzolato, Professor Anthony Zander, and Dr Nima Sedaghatizadeh for their guidance, insightful input, support and friendship throughout my study.

Next, I would also like to thank Dr Ross Roberts-Thomson from South Australian Health and Medical Research Institute, Adelaide, Australia and Dr Adam Nelson from Duke Clinical Research Institute, Durham, USA, for their support and contribution in completion of this thesis.

I would also like to acknowledge Professor Ajit Yoganathan from Wallace H. Coulter Department of Biomedical Engineering, Georgia Institute of Technology, for his contribution and help in this research.

Thanks to Professor Marcel Rutten from the Department of Biomedical Engineering, Cardiovascular Biomechanics Research Group, Eindhoven University of Technology, for his help and technical guidance with the design of experimental apparatus.

Many thanks are extended to Dr Fabien Voisin and his colleagues from the Phoenix HPC team for all their help with technical support for the high performance computing system.

I would also like to acknowledge Professor Tracie Barber and the lab technician, Vincenzo Carnevale in the Vascular Fluid Dynamics Group Research Laboratory at the University of New South Wales for all of their help in designing the experimental apparatus.

I am also indebted to the technicians in the Electrical and Mechanical Workshops at the University of Adelaide, especially Thomas Stanef, Mike Schneider, and Brandon Pullen for all their help with the design and construction of the electronics and experimental apparatus.

I would gratefully acknowledge the financial support of the Australian Government Research Training Program, and The University of Adelaide.

I owe huge thanks to my family and my girlfriend for their endless support, love and encouragement throughout my studies.

Last but not least, I would like to thank all my friends, fellow postgraduate students, my officemates from the School of Mechanical Engineering and our faculty whose sincere friendship and help at various stages of my PhD work made the course of my research enjoyable.

Thesis Formatting

All publication within this thesis are identical to the original article as published or submitted, with the following exceptions:

- Typesetting and referencing have been altered so that there is a consistent format throughout the entire thesis.
- The positions of the figures and tables may differ from the final published version of the papers to improve readability.
- The numbering of tables, figures and equations of each publication has been changed to include the number of the chapter.

Nomenclature

ALE	Arbitrary Lagrangian-Eulerian
AVA	Aortic valve area
AVS	Aortic valve stenosis
AWSS	Average wall shear stress
CAVD	Calcific aortic valve disease
CCW	Contraclockwise
CFD	Computational fluid dynamics
CW	Clockwise
FEA	Finite element analysis
FD	Finite difference
FSI	Fluid structure interaction
STJ	Sinotubular junction
TPG	Transvalvular pressure gradient
VHD	Valvular heart disease
VO	Valve orifice
VOD	Valve orifice diameter
WSS	Wall shear stress

Table of Contents

List of Figures

List of Tables

Chapter 1

Introduction and Motivation of Research

1.1 Introduction

In the following sections, the anatomy and physiology of the heart and aortic valve, the characteristics of the coronary artery blood flow, and the prevalent heart diseases associated with the aortic valve, particularly calcific aortic valve disease (CAVD), are explained. Treatments for aortic valve disease such as different methods of aortic valve replacement (AVR) are also presented. The motivation and objectives of this project are defined. Finally, the outline of this thesis and information included in different chapters are extensively outlined.

1.2 Anatomy and physiology of the heart

The heart is the primary organ of a cardiovascular system. Its function is to pump blood throughout the entire body during the cardiac cycle in order to provide blood to the different organs. The heart comprises two main chambers of left and right atriums [1]. The ventricular septum (shown in Figure 1.1), is a large muscular wall within the heart which separates the heart into two sides, right and left. Each side of the heart is separated into two interior and superior chambers known as the ventricle and atria, respectively [2]. The main function of the left side of the heart is to circulate oxygenated blood flow into the body via systemic circulation, while the right side of the heart has responsibility to oxygenate the oxygen-poor blood by pumping it into the lungs for absorbing fresh oxygen and exchanging gas through pulmonary circulation [3].

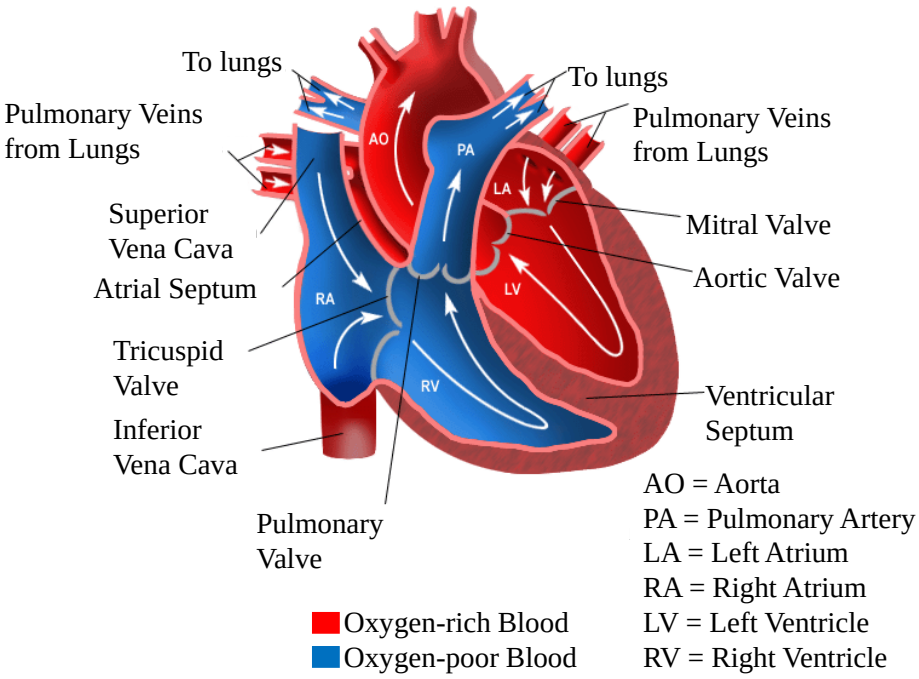

Figure 1.1 Anatomy of the heart [4]

1.2.1 Heart valves

During a cardiac cycle, unidirectional blood flows through the different chambers of the heart via four valves, including the mitral and aortic valves within the left side of the heart, and the pulmonary and tricuspid valves in the right side of the heart [5]. The mitral and tricuspid valves are located between the superior and interior chambers of each side of the heart, while the aortic and pulmonary valves are positioned between each ventricle and their corresponding artery [6].

The cardiac cycle encompasses two phases; systole and diastole. During the diastole phase, the blood flow returning from different organs is accumulated in the right atrium which leads to an increase in the right atrium pressure [7]. When the pressure inside the right atrium exceeds the right ventricle pressure, the tricuspid valve opens (shown in Figure 1.2a) and allows blood to flow into the right ventricle. A similar scenario occurs inside the left atrium in which the oxygenated blood returns from the lungs, increasing the left atrium pressure. Due to the increased pressure, the mitral valve opens and allows the blood to flow into the left ventricle. During the systole phase (as shown in Figure 1.2b), when the heart starts a pumping cycle, the ventricular pressure increases and opens the aortic valve. The ejected blood from the left ventricle flows into the aorta to feed the organs. By the end of a systole, the muscles of the heart relax and the diastole phase restarts [8].

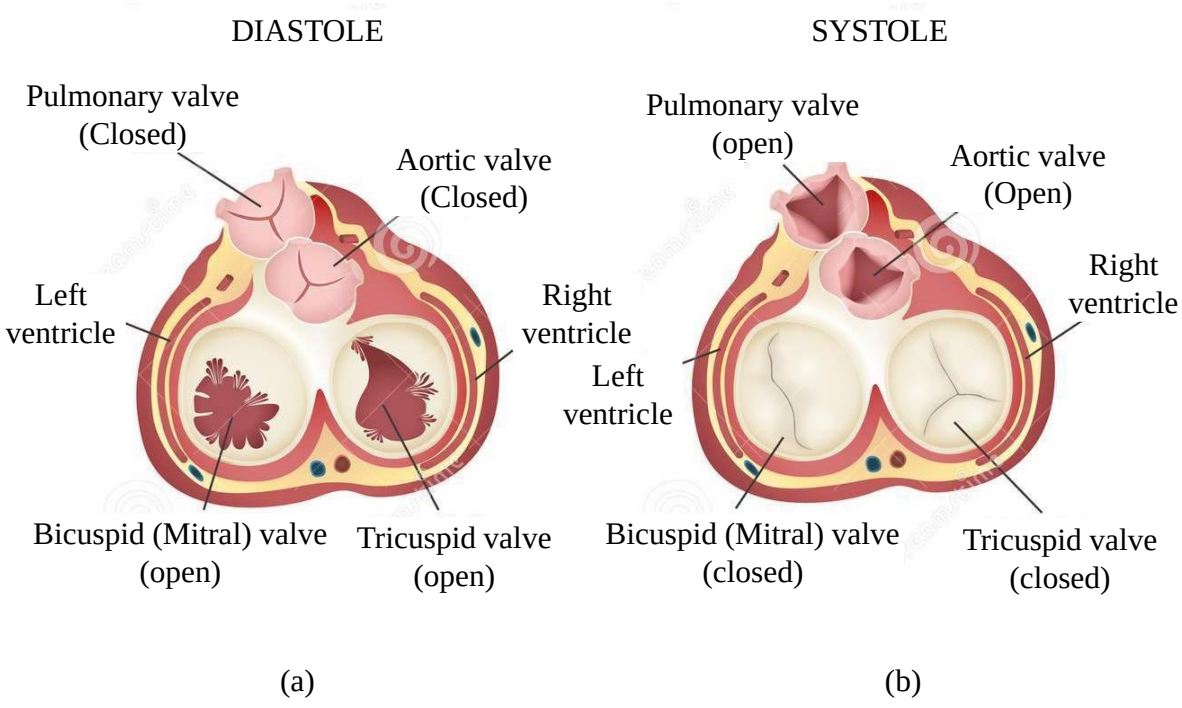

Figure 1.2 Schematic view of heart valve function during (a) diastole and (b) systole phases [9]

1.2.2 Anatomy and physiology of the left ventricle and aortic valve

The left ventricle (LV) is the largest chamber inside the heart and is located at the bottom left of a heart. It has a thick muscular wall which expands and contracts during a cardiac cycle to provide the organs with sufficient blood flow [2]. During the systole, the contraction of the

left ventricle increases the LV pressure from 0 mmHg to 120 mmHg (shown in Figure 1.3) which is the peak pressure at the systolic phase. The increased pressure overcomes the resistance of the aortic valve and opens it. As the valve opens, the oxygenated blood flows into the aorta and all the other organs. The cardiac output (CO) is a parameter which quantifies the functionality of the heart and is defined as the product of heart rate and stroke volume. CO for adults is approximately 5 L/min. Stroke volume and heart rate for adults are typically 70 ml and 70 beats per minute [3].

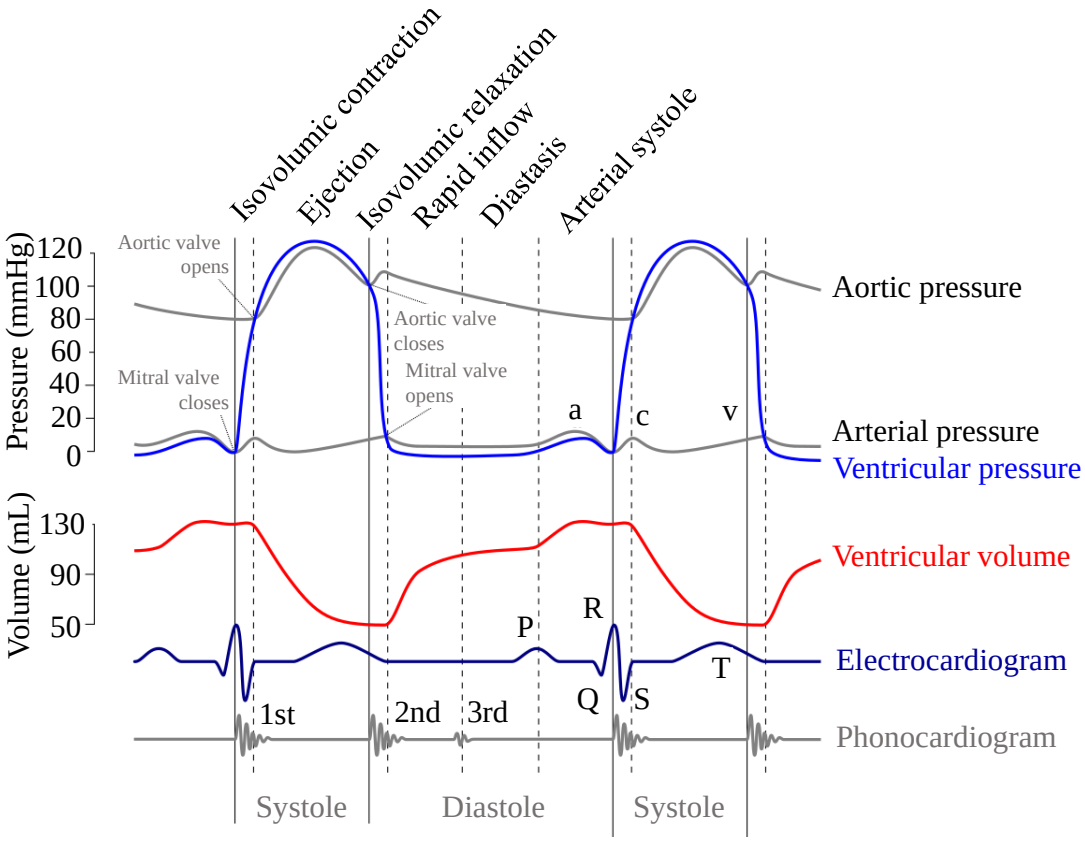

Figure 1.3 Aortic, arterial, ventricle pressure profile, ventricle volume, electrocardiogram, phonocardiogram of the human body during the cardiac cycle [9]. The opening/closing times of the aortic/mitral valves during systole and diastole are shown. The range of the aortic pressure as well as the ejection volume per millilitre are illustrated.

The aortic valve (AV) opens because of the positive transvalvular pressure gradient (TPG) generated between the LV (reaches to 12 mmHg) and the aorta (changing from 80 mmHg to 120 mmHg). It closes during the diastole due to the negative TPG generated between the LV (with pressure 0 mmHg) and the aorta with 80 mmHg pressure [1].

The AV comprises two or three leaflets positioned inside a region known as the aortic root at the base of the aorta. Sinuses are located between the aortic root and the aorta, which are known as the sinuses of Valsalva. There are three sinuses named: the left posterior aortic sinus, the anterior aortic sinus, and the right posterior aortic sinus. These sinuses encompass only two coronary artery ostia which are the connectors between the left/right posterior sinuses and their corresponding coronary arteries (right and left coronary arteries) as shown in Figure 1.4. The leaflets of the AV consist of three different regions including the base, belly and tip

of the leaflets [2]. The bottom section of the leaflet is called the base which connects the leaflets to the wall of the sinuses. The top free edge of the leaflets is called the tip and the belly is the section between the free edges and the base of the leaflets. Each leaflet has three layers named fibrosa, spongiosa and ventricularis [10]. The fibrosa layer of the leaflets is on the aorta side and made of collagen fibres, interstitial cells, elastin fibres and endothelial cells, the combination of which provide strength, flexibility, and structural integrity of the leaflets as well as protection from cell infiltration and lipid accumulation. The ventricularis layer of the leaflets is on the LV side and consists of more interstitial and endothelial cells which provide the required bending strength for the leaflets during the systole and diastole phases. The spongiosa layer of the leaflets is positioned between the fibrosa and ventricularis layers of the leaflets which, in turn, has the function to damp the dynamic motion of the leaflets [11].

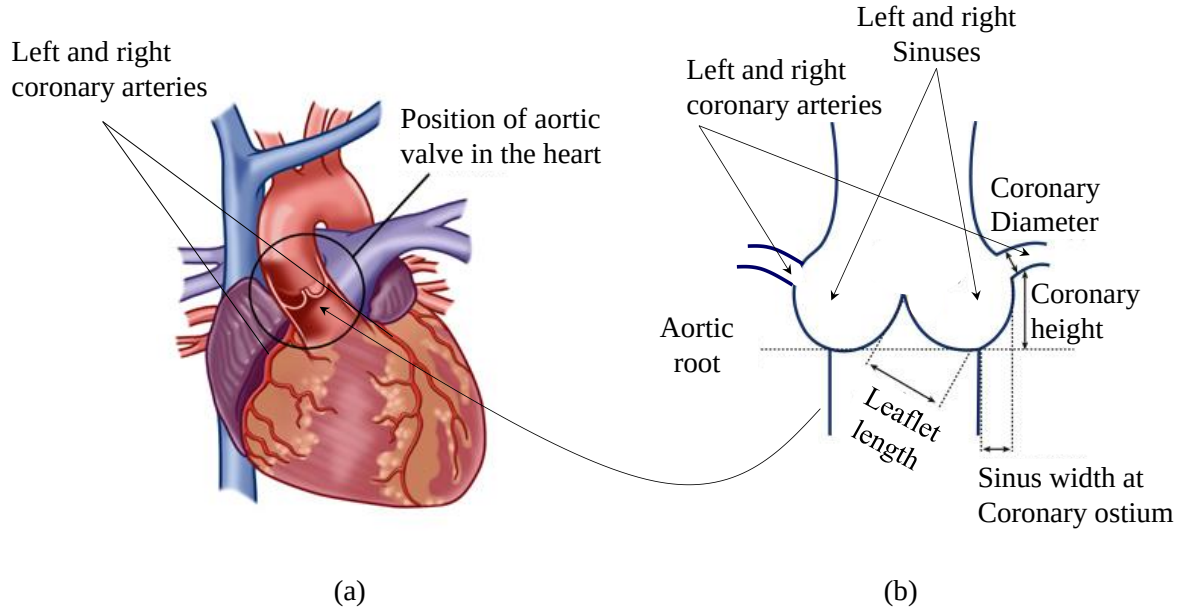

Figure 1.4 (a) Position of the aortic valve inside the heart (b) A schematic view of the left and right sinus cavity with its corresponding coronary artery ostia [12]

1.3 Characteristics of the coronary artery blood flow

The coronary arteries are responsible for providing sufficient blood to feed the heart itself. They originate from the right and left coronary artery ostia within the sinuses (as shown in Figure 1.5) [13]. At the early systole, when the heart starts a pumping cycle and the aortic valve starts to open, the coronary artery blood flow rate increases. At peak systole, when the valve is completely open, the coronary artery blood flow rate decreases due to the myocardial contraction which originates from the arterial resistance [14]. Generally, at peak systole the heart muscles expand which leads to a reduction in the diameter of the coronary artery. This reduction in the diameter of the coronary arteries leads to a decrease in the coronary artery flow rate. At early diastole, when the heart muscles relax and the aortic valve is closed, a back-flow is generated in the cavities of the sinuses because of the pressure difference between the left ventricle and aorta, and flows through the coronary arteries and increases the coronary artery blood flow rate [15].

The presence of coronary artery flow plays an important role in the aortic valve hemodynamics. Due to the formation of complex vortex structures in the sinus cavity, the coronary artery blood flow affects the dynamics of the leaflets during the cardiac cycle. The vortices generated in the sinuses not only affect the dynamic motion of the aortic valve but also change the hemodynamic parameters in the aortic root, the cavities of the sinuses and the coronary arteries. Changes in the hemodynamic parameters in the coronary arteries and the aortic sinuses are the main reasons for aortic valve and coronary artery diseases [16].

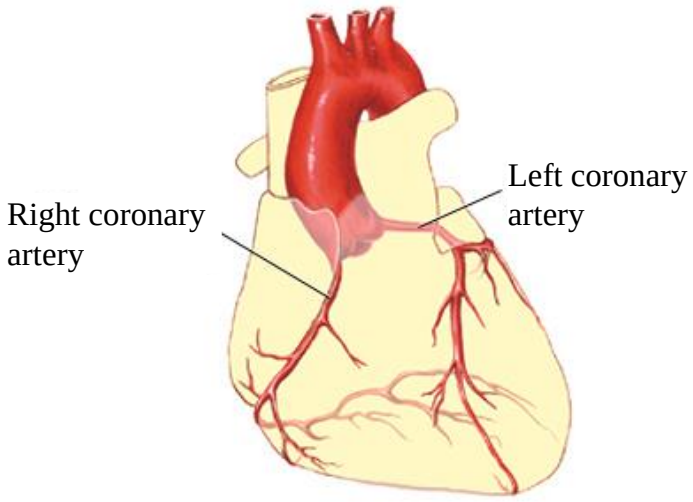

Figure 1.5 Schematic view of the position of the left and right coronary arteries [4]

1.4 Aortic valve diseases

Valvular heart disease (VHD) is one of the main causes of mortality and morbidity across the world. VHD is mainly categorised into congenital and acquired valvular heart diseases, in which acquired VHD is the most prevalent type, especially among adults. Acquired VHD is caused by long term injuries or diseases such as myxomatous degeneration, endocarditis, rheumatic fever, and calcification of the leaflets. Generally, Aortic Stenosis (AS) and Aortic Regurgitation (AR) are the most common diseases associated with VHD [8].

Aortic Stenosis (AS) is a disease in which the aortic valve opening is narrowed or blocked (shown in Figure 1.6b) over time because of the stiffening of the aortic valve leaflets [7]. The stiffened aortic valve leaflets cannot fully open during the systole phase. The incomplete opening of the valve leads to an increased load on the heart as it works to provide sufficient blood flow to the organs. As a result the heart muscles become thicker and less flexible reducing their performance. Furthermore, in order to overcome the increased valve resistance, the heart has to generate higher pressure which leads to higher blood pressure. These factors make it difficult for the heart to work in a proper condition. This changes the flow behaviour as well as the wall shear stress distribution on the leaflets, facilitating calcification on the aortic valve leaflets and results in heart failure over time [17].

Aortic Regurgitation (AR) is another prevalent disease associated with VHD (shown in Figure 1.6). AR occurs because the aortic valve is incapable of full closure which results in

blood being partially returned to the left ventricle [18]. During the diastole, incomplete closure leads to return of the ejected flow from the heart into the left ventricle. As a result, in each cycle the heart has to work harder to compensate for the insufficient blood flow. Furthermore, the blood flow returned to the heart can, in turn, affect the performance of the mitral valve during the diastole phase when the heart is at rest and the mitral valve opens to refill the left ventricle. The regurgitated blood flow not only needs to be pumped twice but also enlarges the left ventricle chamber of the heart. AR disease affects the heart performance and can lead to a heart attack and failure over time.

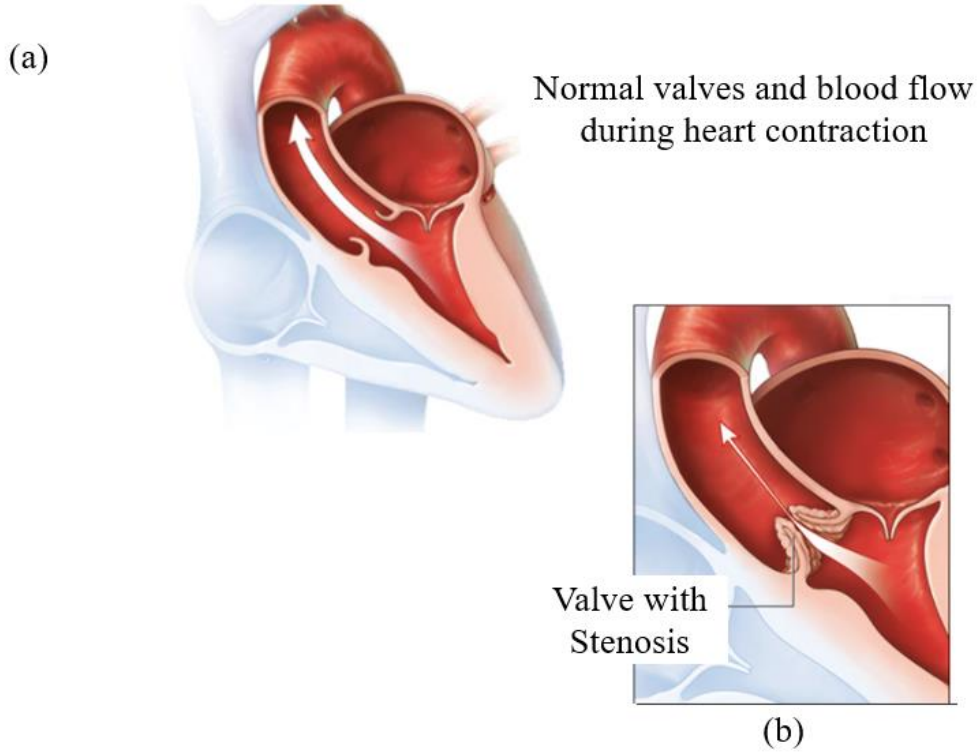

Figure 1.6 (a) normal valves and blood flow during heart contraction, (b) Aortic stenosis [12]

1.5 Calcific aortic valve disease

Calcific aortic valve disease (CAVD) occurs when calcium deposits on the aortic valve leaflets and the valve leaflets become stiffer [19]. CAVD is the third most prevalent heart disease worldwide [19]. CAVD usually starts with a very low level of calcification on the leaflets which is called aortic sclerosis. Once aortic sclerosis progresses, the leaflets become stiffer which results in aortic stenosis (AS) which affects valve performance during the cardiac cycles and significantly decreases the valve orifice diameter (shown in Figure 1.7) during opening time.

AS is a very common disease among adults with 1.7% of the worldwide, population diagnosed with AS. Aortic stenosis has a higher rate of mortality among the valvular heart diseases so that more than 50% of patients with initial symptoms lose their life within two years. Shortness of breath, chest pain, fatigue, and murmuring of the heart are the most common symptoms of CAVD. Calcific aortic valve disease can lead to blocking of the aortic valve,

coronary artery diseases, and obstruction in the aortic and coronary artery blood flow. It can be lethal if it is left untreated. Various factors can initiate CAVD and increase its risk. Age, male sex, smoking, diseases such as hypertension, diabetes as well as higher lipoprotein are the most common risk factors [20].

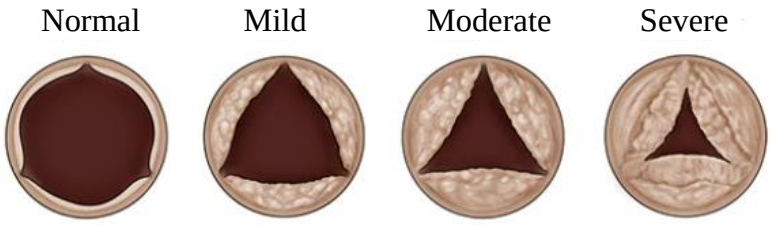

Figure 1.7 Valve orifice area corresponding to healthy, mildly, moderately, and severely calcified aortic valve [4]

1.6 Etiologies of calcific aortic valve disease

The most common causes of CAVD are genetic factors which generally affect the process of osteogenic differentiation and lead to CAVD. For example, higher lipoprotein and hypertension problems have been identified in patients who are suffering from CAVD [21]. Basically, it is believed that genetic factors and CAVD are interdependent. Beside genetic factors, valvular abnormal hemodynamics can affect the stress profile on the leaflets. An abnormal stress profile generated on the aortic valve leaflets can initiate calcium deposition on the leaflets and result in sclerosis. Over time, sclerosis progresses at a higher degree of calcification and leads to CAVD [22].

Wall shear stress (WSS) is the fractional viscous stress generated on the aortic valve leaflets due to the viscosity of the blood flow. The level of the WSS on the aortic valve leaflets is a very important factor in determining the stability of the valvular homeostasis. It is believed that alteration in the level of the WSS on the aortic valve leaflets can lead to endothelial dysfunction, remodelling of the valve, and inflammatory responses. These changes can result in the initiation and progression of CAVD [23].

1.7 Treatment of calcific aortic valve disease

Treatments of CAVD used by cardiologists are highly dependent on the severity of the aortic valve stenosis and consist of invasive and non-invasive techniques. Aortic valve replacement (AVR) is one of the most common invasive techniques which is used by cardiologists to treat the aortic valve stenosis. AVR is a technique in which the patient's valve is replaced by a bileaflet mechanical or bioprosthetic aortic valve. In this technique, cardiologists perform surgery in order to replace the diseased valves. On the other hand, Transcatheter aortic valve replacement (TAVR) is a method in which cardiologists utilise a catheter to position the artificial valve inside the aorta such that there is no need to perform open heart surgery. The positioned valve is then inflated and replaces the original valve.

1.7.1 Performance assessment of the aortic valve

In the following sections, first the parameters which are used to diagnose the severity of the aortic valve are explained. Then, both aortic valve replacement (AVR) and transcatheter

aortic valve replacement (TAVR) techniques and their advantage and disadvantage are explained in detail.

Transvalvular pressure gradient (TPG) and valve orifice diameter (shown in Figure 1.8) are the two main parameters measured to diagnose stenosis of the aortic valve. After measuring the valve orifice diameter (VOD), various formulas are utilised to calculate the valve orifice area based on the continuity mass law, Gorlin [24] or Hakki [25] equations.

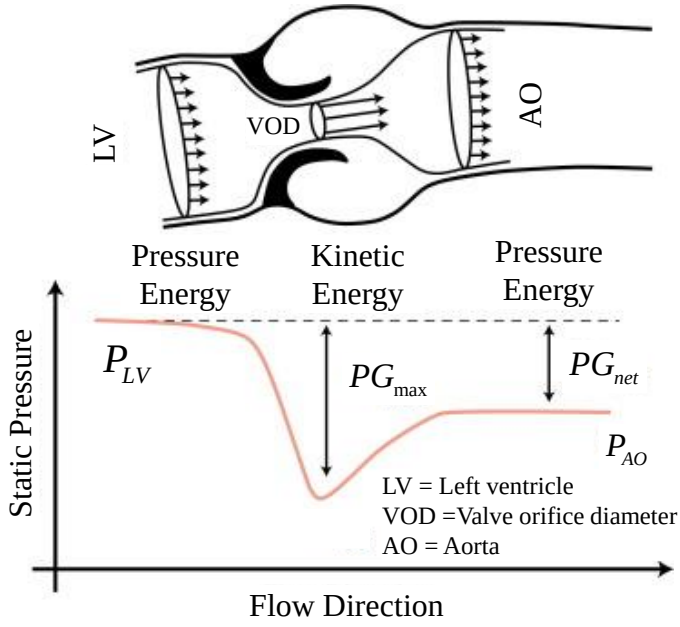

Figure 1.8 Schematic view of the transvalvular pressure gradient (TPG) and aortic valve orifice diameter [9]

Based on the mass continuity equation, the blood flow rate ejected from the left ventricle (LV) of the heart (i.e. left ventricle outflow tract (LVOT)) is equal to the blood flow passing through the valve orifice area (VOA). In order to apply the continuity equation, the time dependent average velocity (i.e. time velocity integral (TVI)) corresponding to each cross section area is measured at the LV and VOA based on the electrocardiography technique. To calculate the cross sectional areas of the LVOT, the diameter of the LVOT is measured using the data collected by Doppler Echocardiography machines. Then, the aortic valve area can be calculated based on the continuity equation. Measuring the LVOT diameter based on Doppler echocardiography has some discrepancy due to assuming uniform velocity through the valve. This discrepancy in measuring LOVT diameter is one of the disadvantage of this method.

The second method which is used by cardiologists to diagnose aortic valve stenosis is based on the Gorlin equation [24] in which the pressure gradient through the aortic valve is correlated with the blood flow rate passing across the aortic valve during systole. In order to calculate the mean pressure gradient, the velocity measured by Doppler techniques along the aortic valve is converted to the pressure difference between the left ventricle and the aorta based on Bernoulli's equation ($PG = 4 \times V^2$). Since the Gorlin equation calculates AVA based on the blood flow across the aortic valve, therefore there is inaccuracy in diagnosing aortic valve stenosis especially at lower cardiac output.

The third method used to assess aortic valve stenosis is based on the Hakki equation [25]. The Hakki equation is the simplified form of the equation represented by Gorlin [24] in which an assumption is made based on the fact that in most cases the final value of the product of the heartbeat and the systolic ejection time is equal to approximately 1000. Finally, in order to diagnose aortic valve stenosis, the outcome of the calculated AVA needs to be compared with the AVA of a healthy aortic valve [9].

1.7.2 Aortic valve replacement

As mentioned previously, the main methods used in the treatment of the aortic valve stenosis are AVR and TAVR [26]. In AVR, the original valve is replaced by a bileaflet mechanical or bioprosthetic aortic valve (shown in Figure 1.9 a and b) via surgery. The mechanical valve is made of two semilunar disks connected together through a spring mechanism and a circular ring [26]. The mechanical valves in general are very durable but the patients with a mechanical valve need to have anticoagulation medication frequently. This is because the blood flow coagulates around the mechanical valve over time. The coagulated blood forms clots on the leaflets and behind the hinge which put the patient into risk if not treated. Another type of surgical valve is the bioprosthetic aortic valve which is made of the porcine or bovine aortic valve leaflets surrounded by polymer material. This type of valve, in contrast to the mechanical one, does not require frequent anticoagulation check-ups. However, they need to be replaced every 10-15 years because of their decreased durability. As mentioned, installation of mechanical and bioprosthetic valves requires open heart surgery which potentially puts patients at risk [27].

(a) (b) (c)

Figure 1.9 Different types of artificial aortic valves (a) mechanical (b) bioprosthetic (c) transcatheter (stented) aortic valves [4]

To avoid the risks associated with open heart surgery and to reduce the cost, TAV was introduced (shown in Figure 1.9 c) in 2002. TAVR is a novel technique in which patients do not require to undergo open heart surgery [27]. In this method, a bioprosthetic stented aortic valve is attached to a catheter which can carry the valve through the femoral artery and position it inside the diseased valve (shown in Figure 1.10). Once the catheter reaches the desired position, the stent is inflated and the diseased original aortic valve is replaced by the transcatheter one.

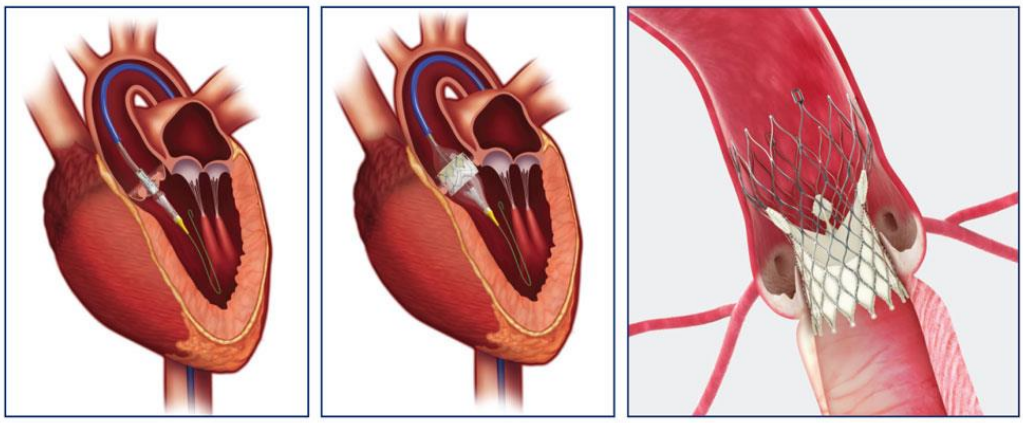

(a) (b) (c)

Figure 1.10 Transcatheter aortic valve replacement (TAVR) procedure (a) positioning (b) inflating (c) replacement of the TAV [9]

1.8 Motivation and objectives of the research

Medical imaging such as Magnetic Resonance Imaging (MRI), Computed Tomography (CT) scans, as well as echocardiography techniques are mostly used by cardiologists to diagnose aortic valve stenosis. These techniques are extremely expensive and their implementation requires a high level of skill as well as sophisticated equipment. In addition, in laboratory environment in-vitro measurements are used to evaluate the performance of artificial valves such as bioprosthetic, mechanical, and transcatheter aortic valves. The main objective of in-vitro experiments is to test the durability of the artificial valves over time. While both in-vitro and in-vivo techniques have been broadly used for investigation of aortic valve stenosis in the past decades, some of the hemodynamic parameters such as the wall shear stress distribution on the leaflets, which has a significant impact on initiation and progression of valvular heart diseases, cannot be easily measured through these time-consuming and expensive experiments [9].

With the advancement in modelling techniques and computational power, numerical methods such as computational fluid dynamics (CFD), finite element analysis (FEA), and fluid-structure interaction (FSI) are used as alternatives for calculation of hemodynamic parameters required for diagnosing stenosis of the aortic valve. Among the numerical methods, the 2-way FSI modelling technique is broadly used to study the hemodynamics of the aortic valve and its leaflets due to its capability of modelling the structure and fluid domains and their interaction simultaneously. While this method is able to model the dynamic motion of the aortic valve leaflets, it is very challenging to model the large deflection of the leaflets during the cardiac cycle considering the coronary artery ostia and their effects on the flow patterns in the sinuses as well as their hemodynamic parameters.

This research aims to develop a deep understanding of the flow behaviour inside the sinus cavity of the aortic valve in order to predict the wall shear stress distribution on the aortic valve leaflets and its correlation with CAVD. This aim has been achieved by answering the following research questions:

- How does the coronary artery blood flow affect the hemodynamic parameters within the aortic root, the vortex structures in the sinus cavity, and the shear variation on the leaflets and arterial walls?
- How does the position of the coronary artery ostia influence the sinus vortex structures and accordingly the wall shear stress distribution on the aortic valve leaflets?
- How interdependent are the calcification of the aortic valve leaflets and the presence of coronary artery atherosclerosis?
- How does geometrical variation affect the wall shear stress distribution on the leaflets and what is its correlation with CAVD?

1.9 Thesis outline

In this section a brief overview of the different chapters of the thesis is presented. The format of the current thesis is based on publications; i.e. the chapters includes manuscripts that have been published or are currently under review in peer-reviewed journals. In the following paragraphs, brief information about the content of each chapter is explained. This includes a comprehensive literature review on the recent research which has been carried out in the field of cardiovascular fluid mechanics with a focus on calcification of the aortic valve and its effect on hemodynamic parameters. It is hypothesised that the hemodynamic variations within the sinus cavity and the initiation and progression of CAVD can be correlated. Furthermore, it is also hypothesised whether the presence of aortic valve stenosis and the initiation of coronary artery atherosclerosis can be independent. The presented hypothesis is then supported by a comprehensive numerical study which is validated with an in-vitro in-house experiment.

In Chapter 2, a comprehensive literature review is presented including different numerical methods used for modelling of the aortic valve leaflets as well as in-vitro experiments. Initially, various in-vitro experimental techniques used by researchers to investigate the dynamic motion of artificial aortic valve leaflets are presented. Then, studies in which the two most commonly used techniques used for modelling of the aortic valve leaflets behaviour, named CFD and FEA, accompanied with a discussion on their achievements, accuracy, applicability, and limitations is presented. Then, the two-way FSI technique is introduced and its advantages compared to the other numerical methods are discussed in detail. The challenges associated with the FSI modelling of the aortic valve leaflets are presented. Finally, the most recent achievements in modelling the dynamic behaviour of the aortic valve leaflets based on the FSI numerical method are introduced.

In Chapter 3, an FSI model of aortic valve leaflets with the coronary arteries is developed and validated against experimental data. Then, the model is extended to specify whether calcification of the aortic valve leaflets can affect initiation and progression of coronary artery diseases. The effect of calcification of the aortic valve leaflets on the hemodynamic parameters in the aortic root, the sinus cavity, and the coronary arteries are investigated. The results revealed that leaflet stiffening not only changes the hemodynamic parameters within the aortic root but also significantly affects the wall shear stress on the wall of the coronary arteries. It is hypothesised that the changes in the wall shear stress on the wall of the coronary arteries could be one of the reasons for initiation of coronary artery atherosclerosis.

Chapter 4 presents an FSI model of the aortic valve with different positions of the coronary artery ostia (i.e. distal, middle and proximal coronary artery ostia). The main

objectives of the study carried out in this chapter is to answer the question as to whether the position of the coronary artery ostia can influence the sinus vortex structures and accordingly its hemodynamics. Results show that the aortic valve with a proximal coronary artery ostia experiences a higher Transvalvular Pressure Gradient (TPG) compared to that with a middle or a distal coronary artery ostia. It means that an aortic valve with a coronary artery ostia closer to the aortic root is more prone to have a higher TPG in each cardiac cycle. This can, in turn, affect the durability and lifetime of the transcatheter and bioprosthetic aortic valves. Furthermore, the influence of the size of the sinus cavity accompanied with the position of the coronary artery ostia is investigated. The results reveal that an aortic valve with a smaller sinus and a proximal coronary artery ostia has a larger TPG during the cardiac cycle, however, the coronary artery flow rate corresponding to this case is higher at peak systole compared to that for a middle or distal coronary artery. This is due to the shorter distance between the coronary artery ostia position and the leaflets.

Chapter 5 of this thesis focuses on developing an FSI model and validates it against experiment to model the stenosis inside coronary arteries in order to investigate its effect on the sinus vortex structures and the aortic root hemodynamics. The study in this chapter is motivated by the lack of information about the effect of the coronary artery blockage on the hemodynamic parameters inside the sinus cavity and the wall shear stress distribution on the leaflets. Clinical data reveals that approximately 45% of patients who require aortic valve replacement suffer from a stenosed coronary artery [19]. The study presented in this chapter is dedicated to investigation of the relationship between the calcification of the aortic valve and coronary artery atherosclerosis. The results reveal that an aortic valve with a 75% stenosed coronary artery experiences less wall shear stress on the aortic valve leaflets compared with that for a healthy coronary artery. This means that a healthy valve with a stenosed coronary artery is more prone to calcification over time.

Chapter 6 of this thesis presents a numerical model for prediction of the wall shear stress distribution on the leaflets in order to find a correlation between the wall shear stress on the leaflets and CAVD. The developed FSI model of the aortic valve is validated against in-vitro in-house experiments. The effects of the geometrical parameters such as the sinus diameter and the locations of the coronary artery ostia on the wall shear stress distribution on the leaflets are investigated. Probability density functions of the wall shear stress distribution on the aortic valve leaflets corresponding to a healthy and a calcified aortic valve are calculated. The results reveal that a severely calcified valve witnesses less wall shear stress on the leaflets with a higher probability of having smaller wall shear stress compared to a healthy valve. Furthermore, a healthy valve with a proximal coronary artery ostia experiences less wall shear stress with a higher probability of having smaller wall shear stress on the leaflets compared to that of a distal coronary artery ostia. It means that a healthy valve with a proximal coronary artery ostia is more prone to calcification over time.

In the final chapter, Chapter 7, the key findings and achievements of the current study are presented followed by conclusions. Moreover, suggestions are proposed which can be used as motivations and research objectives by other researchers in the field of cardiovascular fluid mechanics.

1.10 Publications arising from the current thesis

The current study has resulted in several articles which are published or under review in different international journals and peer-reviewed conference proceedings.

1.10.1 Published Journal Papers

- **Araz R. Kivi**, Nima Sedaghatizadeh, Benjamin S. Cazzolato, Anthony C. Zander, Ross Roberts-Thomson, Adam J. Nelson, Maziar Arjomandi, Fluid structure interaction modelling of aortic valve stenosis: Effects of valve calcification on corona artery flow and aortic root hemodynamics, Journal of Computer Methods and Programs in Biomedicine, 196 (2020), 105647.
- **Araz R. Kivi**, Nima Sedaghatizadeh, Benjamin S. Cazzolato, Anthony C. Zander, Adam J. Nelson, Ross Roberts-Thomson, Ajit Yoganathan, Maziar Arjomandi, Hemodynamics of a stenosed aortic valve: effects of the geometry of the sinuses and the position of the coronary ostia, International Journal of Mechanical Sciences, 188 (2020), 106015.

1.10.2 Submitted Journal Papers

- **Araz R. Kivi**, Nima Sedaghatizadeh, Benjamin S. Cazzolato, Anthony C. Zander, Adam J. Nelson, Ross Roberts-Thomson, Kelvin K. L. Wong, Maziar Arjomandi, Prediction of calcium deposition on aortic valve leaflets in the presence of coronary artery atherosclerosis, Submitted to Medical & Biological Engineering & Computing.
- **Araz R. Kivi**, Nima Sedaghatizadeh, Benjamin S. Cazzolato, Anthony C. Zander, Adam J. Nelson, Ross Roberts-Thomson, Kelvin K. L. Wong, Maziar Arjomandi, Calcific aortic valve disease prediction based on wall shear stress distribution on the leaflets, Submitted to Annals of Biomedical Engineering.

1.10.3 Published Conference Papers

- **Araz R. Kivi**, Nima Sedaghatizadeh, Benjamin S. Cazzolato, Anthony C. Zander, Ross Roberts-Thomson, Adam J. Nelson, Maziar Arjomandi, Calcification effect on the wall shear stress distribution of the aortic valve leaflets, 22nd Australian Fluid Mechanics Conference (2020), Brisbane, Australia.
- **Araz R. Kivi**, Nima Sedaghatizadeh, Maziar Arjomandi, Anthony C. Zander, Benjamin S. Cazzolato, Fluid structure interaction analysis of a calcified aortic valve, 21st Australian Fluid Mechanics Conference (2018), Adelaide, Australia.

1.11 References

[1] M.A. Chizner, D.L. Pearle, A.C. Deleon, The natural history of aortic stenosis in adults, American Heart Journal, 99 (1980) 419-424.
[2] F. Rader, E. Sachdev, R. Arsanjani, R.J. Siegel, Left ventricular hypertrophy in valvular aortic stenosis: Mechanisms and clinical implications, American Journal of Medicine, 128 (2015) 344-352.
[3] C. Cuspidi, C. Sala, F. Negri, G. Mancia, A. Morganti, Prevalence of left-ventricular hypertrophy in hypertension: An updated review of echocardiographic studies, Journal of Human Hypertension, 26 (2012) 343-349.

[4] S. Kadel, Computational assessment of aortic valve function and mechanics under hypertension, Conventional Thesis, Wright State University (2020).
[5] P. Youssefi, A. Gomez, T. He, L. Anderson, N. Bunce, R. Sharma, A. Figueroa, M. Jahangiri, Patient-specific computational fluid dynamics-assessment of aortic hemodynamics in a spectrum of aortic valve pathologies, The Journal of Thoracic and Cardiovascular Surgery, 153 (2017) 8-20.
[6] I.C. Howard, E.A. Patterson, A. Yoxall, On the opening mechanism of the aortic valve: Some observations from simulations, Journal of Medical Engineering & Technology, 27 (2003) 259-266.
[7] R. Rosenhek, U. Klaar, M. Schemper, C. Scholten, M. Heger, H. Gabriel, T. Binder, G. Maurer, H. Baumgartner, Mild and moderate aortic stenosis. Natural history and risk stratification by echocardiography, European Heart Journal, 25 (2004) 199-205.
[8] C.M. Otto, I.G. Burwash, M.E. Legget, B.I. Munt, M. Fujioka, N.L. Healy, C.D. Kraft, C.Y. Miyake-Hull, R.G. Schwaegler, Prospective Study of Asymptomatic Valvular Aortic Stenosis, Circulation, 95 (1997) 2262-2270.
[9] E. Kouhi, An advanced fluid structure interaction study of tri-leaflet aortic valve, Conventional Thesis, Swinburne University of Technology (2012).
[10] J.T. Butcher, R.M. Nerem, Valvular endothelial cells and the mechanoregulation of valvular pathology, Philosophical Transactions of the Royal Society B: Biological Sciences, 362 (2007) 1145-1157.
[11] E. Poggianti, L. Venneri, V. Chubuchny, Z. Jambrik, L.A. Baroncini, E. Picano, Aortic valve sclerosis is associated with systemic endothelial dysfunction, Journal of the American College of Cardiology, 41 (2003) 136-141.
[12] H. Maleki, Structural and fluid-structure interaction analysis of stenotic aortic valves: application to percutaneous aortic valve replacement, Conventional Thesis, Concordia University (2010).
[13] B.L. Moore, L.P. Dasi, Coronary Flow Impacts Aortic Leaflet Mechanics and Aortic Sinus Hemodynamics, Annals of Biomedical Engineering, 43 (2015) 2231-2241.
[14] K. Cao, P. Sucosky, Aortic valve leaflet wall shear stress characterization revisited: impact of coronary flow, Computer Methods in Biomechanics and Biomedical Engineering, 20 (2017) 468-470.
[15] A. Nemes, T. Forster, M. Csanády, Relationship between coronary flow velocity reserve and aortic stiffness, The American Journal of Physiology-Heart and Circulatory Physiology, 290 (2006) 1152-1187.
[16] H. Hatoum, Fluid mechanics of transcatheter aortic valve replacement, Conventional Thesis, The Ohio State University (2018).
[17] Y.S. Morsi, Tissue engineering of the aortic heart valve: fundamental and developments, Nova Science Publisher Inc, New York, United States (2012).
[18] N.M. Rajamannan, F.J. Evans, E. Aikawa, K.J. Grand-Allen, L.L. Demer, D.D. Heistad, C.A. Simmons, K.S. Masters, P. Mathieu, K.D. O'Brien, F.J. Schoen, D.A. Towler, A.P. Yoganathan, C.M. Otto, Calcific aortic valve disease: Not simply a degenerative process: A review and agenda for research from the national heart and lung and blood institute aortic stenosis working group, Circulation, 124 (2011) 1783-1791.
[19] D.A. Lerman, S. Prasad, N. Alotti, Calcific aortic valve disease: Molecular mechanisms and therapeutic approaches, European Cardiology Review 10 (2015) 108-112.
[20] K.D. O'Brien, Pathogenesis of calcific aortic valve disease, Arteriosclerosis, Thrombosis, and Vascular Biology, 26 (2006) 1721-1728.
[21] S. Koenig, J. Lincoln, V. Vidua Garg, Genetic basis of aortic valvular disease, Current Opinion in Cardiology, 32 (2017) 239-245.

[22] J. Ortlepp, R. Hoffmann, F. Ohme, J. Lauscher, F. Bleckmann, P. Hanrath, The vitamin D receptor genotype predisposes to the development of calcific aortic valve stenosis, Heart 85 (2001) 635-638.
[23] S. Chandra, N.M. Rajamannan, P. Sucosky, Computational assessment of bicuspid aortic valve wall-shear stress: Implications for calcific aortic valve disease, Biomechanics and Modeling in Mechanobiology, 11 (2012) 1085-1096.
[24] M.G. Yussman, T. Toyokawa, A. Odley, R.A. Lynch, G. Wu, M.C. Colbert, B.J. Aronow, J.N. Lorenz, G.W. Dorn, Mitochondrial death protein Nix is induced in cardiac hypertrophy and triggers apoptotic cardiomyopathy, Nature Medicine, 8 (2002) 725-730.
[25] A. Hakki, A.S. Iskandrian, C. Bemis, D. Kimbiris, G.S. Mintz, B.L. Segal, C. Brice, A simplified valve formula for the calculation of stenotic cardiac valve areas, Circulation, 63 (1981) 1050-1055.
[26] S.J. Head, M. Çelik, A.P. Kappetein, Mechanical versus bioprosthetic aortic valve replacement, European Heart Journal, 38 (2017) 2183-2191.
[27] J.R.G. Etnel, S.A. Huygens, P. Grashuis, B. Pekbay, G. Papageorgiou, J.W.R. Hesselink, A.J.J.C. Bogers, J.J.M. Takkenberg, Bioprosthetic aortic valve replacement in nonelderly adults: A systematic review, meta-analysis, and microsimulation, Circulation: Cardiovascular Quality and Outcomes, 12 (2019) 1161-1182.

Chapter 2

Literature review

The cardiovascular system has been investigated by many researchers studying its dynamical behaviour, function, and physics. Among all the previous studies in the field of cardiovascular fluid mechanics, modelling of the aortic valve still requires further improvement and investigation. The importance of studying the aortic valve can be understood when reviewing the relevant statistics. Each year approximately 1.2 million (5.6%) Australian adults aged 18 and over encountered one or more conditions associated with vascular heart diseases, including stroke [1]. More importantly, each year approximately 40,000 Australians aged 55yrs or over need surgical aortic valve replacement (SAVR) and 7,000 Australian aged 75yrs or over require transcatheter aortic valve replacement (TAVR) [1]. Various techniques have been used to investigate the diseases associated with the aortic valve: in-vivo studies such as echocardiography and magnetic resonance imaging (MRI), and in-vitro experiments such as flow visualisation through particle imaging velocimetry (PIV) techniques and numerical simulations. Numerical simulations have attracted the attention of researchers in recent years because they can provide better understanding of the flow behaviour through the aortic valve, the dynamical motion of the aortic valve leaflets and the hemodynamics of the valve. Furthermore, they can help cardiologists to better understand the roots of the diseases associated with the aortic valve and also predict the efficiency and durability of artificial aortic valves.

Numerical simulation plays an important role in modelling of the dynamical motion of the aortic valve. There are three main modelling techniques: structural modelling, computational fluid dynamics and fluid structure interaction modelling. In structural modelling, only the structural part is modelled and the pressure is applied to the surfaces of the structure as a boundary condition instead of the blood flow. This method can only model the dynamical motion of the leaflet and find the stress and strain components on the leaflets. In this modelling, there is no way to model the fluid part and find the velocity components, the vorticity inside the sinuses and the flow shear stress. In computational fluid dynamics modelling, only the fluid part is considered. The behaviour of the fluid can be modelled via this technique, however the interaction between the structural and fluid parts is completely ignored. Since the dynamical motion of the leaflets can significantly affect the fluid domain and accordingly the velocity and vorticity components as well as the sinus vortex structures, the interaction between the fluid and structural domains should be accounted for. Therefore, fluid structure interaction methodology is used in order to have better understanding of the flow behaviour through the aortic valve and vortices inside the sinus cavity which play a main role in formation of the thrombosis of the blood flow, and most importantly shear stress in the vicinity of the leaflets. This method is used to model the interaction between the blood flow and leaflets. It can provide more accurate information on the shear stress in the vicinity of the leaflets, the vortices inside the sinus cavity, and the hemodynamic characteristics of the aortic valve leaflets. This information on the blood flow behaviour can be used to identify the

correlation between the hemodynamic parameters and aortic valve diseases such as calcification of the aortic valve.

In this chapter, a comprehensive literature review is performed in order to define the objectives of the project. In-vitro and in-vivo experimental techniques as well as numerical approaches which are used to analyse the performance of the aortic valve leaflets, model the dynamical behaviour of the leaflets, and study the flow behaviour through the valve, are thoroughly discussed.

2.1 Effect of aortic stenosis on aortic valve hemodynamics and coronary artery flow

Aortic valve stenosis is the second most common heart disease after coronary artery disease, and it is associated with abnormalities of the arterial system such as systolic dysfunction of the left ventricle, reduced aortic flow rate, reduced arterial compliance and increased transvalvular pressure gradient [2]. Stenosis of the aortic valve is the narrowing of the aortic valve because of calcium deposition on the leaflets. The stenosed valve cannot open properly and this affects the hemodynamic parameters inside the aortic root, mainly the valve orifice diameter/area, and the transvalvular pressure gradient.

Stenosis of the aortic valve not only changes the hemodynamic parameters within the aortic root, but also affects the coronary artery hemodynamics. Clinical data shows that patients with aortic valve stenosis and healthy coronary arteries are reported to have reduced coronary artery flow during the cardiac cycle [3]. The reduced coronary artery flow in patients with aortic valve stenosis may lead to myocardial ischemia and left ventricle dysfunction which results in heart failure over time [3]. The mechanism underlying the reduction of coronary artery flow in patients with aortic valve stenosis is still unknown [4]. It is believed that concentric LV hypertrophy may be the main reason for coronary artery flow reduction in patients with aortic stenosis. It was also shown that higher left ventricle pressure caused due to the presence of aortic stenosis, may lead to a reduction of the coronary artery flow [4]. Furthermore, in-vivo data shows that patients with aortic valve stenosis have symptoms of coronary artery disease. It is also believed that coronary artery disease and aortic valve stenosis are interdependent, however, the mechanism behind is not clear as yet [4].

The stenosis of the aortic valve and its effect on the sinus vortex structures and the wall shear stress on the leaflets is very important due to its effect on initiation and progression of the calcific aortic valve disease [5]. Genetic factors impact on the initiation of calcific aortic valve disease, however the alteration of fluid shear stresses in the vicinity of the leaflets is believed to be one of the main factors impacting on initiation of CAVD [6]. Although, it is not well understood how CAVD initiates and progresses, it is believed that there is a link between the wall shear stress on the leaflets and the imitation and progression of CAVD [7].

2.2 Wall shear stress and its relation with aortic valve and coronary artery disease

Wall shear stress (WSS) is defined as the fractional viscous stress on the wall produced due to the velocity variation of the blood flow near the wall. It is shown that the physiologic WSS levels are very important in the maintenance of the homeostasis of the aortic valve,

however variation in the WSS is one the main reasons for initiation of pathologies associated with the aortic valve [8].

Invasive and in-vitro investigations also demonstrated that the wall shear stress plays a significant role in the initiation of atherosclerosis within the coronary arterial wall and the progression of the calcium deposition on the leaflets [9]. Calcification and atherosclerosis are, however, complex multifactorial processes which remain incompletely understood. It is believed that blood flow-induced shear stress affects the endothelial cells leading to endothelial dysfunction, inflammatory responses, oxidative stress which remodels the artery wall and valve structure and eventually results in the progression of calcification and initiation of atherosclerosis [10, 11].

Mohammadi et al. [12] presented a 3D global fluid structure interaction model of the aortic valve leaflets including left and right coronary arteries. They investigated the effect of the leaflets stiffening on the coronary artery hemodynamics. They showed that the wall shear stress on the left and right coronary arteries during the systole decreases by increasing the leaflets' stiffness due to calcification. By contrast, the wall of the coronary arteries experiences higher shear stress at diastole phases. Moreover, the results revealed that the coronary artery flow rate decreases due to the calcification of the aortic valve. This can be correlated with coronary artery diseases.

Another study by Nobari et al. [13] investigates the influence of the stiffness of the coronary artery wall on coronary artery hemodynamics. They showed that the stiffened coronary artery experiences a lower amount of wall shear stress compared to healthy coronary arteries. They also studied the effect of calcification accompanied by stiffness of the coronary arteries wall on coronary artery flow rates. They showed that calcified valve with stiffened coronary artery wall witnesses lower shear stress on the leaflets during the systole and higher amount of shear stress on the leaflets during the diastole.

2.3 Coronary artery flow and its importance in fluid structure interaction modelling of the aortic valve

Fluid structure interaction modelling of the aortic valve is a very challenging task because of the complexity associated with modelling the large deformation of the leaflets during the systole [14]. Many researchers have developed 2D and 3D models of the aortic valve neglecting the presence of the coronary arteries because considering the coronary arteries in FSI simulation increases the complexity of the modelling and accordingly the instability of the solution [15, 16]. On the other hand, coronary artery blood flow can significantly affect the sinus vortex structures and accordingly the hemodynamic parameters inside the aortic root and the sinus cavity [17]. Therefore, it is crucial to include coronary arteries when modelling the pathologies associated with the aortic valve. There are a few analytical and numerical studies based on FSI models of the aortic valve considering coronary arteries [12, 13, 16], however there is still lack of knowledge related to the effect of coronary artery flow on the sinus flow characteristics as well as the hemodynamic parameters of the aortic valve.

Cao et al. [16] investigated the impact of coronary flow on aortic sinus hemodynamics as well as wall shear stress on the leaflets. They reported that the presence of the coronary artery increases the complexity of the fluid structure interaction modelling as well as instability of the solution. They calculated the oscillatory shear stress on the different locations of the

leaflets (base, belly, and tip) corresponding to coronary and non-coronary sinuses. The results showed that the belly of the leaflets corresponding to the coronary sinuses experiences lower shear stress compared to that of with non-coronary sinus. Moreover, the tip of the leaflets of the coronary sinuses witnesses the lowest magnitude of shear stress among the others. They also showed that the sinus vortex structure of the coronary sinuses are completely different from that of with non-coronary sinuses. It is believed that different sinus vortex structures affects oscillatory shear stress on the leaflets of the coronary sinuses.

Therefore, there is a need to develop a model of the aortic valve taking into account the presence of the coronary arteries and their effect on the sinus flow structure as well as the wall shear stress on the leaflets. There is still a gap in knowledge related to the effects of aortic valve stenosis on the coronary artery hemodynamics as well as the initiation of coronary artery diseases. The correlation between the wall shear stress on the aortic valve leaflets and the initiation and progression of calcific aortic valve diseases is not well understood.

2.4 Positions of the coronary artery ostia and its effect on sinus flow patterns and hemodynamic parameters

Coronary angiographic images show that the position of the coronary artery ostia varies among different people [18], from proximal to distal position relative to the aortic valve [19, 20]. Clinical data shows that a considerable percentage of patients who undertook aortic valve replacement (mainly transcatheter aortic valve replacement) died within 2 years of surgery [18, 21]. The reason behind this number of deaths is still unknown. It is believed that it is related to the diet of the patients, the geometrical properties of the coronary arteries and aortic valve, the hemodynamic variation inside the aortic root, and coronary artery obstructions generated due to the presence of stents in transcatheter aortic valve replacement (TAVR) [21]. It can be hypothesised that the locations of the coronary artery ostia in different patients can affect the sinus flow structures, the wall shear stress on the leaflets and the transvalvular pressure gradient and accordingly lead to the initiation of aortic valve stenosis. Consequently, there is a gap in knowledge about the influence of geometrical parameters such as the locations of the coronary artery ostia on the sinus vortex structures and the flow characteristics inside the aortic root and sinuses. It is not well understood yet how the locations of the coronary artery ostia can alter the sinus vortex structures and most importantly the wall shear stress on the leaflets which is the greatest risk factor associated with CAVD.

In the following sections, previous in-vitro and in-vivo experimental studies, and numerical simulations conducted to model the dynamical behaviour of artificial aortic valves, the flow behaviour through the aortic valve, and the variation of hemodynamic parameters due to abnormalities of the aortic valve, are explained. From the findings of these sections, the objectives of the project are defined.

2.5 In-vitro and in-vivo experiments

Aortic valve replacement (AVR) is one of the most common treatment methods for aortic valve stenosis. Mechanical, bioprosthetic, and transcatheter aortic valves are used to replace the original aortic valve via open heart surgery or transcatheter aortic valve replacement techniques. Therefore, considerable research has focused on developing accurate in-vitro and in-vivo methods in order to evaluate the performance and durability of artificial valves.

2.5.1 Hemodynamic assessment of artificial aortic valves

Pioneering experimental research in this field was done by Brown et al. [22] who found that excessive wall shear stress (shear stress > 50 dyne cm^{-2}) on the leaflets could activate platelets and result in thrombosis over time. Following their work, Yoganathan et al. [23, 24] investigated the probability of thrombosis in a Starr-Edward aortic valve using Laser-Doppler Anemometry (LDA). They tested thirteen autopsy models of aortic valves considering steady-state flow and measured shear stress, pressure difference and flow rate. They found that the pressure significantly drops in the vicinity of the prosthetic valve where the stresses are very high. It was also shown that the flow pattern is highly affected by recirculation zone generated behind the leaflets due to separation. Their results showed that the recirculation zone behind the leaflets, and reduction in the pressure accompanied with turbulent stresses affect the formation of the thrombus which leads to prosthetic valve failure over time. A similar in-vitro test was conducted by the same group in which a Medtronic-Hall pivoting disc heart valve was tested under similar conditions. The results of this work also confirmed their previous findings, however the stagnation region corresponding to this type of valve was shifted to different locations.

Later on, Woo et al. [25] and Yoganathan et al. [26] conducted series of investigations to study the hemodynamic performance of the polymeric, Carpentier-Edwards, and Ionescu-Shiley tissue valves considering steady-state flow. Their finding showed that the polymeric valve experiences less turbulent blood flow at peak systole with a larger effective orifice area (EOA) compared to the other ones. The LDA approach was also used by Chandran et al. [27] for studying the flow characteristics corresponding to the different types of mechanical valves. Their findings showed that turbulent stresses related to the ball caged prostheses were lower than that of the disk valve. Later, studies were conducted by the same group in which they focused more on the valve closure, investigating the effect of the increased pressure in the left ventricle of the heart on the generation of cavitation in the mechanical valves [28, 29]. Their results revealed that there is a large negative pressure difference between the location of the valve hinge and the tips of the leaflets in both in-vitro and in-vivo tests [30].

Several experimental studies were carried out by researchers in which various types of mechanical and bio-prosthetic valves were tested considering pulsatile blood flow under physiological conditions [26, 31-33]. Hemodynamic parameters were measured for all the common types of artificial valves using a 2D LDA method. The results show that the valves witness a uniform flow pattern during the systole. However, a separation zone occurred in the area close to the hinge where the wall shear stress and turbulent stress are high. They showed that blood cells are more prone to damage around the hinge of the leaflets.

Significant progress in investigating the performance of prosthetic valves was achieved by Fan et al. [34] who presented a novel technique named colour Doppler flow mapping to assess the flow velocity field. This technique is medical ultrasonography which utilises the Doppler effect to provide images of the body organs and blood flow. However, colour Doppler flow mapping provides accurate data of the velocity and direction of the blood flow inside the body, the ultrasound beam should be placed parallel to blood flow in order to record precise data. This can be one of the limitations of these techniques. Later, Cape et al. [35] investigated the effects of different factors such as the physical characteristics of the system, the settings of the instrument, and the interaction of the solid parts on the resolution of the images taken through this technique. Accordingly, a study was carried out by Cape et al. [36] in which the

colour Doppler flow mapping technique was used to study the influence of the regurgitated blood flow on hemodynamic parameters. They found that the conditions of the adjacent walls (stiffened wall) significantly reduces the maximum magnitude of the velocity in the flow field. This technique was also used by Recusani et al. [37] in order to accurately measure the effective orifice area (EOA) specifically inside the turbulent flow.

Later, Baldwin et al. [38] utilised a Laser Doppler Velocimetry (LDV) approach to investigate the flow behaviour around the pivot and hinge regions of the different disk valves. They found that the maximum value of turbulent shear stress has the same trend in different models of disk valves. After the introduction of 2D LDV, they conducted a research in which they compared the hemodynamic characteristics of the Bjork-Shiley and SJM prosthetic aortic valves. Turbulent shear stress comparison between the results of the 2D and 3D Laser Doppler Velocimetry approach showed significant measurement errors (greater than 10%). These observed errors are highly dependent on the components of the velocity used in the 2D technique.

Kini et al. [39] utilised Particle Imaging Velocimetry (PIV) and LDV approaches in their in-vitro experiment to investigate the regurgitation phenomenon generated downstream of the prosthesis during the systole. They compared the flow structures inside the sinuses considering constant and pulsatile flow rates. They showed that the sinuses of the model with pulsatile flow experience complicated vortex structures with a higher magnitude of vorticity strength compared to the model with constant flow. They visualised the complex regurgitated flow structures downstream of the prosthesis considering the pulsatile blood flow at the inlet. Later, Manning et al. [40] proposed a PIV technique to measure the regurgitated blood flow during the cardiac cycle, focusing on cavitation. The captured images showed that the generation of the vortex in the vicinity of the prosthesis tips could generate cavitation. Ellis et al. [41] and Leo et al. [42] utilised similar experimental methods in which they provided more detail on the blood flow patterns near the hinge region of the prosthesis. They showed that complicated vortex structures near the hinge region of the valve increases average wall shear stress on the valve's leaflets.

Morsi et al. [43] analysed the performance of the jellyfish valve using a LDA method and compared it with the artificial St. Vincent disk valve. They showed that the shear stress corresponding to the jellyfish valve was much less than that related to the St. Vincent disk valve due to the difference in the material properties as well as the design of the valves. Another work carried out by Morsi et al. [44] in which they visualised the turbulent flow behaviour near the outlet region of the jellyfish valve. They measured the pressure difference across the valve orifice, and the energy losses and regurgitated blood flow during the systole [45, 46]. They found that the jellyfish valve model witnessed less back flow and energy losses compared to the mechanical aortic valve. Furthermore, the regurgitated blood flow related to the mechanical valve was twice that of the jellyfish valve model.

Another study carried out by Morsi et al. [47] in which they investigated the probability of formation of thrombus and activation of the platelet under the same conditions as the abovementioned experiments. They proposed a mathematical model in which they correlated the peak shear stress with the blood damage index to find the probability of thrombus formation. They reported a lower blood damage index for the jellyfish valve model compared to the mechanical valve. Later, in a similar study conducted by Morsi at al. [48], the influences of the shape of the sinus (real, elliptical, and cylindrical chambers) on the formation of

thrombus was investigated. They determined that the jellyfish valve model with an elliptical chamber witnesses the lowest magnitude of shear stress.

In the past two decades, researchers have benefitted from in-vitro experiments [49-51] and in-vivo methods such as Ultrasound [52], Echocardiography [53], and Cardiac Magnetic Resonance (CMR) [54] in order to assess the performance of the prosthesis. For example, Leo at al. [55] characterised the velocity and shear stress fields inside the polymeric aortic valves. They evaluated the performance of the three different polymeric aortic valves with various thickness of the leaflets under physiological conditions. They showed that the leaflet thickness affects the valve dynamics and increases the possibility of thrombus formation near the hinge of polymeric trileaflet aortic valves. Another study carried out by Ge et al. [56] in which they analysed the possible complications caused to blood cells by a bileaflet mechanical aortic valve. They linked the Reynolds shear stresses and viscous stress as factors which caused damage to the blood cells downstream of the leaflets. They indicated that the damaged blood cells can promote thrombus formation in the vicinity of the valve leaflets.

Yap et al. [57] presented an in-vitro technique to link the energy losses of an aortic valve caused by aortic valve stenosis in each cardiac cycle to heart attack and failure. They tested various porcine aortic valves under a number of physiological conditions such as different stroke volumes and heart beats and considered healthy, calcified and severely calcified aortic valves. They showed a severely stenosed aortic valve experiences higher energy losses during each cycle with the abnormal shape of the energy loss waveform compared to that of a healthy valve. Based on their results, increasing the level of the severity of stenosis increases energy losses. This energy loss was determined as a clinical tool to evaluate the aortic valve stenosis.

2.5.2 Sinus flow visualisation based on experimental techniques

Sinus flow structures have a strong relation with the hemodynamic parameters inside the sinus cavity. To show this, researchers have conducted experiments over the last decade to visualise the sinus flow characteristics. For example, Forleo et al. [58] presented a new in-vitro technique for quantifying the effects of the vortex formation and regurgitated jet flow near the hinge of a bileaflet mechanical aortic valve on blood damage index (BDI). Their results showed that mechanical valve replacement affects BDI by reducing the valve closing time by 10ms and increasing the mean aortic pressure by 40 mmHg. This increased mean pressure generates stronger vortex structures which leads to the activation of the platelet and subsequently increased BDI. Another study carried out by Moore et al. [7] in which the effects of the sinus vortex structure on the performance of the aortic valve was shown. The results of this study demonstrated that the flutter of the leaflets during the systole was considerably induced by various heartbeats and complex spatiotemporal vortex structures generated in the sinuses (shown in Figure 2.1).

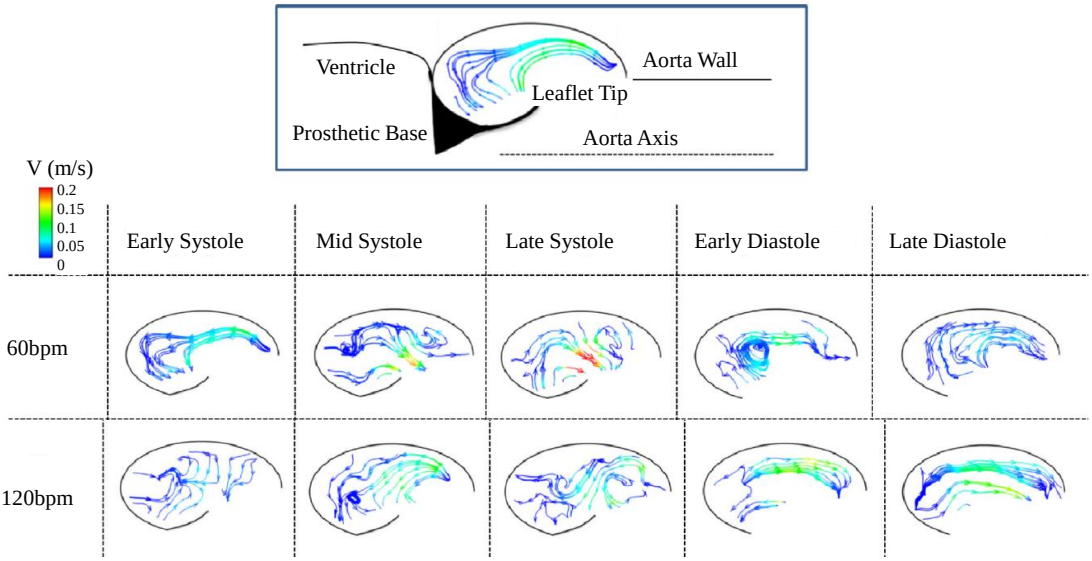

Figure 2.1 Velocity streamlines and contours inside the sinus cavity during cardiac cycle corresponding to hearts with different heartbeats (i.e. 60 and 120bpm) [7]

Later, in another work conducted by the same research group, Moore et al. [59] investigated the effects of the coronary artery flow on aortic leaflet mechanics and the hemodynamics of the sinus using a bioprosthetic aortic valve. The vortex structures between the coronary and non-coronary sinuses were compared in order to elucidate the hypothesis that the non-coronary sinus is calcified before the other sinuses. The results showed that the presence of coronary flow affects the leaflet dynamics and reduces the wall shear stress on the leaflets (shown in Figure 2.2), however it improved washout time (the time taken for the blood to flow from the sinuses to the aorta) at the base of the leaflet. In similar work by Yousefi at al. [60] the effect of arched leaflets and the stent profile on the performance of a polymeric aortic valve was analysed. They found that a higher stent profile and arches decreases the regurgitated blood flow and the Reynolds shear stress by 5 and 40 percent, respectively. Based on their results, a valve with arched leaflets witnesses lower energy losses and accordingly lower probability of aortic valve stenosis.

Hatoum et al. [61] studied the effect of transcatheter aortic valve replacement on the blood flow structures and in order to identify the thrombus formation process after valve-in-valve aortic valve replacement. Their findings showed a significant reduction in the peak velocity along the valve orifice, the vorticity magnitude inside the sinuses of the replaced transcatheter aortic valve, and the peak shear stress on the leaflets of the transcatheter aortic valve. They demonstrated that a lower shear stress on the leaflets increases the risk of formation of thrombosis in the vicinity of the leaflets. Later, the same group conducted research associated with the effect of transcatheter aortic valve replacement (TAVR) on valve hemodynamics [62]. They analysed the influence of TAVR on a wide range of hemodynamic parameters such as pressure gradient (PG), leakage fractions (LF), shear stress on the leaflets and the sinus washout mechanism. Based on their results, PG was highly affected by the axial position and angular orientation of the TAV. Furthermore, the flow shear stress, as well as the washout mechanism inside the sinus cavity at peak systole, were highly influenced by the deployment depth of the TAV.

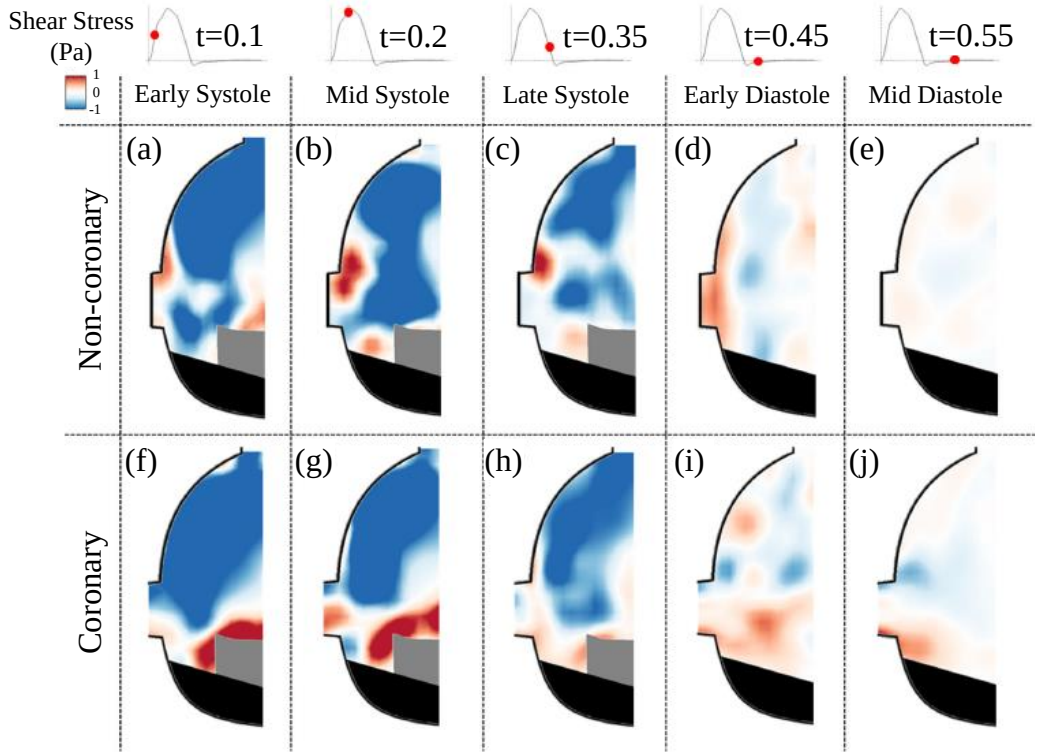

Figure 2.2 Shear stress contours for the coronary and non-coronary sinuses during the cardiac cycle [59]

Later, a similar in-vitro experimental study was carried out by the same research group, but this time the presence of congenital aortic valve diseases (i.e. bicuspid aortic valve leaflets) and their effects on valve hemodynamics were analysed [63]. They compared the sinus vortex structures and hemodynamic parameters between the tricuspid and bicuspid aortic valves (TrAV and BAV). Their results demonstrated that the leaflets of a TrAV witness higher shear stress on the leaflets and quicker washout time compared to those of a BAV. Regarding valvular heart diseases, Hatoum et al. [17] also studied the effect of the calcification of the bioprosthetic aortic valve on the sinus vortex structures and the valve hemodynamics using the PIV technique. Their results showed that a severely calcified aortic valve has a lower valve orifice area with a higher vorticity magnitude inside the sinuses compared to those related to the healthy valve. Furthermore, the circulation strength of vortices inside the sinuses of the healthy valve are stronger than for a calcified valve. Based on their results, the strong vortices are more prone to move towards the aorta instead of being trapped in the sinuses. This led to different vortex structures and a slower washout mechanism inside the non-coronary sinus corresponding to the diseased valve. Similar studies were conducted by Hatoum et al. [64], but this time, the same scenario was examined for the TAV-in-TAV replacement. They compared the washout times of the TAV-in-TAV, valve-in-valve, and TAV replacements. Their findings demonstrated that the washout mechanism is not significantly affected in TAV-in-TAV compared with valve-in-valve and TAV replacements. However, the shear stress distribution on the leaflets and the jet velocity along the valve were highly dependent on the various types of aortic valve replacements (AVR).

In-vitro and in-vivo experiments have been successful in analysing the performance of the different types of artificial aortic valves, and a huge amount of achievements in the last two decades, however measuring hemodynamic parameters such as the wall shear stress based on

experiments is still very challenging. Additionally, enormous cost needs to be invested in the facilities used for in-vitro and in-vivo experiments. Therefore, researchers have been looking for an alternative and cost-effective solution to test and simulate aortic valve diseases. The most common numerical approaches used to simulate the dynamical motion of the leaflets and investigate the sinus flow patterns are: Finite Element Analysis (FEA), Computational Fluid Dynamic (CFD), and Fluid Structure Interaction (FSI) methods.

In the following sections, the above numerical methods used to model the dynamical motion of the aortic valve are explained along with some of their advantages and disadvantages.

2.6 Finite element analysis numerical approach

Researchers have used FEA to characterise the material properties, parametrically design biomedical aortic valves, and test the durability of bioprosthetic, mechanical and stented aortic valves in the past two decades. FEA has been widely used to simulate the dynamic motion of the leaflets and to analyse the stress distribution on the leaflet cusps undergoing uniform pressure or forces extracted from the fluid. FEA considers only the structural part of the aortic valve leaflets, ignoring the interaction of the fluid and structural domains. In recent years many researchers have used FEA as a numerical method to model the dynamic motion of the leaflets in order to improve the design of the bioprosthetic, mechanical and stented aortic valves. The following sections focus on the achievements and developments of FEA in the design and analysing the performance of the different types of artificial aortic valves.

2.6.1 Simulation of dynamical motion of the leaflets based on finite element analysis

To characterise the deformation of the leaflets subjected to uniform pressure, Huang et al. [65] developed a 2D model of a bio-prosthetic aortic valve. They reported that a large amount of stress is generated during systole. Later, a 3D model of a bileaflet mechanical valve was designed by Black et al. [66] based on the finite element method (FEM) in which they reported that utilising a 2D membrane model to simulate the dynamic motion of the leaflets could lead to significant errors in calculating the maximum stress magnitudes on the leaflets.

Chandran et al. [67] investigated the influence of geometrical parameters such as the length of the stent, the thickness of the leaflet and the coaptation area on the magnitude of the stress on polymeric aortic valve at early diastole (when the valve is completely closed). A rigid model of the stent was designed and the FE method was utilised to analyse the stress distribution on the leaflets. Their results demonstrated that commissural attachment is where the peak stresses occur on the leaflets. Furthermore, they showed that the stress reduces significantly as the length of the leaflets increases. However, no information was reported on the effects of the leaflet thickness and coaptation area.

Krucinski et al. [68] presented novel modelling of the flexible stent in trileaflet bovine bioprosthetic aortic valves based on the FE method. They studied the stress on the proposed model and reported that the region in which the stress concentrated is near to the commissural area of the leaflets, which occurs with the same finding of Chandran et al. [67]. Based on their findings, the introduced novel stent design showed 40% lower stress at critical areas compared with the previous stents designs.

Later, the influence of the nonlinearity of the leaflet materials on the dynamical behaviour of the aortic valve leaflets was discussed by Patterson et al. [69]. They compared the deformation of the leaflets of a bicuspid aortic valve using linear and nonlinear material properties and under uniform pressure. Their results showed that the nonlinear model of the leaflets demonstrates a larger deformation and quicker response to the external pressure compared with those of leaflets with linear material properties. Another study carried out by Thornton et al. [70] using the same FE model of the aortic valve with nonlinear material properties of the leaflets was considered. However, this time they studied the effects of the changes in the thickness and the Yong's modulus of the leaflets on the stress distribution on the leaflet cusps. Their results showed that thicker leaflets experience lower values of stress during the diastole phase. However, the influence of the higher pressure drop and the energy losses of the system were ignored during the systole phase.

A numerical study of the proposed design by De Hart et al. [71] shows considerable improvement in the durability of the artificial aortic valves using novel fibre-reinforced material. A novel fibre-reinforced material inside the stented model of the aortic valve was examined via the FE method. Based on their results, the proposed model reduced the maximum stress on the leaflets by 60%. A similar study carried out by Cacciola et al. [72, 73] considered the same material properties used by De Hart et al. [71], but this time without a stent. Their results demonstrated that the peak stress on the leaflets decreases by 75% which could considerably improve the durability of the proposed bioprosthetic aortic valve.

2.6.2 Performance evaluation of the artificial aortic valves based on finite element analysis

A novel technique was introduced by Grande-Allen et al. [74] to extract the geometry for a realistic model of the aortic valve. They studied the effect of various graft shapes of the original and artificial aortic valves on their performance using the FE method. A 3D realistic model of the healthy aortic valve was developed using available MRI images. Then, two novel graft models considering pseudosinus and cylindrical elements shape in addition to the natural bioprosthetic elements were developed. Three numerical models corresponding to two grafted and one natural models were introduced considering linear material properties in developing the models. An unsteady pressure profile was applied to all of the developed FE models. Their results showed that the prosthetic model witnesses a higher stress concentration in critical areas compared with the natural model. Their finding emphasized the importance of the graft element shape in FE modelling of the artificial valves rather than the linear or non-linear material properties.

Luo et al. [75] investigated the influence of geometrical parameters such as the height of the stent, the diameter of the valve, and different thickness of the aortic valve leaflets on the stress distribution on the leaflets of a porcine bio-prosthetic aortic valve. In the numerical modelling, a constant pressure (16kPa) was applied on the leaflets and the influence of the isotropic and anisotropic material properties were studied. Their findings showed that a bioprosthetic valve with the thickness of the leaflets varying along the length could considerably reduce the maximum stress at the commissural attachments. Furthermore, the longer stent with smaller diameter size could also lead to stress reduction on the leaflets. The main limitation of their work was that they only analysed one-third of the leaflets and ignored the influences of the contact stress on the deformation of the leaflets during systole.

A 3D FE model of the aortic valve considering aortic roots and sinuses was proposed by Howard et al. [76] in which the unsteady pressure was used as the boundary condition to generate the dynamic motion of the leaflets. Their results showed that the presence of aortic roots and sinuses in their model could considerably differentiate (65% difference) the effective orifice area (EOA). Later, they improved their FE model to a one-way fluid structure interaction (FSI) model using the operator split method in which the fluid forces indirectly became updated in each cycle [77].

The effect of the orthotropic nature of the aortic valve leaflets on the dynamic behaviour of the leaflets was studied by Arcindiacono et al. [78] in which a 3D model of orthotropic tri-leaflet aortic valves was developed using the FE method. Two different orthotropic models of the leaflets were introduced considering different Young's moduli in the circumferential and radial directions. In order to investigate the dynamic motion of the leaflets, the physiological pressure profile was defined as a boundary condition. The results demonstrated considerable changes in the deformation and stress values in the different directions on the leaflets by defining the orthotropic axes over the leaflets.

Later, Sun et al. [79] developed more accurate results for the deformation and stresses on 2D leaflets using quasi-static FE modelling. Their results showed an approximate 2% error between the outcomes of their study and the experimental measurements. However, they extended their 2D model into a 3D model in which they observed a significant amount of variation in the distribution of the principal stresses on the leaflets. Then, Kim et al. [80] presented a FE model of a bioprosthetic aortic valve using shell elements. The results of their modelling could accurately model the dynamic motion of the bioprosthetic aortic valve with more precise results relating to the deformation of the leaflets because of their considering anisotropic material properties along the aortic valve leaflets.

Haj-Ali et al. [81] combined experimental and numerical techniques in order to design and evaluate the performance of a polymeric aortic valve. The dynamical behaviour of the leaflets was modelled using FEM and nonlinear shell elements. Quasi-static TPG data collected from the in-vitro experiment was defined as the boundary condition in the numerical modelling. The results of the experimental and numerical methods had only 10% discrepancy in the measurement of the leaflet deformation. They reported that the stress and strain results obtained from their work were more accurate compared with the previous numerical models [76]. Their results also confirmed that the peak values of stress occur in the vicinity of the commissural area.

The effect of different shape of the commissural attachment on the dynamic performance of the tri-leaflet valve was studied by Nedoom et al. [82] in which two models of the leaflets (i.e. moulded and tubular models) were developed. In the developed models, the physiological pressure waveform during the cardiac phases was applied. Based on their findings, the leaflets in the moulded model demonstrated a quick response, higher EOA (effective orifice area) and coaptation during the systole compared with that for the tubular model. The stress values corresponding to the moulded model were lower than that of the tubular model. This meant that the moulded model could be used in the natural design of the bio-prosthetic aortic valve.

Burriesci et al. [83] presented a comprehensive investigation based on FE methods in order to parametrise and optimise the performance of a polymeric aortic valve. In their study, a single curved profile for the leaflets was introduced in order to improve the stress distribution

on the leaflets at commissural attachments. The physiological TPG was considered as a boundary condition in order to model the dynamical behaviour of the aortic valve. Their findings showed an approximate 10% increase in the EOA and a decrease in the peak von Mises stress on the leaflets and the pressure difference along the valve compared with previous designs. The results were validated against the previous experimental study and found to be more accurate in calculating EOA and PG using the new design.

Labrosse et al. [84] developed FE models for a normal, a diseased and a repaired valve in order to simulate cusp prolapse disease associated with diseased or repaired aortic valves. The performance of the diseased and repaired valve was compared with the normal healthy valve by calculating and comparing maximum leaflet stress, valve orifice area, coaptation area at early diastole, and opening/closing times of the leaflets. Later, Gilmanov et al. [85] used a hyperelastic materials model and a shell FE formulation in order to simulate the large deformation of the aortic valve leaflets during the cardiac cycle (shown in Figure 2.3). The proposed model showed that the nonlinear hyperelastic anisotropic material properties of the leaflets affects the durability of the bioprosthetic aortic valve to tolerate higher levels of TPG during the diastole phases. A similar study was carried out by Abbasi et al. [86] considering viscous damping effects of surrounding fluid. Based on their findings, the anisotropic FE model could accurately simulate the coaptation and large deformation of the leaflets during early diastole, and systole, respectively.

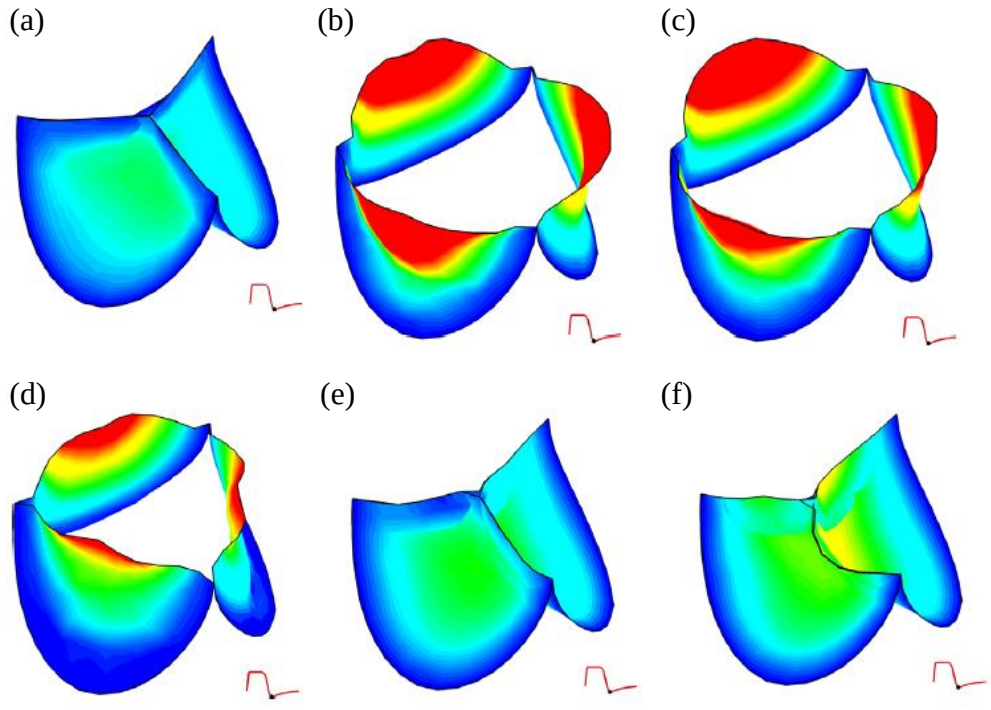

Figure 2.3 Displacement contour and dynamic opening and closing of the trileaflet aortic valve during the cardiac cycle (a) early systole, (b) middle systole, (c) peak systole, (d) early diastole, (e) middle diastole, and (f) late systole [85].

FEA has a significant impact on simulating the dynamic behaviour of the aortic valve leaflets and analysing the performance of the bioprosthetic, mechanical, and stented aortic valves, however the accuracy of the proposed models could be seriously questioned, as the

direct interaction between the fluid and structural domain has been completely neglected in all of the FEA simulations. For instance, the calculated values of maximum stress and the distribution of the stress on the leaflets could not be considered completely accurate, as the exchanged force between the structure and fluid domains is not similar to the pressure difference boundary condition which was used in most of the above-mentioned FE simulations. Eventually, EOA estimation and pressure drop calculations based on these models could not provide a clear picture of the dynamical performance of the bio-prosthetic aortic valve due to the fluid domain being neglected in the simulations [15].

2.7 Computational fluid dynamics numerical approaches

Computational fluid dynamics is a numerical method used to model fluid dynamics. In the context of the current research topic, it is able to analyse flow characteristics and measure the hemodynamic parameters along the aortic valve excluding the structural deformation. Whilst this method is powerful in modelling the fluid domain, the interaction between the fluid and structural domains is neglected. In the following, the previous studies in the modelling of blood flow through the aortic valve based on the computational fluid dynamics method are explained.

CFD modelling of the aortic valve was introduced by Peskin et al. [87]. Later, the immersed boundary techniques were utilised to model the fluid mechanics of mitral and aortic valves [87, 88]. Greenfield et al. [89] visualised the flow in the vicinity of ball and tilting disk valves in order to measure the velocity, pressure and stress contours. Then, Thalassoudis et al. [90] utilised the CFD method to study the influence of inflow variation on the shear stress values of the prosthetic Edwards caged ball aortic valve. They used a numerical finite difference technique to solve the Navier-Stokes equations and predict the blood flow behaviour inside the valve.

A three dimensional model of bi-leaflet mechanical aortic valves was presented by Borgersen et al. [91] in which they modelled the fluid domain at three different static positions of the aortic valve leaflets. Then, Shim et al. [92, 93] investigated the flow behaviour of a similar valve when the valve was half-opened. The 3D Navier-Stokes equations were solved assuming laminar flow along the valve. Based on their findings, the shear stress magnitudes inside the sinus area was found to be very high due to the circulatory flow. King et al. [94] investigated experimentally and numerically the unsteady Newtonian flow behaviour of the blood flow along a bi-leaflet mechanical valve. The model included the sinuses, the aortic root and the left ventricle of the heart and was carried out when the valve was semi-open. They compared the results of their experiments with the numerical results from CFD. They found that the wall shear stress on the leaflets of the model considering sinuses is larger than that without sinuses.

The dynamical behaviour of a prosthetic valve was studied by Gardner et al. [95] in which CFD accompanied with Newton-Euler methods were used to map the pressure difference from the fluid domain onto the surfaces of the leaflets. The leaflets were assumed to have rotational and translational degrees of freedom with the ability to slide as well. Although, they extracted forces from the fluid domain and applied them to the structural domain, the lack of dynamic mesh updating in the structural domain affected the accuracy of the stress-strain fields.

Keshavarz Motamed et al. [96] numerically modelled a simplified model of the aorta considering coarctation of the aorta and aortic stenosis which are common valvular heart

diseases. The formulated Navier-Stokes equation was solved using CFD and the results were validated against a simplified experiment using a curved pipe mimicking ascending aorta. Their findings demonstrated that the presence of a coarctation considerably modifies the flow behaviour, the average wall shear stress, and the velocity magnitudes within the curved pipe model. More importantly, they reported that PG was reduced by 36mmHg considering both coarctation and aortic stenosis. A similar study conducted by the same group [97] in which they studied the effect of the presence of aortic stenosis and coarctation of the aorta on the workload of the left ventricle. Their results demonstrated that the left ventricle stroke changes from 0.98J for a healthy valve to approximately 2.15J for the valve with all aortic stenosis and coarctation. Their models were able to non-invasively predict the maximum left ventricle systolic pressure and the workload of the left ventricle because of existing aortic stenosis accompanied with coarctaion. The influence of the congenital bicuspid valve diseases accompanied with coarctation on the flow behaviour inside the aortic root was also studied by the same group.

Later, Motamed et al. [98] proposed a new approach to evaluate the severity of coarctation of the aorta (COA) based on the Doppler velocity index and EOA. Three different models of COA were developed and examined considering different flow rates and in the presence of healthy and stenosed aortic valves (shown in Figure 2.4). Their results showed that the peak-to-peak PG related to COA is highly dependent on the flow rate. Their findings demonstrated that the COA Doppler velocity index and COA are independent of the flow rate and the aortic valve conditions (i.e. healthy or stenosed aortic valve). In similar work by the same group [99], a non-invasive technique to diagnose the higher workload of the left ventricle using Magnetic Resonance Imaging (MRI) and Doppler Echocardiography was proposed. They presented a novel lumped model to represent the ventricular-valvular-arteria interaction in order to predict the stroke work of the left ventricle. They also introduced a new index named normalised stroke work (N-SW) to evaluate the workload of the left ventricle. Their model was validated against in-vivo data taken from 49 patients. Their results suggested that the N-SW method used to diagnose the severe aortic stenosis is more valid for patients with lower flow rate and TPG compared with patients with higher flow rate and TPG.

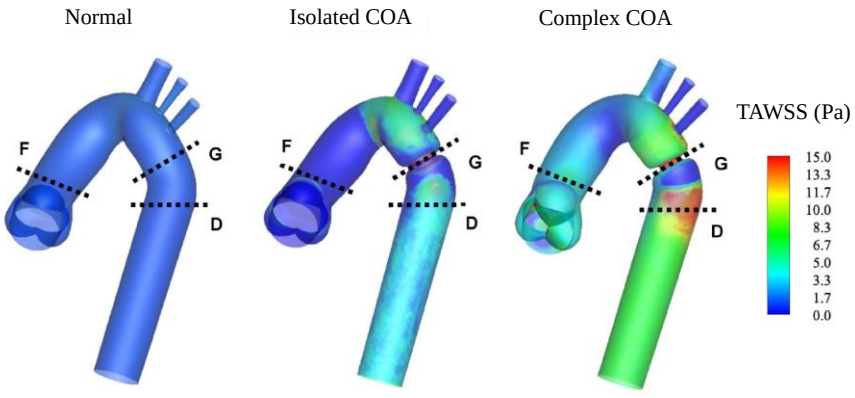

Figure 2.4 Time-averaged wall shear stress at peak systole corresponding to normal (healthy valve and aorta), isolated COA (healthy valve with coarctation in the aorta) and complex COA (bicuspid valve with coarctation in the aorta) models of the aorta [98, 100].

Djebbari et al. [101] investigated the influences of aortic stenosis and regurgitation on aortic valve hemodynamics using CFD and mathematical modelling. They developed a non-

invasive mathematical model to simulate the aortic stenosis and regurgitation based upon parameters such as EOA, blood pressure (BP) and stroke volume (SV) of the heart. They used the proposed approach on two groups of patients who were suffering from different levels of aortic stenosis and aortic regurgitation. Their results showed that patients with mild aortic stenosis and moderate aortic regurgitation were at risk of having higher workload on the left ventricle.

Keshavarz-Motamed et al. [102] presented an analytical model of the aortic valve in order to estimate TPG for patients with aortic stenosis. The proposed model solved Navier Stokes and elastic-deformation equations corresponding to the fluid and structural parts, respectively. The mode was validated against in-vivo and in-vitro published data. Their results showed that the proposed model could better estimate TPG in patients with a lower heart flow rate compared to other in-vivo techniques [96].

Later, Keshavarz-Motamed et al. [103] developed a CFD and a lumped parametric model taking benefit from the clinical data extracted from Doppler echocardiography, CT scan, and MRI in order to simulate the left ventricle hemodynamics considering different levels of paravalvular leakage (PVL) (i.e. mild, moderate, and severe PVL). Their results showed that the presence of a PVL affects the structure of the vortices inside the left ventricle and sinuses. Furthermore, their findings demonstrated that the abnormal flow characteristic, due to the presence of the PVL, significantly changes the shear stress on the aortic valve leaflets which affected the durability of the valve after the TAV replacement. Moreover, their results reveal that PVL also influences the flow behaviour as well as the shear stress values inside the left ventricle which leads to higher workload on the left ventricle. This eventually results in a higher risk of heart failure over time.

Despite valuable achievements and developments in CFD simulation of the aortic valve diseases such as aortic valve stenosis, coarctation, and aortic regurgitation, the effect that the structural motion has on the fluid flow is not accounted for in the CFD modelling. The fluid and structural domains must be simultaneously resolved in order to accurately model the dynamic motion of the aortic valve. In the following section, a well-known approach named two-way FSI will be introduced. Then, a comprehensive review will be presented associated with two-way FSI modelling of aortic valve pathologies.

2.8 Two-way fluid structure interaction (FSI) numerical approach

The past three decades have seen significant achievements in computational and mathematical modelling through novel techniques to model fluid dynamics and structural domains separately. However, these numerical techniques were not able to solve fully coupled moving boundary problems associated with heart valves which involve interaction between the blood flow and the deformable structural domain (leaflets). During the last two decades, two novel techniques named Arbitrary-Lagrangian, Eulerian (ALE) and Cartesian and/or Immersed boundary (IB) [104] methods were developed to model the interaction between the fluid and structural domains. However, researchers recently suggested that a method which combines both numerical techniques (ALE & IB) would be beneficial to simulate the complex fluid dynamics within the artificial heart valves [104].

In the following sections, various developed FSI techniques for the modelling of the dynamic behaviour of aortic valves accompanied by their stability to evaluate the performance of bioprosthetic and polymeric aortic valves will be reviewed.

2.8.1 Fluid structure interaction simulation of aortic valves

Fluid structure interaction modelling has been widely used to model the interaction between the blood flow and dynamical motion of the leaflets in the past few decades. For example, Campen et al. [105] presented a 2D model of the disc-type prosthetic aortic valve based on FSI simulation. They compared the results of a numerical simulation and experimental data and showed that numerical simulation could model the dynamic motion of the aortic valve leaflets. Krafczyk et al. [106] utilised a novel method of modified Lattice-Boltzmann (LB) technique to model the deformation of the leaflets considering transient blood flow. Another method was introduced by Cheng et al. [107] in which they used coupled 2D Navier-Stokes equations accompanied with the ALE technique to model the dynamic behaviour of mechanical aortic valves leaflets during the late systole phase (closure time). They parametrically investigated the influence of the geometrical parameters such as the size of the valve and the material properties of the leaflets. Their findings showed that the presence of negative pressure values generated during the closure period and in the vicinity of the hinges of the valve, increase the probability of thrombosis.

Later, Stijen et al. [108] simulated a 2D model of a mechanical aortic valve based on the FSI method in order to investigate the hemodynamic characteristics of the bio-prosthetic aortic valve in addition to various Reynolds and Strouhal numbers. The model includes two elastic membranes surrounded by solid frame. They used FE and FV to solve the structural and fluid domain, respectively. Their results showed that the shear stress around the hinges of the valve is highly dependent on the Reynolds and Strouhal number especially during the systole.

Krishnan et al. [109] and Govindarajan et al. [110] investigated the probability of activation of the platelets and formation of thrombosis in the vicinity of the hinge of the mechanical aortic valve during the closure period. The Lagrangian particle tracking technique was utilised in order to model the platelets considering all the forces. Their finding demonstrated that the circulatory flow generated due to flow separation in the vicinity of the leaflets apply higher shear stress on the particle which results in platelet activation.

Guivier et al. [111] utilised a similar method to compare the hemodynamic variation of a healthy and stenosed aortic valve using a 2D numerical model. They used Lagrangian particle tracking technique in their simulation. They reported that the stenosed aortic valve was unable to close properly at the late systole, because of the reduced diameter of the valve generating asymmetric and turbulent flow downstream of the leaflets which affect the dynamic motion of the leaflets and their hemodynamics.

Cheng et al. [112] introduced a novel technique which was a combination of the Immersed Boundary (IB) method, mathematical techniques, and Lattice Boltzmann (LB) method in order to improve the accuracy of the FSI simulation. The proposed techniques were successfully employed in a 2D model of the deformable leaflets of the mitral valve. The model was validated against previously published numerical data in terms of flow characteristics and dynamic deformation of the leaflets.

Choi et al. [113-116] conducted a series of investigations to analyse the performance of a mechanical aortic valve based on the FSI technique. They utilised FE and FV in order to couple the fluid and structural domains. They investigated the effects of the Newtonian and Non-Newtonian pulsatile blood flow on the aortic valve hemodynamics and performance in 2D and 3D simulations. Their findings showed that large vortices were generated inside the

sinuses at the peak systole. Their main findings were related to the effects of the angular velocity of the leaflets at late systole which significantly affects the turbulent flow surrounding the leaflets and also downstream of the leaflet. It was reported that the diverged turbulent flow in the above-mentioned regions generated a higher wall shear stress in the vicinity of the leaflets which results in blood cell damage.

The advantages of FSI simulation over purely FEA or CFD is the capability for modelling the interaction between multiple domains. Consequently, the above-mentioned FE/FV commercial codes used by the researchers obtained large popularity for evaluating the performance of the bioprosthetic aortic valve. Dumont et al. [117] presented a 2D FSI model of a bi-leaflet mechanical aortic valve at late systole (during closure time) using the FLUENT commercial code. Later, the same method was utilised by Redaelli et al. [118] to develop a 3D model of mechanical aortic valve. They used the coupled approach accompanied with an in-house code to correlate the displacement of the leaflets to the forces measured in the fluid domain. The obtained results of the angular velocity and displacement of the leaflets were compared with the experimental results showing an approximately 7% error between the experimental and numerical results.

Later, Nobili et al. [119] used FLUENT to investigate the effect of using weak and strong coupling techniques in the FSI simulation of bileaflet mechanical valves. However, the overall results of the displacement of the leaflets and flow patterns obtained from both methods (i.e. weak and strong coupling) were similar. There were considerable differences between the results obtained using the weak coupling method and the experimental data within the specific regions. For example, the peak opening time and velocity obtained using the weak coupling module had around 15% and 8% errors, respectively, compared with the experimental data. Another study carried out by Nobili et al. [120] in which they utilised a commercial FV solver accompanied with an implicit FEA package to perform coupled FSI simulation of the same mechanical aortic valve. The results of this study were compared with the experimental data and above-mentioned numerical work conducted by the same group, which showed that using a novel coupled FV and FEA can provide more accurate results compared to that with weak and strong coupling techniques. In the proposed novel coupled FV and FEA technique, they used FV to model the fluid domain and FEA to model the structural domain. Then, they developed a code in order to couple these two methods with a semi-coupled FSI model.

Dumont et al. [121] used FLUENT to study the hemodynamic and dynamic performance of two different models of mechanical valves (SJM and ATS) in order to predict possibility of formation of thrombosis. They utilised implicit FEA and FVA methods to simulate the interaction between the fluid and structural domains. The calculated mean pressure and velocity distribution during the systole and through the valve for both types of valves were nearly identical. However, the SJM model of the mechanical valve experienced a higher stress on the blood platelets compared with that of the ATS model. Their findings showed that the presence of a higher stress on the blood platelets increased the probability of thrombosis formation in the SJM type of mechanical valve.

Although using commercial software has helped researchers to obtain reliable results required for designing and evaluating the performance of bioprosthetic valves, better results were obtained by modifying the FE/FV coupling method by incorporating tailored codes. For example, researchers utilised an alternative technique to model a two-way FSI simulation of the aortic valve such as Arbitrary Lagrangian-Eulerian method in order to synchronise the

dynamic motion of the leaflets with the corresponding fluid force. Cheng et al. [122] used the above-mentioned method to simulate a quarter of the 3D model of the Medtronic mechanical valve. Their results showed that the possibility of thrombosis formation between the housing of the valve and the leaflet edge.

Tai et al. [123] developed a fully immersed object technique in order to model the interaction between the multiple domains of mechanical aortic valves. The fluidic forces were obtained directly from the momentum equations considering the initial values of the velocity distribution. This method was utilised by other researchers [124, 125] in which they reported that the flow shear moment had almost no impact on the dynamic behaviour of the aortic valve leaflets compared with the pressure difference moment which had a considerable effect on the leaflet dynamics.

Pelloccioni et al. [126] presented a novel modelling technique for 3D FSI modelling of a bi-leaflet mechanical aortic valve using General Lattice Boltzmann (LB) equations accompanied by the multi-relaxation module. The mesh generation based on the modified LB method was capable of capturing the dynamic behaviour of the leaflets during the systole phase. The jet velocity along the valve was calculated based on the numerical technique, with a good agreement between the flow pattern obtained through this study and experimental data captured from high-speed photography.

The comprehensive study carried out by Borazjani et al. [127] who modified the sharp-interface curvilinear method presented by Ge et al. [128] in order to simulate the large deformation of the bi-leaflet mechanical aortic valve. Both weak and strong coupling modules for FSI modelling of the aortic valve were implemented considering moving immersed structure and Lagrangian grids fluid domains. They reported that stability of the FSI simulation depends upon the material properties of the leaflets and physiological condition of the blood flow domain. Furthermore, they proposed a novel Aitken's acceleration method accompanied by a coupling technique to increase the stability of the FSI simulation. The results showed that the generation of high quality grids not only plays an important role in capturing the flow characteristics during the systole, but also has an impact on the structural domain dynamic stability. Later, another study conducted by the same group [127] in which they presented a more accurate image showing the distribution of the flow along the same valve considering the realistic shape of the sinuses. The MRI images of a healthy aortic valve were used to extract the realistic shape of the aortic root and sinuses. The dynamic response of the leaflets under the physiological flow conditions was analysed. Their results showed that the realistic model witnesses higher shear stress in the vicinity of the leaflets compared with those of the simplified sinus model.

Morbiducci et al. [129] developed a new FSI model accompanied by a Lagrangian technique to analyse the dynamic performance of an aortic valve in order to predict platelet activation. Their model showed that the probability of platelet activation at early systole is higher than that at late systole. Furthermore, further investigations showed that the possibility of thrombosis formation in a mechanical aortic valve is highly dependent on the magnitude and orientation of the velocity and vorticity vectors. Their finding demonstrated that the rate of platelet activation is more dependent on the spanwise vorticity magnitude (Rate > 0.94) rather than streamwise vorticity magnitude (Rate > 0.78).

Later, Simon et al. [130] developed a new micro scale silicon-based model of a prosthetic aortic valve extracted from tomography scan images. They utilised both fully coupled sharp Immersed Boundary and a second-order fractional-step technique to simulate the FSI model of the leaflets and their corresponding hinges. A fine mesh around the hinge was generated in order to obtain accurate results for the shear stress downstream of the leaflets and to capture the complex turbulent flow in the vicinity of the leaflets as well as the vortical structures during the systole and diastole. The findings of this study were used by the same group later [131] where they investigated the possibility of thrombosis formation for the same aortic valve model. The results showed that the formation of thrombosis is highly dependent on geometrical factors such as the shape of the leaflets, the orientation of the leaflets hinge, and the width of the leaflets gap.

De Hart et al. [132] used a fictitious domain method to develop a 2D model of an aortic valve considering flexible leaflets and rigid sinus walls. The materials of the leaflets were considered to be isotropic and incompressible. The dynamic motion of the leaflets was validated against experimental data considering various physiological boundary conditions. The proposed model was extended to a 3D model of the heart valve during diastole phases [133]. Their results showed that the flow pattern is disturbed around the tips of the leaflets at mid-diastole accompanied by maximum Cauchy stresses in the vicinity of the commissural attachments. Another study carried out by the same group [134, 135] examined the influence of the compliance of the aortic root on the stability of the bioprosthetic aortic valve. The stentless fibre-reinforced biprosthetic aortic valve was modelled during the cardiac cycle and the significance of the compliance of the aortic root was investigated. Their findings demonstrated that the presence of the compliance of the aortic root not only affects the opening and closing time of the aortic valve leaflets, but also significantly decreases stresses on the leaflets of the aortic valve.

Despite various studies carried out by de Hart using FSI simulation of the bioprosthetic and polymeric aortic valve, the validity of their simulation in terms of stress magnitude estimation and symmetrical flow behaviour along the valve are questionable. Since the 3D FE/FV model analysed only one-sixth of the entire valve, therefore assuming symmetrical modelling without considering the effect of contact stress in the vicinity of the leaflets was completely questioned. This assumption could influence the accuracy of the results especially in the early and late systole phases. Moreover, due to limitations related to the mesh updating technique, the number of elements used in the fluid domain were not sufficient to provide accurate results in some sensitive areas such as the recirculation zones inside sinuses as well as the shear stress near the walls [136].

Later, Loon et al. [136, 137] presented a new FSI technique to model the large deformation of aortic valve leaflets in which the fluid and structural parts were meshed independently. To consider the non-conformal fields at the contact area, a Lagrange multiplier was defined in which the stability of the system was controlled by taking advantage of adaptive meshing techniques. However, the mesh inside the contact area was not well defined in the modelling, and they assumed that the presence of the non-conformal mesh in either the fluid and structural domains could compensate for the complexity of the mesh inside this region.

Vierendeels et al. [138] developed a novel coupling algorithm in order to simulate an FSI model of flexible leaflets in which they utilised CFD code to solve the fluid domains accompanied with an in-house solver code for the structural part. The proposed simulation was

a 2D model of a single aortic valve leaflet inside the sinus cavity. The pressure difference was applied as a boundary condition in order to investigate the dynamic motion of the leaflets.

Nicosia et al. [139] developed a FE aortic valve model in which they introduced a new fully coupled FV/FE model of the aortic valve considering the aortic root. The realistic model of an aortic valve extracted from MRI images and the LS-Dyna software was used to model the dynamic behaviour of the leaflets considering the physiological pressure profile as boundary conditions in the model. The general motion of the aortic valve leaflets was compared with the motion of a natural valve. Furthermore, the vortical structure within the sinus cavity was compared with that available in the literature for validation purposes. Later, Einstein et al. [140] proposed a 3D dynamic model of a mitral valve based on a 3D membrane formulation technique. The model was validated against in-house experiment in which they used a left-ventricle heart simulator working under physiological blood flow conditions.

Ranga et al. [141] proposed an FSI numerical model of an aortic valve which was validated against in-vivo data. The total displacement of the leaflets and stress distributions (von Mises Stress) on the leaflets was calculated. Furthermore, the MRI data such as valve opening, closing, and ejection times were compared with those calculated through numerical simulation. Their findings showed that the lack of compliance in the modelling of the aortic root affects the measured stress values on the leaflets. Moreover, their results revealed that different geometry of the sinuses not only affects the dynamic motion of the leaflets during the systolic phase but also impacts the valve closure time. Generally, the results showed the vortical structures generated inside the sinuses affect the dynamic performance of the leaflets.

2.8.2 Sinus vortex structural modelling based on fluid structure interaction

The sinus vortex structure of the aortic valves can, in turn, affect hemodynamic parameters inside the aortic root. To investigate this, Morsi et al. [142] investigated the dynamical and hemodynamic performance of a polymeric aortic valve using a weak coupling FSI technique. The model was examined based on the ALE method in ANSYS software and considered various Reynolds numbers. Their results demonstrated that the dominant recirculation zone initiated downstream of the leaflets and developed towards the axis of symmetry of the leaflets during the systole phase. Wall shear stress (WSS) was measured on the leaflet and higher WSS reported in the vicinity of the tips of the leaflets.

Watton et al. [143] proposed a fully coupled FSI model of a bileaflet mechanical mitral valve based on the IB method. The proposed model was examined under four different non-physiological flow conditions in order to find the optimised design of the bioprosthetic mitral valve. The proposed FSI model captured the dynamic motion of the leaflets and flow patterns through the valve with some discrepancies compared to the reported experimental data. The errors were mostly due to the inaccurate modelling of the material properties of the leaflets as well as the quality of the mesh, especially in critical areas. Another study conducted by Watton et al. [144] in which a similar approach was used based on the Immersed Boundary method, but this time with more realistic boundary conditions (physiological flow). The results of this study were compared with in-vivo data showing less error due to using the physiological blood flow rate profile.

Later, Katayama et al. [145] developed an FSI model of a bioprosthetic aortic valve in which the effects of the presence (and lack of) the sinuses on the stress distribution on the leaflets were investigated. The physiological pressure waveform was considered at the inlet and outlet of the model as boundary conditions. Their results showed that the leaflets of the model incorporating sinuses experience lower bending stress values at the late diastole compared with that without sinuses.

Chandra et al. [146] presented new FSI models of bicuspid and tricuspid aortic valve (BAV and TAV) in order to compare the hemodynamic variations inside the aortic root in terms of the presence of the TAV and BAV. The study aimed to quantify the influence of the abnormalities of the aortic valve on the initiation of aortic valve pathologies such as calcific aortic valve (CAVD). The proposed FSI models of the bicuspid and tricuspid aortic valve were validated against experimental data using particle imaging velocimetry (PIV) techniques. The flow velocity field, the effective orifice area of the valve and the wall shear stress on the leaflets were compared with those measured in the experiment. Their results showed significant changes in hemodynamic parameters, especially the WSS on the leaflets corresponding to the BAV may result in a rapid progression of CAVD.

Another study carried out by the same group [147] on the wall shear stress distribution on different layers of the leaflets (i.e. fibrosa and ventricularis layers) for the BAV and TAV. They presented 2D FSI models of the normal TAV and abnormal BAV using a Lagrangian-Eulerian method. The performance analysis of the aortic valve was conducted by calculating the valve effective orifice area (EOA), oscillatory shear index (OSI) and temporal shear magnitude (TSM). Their results showed that the EOA corresponding to BAV reduces by 49 percent compared to that of the TAV. Furthermore, the results demonstrated that different segments of the leaflets (i.e. tip, belly, and base of the leaflets) experienced varying magnitudes of WSS (shown in Figure 2.5).

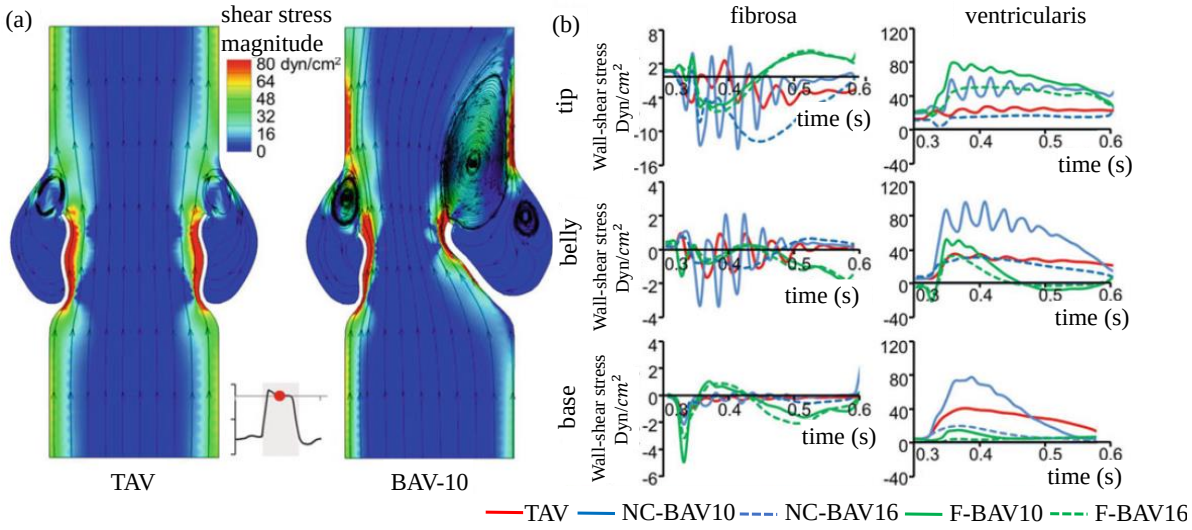

Figure 2.5 Shear stress distribution on aortic valve leaflets: (a) shear stress contour in the TAV and BAV10 at peak systolic phase, (b) variation of temporal shear stress in different segments of the leaflets (i.e. tip, belly, and base) for TAV, BAV10 and BAV16; NC and F refer to non-coronary and fused leaflets, respectively [147].

Later, Cao et al. [148] proposed a 3D FSI model of a tricuspid aortic valve in which the dynamic behaviour of the leaflets and valvular flow pattern were simulated based on an Arbitrary Langrangian-Eulerian approach. The performance evaluation of the tricuspid aortic valve was conducted by calculating and analysing temporal shear magnitude (TSM), oscillatory shear index (OSI), and temporal shear gradient (TSG). Their results revealed that the ventricularis side of the leaflets experienced a higher magnitude of WSS compared to the fibrosa side of the leaflets. Furthermore, the WSS in different areas of the leaflets (i.e. base, belly, and tips) were calculated and compared. Based on their results, the average wall shear stress (AWSS) on the belly segments of the leaflet was the highest compared to the other areas. This study provided a new insight in the 3D modelling of the dynamical motion of the aortic valve leaflets, however the presence of the coronary arteries were completely neglected.

A similar study was conducted by Cao et al. [16, 149] in which a 3D model of an ascending aorta was simulated based on FSI methodology. The influences of the aortic dilation, abnormality of the aortic valve, and fusion in the bicuspid aortic valve on the hemodynamic parameters within the ascending aorta and at a particular segment were investigated. The flow pattern inside the ascending aorta was compared considering the presence of either a tricuspid aortic valve or a bicuspid aortic valve with different fusion morphologies such as left-right coronary cusp fusion, right-non coronary cusp fusion and non-left coronary cusp fusion. Their results emphasised that the presence of an abnormal valve condition generates velocity and WSS abnormalities (shown in Figure 2.6) within the ascending aorta which result in arterial dilation. Another study carried out by the same group [150] in which the transvalvular pressure gradient corresponding to tricuspid and bicuspid aortic valves with different morphologies, were calculated and compared based on ALE/FSI simulation.

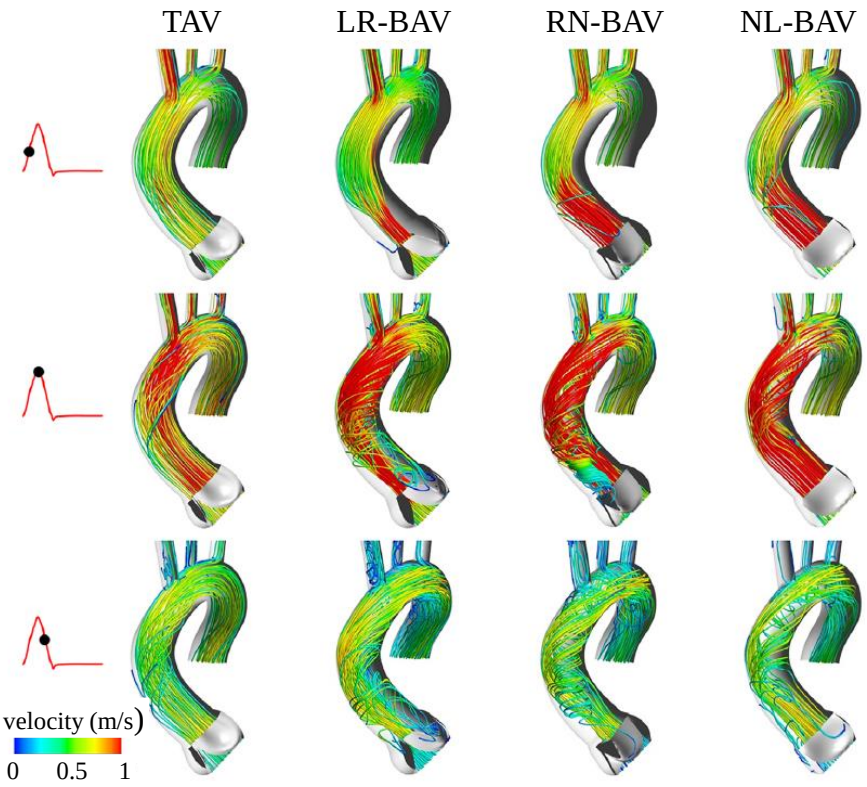

Figure 2.6 Velocity streamlines inside the ascending aorta during cardiac cycle considering different types of the aortic valve: tricuspid aortic valve, bicuspid aortic valve with left-right coronary cusp fusion (LR-BAV), right-non coronary cusp fusion (RN-BAV), and non-left coronary cusp fusion (NL-BAV) [16, 149].

Amindari et al. [15] developed 2D models of a healthy and a calcified aortic valve based on FSI simulation using ASNYS software. They investigated the influence of the calcification of the aortic valve on the hemodynamic parameters inside the aortic root in the absence of coronary arteries. The WSS on different sides of the leaflets (fibrosa and ventricularis sides) were calculated and validated against in-vivo data. Their findings show that calcification significantly affects the TPG through the aortic valve as well as the WSS on the leaflets. Their finding elucidated that the difference between the WSS of the different sides of the leaflets may contribute to the initiation of CAVD.

Tango et al. [151] developed a 3D FSI model of a healthy bioprosthetic aortic valve in order to better understand the bioprosthetic valve function during opening and closing times, and the sinus vortex structures. The model was qualitatively and quantitatively validated against PIV experimental data. Their findings mainly emphasised that the proposed FSI modelling plays an important role in the prediction of pathologies corresponding to the aortic valve. The main limitation of the proposed model was the lack of coronary artery ostia in their FSI simulation. The presence of the coronary artery ostia in the modelling is very crucial because it not only changes the flow pattern inside the sinus cavity and accordingly affects the hemodynamics of the coronary artery and aortic root, but also increases the instability of the FSI simulation and make it challenging to be modelled.

Despite significant achievements and development in the design and analysis of aortic valves based on the FSI technique, to the best of the authors knowledge, the FSI simulation of aortic valves considering the effect of the presence of the coronary arteries still has not been completely analysed. The influence of calcification on the hemodynamic parameters within the aortic root, as well as the coronary artery flow pattern and hemodynamics, still remain unknown. Furthermore, based on clinical data, the location of the coronary artery ostia varies in different patients. Therefore, it is hypothesised that the locations of the coronary artery ostia may affect the hemodynamic parameters of the aortic valve and result in initiation and progression of the CAVD.

2.9 Concluding remarks

This chapter provides a comprehensive overview of the common modelling techniques used in numerical simulation of the aortic valve and its corresponding pathologies such as aortic valve stenosis, congenital abnormalities (i.e. bicuspid aortic valve and cusp fusions), dilation of the aorta, and coarctation of the ascending aorta. It was determined that the presence of the coronary artery ostia inside the sinus cavity not only affects the hemodynamic parameters within the aortic root and vortical structures inside the sinus cavity but also changes the hemodynamic parameters inside the coronary arteries which leads to the initiation and progression of coronary artery diseases. Furthermore, based on clinical data, the location of the coronary artery ostia inside the sinus cavity affects the sinus vortex structures and the wall shear stress on the aortic valve leaflets which result in the initiation and progression of calcific aortic valve diseases. Hence, in light of the literature review, the primary objectives of this research are defined as follows:

- To develop a numerical two-dimensional simplified model of the aortic valve in order to understand the effects of calcification of the aortic valve leaflets (stiffening of the aortic valve leaflets) on flow behaviour inside the sinus cavity, sinus vortex structures, hemodynamic variation within the aortic root as well as coronary arteries.
- To investigate the importance of the location of the coronary artery ostia on the flow patterns and vortical structures inside the sinus cavity as well as the hemodynamic variation within the coronary arteries such as the wall shear stress on the walls of the coronary arteries. The proposed model can be used to predict the TPG for different aortic valve models in terms of the positions of the coronary artery ostia.
- To investigate the effects of coronary artery stenosis on sinus vortex structures and hemodynamics, as well as the wall shear stress variation on the aortic valve leaflets. The model can be used to predict the variations of the wall shear stress on the leaflets and its correlation with CAVD.
- To develop a numerical model validated against in-vitro in-house experiments in order to predict the probability of the wall shear stress distribution on the leaflets for different valve types. The model can be used to find the relationship between the wall shear stress on the leaflet and the possibility of CAVD.

2.10 References

[1] P.D. Sciscio, J. Brubert, M.D. Sciscio, Aortic stenosis in Australia: disease prevalence and patient eligibility for aortic valve replacement, Heart, Lung and Circulation, 24 (2015) 409-419.

[2] P. Pibarot, J.G. Dumesnil, New concepts in valvular hemodynamics: Implications for diagnosis and treatment of aortic stenosis, The Canadian Journal of Cardiology, 23 (2007) 40-47.
[3] D. Garcia, P.G. Camici, L.-G. Durand, K. Rajappan, E. Gaillard, O.E. Rimoldi, P. Pibarot, Impairment of coronary flow reserve in aortic stenosis, Journal of Applied Physiology, 106 (2009) 113-121.
[4] J.-M. Paradis, J. Fried, T. Nazif, A. Kirtane, K. Harjai, O. Khalique, K. Grubb, I. George, R. Hahn, M. Williams, M.B. Leon, S. Kodali, Aortic stenosis and coronary artery disease, European Heart Journal, 35 (2014) 2069-2082.
[5] D. A. Towler, Molecular and cellular aspects of calcific aortic valve disease, Circulation Research, 113 (2013) 198-208.
[6] J. Lincoln, V. Garg, Etiology of valvular heart disease, Circulation, 78 (2014) 1801-1807.
[7] B. Moore, L.P. Dasi, Spatiotemporal complexity of the aortic sinus vortex, Experiments in Fluids, 55 (2014) 1770-1780.
[8] J.T. Butcher, A.M. Penrod, A.J. Garcia, R.M. Nerem, Unique morphology and focal adhesion development of valvular endothelial cells in static and fluid flow environments, Arteriosclerosis, Thrombosis, and Vascular Biology, 24 (2004) 1429-1434.
[9] D. Hoehn, L. Sun, P. Sucosky, Role of pathologic shear stress alterations in aortic valve endothelial activation, Cardiovascular Engineering and Technology, 1 (2010) 165-178.
[10] P. Sucosky, K. Balachandran, A. Elhammali, H. Jo, A.P. Yoganathan, Altered shear stress stimulates upregulation of endothelial VCAM-1 and ICAM-1 in a BMP-4- and TGF-β1-dependent pathway, Arteriosclerosis, Thrombosis, and Vascular Biology, 29 (2009) 254-260.
[11] L. Sun, N.M. Rajamannan, P. Sucosky, Defining the role of fluid shear stress in the expression of early signaling markers for calcific aortic valve disease, PLoS One, 8 (2013) 844-853.
[12] H. Mohammadi, R. Cartier, R. Mongrain, 3D physiological model of the aortic valve incorporating small coronary arteries, International Journal for Numerical Methods in Biomedical Engineering, 33 (2016) 2829-2834.
[13] S. Nobari, R. Mongrain, R. Leask, R. Cartier, The effect of aortic wall and aortic leaflet stiffening on coronary hemodynamic: a fluid–structure interaction study, Medical & Biological Engineering & Computing, 51 (2013) 923-936.
[14] S. Nobari, R Mongrain, R Leask, R Cartier, The Effect of Aortic Wall and Aortic Leaflet Stiffening on Coronary Hemodynamic: A Fluid-Structure Interaction Study, Medical & Biological Engineering & Computing, 51 (2013) 923-936.
[15] A. Amindari, L. Saltik, K. Kirkkopru, M. Yacoub, H.C. Yalcin, Assessment of calcified aortic valve leaflet deformations and blood flow dynamics using fluid-structure interaction modeling, Informatics in Medicine Unlocked, 9 (2017) 191-199.
[16] K. Cao, P. Sucosky, Aortic valve leaflet wall shear stress characterization revisited: impact of coronary flow, Computer Methods in Biomechanics and Biomedical Engineering, 20 (2017) 468-470.
[17] H. Hatoum, L.P. Dasi, Spatiotemporal complexity of the aortic sinus vortex as a function of leaflet calcification, Annals of Biomedical Engineering, 47 (2019) 1116-1128.
[18] P. Kaul, K. Javangula, Single left coronary artery with separate origins of proximal and distal right coronary arteries from left anterior descending and circumflex arteries – a previously undescribed coronary circulation, Journal of Cardiothoracic Surgery, 2 (2007) 18-25.
[19] B.F. Waller, C.M. Orr, J.D. Slack, C.A. Pinkerton, J.V. Tassel, T. Peters, Anatomy, histology, and pathology of coronary arteries: a review relevant to new interventional and imaging techniques, Clinical Cardiology, 15 (1992) 451-457.

[20] K. Barszcz, M. Kupczyńska, M. Polguj, J. Klećkowska-Nawrot, M. Janeczek, K. Goździewska-Harłajczuk, M. Dzierzęcka, P. Janczyk, Morphometry of the coronary ostia and the structure of coronary arteries in the shorthair domestic cat, PLoS One, 12 (2017) 177-186.
[21] E. Prifti, F. Ademaj, K. Krakulli, E. Rruci, M. Zeka, A. Demiraj, A rare coronary anomaly consisting of a single right coronary ostium in an adult undergoing surgical coronary revascularization: a case report and review of the literature, Journal of Medical Case Reports, 10 (2016) 180-192.
[22] C.H. Brown, L.B. Leverett, C.W. Lewis, C.P. Alfrey, J.D. Hellums, Morphological, biochemical, and functional changes in human platelets subjected to shear stress, Journal of Laboratory and Clinical Medicine 86 (1975) 462-471.
[23] A.P. Yoganathan, H.H. Reamer, W.H. Corcoran, E.C. Harrison, I.A. Shulman, W. Parnassus, The Starr-Edwards aortic ball valve: Flow characteristics, thrombus formation, and tissue overgrowth, Artificial Organs, 5 (1981) 6-17.
[24] A.P. Yoganathan, A. Chaux, R.J. Gray, M.D. Robertis, J.M. Matloff, Flow characteristics of the st. jude prosthetic valve: An in vitro and in vivo study, Artificial Organs, 6 (1982) 288-294.
[25] Y.R. Woo, F.P. Williams, A.P. Yoganathan, In-vitro fluid dynamic characteristics of the abiomed trileaflet heart valve prosthesis, Journal of Biomechanical Engineering, 105 (1983) 338-345.
[26] Y.R. Woo, A.P. Yoganathan, Pulsatile flow velocity and shear stress measurements on the St. Jude bileaflet valve prosthesis, Scandinavian Journal of Thoracic and Cardiovascular Surgery, 20 (1986) 15-28.
[27] K.B. Chandran, G.N. Cabell, B. Khalighi, C.J. Chen, Laser anemometry measurements of pulsatile flow past aortic valve prostheses, Journal of Biomechanics, 16 (1983) 865-873.
[28] K.B. Chandran, S. Aluri, Mechanical valve closing dynamics: Relationship between velocity of closing, pressure transients, and cavitation initiation, Annals of Biomedical Engineering, 25 (1996) 926-938.
[29] K.B. Chandran, C.S. Lee, Pressure distribution near the occluders and impact forces on the outlet struts of Shiley convexo-concave valves during closing, Journal of Heart Valve Disease, 5 (1996) 199-206.
[30] K.B. Chandran, E.U. Dexter, S. Aluri, W.E. Richenbacher, Negative pressure transients with mechanical heart-valve closure: correlation between in vitro and in vivo results, Annals of Biomedical Engineering, 26 (1998) 546-556.
[31] D.D. Hanle, E.C. Harrison, A.P. Yoganathan, W.H. Corcoran, In vitro velocity measurements down stream from the lonescu-Shiley aortic bioprosthesis in steady and pulsatile flow, Medical and Biological Engineering and Computing, 24 (1986) 449-459.
[32] D.D. Hanle, E.C. Harrison, A.P. Yoganathan, W.H. Corcoran, Turbulence downstream from the Ionescu-Shiley bioprosthesis in steady and pulsatile flow, Medical & Biological Engineering & Computing, 25 (1987) 645-649.
[33] A.P. Yoganathan, Y.R. Woo, H.W. Sung, F.P. Williams, R.H. Franch, M. Jones, In vitro hemodynamic characteristics of tissue bioprostheses in the aortic position, The Journal of Thoracic and Cardiovascular Surgery, 92 (1986) 198-209.
[34] P. Fan, N.C. Nanda, J.W. Cooper, E. Cape, A. Yoganathan, Color Doppler assessment of high flow velocities using a new technology: In vitro and clinical studies, Echocardiography, 7 (1990) 763-769.
[35] E.G. Cape, R. Monheit, H.W. Sung, S.H. Winoto, A.E. Weyman, R.A. Levine, A.P. Yoganathan, The effect of receiving chamber environment on the visualization of cardiac jets by color Doppler flow mapping, Proceedings of the First Conference on Visualization in Biomedical Computing, IEEE (1990) 179-184.

[36] E.G. Cape, A.P. Yoganathan, A.E. Weyman, R. A.Levine, Adjacent solid boundaries alter the size of regurgitant jets on Doppler color flow maps, Journal of the American College of Cardiology, 17 (1991) 1094-1102.
[37] F. Recusani, G.S. Bargiggia, A.P. Yoganathan, A. Raisaro, L.M.V. Cruz, H.W. Sung, C. Bertucci, M. Gallati, V.A. Moises, A. Simpson, A new method for quantification of regurgitant flow rate using color Doppler flow imaging of the flow convergence region proximal to a discrete orifice. An in vitro study.", Circulation, 83 (1991) 594-604.
[38] J.T. Baldwin, J.M. Tarbell, S. Deutsch, D.B. Geselowitz, Mean velocities and Reynolds stresses within regurgitant jets produced by tilting disc valves, ASAIO Transactions, 37 (1991) 60-75.
[39] V. Kini, C. Bachmann, A. Fontaine, S. Deutsch, J.M. Tarbell, Integrating particle image velocimetry and laser Doppler velocimetry measurements of the regurgitant flow field past mechanical heart valves, Artificial Organs, 25 (2001) 136-145.
[40] K.B. Manning, V. Kini, A.A. Fontaine, S. Deutsch, J.M. Tarbell, Regurgitant flow field characteristics of the St. Jude bileaflet mechanical heart valve under physiologic pulsatile flow using particle image velocimetry, Artificial Organs, 27 (2003) 840-846.
[41] J.T. Ellis, T.M. Healy, A.A. Fontain, R. Saxena, A.P. Yoganathan, Velocity measurements and flow patterns within the hinge region of a Medtronic Parallel(TM) bileaflet mechanical valve with clear housing, Journal of Heart Valve Disease, 5 (1996) 591-599.
[42] H.L. Leo, Z. He, J.T. Ellis, A.P. Yoganathan, Microflow fields in the hinge region of the CarboMedics bileaflet mechanical heart valve design, Journal of Thoracic and Cardiovascular Surgery, 124 (2002) 561-574.
[43] Y.S. Morsi, A. Sakhaeimanesh, B.R. Clayton, Measurements of steady flow velocity and turbulent stress downstream from jellyfish and St. Vincent aortic heart valves, Artificial Organs, 2 (1999) 176-183.
[44] Y.S. Morsi, M. Kogure, M. Umezu, In vitro laser Doppler anemometry of pulsatile flow velocity and shear stress measurements downstream from a jellyfish valve in the mitral position of a ventricular assist device, Journal of Artificial Organs, 2 (1999) 62-73.
[45] A.A. Sakhaeimanesh, Y.S. Morsi, Analysis of regurgitation, mean systolic pressure drop and energy losses for two artificial aortic valves, Journal of Medical Engineering and Technology, 23 (1999) 63-68.
[46] Y.S. Morsi, A.A. Sakhaeimanesh, Flow characteristics past Jellyfish and St. Vincent valves in the aortic position under physiological pulsatile flow conditions, Artificial Organs, 24 (2000) 564-574.
[47] Y. Morsi, M. Kogru, M. Umezu, Relative blood damage index of the jellyfish valve and the Bjork-Shiley tilting-disk valve, Journal of Artificial Organs, 2 (1999) 163-169.
[48] Y.S. Morsi, A. Sakhaeimanesh, B.R. Clayton, Hydrodynamic evaluation of three artificial aortic valve chambers, Artificial Organs, 24 (2000) 57-63.
[49] K.B. Manning, L.H. Herbertson, A.A. Fontaine, S. Deutsch, A detailed fluid mechanics study of tilting disk mechanical heart valve closure and the implications to blood damage, Journal of Biomechanical Engineering, 130 (2008) 141-146.
[50] D.W. Murphy, L.P. Dasi, J. Vukasinovic, A. Glezer, A.P. Yoganathan, Reduction of procoagulant potential of b-datum leakage jet flow in bileaflet mechanical heart valves via application of vortex generator arrays, Journal of Biomechanical Engineering, 132 (2010) 150-168.
[51] L.P. Dasi, H.A. Simon, P. Sucosky, A.P. Yoganathan, Fluid mechanics of artificial heart valves, Clinical and Experimental Pharmacology and Physiology, 36 (2009) 225-237.
[52] B. Travis, T. Christensen, M. Smerup, M.S. Olsen, J.M. Hasenkam, H. Nyhaard, An in vivo method for measuring turbulence in mechanical prosthesis leakage jets, Journal of Biomechanical Engineering, 126 (2004) 26-35.

[53] R.S. Arias, I.P. Uribe, F. Carreras, S. Pujadas, R. Leta, G. Pons-Llado, Misleading echocardiographic diagnosis of a posthetic heart valve vegetation due to the cavitation phenomenon, Experimental and Clinical Cardiology, 14 (2009) 53-55.
[54] S. Kutty, K.K. Whitehead, S. Natarajan, M.A. Harris, G. Wernovsky, M.A. Fogel, Qualitative echocardiographic assessment of aortic valve regurgitation with quantitative cardiac magnetic resonance: a comparative study, Pediatric cardiology, 30 (2009) 971-977.
[55] H.L. Leo, L.P. Dasi, J. Carberry, H.A. Simon, A.P. Yoganathan, Fluid dynamic assessment of three polymeric heart valves using particle image velocimetry, Annals of Biomedical Engineering, 34 (2006) 936-952.
[56] L. Ge, L.P. Dasi, F. Sotiropoulos, A.P. Yoganathan, Characterization of hemodynamic forces induced by mechanical heart valves: reynolds vs. viscous stresses, Annals of Biomedical Engineering, 36 (2008) 276-297.
[57] C.H. Yap, L.P. Dasi, A.P. Yoganathan, Dynamic hemodynamic energy loss in normal and stenosed aortic valves.", Journal of Biomechanical Engineering, 132 (2010) 150-166.
[58] M. Forleo, L.P. Dasi, Effect of hypertension on the closing dynamics and lagrangian blood damage index measure of the B-Datum Regurgitant Jet in a bileaflet mechanical heart valve, Annals of biomedical engineering, 42 (2014) 110-122.
[59] B. Moore, L.P. Dasi, Coronary flow impacts aortic leaflet mechanics and aortic sinus hemodynamics, Annals of Biomedical Engineering, 43 (2015) 2231-2241.
[60] A. Yousefi, D.L. Bark, L.P. Dasi, Effect of arched leaflets and stent profile on the hemodynamics of tri-leaflet flexible polymeric heart valves, Annals of Biomedical Engineering, 45 (2017) 464-475.
[61] H. Hatoum, B.L. Moore, P. Maureira, J. Dollery, J.A. Crestanello, L.P. Dasi, Aortic sinus flow stasis likely in valve-in-valve transcatheter aortic valve implantation, The Journal of Thoracic and Cardiovascular Surgery, 154 (2017) 32-43.
[62] H. Hatoum, J. Dollery, S.M. Lilly, J.A. Crestanello, L.P. Dasi, Implantation depth and rotational orientation effect on valve-in-valve hemodynamics and sinus flow, The Annals of Thoracic Surgery, 106 (2018) 70-78.
[63] H. Hatoum, L.P. Dasi, Sinus hemodynamics in representative stenotic native bicuspid and tricuspid aortic valves: an in-vitro study, Fluids, 3 (2018) 56-65.
[64] H. Hatoum, S. Lilly, P. Maureira, J. Crestanello, L.P. Dasi, Sinus hemodynamics after transcatheter aortic valve in transcatheter aortic valve, The Annals of Thoracic Surgery, 110 (2020) 1348-1356.
[65] X. Huang, M.M. Black, I.C. Howard, E.A. Patterson, two-dimensional finite element analysis of a bioprosthetic heart valve, Journal of Biomechanics, 23 (1990) 753-762.
[66] M.M. Black, I.C. Howard, X. Huang, E.A. Patterson, A three-dimensional analysis of a bioprosthetic heart valve, Journal of Biomechanics, 24 (1991) 793-801.
[67] K.B. Chandran, S.H. Kim, G. Han, Stress distribution on the cusps of a polyurethane trileaflet heart valve prosthesis in the closed position, Journal of Biomechanics, 24 (1991) 385-395.
[68] S. Krucinski, I. Vesely, M.A. Dokainish, G. Campbell, Numerical simulation of leaflet flexure in bioprosthetic valves mounted on rigid and expansile stents, Journal of Biomechanics, 26 (1993) 929-943.
[69] E.A. Patterson, I.C. Howard, M.A. Thornton, A comparative study of linear and nonlinear simulations of the leaflets in a bioprosthetic heart valve during the cardiac cycle, Journal of Medical Engineering and Technology, 20 (1996) 95-108.
[70] M.A. Thornton, I.C. Howard, E.A. Patterson, Three-dimensional stress analysis of polypropylene leaflets for prosthetic heart valves, Medical Engineering and Physics, 19 (1997) 588-597.
[71] J.D. Hart, G. Cacciola, P.J. Schreurs, G.W. Peters, A three-dimensional analysis of a fibre-reinforced aortic valve prosthesis, Journal of Biomechanics, 31 (1998) 629-638.

[72] G.R. Cacciola, G.W.M. Peters, P.J.G. Schreurs, J.D. Janssen, Development of a reinforced polymer heart valve prosthesis, American Society of Mechanical Engineers, (1997) 435-436.
[73] G. Cacciola, G.W.M. Peters, P.J.G. Schreurs, A three-dimensional mechanical analysis of a stentless fibre-reinforced aortic valve prosthesis, Journal of Biomechanics, 33 (2000) 521-530.
[74] K.J. Grande-Allen, R.P. Cochran, P.G. Reinhall, K.S. Kunzelman, Finite-element analysis of aortic valve-sparing: Influence of graft shape and stiffness, IEEE Transactions on Biomedical Engineering, 48 (2001) 647-659.
[75] X.Y. Luo, W.G. Li, J. Li, Geometrical stress-reducing factors in the anisotropic porcine heart valves, Journal of Biomechanical Engineering, 125 (2003) 735-744.
[76] I.C. Howard, E.A. Patterson, A. Yoxall, On the opening mechanism of the aortic valve: Some observations from simulations, Journal of Medical Engineering & Technology, 27 (2003) 259-266.
[77] C.J. Carmody, G. Baurriesci, I.C. Howard, E.A. Patterson, An approach to the simulation of fluid-structure interaction in the aortic valve, Journal of Biomechanics, 39 (2006) 158-169.
[78] G. Arcindiacono, A. Corvi, T. Severi, Functional analysis of bioprosthetic heart valves, Journal of Biomechanics, 38 (2005) 1483-1490.
[79] W. Sun, A. Abad, M.S. Sacks, Simulated bioprosthetic heart valve deformation under quasi-static loading, Journal of Biomechanical Engineering, 127 (2005) 905-914.
[80] H. Kim, K.B. Chandran, M.S. Sacks, J. Lu, An experimentally derived stress resultant shell model for heart valve dynamic simulations, Annals of Biomedical Engineering, 35 (2007) 30-44.
[81] R. Haj-Ali, L.P. Dasi, H.S. Kim, J. Choi, H.W. Leo, A.P. Yoganathan, Structural simulations of prosthetic tri-leaflet aortic heart valves, Journal of Biomechanics, 41 (2008) 1510-1519.
[82] F.L. Xiong, W.A. Goetz, C.K. Chong, Y.L. Chua, S. Pfeifer, E. Wintermantel, J.H. Yeo, Finite element investigation of stentless pericardial aortic valves: Relevance of leaflet geometry, Annals of Biomedical Engineering, 38 (2010) 1908-1918.
[83] G. Burriesci, F.C. Marincola, C. Zervides, Design of a novel polymeric heart valve, Journal of Medical Engineering and Technology, 34 (2010) 7-22.
[84] M.R. Labrosse, M. Boodhwani, B. Sohmer, C.J. Beller, Modeling leaflet correction techniques in aortic valve repair: a finite element study, Journal of Biomechanics, 44 (2011) 2292-2298.
[85] A. Gilmanov, H. Stolarski, F. Sotiropoulos, Non-linear rotation-freeshell finite-element models for aortic heart valves, Journal of Biomechanics, 50 (2017) 56-62.
[86] M. Abbasi, M.S. Barakat, K. Vahidkhah, A.N. Azadani, Characterization of three-dimensional anisotropic heart valve tissue mechanical properties using inverse finite element analysis, Journal of the Mechanical Beahviour of Biomedical Materials, 62 (2016) 33-44.
[87] C.S. Peskin, Flow patterns around heart valves: A numerical method, Journal of Computational Physics, 10 (1972) 252-271.
[88] D.M. McQueen, C.S. Peskin, Computational studies of blood flow in the heart in two and three dimensions, Bioengineering, Proceedings of the Northeast Conference, IEEE (1991) 77-78.
[89] H. Greenfiled, A. Au, Computer visualization of flow patterns for prosthetic heart valves, Scandinavian Journal of Thoracic and Cardiovascular Surgery, 10 (1976) 197-204.
[90] K. Thalassoudis, J. Mazmudar, B.J. Noye, I.H. Craig, Numerical study of turbulent blood flow through a caged-ball prosthetic heart valve using a boundary-fitted co-ordinate system, Medical and Biological Engineering and Computing, 25 (1987) 173-180.
[91] S.E. Borgersen, A. Hajiloo, Simulation of flow characteristics through heart valves using 3-dimensional computational fluid dynamics, American Society of Mechanical Engineers, 80-82 (1994).

[92] E.B. Shim, K.S. Chang, Numerical analysis of three-dimensional Bjork-Shiley valvular flow in an aorta, Journal of Biomechanical Engineering, 119 (1997) 45-51.
[93] E.B. Shim, K.S. Chang, Three-dimensional vortex flow past a tilting-disc valve using a segregated finite element scheme, Computational Fluid Dynamics journal, 3 (1994) 200-205.
[94] M.J. King, J. Corden, T. David, J. Fisher, A three-dimensional, time-dependent analysis of flow through a bileaflet mechanical heart valve: Comparison of experimental and numerical results, Journal of Biomechanics, 29 (1996) 609-618.
[95] J.F. Gardner, T.A. Waniewski, Newton-Euler model of prosthetic heart valve dynamics, American Society of Mechanical Engineers, (1995) 265-366.
[96] Z. Keshavarz-Motamed, L. Kadem, 3D pulsatile flow in a curved tube with coexisting model of aortic stenosis and coarctation of the aorta, Medical Engineering & Physics, 33 (2011) 315-324.
[97] Z. Keshavarz-Motamed, J. Garcia, P. Pibarot, E. Larose, L. Kadem, Modeling the impact of concomitant aortic stenosis and coarctation of the aorta on left ventricular workload, Journal of Biomechanics, 44 (2011) 2817-2825.
[98] Z.K. Motamed, J. Garcia, N. Maftoon, E. Bedard, P. Chetaille, L. Kadem, A new approach for the evaluation of the severity of coarctation of the aorta using Doppler velocity index and effective orifice area: In vitro validation and clinical implications, Journal of Biomechanics, 45 (2012) 1239-1245.
[99] Z. Keshavarz-Motamed, J. Garcia, E. Gaillard, R. Capoulade, F.L. Ven, G. Cloutier, L. Kadem, P. Pibarot, Non-invasive determination of left ventricular workload in patients with aortic stenosis using magnetic resonance imaging and Doppler echocardiography, PLoS One, 9 (2014) 867-893.
[100] Z.K. Motamed, J. Garcia, L. Kadem, Fluid dynamics of coarctation of the aorta and effect of bicuspid aortic valve, PLoS One, 8 (2013) 723-734.
[101] A. Djbbari, W. Mawad, N. Dahdah, E. Benevento, Z. Keshavarz-Motamed, L. Kadem, Contribution of aortic regurgitation to left ventricle load in patients with aortic stenosis: A mathematical model analysis, Canadian Journal of Cardiology, 30 (2014) 105-111.
[102] Z. Keshavarz-Motamed, P.K. Motamed, N. Maftoon, Non-invasive determination of transcatheter pressure gradient in stenotic aortic valves: An analytical model, Medical Engineering & Physics, 37 (2015) 321-327.
[103] Z. Keshavarz-Motamed, S.J. Lee, E. Edelman, Quantification and systematic differentiation of impact of paravalvular leeakage following transcatheter aortic valve replacement, Journal of the American College of Cardiology, 67 (2016) 2212-2214.
[104] A.P. Yoganathan, K.B. Chandran, F. Sotiropoulos, Flow in prosthetic heart valves: State-of-the-art and future directions, Annals of Biomedical Engineering, 33 (2005) 1689-1694.
[105] V. Campen, A.M. Horsten, Modelling the fluid dynamics of a moving aortic disc-value, Annals of Biomedical Engineering, 19 (1991) 581-589.
[106] M. Krafczyk, M. Cerrolaza, M. Schulz, E. Rank, Analysis of 3D transient blood flow passing through an artificial aortic valve by Lattice–Boltzmann methods, Journal of Biomechanics, 31 (1998) 453-462.
[107] R. Cheng, Y.G. Lai, K.B. Chandran, Two-dimensional fluid-structure interaction simulation of bileaflet mechanical heart valve flow dynamics, Journal of Heart Valve Disease, 12 (2003) 772-780.
[108] J.M.A. Stijen, J.D. Hart, P.H.M. Bovendeerd, F.V.D. Vosse, Evaluation of a fictitious domain method for predicting dynamic response of mechanical heart valves, Journal of Fluids and Structures, 19 (2004) 835-850.
[109] S. Krishnan, H.S. Udaykumar, J.S. Marshall, K.B. Chandran, Two-dimensional dynamic simulation of platelet activation during mechanical heart valve closure, Annals of Biomedical Engineering, 34 (2006) 1519-1534.

[110] V. Govindarajan, H.S. Udaykumar, K.B. Chandran, Two-dimensional simulation of flow and platelet dynamics in the hinge region of a mechanical heart valve, Journal of Biomechanical Engineering, 131 (2009) 31-38.
[111] C. Guivier, V. Deplano, P. Pibarot, New insights into the assessment of the prosthetic valve performance in the presence of subaortic stenosis through a fluid-structure interaction model, Journal of Biomechanics, 40 (2007) 2283-2290.
[112] Y. Cheng, H. Zhang, Immersed boundary method and lattice Boltzmann method coupled FSI simulation of mitral leaflet flow, Computers and Fluids, 39 (2010) 871-881.
[113] C.R. Choi, C.N. Kim, Analysis of blood flow interacted with leaflets in MHV in view of fluid-structure interaction, KSME International Journal, 15 (2001) 613-622.
[114] C.R. Choi, C.N. Kim, Numerical analysis on the hemodynamics and leaflet dynamics in a bileaflet mechanical heart valve using a fluid-structure interaction method, ASAIO Journal, 55 (2009) 428-437.
[115] C.R. Choi, C.N. Kim, M.J. Choi, Characteristics of transient blood flow in MHVs with different maximum opening angles using Fluid-Structure Interaction method, Korean Journal of Chemical Engineering, 18 (2001) 809-815.
[116] C.R. Choi, C.N. Kim, Y.J. Kwon, J.W. Lee, Pulsatile blood flows through a bileaflet mechanical heart valve with different approach methods of numerical analysis; Pulsatile flows with fixed leaflets and interacted with moving leaflets, KSME International Journal, 17 (2003) 1073-1082.
[117] K. Dumont, J.M.A. Stijnen, J. Vierendeels, F.N.V.D. Vosse, P.R. Verdonck, Validation of a fluid-structure interaction model of a heart valve using the dynamic mesh method in fluent, Computer Methods in Biomechanics and Biomedical Engineering, 7 (2004) 139-146.
[118] A. Redaelli, H. Bothorel, E. Votta, M. Soncini, 3-D simulation of the St. Jude Medical bileaflet valve opening process: fluid-structure interaction study and experimental validation, The Journal of Heart Valve Disease, 13 (2004) 804-813.
[119] M. Nobili, G. Passoni, A. Redaelli, Two fluid-structure approaches for 3D simulation of St. Jude Medical bileaflet valve opening, Journal of Applied Biomaterials and Biomechanics, 5 (2007) 49-59.
[120] M. Nobili, U. Morbiducci, R. Ponzini, C.D. Gaudio, A. Balducci, M. Grigioni, F.M. Montevencchi, A. Redaelli, Numerical simulation of the dynamics of a bileaflet prosthetic heart valve using a fluid-structure interaction approach, Journal of Biomechanics, 41 (2008) 2539-2550.
[121] K. Dumont, J. Vierendeeld, R. Kaminsky, G.V. Nooten, P. Verdonck, D. Bluestein, Comparison of the hemodynamic and thrombogenic performance of two bileaflet mechanical heart valves using a CFD/FSI model, Journal of Biomechanical Engineering, 129 (2007) 558-565.
[122] R. Cheng, Y.G. Lai, K.B. Chandran, Three-dimensional fluid-structure interaction simulation of bileaflet mechanical heart valve flow dynamics, Annals of Biomedical Engineering, 32 (2004) 1471-1483.
[123] C.H. Tai, K.M. Liew, Y. Zhao, Numerical simulation of 3D fluid-structure interaction flow using an immersed object method with overlapping grids, Computers and Structures, 85 (2007) 749-762.
[124] G.H. Xia, M.Y. Zhao, J.H. Yeo, Numerical simulation of 3D fluid-structure interaction using an immersed membrane method, Modern Physics Letters B, 19 (2005) 1447-1450.
[125] G.H. Xia, Y. Zhao, J.H. Yeo, Parallel unstructured multigrid simulation of 3D unsteady flows and fluid–structure interaction in mechanical heart valve using immersed membrane method, Computers & Fluids, 38 (2009) 71-79.
[126] O. Pelliccioni, M. Cerrolaza, R. Suros, A biofluid dynamic computer code using the general lattice Boltzmann equation, Advances in Engineering Software, 39 (2008) 593-611.

[127] I. Borazjani, L. Ge, F. Sotiropoulos, Curvilinear immersed boundary method for simulating fluid structure interaction with complex 3D rigid bodies, Journal of Computational Physics, 227 (2008) 7587-7620.
[128] L. Ge, F. Sotiropoulos, A numerical method for solving the 3D unsteady incompressible Navier-Stokes equations in curvilinear domains with complex immersed boundaries, Journal of Computational Physics, 225 (2007) 1782-1809.
[129] U. Morbiducci, R. Ponzini, M. Nobili, D. Massai, F.M. Montevencchi, D. Bluestein, A. Redaelli, Blood damage safety of prosthetic heart valves. Shear-induced platelet activation and local flow dynamics: A fluid-structure interaction approach, Journal of Biomechanics, 42 (2009) 1952-1960.
[130] H.A. Simon, L. Ge, F. Sotiropoulos, A.P. Yoganathan, Simulation of the three-dimensional hinge flow fields of a bileaflet mechanical heart valve under aortic conditions, Annals of Biomedical Engineering, 38 (2009) 841-853.
[131] H.A. Simon, L. Ge, F. Sotiropoulos, A.P. Yoganathan, Numerical investigation of the performance of three hinge designs of bileaflet mechanical heart valves, Annals of Biomedical Engineering, 6 (2010) 1-16.
[132] J.D. Hart, G.W.M. Peters, P.J.G. Schreurs, F.P.T. Baaijens, A two-dimensional fluid-structure interaction model of the aortic value, Journal of Biomechanics, 33 (2000) 1079-1088.
[133] J.D. Hart, G.W.M. Peters, P.J.G. Schreurs, F.P.T. Baaijens, A three-dimensional computational analysis of fluid-structure interaction in the aortic valve, Journal of Biomechanics, 36 (2003) 103-112.
[134] J.D. Hart, G.W.M. Peters, P.J.G. Schreurs, F.P.T. Baaijens, Collagen fibers reduce stresses and stabilize motion of aortic valve leaflets during systole, Journal of Biomechanics, 37 (2004) 303-311.
[135] J.D. Hart, F.P.T. Baaijens, G.W.M. Peters, P.J.G. Schreurs, A computational fluid-structure interaction analysis of a fiber-reinforced stentless aortic valve, Journal of Biomechanics, 36 (2003) 699-712.
[136] R.V. Loon, P.D. Anderson, F.N.V.D. Vosse, A fluid-structure interaction method with solid-rigid contact for heart valve dynamics, Journal of Computational Physics, 217 (2006) 806-823.
[137] R.V. Loon, P.D. Anderson, F.P.T. Baaijens, F.N.V.D. Vosse, A three-dimensional fluid-structure interaction method for heart valve modelling, Comptes Rendus - Mecanique, 333 (2005) 856-866.
[138] J. Vierendeels, K. Dumont, P.R. Verdonck, A partitioned strongly coupled fluid-structure interaction method to model heart valve dynamics, Journal of Computational and Applied Mathematics, 215 (2008) 602-609.
[139] M.A. Nicosia, R.P. Cochran, D.R. Einstein, C.J. Rutland, K.S. Kuzelman, A coupled fluid-structure finite element model of the aortic valve and root, Journal of Heart Valve Disease, 12 (2003) 781-789.
[140] D.R. Einstein, K.S. Kuzelman, P.G. Reinhall, M.A. Nicosia, R.P. Cochran, Non-linear fluid-coupled computational model of the mitral valve, Journal of Heart Valve Disease, 14 (2005) 376-385.
[141] A. Ranga, O. Bouchot, R. Mongrain, P. Uglini, R. Cartier, Computational simulations of the aortic valve validated by imaging data: Evaluation of valve-sparing techniques, Interactive Cardiovascular and Thoracic Surgery, 5 (2006) 373-378.
[142] Y.S. Morsi, W.W. yANG, A. Owida, C.S. Wong, Development of a novel pulsatile bioreactor for tissue culture, Journal of Artificial Organs, 10 (2007) 109-114.
[143] P.N. Watton, X.Y. Luo, X. Wang, G.M. Bernacca, P. Molloy, D.J. Wheatley, Dynamic modelling of prosthetic chorded mitral valves using the immersed boundary method, Journal of Biomechanics, 40 (2007) 613-626.

[144] P.N. Watton, X.Y. Luo, M. Yin, G.M. Bernacca, D.J. Wheatley, Effect of ventricle motion on the dynamic behaviour of chorded mitral valves, Journal of Fluids and Structures, 24 (2008) 58-74.
[145] S. Katayama, N. Umetani, S. Surgiura, T. Hisada, The sinus of Valsalva relieves abnormal stress on aortic valve leaflets by facilitating smooth closure, Journal of Thoracic and Cardiovascular Surgery, 136 (2008) 1528-1535.
[146] S. Chandra, C. Seaman, N.M. Rajamannan, P. Sucosky, Computational comparison between normal and bicuspid aortic valve hemodynamics, The American Society of Mechanical Engineering, Summer Bioengineering Conference (2011) 1211-1212.
[147] S. Chandra, N. Rajamannan, P. Sucosky, Computational assessment of bicuspid aortic valve wall-shear stress: implications for calcific aortic valve disease, Biomechanics and modeling in mechanobiology, 11 (2012) 1085-1096.
[148] K. Cao, M. Bukac, P. Sucosky, Three-dimensional macro-scale assessment of regional and temporal wall shear stress characteristics on aortic valve leaflets, Computer Methods in Biomechanics and Biomedical Engineering, 19 (2015) 603-613.
[149] K. Cao, P. Sucosky, Effect of bicuspid aortic valve cusp fusion on aorta wall shear stress: Preliminary computational assessment and implication for aortic dilation, World Journal of Cardiovascular Diseases, 5 (2015) 120-132.
[150] K. Cao, P. Sucosky, Computational comparison of regional stress and deformation characteristics in tricuspid and bicuspid aortic valve leaflets, International Journal for Numerical Methods in Biomedical Engineering, 33 (2017) 27-35.
[151] A.M. Tango, J. Salmonsmith, A. Ducci, G. Burriesci, Validation and extension of a fluid–structure interaction model of the healthy aortic valve, Cardiovascular Engineering and Technology, 9 (2018) 739-751.

Chapter 3

Effect of Calcification of the aortic valve on coronary artery hemodynamics

In Chapter 1, a brief introduction regarding the anatomy of the aortic valve, its function inside the body, common aortic valve diseases, and treatments and methods to diagnose stenosis of the aortic valve were presented. The techniques used to replace the stenosed aortic valves were also discussed. In Chapter 2, a comprehensive literature review encompassing the experimental and numerical approaches used to simulate the pathologies of the aortic valve were explained. The chapter concluded by defining the objectives of the project based on the identified gaps.

Clinical data shows that patients with aortic valve stenosis are reported to have reduced coronary artery flow during the cardiac cycle. The reduced coronary artery flow in patients with aortic valve stenosis may lead to myocardial ischemia and left ventricle dysfunction which results in heart failure over time. Furthermore, in-vivo data shows that patients with aortic valve stenosis have symptoms of coronary artery disease. It is also believed that coronary artery disease and aortic valve stenosis are interdependent, however, the mechanism behind this is not clear. This chapter is focused on providing an answer to the following research question which is the first objective of the project: *whether leaflet stiffening affect coronary artery hemodynamics and results in the initiation of coronary artery disease?*

A fluid structure interaction model of the simplified aortic valve leaflets incorporating coronary artery ostia extracted from a two-dimensional echocardiography image is presented. The effect of calcification of the aortic valve leaflets on the hemodynamic parameters within the aortic root and coronary arteries, the flow pattern inside the sinus cavity, and the transvalvular pressure gradient along the valve are investigated. The correlation between the calcification of the aortic valve and coronary artery diseases is elucidated. To reveal this, the influence of aortic valve stenosis (leaflet thickening) on the wall shear stress inside the coronary arteries is analysed and the susceptible locations for initiation and progression of coronary artery atherosclerosis are found.

Details of the methodology, supporting evidence and data are presented and explained in this chapter which consists of the published journal article:

Araz. R. Kivi, Nima Sedaghatizadeh, Benjamin S. Cazzolato, Anthony C Zander, Ross Roberts-Thomson, Adam J. Nelson, Maziar Arjomandi, Fluid structure interaction modelling of aortic valve stenosis: Effects of valve calcification on coronary artery flow and aortic root hemodynamics, Journal of Computer Methods and Programs in Biomedicine, 196, 2020, 105647.

Statement of Authorship

Title of Paper	Fluid structure interaction modelling of aortic valve stenosis: Effects of valve calcification on coronary artery flow and aortic root hemodynamics
Publication Status	☑ Published ☐ Accepted for Publication ☐ Submitted for Publication ☐ Unpublished and Unsubmitted w ork w ritten in manuscript style
Publication Details	Araz. R. Kivi, Nima Sedaghatizadeh, Benjamin S. Cazzolato, Anthony C Zander, Ross Roberts-Thomson, Adam J. Nelson, Maziar Arjomandi, Fluid structure interaction modelling of aortic valve stenosis: Effects of valve calcification on coronary artery flow and aortic root hemodynamics, Journal of Computer Methods and Programs in Biomedicine, 196, 2020, 105647.

Principal Author

Name of Principal Author (Candidate)	Araz R. Kivi
Contribution to the Paper	Developed Ideas and Concepts • Conducted a comprehensive literature review • Developed the ideas and concepts based on the gaps of the knowledge in the field Performed the Modelling • Developed an aortic valve model in ANSYS workbench software • Developed an appropriate udf code to defined boundary conditions • Simulated the dynamic behaviour of the aortic valve leaflets • Validated the simulated model with the experimental data Interpreted Results • Extracted raw data from simulation • Post processed the data using CFD post and MATLAB • Developed a MATLAB code to extract the averaged data • Interpreted the results and compared them with the experimental results Wrote the Manuscript • Solely developed first full draft of the manuscript • Applied comments given by co-authors • Responsible for revising the manuscript after review • Acted as the corresponding author
Overall percentage (%)	80%
Certification:	This paper reports on original research I conducted during the period of my Higher Degree by Research candidature and is not subject to any obligations or contractual agreements with a third party that would constrain its inclusion in this thesis. I am the primary author of this paper.

Signature		Date	29/01/2021

Co-Author Contributions

By signing the Statement of Authorship, each author certifies that:

i. the candidate's stated contribution to the publication is accurate (as detailed above);

ii. permission is granted for the candidate in include the publication in the thesis; and

iii. the sum of all co-author contributions is equal to 100% less the candidate's stated contribution.

Name of Co-Author	Nima Sedaghatizadeh		
Contribution to the Paper	Supervised the work, participated in developing ideas, and provide feedback on the manuscript.		
Signature		Date	29/01/2021

Name of Co-Author	Benjamin S. Cazzolato		
Contribution to the Paper	Supervised the work, participated in developing ideas, and evaluated the manuscript.		
Signature		Date	29/01/2021

Name of Co-Author	Anthony C Zander		
Contribution to the Paper	Supervised the work, and provide feedback on the manuscript.		
Signature		Date	16/02/2021

Name of Co-Author	Ross Roberts-Thomson		
Contribution to the Paper	Participated in developing ideas, and provide feedback on the manuscript.		
Signature		Date	08/02/2021

Name of Co-Author	Adam J Nelson		
Contribution to the Paper	Participated in developing ideas and evaluated the manuscript.		
Signature		Date	08/02/2021

Name of Co-Author	Maziar Arjomandi		
Contribution to the Paper	Supervised the work, participated in developing ideas, and provide feedback on the manuscript.		
Signature		Date	29/01/2021

Please cut and paste additional co-author panels here as required.

Fluid structure interaction modelling of aortic valve stenosis: effects of valve calcification on coronary artery flow and aortic root hemodynamics

Araz R. Kivi, Nima Sedaghatizadeh, Benjamin S. Cazzolato, Anthony C. Zander, Ross Roberts-Thomson, Adam J. Nelson, Maziar Arjomandi

3.1 Abstract

Coronary artery diseases and aortic valve stenosis are two of the main causes of mortality and morbidity worldwide. Stenosis of the aortic valve develops due to calcium deposition on the aortic valve leaflets during the cardiac cycle. Clinical investigations have demonstrated that aortic valve sclerosis not only affects hemodynamic parameters inside the aortic root but also has a significant influence on the coronary artery hemodynamics and leads to the initiation of coronary artery disease. The aim of this study is to investigate the effect of calcification of the aortic valve on the variation of hemodynamic parameters in the aortic root and coronary arteries in order to find potential locations for initiation of the coronary stenoses. Fluid structure interaction modelling methodology was used to simulate aortic valve hemodynamics in the presence of coronary artery flow. A 2-D model of the aortic valve leaflets was developed in ANSYS Fluent based on the available echocardiography images in literature. The k-ω SST turbulence model was utilised to model the turbulent flow downstream of the leaflets. The effects of calcification of the aortic valve on aortic root hemodynamics including transvalvular pressure gradient, valve orifice dimeter, vorticity magnitude in the sinuses and wall shear stress on the ventricularis and fibrosa layers of the leaflets were studied. Results revealed that the transvalvular pressure gradient increases from 792 Pa (~ 6 mmHg) for a healthy aortic valve to 2885 Pa (~ 22 mmHg) for a severely calcified one. Furthermore, the influence of the calcification of the aortic valve leaflets on the velocity profile and the wall shear stress in the coronary arteries was investigated and used for identification of potential locations of initiation of the coronary stenoses. Obtained results show that the maximum velocity inside the coronary arteries at early diastole decreases from 1 m/s for the healthy valve to 0.45 m/s for the severely calcified case. Calcification significantly decreases the wall shear stress of the coronary arteries. This reduction in the wall shear stress can be a main reason for initiation of the coronary atherosclerosis process and eventually results in coronary stenoses.

3.2 Introduction

Aortic valve disease is the most common form of valvular heart disease (VHD) in the elderly and frequently coexists with coronary artery disease [1]. Contemporary registries suggest the prevalence of coronary artery disease increases with age and the presence of aortic stenosis such that over half of all patients require simultaneous coronary bypass during valve surgery [2]. Aortic valve disease of the elderly occurs when calcium deposits on aortic valve leaflets over time, thereby changing the geometry and material properties of the aortic valve leaflets [3-5]. Invasive studies demonstrate that changes in the geometry and material properties of the aortic valve leaflets not only affect hemodynamics within the aortic root but also have a significant impact on coronary blood flow [6-8]. The hemodynamic variations in coronary arteries due to calcification may lead to accelerated atherosclerosis and eventually result in coronary stenosis [9, 10].

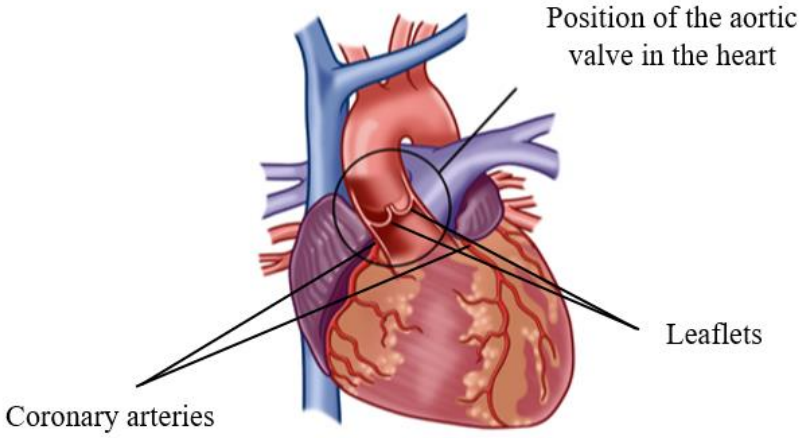

Figure 3.1 Schematic view of the position of the aortic valve inside the heart [11]

Clinical investigations [12] show that the wall shear stress plays a significant role in the initiation of atherosclerosis within the coronary arterial wall and the progression of the calcium deposition on the leaflets. Calcification and atherosclerosis are, however, complex multifactorial processes which are yet to be completely understood [8, 13, 14]. It is believed that blood flow-induced shear stress affects the endothelial cells, leading to endothelial dysfunction, inflammatory responses, oxidative stress which remodels the artery wall and valve structure, and eventually results in progression of calcification and initiation of atherosclerosis [15-17]. For example, a recent study carried out by Hatoum et al. (2019) shows that the recirculation zone in the sinuses for a calcified aortic valve changes the wall shear stress on the aortic valve leaflets and results in progression of calcium deposition. They also demonstrated that the calcified aortic valve leaflet experiences a smaller range of shear stress with higher shear stress probabilities during the systole compared to that of a healthy valve.

During the past decades, researchers have investigated pathologies of aortic valve and coronary arteries using numerical [18, 19], clinical (in-vivo), and experimental (in-vitro) methods [8, 16, 20-22]. In numerical modelling, finite element analysis (FEM) and computational fluid dynamics (CFD) have been used to investigate valve hemodynamics [23-26]. The FEM studies [23, 27] considered only the structural domain and did not account for the effect of fluid in their simulations. Similarly, the CFD simulations are not able to capture the effect of the structural domain on the fluid one.

To overcome the limitations of the aforementioned works not being able to model the fluid and structure domain simultaneously, fluid structure interaction (FSI) modelling has been employed by researchers [28, 29] to study the influence of the valve structure and the coronary wall on the fluid domain. For example, Weinberg and Mofrad [30] developed a FSI model of the aortic valve with nonlinear, anisotropic material properties and investigated the effect of material properties on leaflet strain during the cardiac cycle, comparing the impact of trileaflet and bicuspid valve morphology. They found that nonlinearity in the material properties of the bicuspid aortic valve has a significant effect on leaflet strain compared to that of the trileaflet valve. Katayama, Umetani, Sugiura and Hisada [31] developed a model of the aortic valve to investigate the impact of the presence of sinuses on hemodynamic parameters inside the aortic root, and found that the presence of the sinuses affect the opening time of the valve. These aforementioned studies have not considered coronary arteries in their model, although the

presence of coronary flow is able to change the hemodynamic parameters inside the aortic root [32, 33].

To consider the effect of coronary arteries, Kim, Vignon-Clementel, Coogan, Figueroa, Jansen and Taylor [34] developed an FSI model of the aortic root including coronary arteries. However, the model did not incorporate the leaflets and sinuses. Nobari, Mongrain, Leask and Cartier [32] extended the model of Kim et al. (2010) by adding right and left coronary arteries. They also utilised the ALE approach to simulate an FSI model of the aortic valve. Mohammadi, Cartier and Mongrain [35] improved the previous model by considering the tapered shape and branches of the coronary arteries. They used the combined FD and ALE approaches to simulate the model of the aortic valve. They investigated the effect of narrowing of the coronary arteries on the wall shear stress inside the coronary arteries based on the explicit finite element method using LS-DYNA software. Cao et al. (2017) presented a FSI model of the aortic valve with coronary arteries and investigated the impact of having coronary artery on leaflet wall shear stress. They found that vortex development in sinus due to the presence of coronary arteries can, in turn, changes the magnitude of the leaflet wall shear stress. However, the impact of aortic valve stenosis on the hemodynamic parameters inside the aortic root, flow features in sinuses, and wall shear stress on the leaflets were neglected.

In this paper, the effect of valve stenosis on the aortic root and coronary hemodynamic parameters as well as the shape of the vortices inside the sinuses and the aortic root hemodynamics were investigated. To do this, 2D models of the healthy, calcified and severely calcified aortic valves were developed in ANSYS Fluent based on the echocardiography images available in the literature. In order to capture the turbulent nature of the flow downstream of the leaflets, the k-ω SST turbulence model was used. The influence of the calcification of the aortic-valve leaflets on hemodynamic parameters inside the aortic root, such as transvalvular pressure gradient, valve orifice diameter, maximum jet velocity along the valve orifice, wall shear stress on the fibrosa and ventricularis layers of the leaflets, was investigated. The impact of calcification of the aortic valve leaflets on the flow pattern in the sinuses was also studied; the vorticity magnitude corresponding to different points behind the leaflets was calculated in order to show how strong vortices can become as a result of the stiffening of the aortic valve leaflets. Furthermore, the flow features such as velocity magnitude, and the wall shear stress on the coronary walls inside the coronary arteries were studied in order to show the significance of the calcification on coronary hemodynamics. Based on the calculated hemodynamic parameters, susceptible locations for the initiation of coronary artery disease were determined.

3.3 Methods

In this study, a model of a 2D healthy aortic valve was developed in a commercial software package, ANSYS Workbench 19.1. The model geometry was based on the 2D echocardiography images of a healthy tricuspid aortic valve available in the literature for a healthy person of 27 years of age [36]. The numerical model consists of two different domains: fluid (blood flow field) and structure (deformable leaflets). Fluid structure interaction methodology was used to model the interaction of the fluid and structural domains. In the following paragraphs, the domains are explained.

3.3.1 Fluid domain (blood flow field)

As depicted in Figure 3.2 (a), the fluid domain consists of four regions: inlet, outlets (coronary and aorta) and blood flow region. The blood is considered as a Newtonian,

incompressible fluid with constant viscosity of 0.0035578 Pa.s and density of 1060 kg/m^3 [37]. As seen in Figure 3.2 (b and c), the inlet (ventricle side), sinus and coronary arteries are 16 mm, 25 mm, and 3 mm in diameter, respectively. These data were extracted from the echocardiography images shown in Figure 3.2 (c) [36].

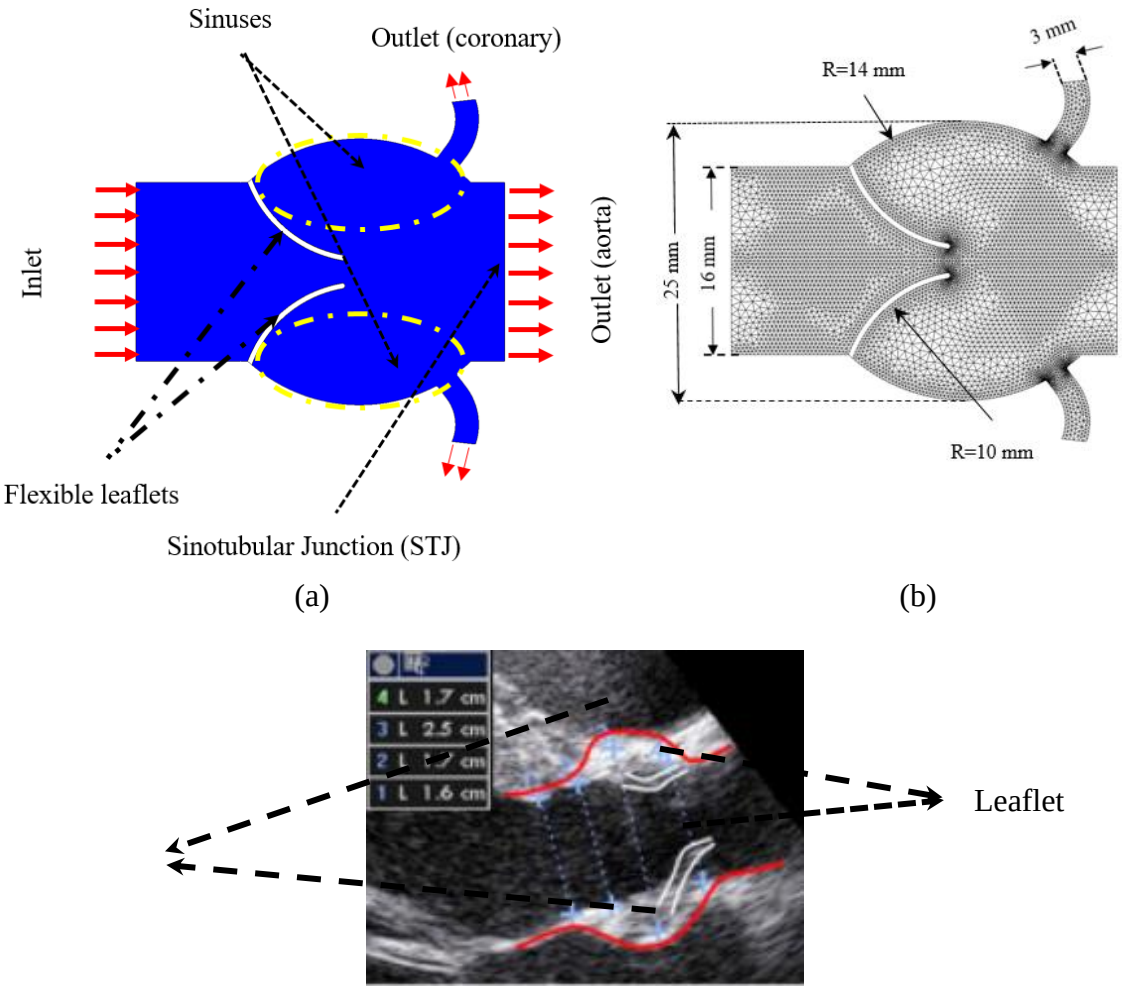

Figure 3.2 Schematic view of (a) healthy aortic valve with flexible leaflets, the sinuses are indicated by a yellow dash-line, flow directions for the inlet and outlet are shown using red arrows, (b) fluid domain mesh and boundary conditions; denser meshes are generated near the wall and leaflets to improve the accuracy of results, (c) echocardiography images from a healthy aortic valve [36]; the shape of the sinuses and leaflets are traced using a red and white line, respectively.

The flow is considered to be incompressible and isothermal conforming to the Navier-Stokes equations based on the *k-ω SST* turbulence model as follows:

$$\frac{\partial}{\partial x_j}\left[\rho k\bar{u}_j-(\mu+\sigma_k\mu_t)\right]\frac{\partial k}{\partial x_j}=\tau_{ij}S_{ij}-\beta^*\rho\omega k \tag{3.1}$$

$$\frac{\partial}{\partial x_j}\left[\rho\omega\bar{u}_j-(\mu+\sigma_\omega\mu_t)\frac{\partial\omega}{\partial x_j}\right]=P_\omega-\beta\rho\omega^2+2(1-F_1)\frac{\rho\sigma_{\omega2}}{\omega}\frac{\partial k}{\partial x_j}\frac{\partial\omega}{\partial x_j} \tag{3.2}$$

in which standard values and the constants are based on values proposed by [38].

For the fluid field, an unstructured mesh was generated based on the sweep method. To improve the accuracy of the results, inflation layers were applied to the walls of the sinuses and

leaflets. To resolve the boundary layers with higher accuracy, the mesh near the artery and leaflets walls was denser with maximum skewness of 0.68. The total number of elements inside the fluid domain is around 10,000, as shown in Figure 3.2 (b). To satisfy the mesh independency requirement, a sensitivity analysis was carried out for the pressure and velocity components for two grid sizes. Results showed that only a 2% difference between the calculated parameters when the number of elements was increased from 10,000 to 14,000. However, the computation time increased by about 40%.

In order to accurately model the deformation and movement of the leaflets, the mesh needs to be updated at every time step. To do this, a spring-based smoothing and re-meshing technique was used to generate a high quality mesh at every time step. Because of the presence of vorticities behind the leaflets and a peak Reynolds number of 2804, the k-ω SST turbulence model was used to model the turbulence flow downstream of the leaflets. ANSYS-Fluent was used to solve the fluid domain. Three sets of boundary conditions were defined in the fluid flow field. At the inlet (ventricular side), a time-dependent velocity profile (shown in Figure 3.3) was considered as the boundary condition. The transient velocity profile for the boundary condition at the inlet was obtained from measured data (based on Doppler imaging) available in the literature [36]. At the coronary outlets, a transient pressure profile (based on the published data) and outflow was considered as the boundary condition (also shown in Figure 3.3), which was obtained from the clinical data of the average coronary flow [39]. To obtain the required information from the interior domain, the outflow boundary condition was considered at the outlet (aorta). The walls of the sinuses were assumed to be rigid. To investigate the validity of this assumption, a sensitivity analysis has been carried out for the pressure and velocity components for two different models: one model with flexible leaflets and sinus walls, and another model with flexible leaflets but solid sinus walls. Results show that a 0.1% difference between the calculated parameters for solid and flexible sinus walls. However, the computation time was increased by about 20% for flexible sinus walls.

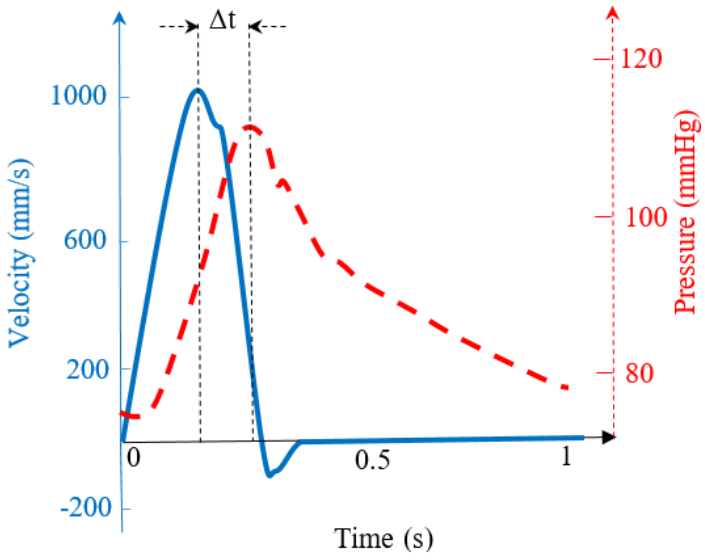

Figure 3.3 Inlet transient velocity profile applied at the inlet plane of the model (blue), physiological pressure at coronary outlets (red). Based on measurements used by [32, 35, 36, and 39].

3.4 Structural domain (deformable leaflets)

The structural domain of the model consists of two flexible leaflets which move as they are exposed to blood flow. The leaflets are assumed to be isotropic with density of 1060 kg/m^3, Poisson's ratio of 0.3 and Young's modulus of 2 MPa [23, 25, 36]. It is considered that calcium is uniformly distributed on the leaflet layers. The Young's modulus for the calcified and severely calcified cases are set to be 10 MPa, and 20 MPa, respectively [23, 25, 36]. ANSYS Mechanical APDL was used to solve the equations of the motion of the leaflets and find the dynamic responses, stresses and strains of the leaflets based on the Newmark time integration method. The mesh used for the leaflets was generated using the sweep method comprising 120 quadratic tetrahedral elements with a minimum of two elements through the thickness. To satisfy the mesh independency requirement, a constant pressure was applied to the leaflets and a mesh convergence study was carried out at steady state. Results show that the accuracy of the solution does not change for the models with more than 100 tetrahedral elements and with a maximum skewness of 0.43. The mechanical properties of the fluid and structural domains and the boundary conditions applied to the fluid domain are presented in Table 3.1 and Table 3.2, respectively.

Table 3.1 Mechanical properties of the fluid and structural domains used in the modelling

Domain	**Dynamic viscosity (Pa.s)**	**Density (kg/m^3)**	**Young's modulus (MPa)**	**Poisson's ratio**
Fluid (blood) Incompressible, Isothermal, Newtonian	0.0035578	1060	---	---
Structure (leaflets) Linear elastic, Isotropic	---	1060	2 (healthy) 10 (calcified) 20 (severely calcified)	0.3

Table 3.2 Boundary conditions used in the modelling

	Inlet	**Outlet (coronary)**	**FSI surface**	**Walls**
Boundary conditions:	Transient pulsatile velocity inlet	Physiological pressure outlet	Fluid structure interaction surface between the flexible elastic leaflets and blood flow	Solid walls for sinuses and aortic root

3.5 Two-way FSI

To model the interaction between the fluid and structure domains, two methods are proposed in the literature: one-way uncoupled and two-way coupled approaches [40]. For a model in which the structural domain undergoes large deformation due to the strong interaction between the domains, a two-way coupling approach is recommended in the literature [41]. A two-way coupled approach is based on either explicit or implicit techniques. In this work, the ANSYS explicit coupling module was used to model the interaction between the fluid flow and the movement of the flexible leaflets. Based on this technique, the continuity, Navier-Stokes, and turbulence equations related to blood flow were solved in Fluent. The deformation equations of the flexible leaflets were solved in Mechanical APDL. At every time step, the data including force and displacement was exchanged between the Fluent and Mechanical APDL modules. The schematic view of the system coupling module in ANSYS is illustrated in Figure 3.4.

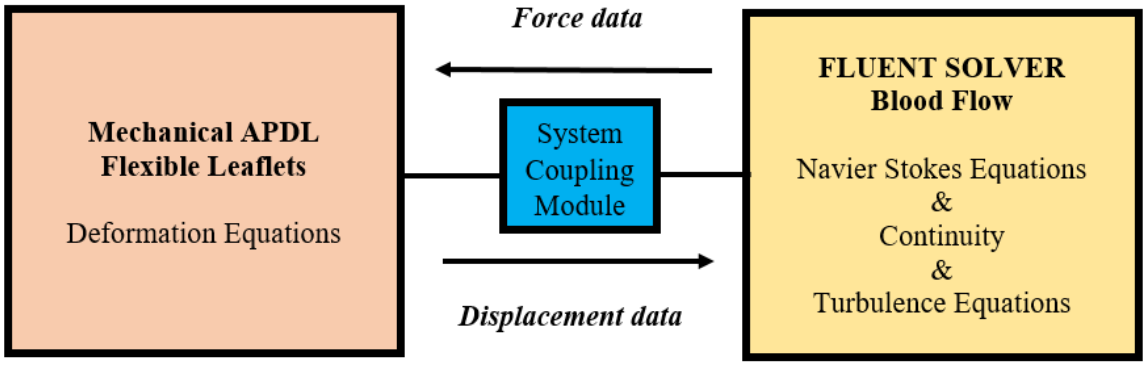

Figure 3.4 Schematic view of the system coupling module in ANSYS. The Navier Stokes, continuity, and turbulence equation were solved by Fluent. The deformation equation related to the flexible leaflets were solved by Mechanical APDL in ANSYS. In order to achieve converged results, the data including force and displacement were iteratively exchanged between the APDL and Fluent based on the System Coupling Module in ANSYS.

3.6 Results and Discussions

3.6.1 Validation of the model

For validation purposes, two hemodynamic parameters calculated for the healthy valve were compared against published data [42, 43]. The calculated transvalvular pressure gradient TPG_{max} and average wall shear stress (AWSS) for the presented work and previous experiments [43, 44] are given in Table 3.3.

Table 3.3 TPG_{max} and AWSS comparison between previous in-vivo experiments and FSI modelling

	TPG_{max} (Pa)	**AWSS (Pa)**
Experiment	799 [43]	7.9 [44]
Present work	792	8.4

To further validate the model, the results were qualitatively compared against recently published PIV data by [17]. Figure 3.5 shows a comparison of streamlines and flow features between the present simulation and the experimental results during systole. As can be seen, the developed model captures the unsteady flow features in the sinuses similar to the observed structures in the PIV experiment. However, there are slight deviations due to the existence of coronary arteries in the present model and differing dimensions.

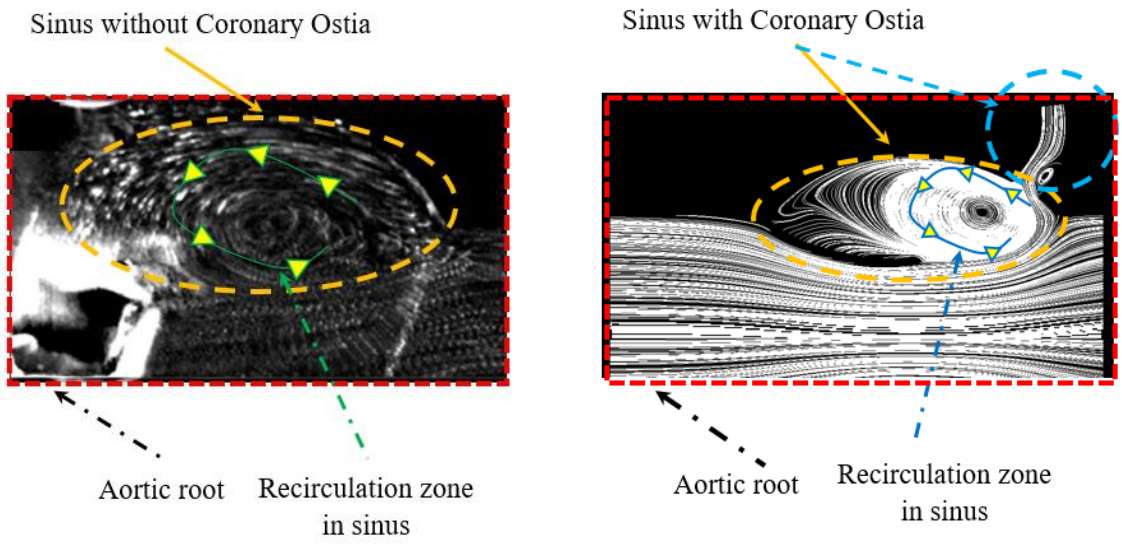

(a) (b)

Figure 3.5 A comparison of the flow streamlines around peak systole in sinus between (a) the PIV experiment [17] and (b) present simulation. The vortices captured in the numerical simulation matches well with those of the PIV experiment.

3.6.2 Effects of calcification on hemodynamic parameters

Velocity contours and streamlines of a healthy aortic valve during a cardiac cycle are depicted in Figure 3.6. As shown, during the systole, when the mass flow rate starts to grow, the pressure on the leaflets (ventricle side) increases and opens the valve. The opening of the valve increases in size by increase in mass flow rate up to maximum flow rate at peak systole when the valve witnesses maximum opening (t=0.1 s). Then, the flow rate starts to decrease and accordingly the leaflets close gradually until early diastole (t=0.32 s). At this time valve closes suddenly due the pressure difference between the left ventricle and the aorta. During closure period, blood flows into the coronary arteries in order to perfuse the myocardium (shown in Figure 3.6 d and e). The flow velocity in the aortic valve reaches its peak value of 1.65 m/s, while the maximum velocity is around 1 m/s at the inlet of the coronary artery; the results reveal that there is a lag between the peak velocity along the aortic valve and that of the coronary arteries. In comparison, the maximum velocity calculated for a healthy aortic valve by Amindari et al. (2017) was around 1.57 m/s. This difference in maximum velocity value is due to a lack of coronary arteries in their model. To show the recirculation zones in the sinuses, the velocity streamlines during cardiac cycle are illustrated in Figure 3.6 (f-j). The streamlines of the flow during the cardiac cycle show formation of various recirculation zones. In mid-systole, a recirculation zone is observed behind the leaflets. These vortices not only result in leaflet closure but also allow blood to flow into the coronary arteries. As seen, at late-systole and mid-diastole, the magnitude of the vortices increase and result in a significant increase in the volume of blood in the coronary arteries. The pressure difference between the left ventricle and aorta changes the magnitude and location of the recirculation zones. As shown, at mid-diastole (shown in Figure 3.6 (i)), three different vortices are observed; one near the tip of the leaflets (shown by red arrows in Figure 3.6 (i)), one attached to the wall of the sinuses (shown by black arrows in Figure 3.6 (i)) and another is located near the base of the ventricularis side of the leaflets (shown with yellow arrows in Figure 3.6 h and i). It is worth mentioning the presence of vortices leads to high amplitude oscillations of the leaflets during the cardiac cycle,

particularly at the diastole phase. It is implied that the vortices affect the dynamic motion of the leaflets.

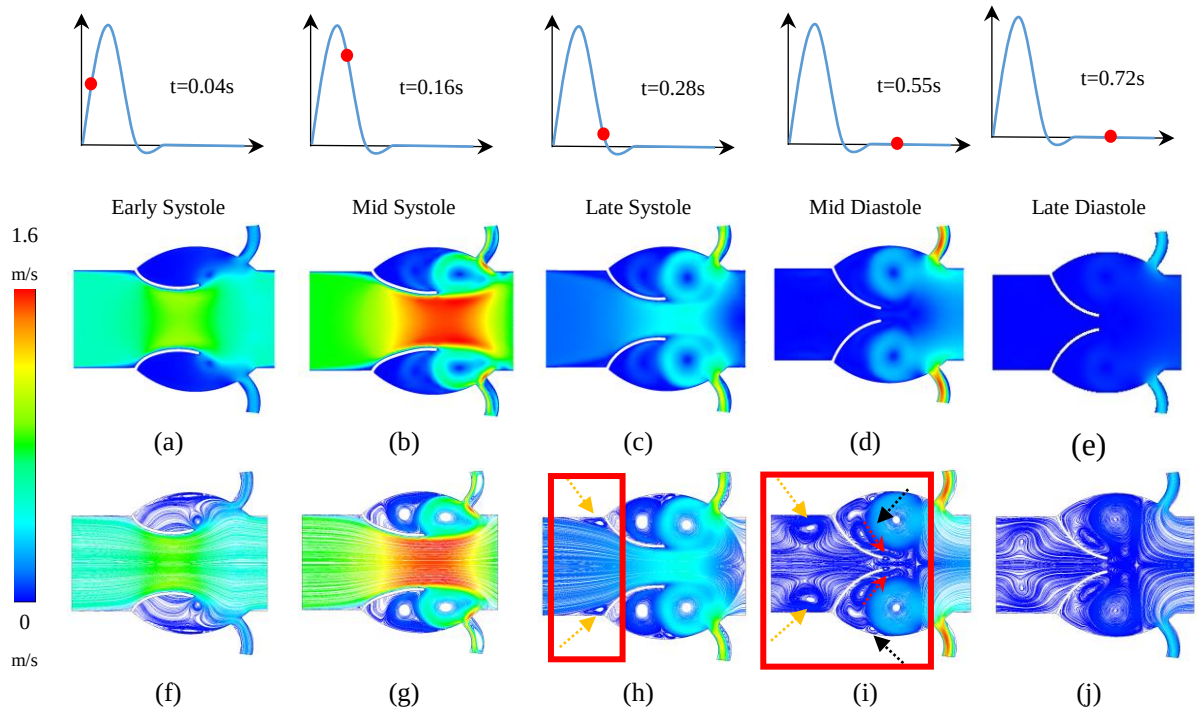

Figure 3.6 Velocity contour (a-e) and streamline (f-j) for a healthy aortic valve during cardiac cycle.

As the healthy valve starts to open, at early systole the shear between the jet and cavity flow results in generation of the primary counter-clockwise (CCW) vortex which grows in size as the valve continues to open. This consequently forms another vortex in the cavity which rotates in the opposite direction. When the valve starts to close, the cavity area increases, resulting in growth of vortices. Theses vortices migrate towards the middle of the cavity to become the dominant flow features occupying the entire cavity area. By the end of cardiac cycle, the flow rate decreases and the vortices migrate to the sinotubular junction (STJ) due to the inertia of the flow.

In order to show the effect of calcification on hemodynamic parameters inside the aortic root, the velocity contours and streamlines of the calcified aortic valve with modulus of elasticity E=10 MPa are illustrated in Figure 3.7. Calcification stiffens the leaflets by changing the material properties of the aortic valve leaflets. The stiffer leaflets do not open or close at the same rate nor to the same extent, which lead to changes in the hemodynamic parameters of the aortic root such as the transvalvular pressure gradient, valve orifice diameter, and maximum jet velocity in the aortic valve. As depicted in Figure 3.7, calcification increases the maximum jet velocity in the aortic valve from 1.65 m/s for the healthy valve to 2.23 m/s for the calcified case. By contrast, the maximum velocity at the inlet of the coronary artery decreases from 1 m/s for the healthy valve to around 0.45 m/s for the severely calcified one at early diastole. Furthermore, the opening diameter of the calcified aortic valve decreases due to an increase in the stiffness of the leaflets, which results in a significant increase in the pressure difference between the left ventricle and the aorta. This pressure difference changes the location of the recirculation zone and its magnitude in the sinuses. As shown in Figure 3.7 h and i, the vortices become larger near the fibrosa and ventricularis side (shown by a dash line) for the calcified aortic valve compared to the healthy one (shown in Figure 3.7 h and i).

The same scenario is repeated for the calcified aortic valve. In this case, at mid-systole, the primary CCW recirculation zone is slightly longer than that of the healthy valve due to the larger area of the sinuses. Furthermore, apart from the primary CCW and CW vortices in the sinuses, two other vortices are generated behind the leaflets (shown in Figure 3.7 i) due to the smaller aortic orifice diameter and larger area of the sinuses. Therefore, the flow behind the sinuses is a combination of small vortices accompanied by primary vortices. The combined vortices behind the leaflets may be a cause of flow stagnation and calcification.

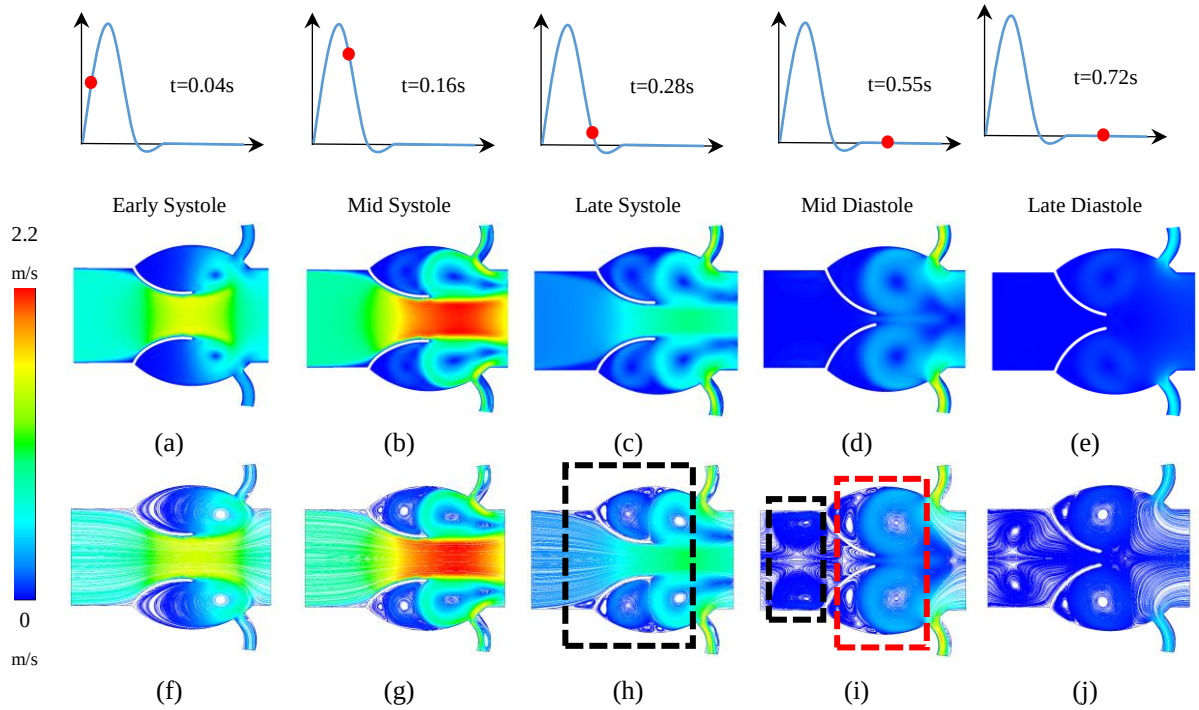

Figure 3.7 Velocity contour (a-e) and streamline (f-j) for a calcified aortic valve during cardiac cycle.

The velocity contours and streamlines for the severely calcified aortic valve with Young's modulus of E=20 MPa are shown in Figure 3.8. The maximum jet velocity along the aortic valve reaches 2.4 m/s for the severely calcified aortic valve. This significant increase in the maximum jet velocity along the aortic valve changes the pressure difference between the left ventricle and the aorta and leads to changes in the recirculation zone (shown in Figure 3.8 h and i). Moreover, calcification modifies the opening, closing, and ejection time of the leaflets. The opening time for the leaflets decreases from around 48 ms for the healthy valve, to 33 ms for the calcified case. On the other hand, calcification increases the valve closing time from 41 ms for the healthy valve, to 74 ms for the calcified case (shown in Table 3.4). Furthermore, the calcified valve has a longer ejection time (for a constant stroke volume of 70 ml). As reported in Table 3.4, the ejection time increases from 202ms for the healthy aortic valve, to 261ms for the calcified aortic valve.

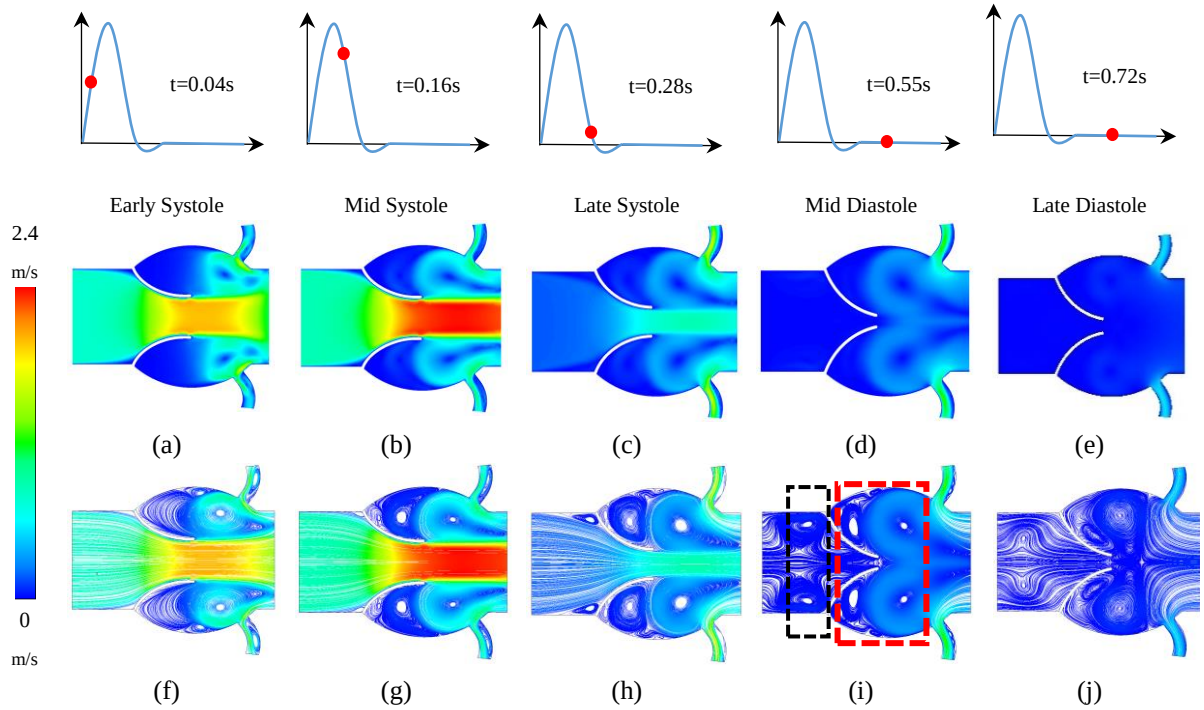

Figure 3.8 Velocity contour (a-e) and streamline (f-j) for a severely calcified aortic valve during cardiac cycle.

As mentioned, calcification has a significant impact on the opening, closing, and ejection time. For the severely calcified aortic valve, the opening time decreases to 26 ms compared to that for the healthy aortic valve which is 48 ms. The ejection and closing times for the severely calcified case are 261 ms and 82 ms, respectively, which is tabulated in Table 3.4 .

Table 3.4 Opening, closing, and ejection time for the healthy, calcified, and severely calcified aortic valve

	Opening time (ms)	**Ejection time (ms)**	**Closing time (ms)**
Healthy	48	202	41
Calcified	33	213	74
Severely calcified	26	261	82

In order to show the impact of calcification on valve orifice diameter, the velocity contours and streamlines for healthy, calcified, and severely calcified aortic valves at mid systole are illustrated in Figure 3.9. As shown, the valve calcification results in a decrease in the valve orifice diameter from 14.2 mm for the healthy aortic valve (and largest opening diameter of 14.4 mm at peak systole) to 10.5 mm for the calcified case, and to 9.6 mm for the severely calcified case. Furthermore, the jet velocity along the aortic valve orifice at mid systole increases from 1.65 m/s for the healthy aortic valve to 2.23 m/s for the calcified case and to 2.47 m/s for the severely calcified case.

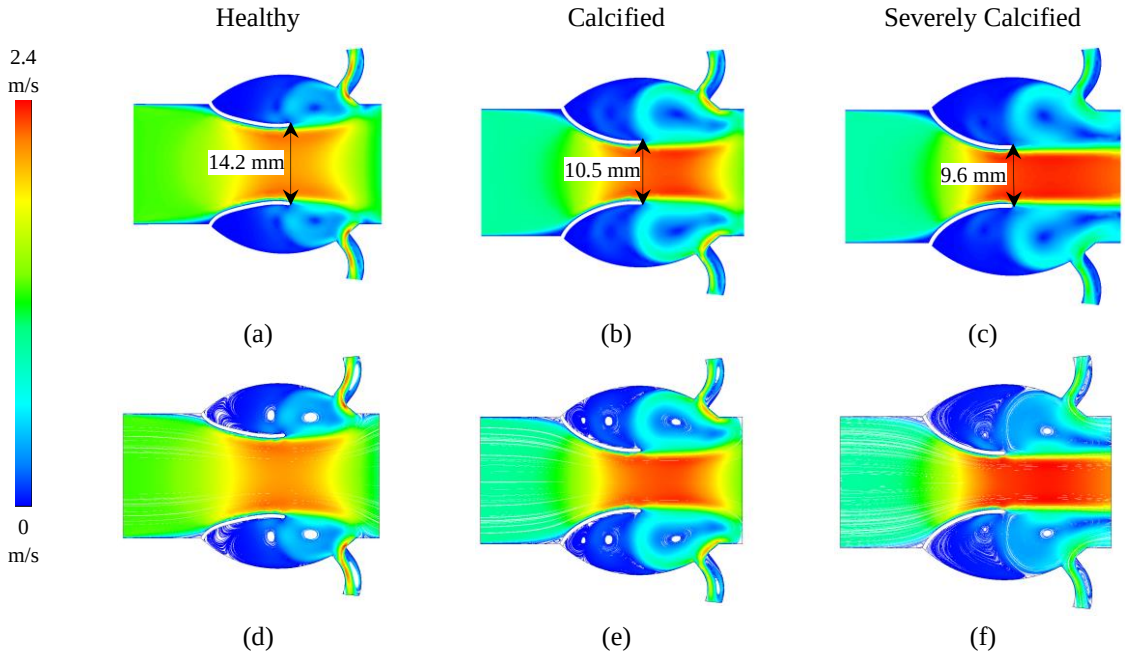

Figure 3.9 Velocity contours and streamlines for a (a,d) healthy, (b,e) calcified, (c,f) severely calcified aortic valve at mid systole.

Improper opening results in a significant increase in the transvavular pressure gradient increases between the left ventricle and the aorta. The transvavular pressure gradients for the healthy, calcified, and severely calcified aortic valves are illustrated in Figure 3.10. As can be seen, the transvalvular pressure gradient for the healthy aortic valve is around 792 Pa (~ 6 mmHg), which significantly increases to 2554 (~ 19 mmHg) and 2885 (~ 22 mmHg) for the calcified and severely calcified cases, respectively. An increase in the TPG might have an effect on valve performance during the cardiac cycle and drives compensatory left ventricular hypertrophy to accommodate the increased wall stress. Over time this process is overwhelmed and systolic dysfunction (heart failure) ensues.

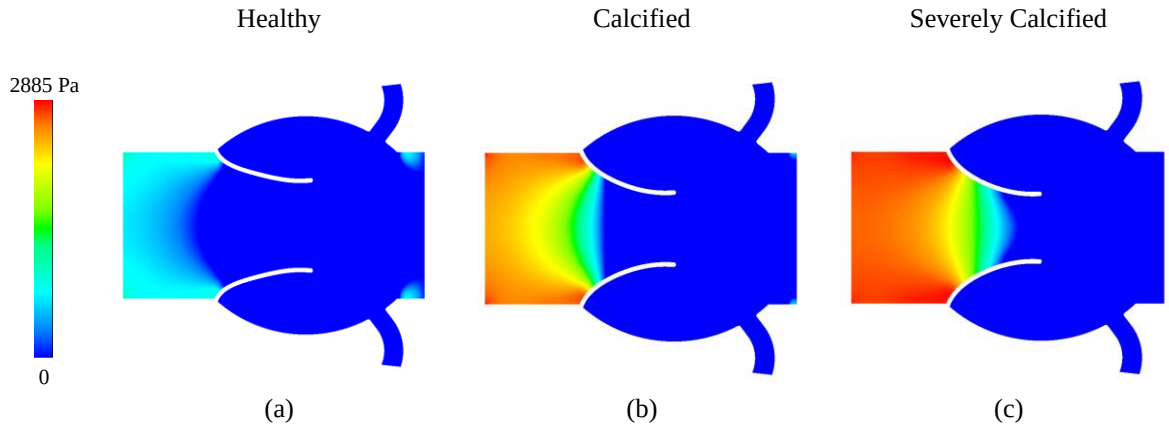

Figure 3.10 Transvalvular pressure gradient for the (a) healthy, (b) calcified, (c) severely calcified aortic valve at peak systole.

Calcification has an impact on jet velocity along the aortic valve. To show this, the variation of the velocity during the cardiac cycle is depicted in Figure 3.11 (b) for a point positioned in the middle of the valve orifice area (shown in Figure 3.11 a). As illustrated, for a constant velocity along the valve orifice area, the diameter of the healthy valve is larger than that of the calcified and severely calcified valves; the more the valve becomes calcified, the less it is able to open during the cardiac cycle. This leads to an increase in the maximum jet velocity during the cardiac cycle. To overcome the left ventricular outflow tract obstruction,

increased intraventricular pressure results, thereby creating a differential in pressure between the left ventricle and the aorta. To illustrate this, TPG for the healthy, calcified, and severely calcified aortic valves are shown in Figure 3.11 (c). As can be seen, the calcified valve experiences greater pressure difference along the valve orifice area during the cardiac cycle. The higher pressure difference can, in turn, affect the performance of the valve and flow features inside the aortic root.

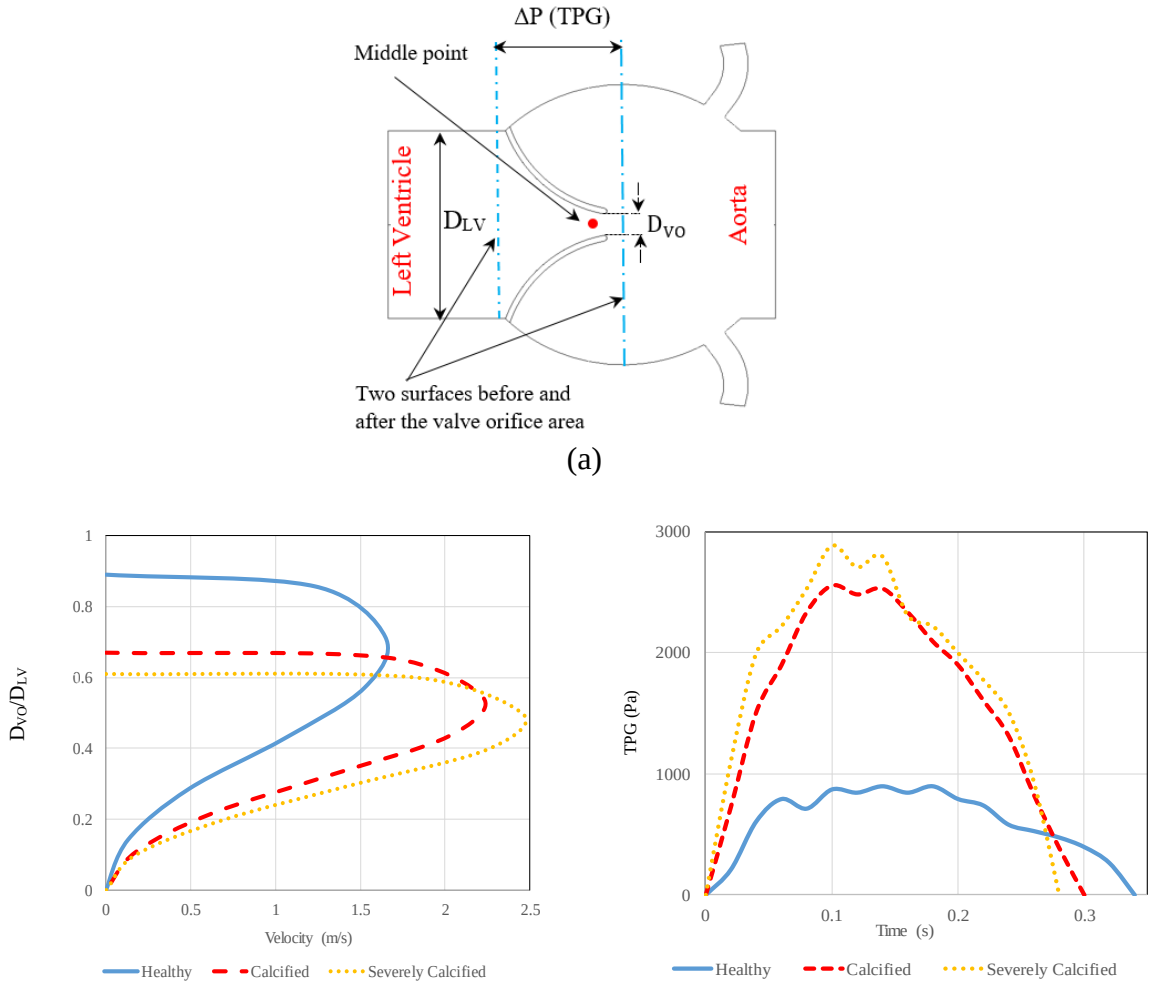

Figure 3.11 (a) Schematic view of the aortic root with leaflets and coronary ostia; D_{LV} and D_{VO} indicate the diameter of the left ventricle and valve orifice, respectively (b) velocity profile corresponding to healthy, calcified, and severely calcified valves at a point located in the middle of the aortic valve orifice showing variation of the valve orifice diameter versus velocity (c) transvalvular pressure gradient (TPG) curves for healthy, calcified, and severely calcified valves indicating the pressure difference between two surfaces before and after the valve orifice area.

The main reason for initiation and progression of calcification is not yet fully understood. However, it is believed that the difference between the wall shear stress of the aortic valve leaflet layers can remodel the valve and has an influence on valve hemodynamics. To investigate this influence, the AWSS of the different layers (ventricularis and fibrosa) of the aortic valve are plotted in Figure 3.12. As depicted, the maximum value of AWSS at ventricularis increases from 25 Pa for the healthy aortic valve to 46 Pa for the severely calcified case, whilst, on the fibrosa side, AWSS decreases from 19 Pa for the healthy aortic valve to 3 Pa for the severely calcified case. As can be seen, the calcified aortic valve is subject to the higher WSS differences between ventricularis and fibrosa layers. As mentioned, these

differences in the wall shear stress of the aortic valve layers are able to damage the valve tissue and lead to progression of calcification.

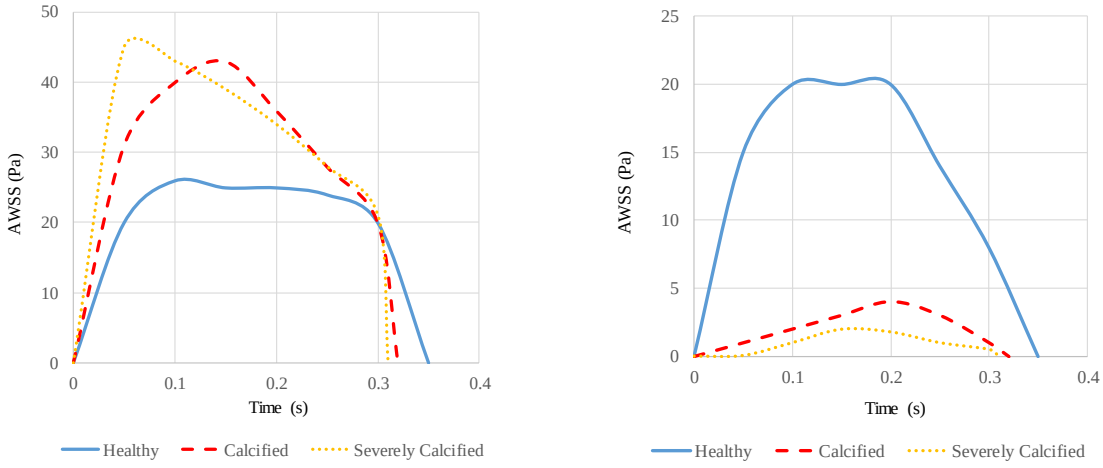

(a) (b)

Figure 3.12 Averaged wall shear stress of the (a) ventricularis and (b) fibrosa layers of the aortic valve.

The velocity profiles of the coronary ostia for healthy, calcified, and severely calcified aortic valves are shown in Figure 3.13. As depicted, at early-systole (shown in Figure 3.13 b), the velocity magnitude has significantly decreased from a maximum value of 0.38 m/s for the healthy aortic valve to around 0.25 m/s for the severely calcified case. Similarly, at early-diastole, the severely calcified case witnesses significant decrease (i.e. from around 1 m/s to 0.45 m/s) in the peak velocity of the coronary artery compared to that of a healthy aortic valve. These velocity reductions result in reduced coronary blood flow. In the context of increased myocardial work (exacerbated by the presence of left ventricular hypertrophy), the myocardial blood supply can be overwhelmed by increased demand leading to ischaemia and the symptom of angina. Chronic ischaemia is believed to be a key component of the abnormal myocardial energetics observed in left ventricular hypertrophy (RFF). The mismatch between increased myocardial oxygen demand from greater intraventricular pressure and reduced coronary flow contributes to the symptoms of angina and heart failure in patients with aortic stenosis.

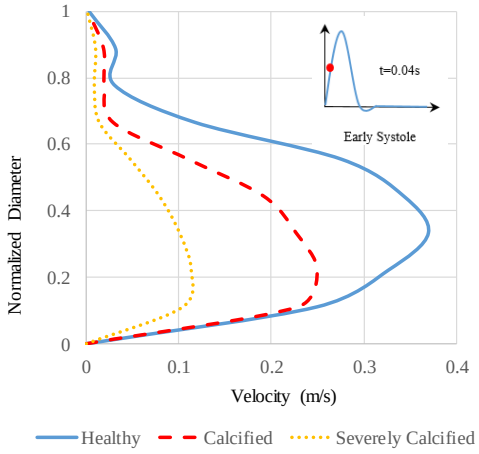

(a)

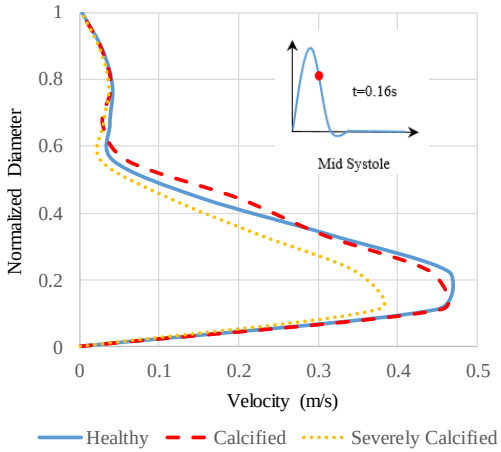

(b)

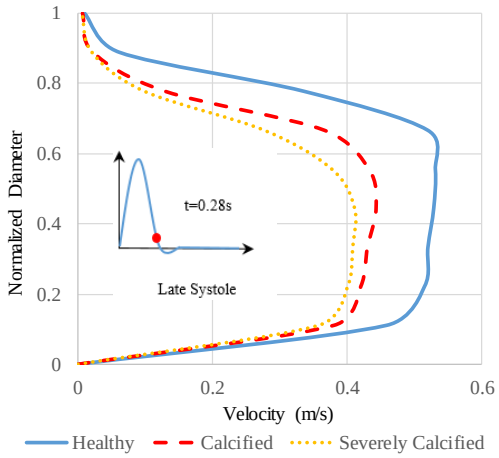

(c)

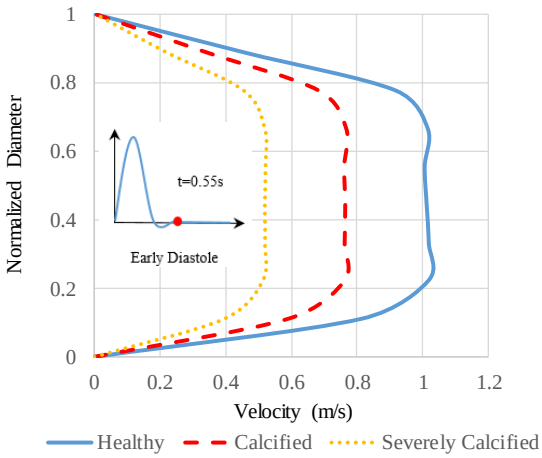

(d)

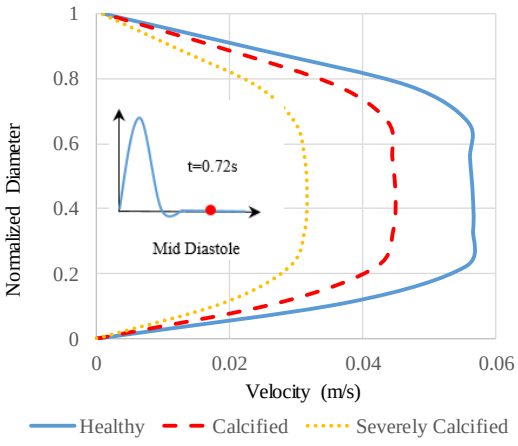

(e)

Figure 3.13 Velocity profile at the coronary ostia for healthy, calcified, severely calcified aortic valve during the cardiac cycle.

The calcification of the aortic valve affects the flow features inside and outside of the aortic root. It is observed that the calcified valve witnesses vortices with different shapes and magnitudes in the sinuses (shown in Figure 3.7 and Figure 3.8). The strength and size of the primary vortex formed in the sinuses can lead to hemodynamic changes inside the coronary arteries. Figure 3.14 shows the vorticity magnitude of three different points positioned in the

sinuses for the healthy, calcified, and severely calcified valves. As shown at point P_1 near the leaflets (shown in Figure 3.14 a), the maximum vorticity magnitude for the healthy aortic valve has two peaks; one around t = 0.2s with a magnitude of 172 rad/s and another one at t = 0.28 s with magnitude of 132 rad/s. As seen, calcification almost doubles the maximum vorticity magnitude of the point P_1 from around 172 rad/s for the healthy valve to 348 rad/s for the severely calcified case. Furthermore, the vorticity magnitude curve corresponding to the calcified valve shifts towards the left compared to the healthy case, which means that the vortices with larger magnitude associated with the severely calcified valve are created over a shorter duration compared to that of the healthy case. This can be explained by the shorter opening/ejection time of the calcified valve in comparison with the healthy one. It is worth mentioning that as the strength of the vortices increases the energy loss becomes more significant. More interestingly, as more energy is lost in the sinuses, the more the blood flow stagnates, and the probability of calcium deposition on the leaflets grows.

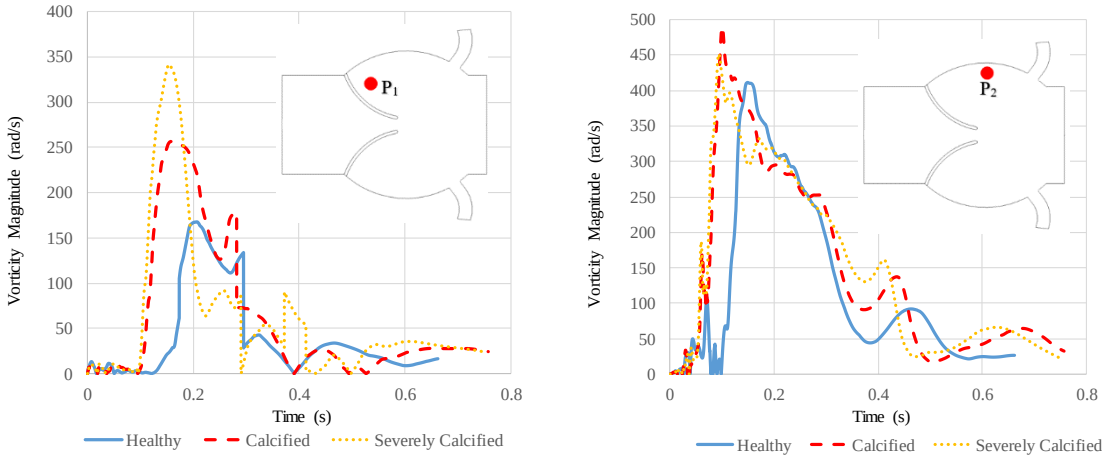

(a)

(b)

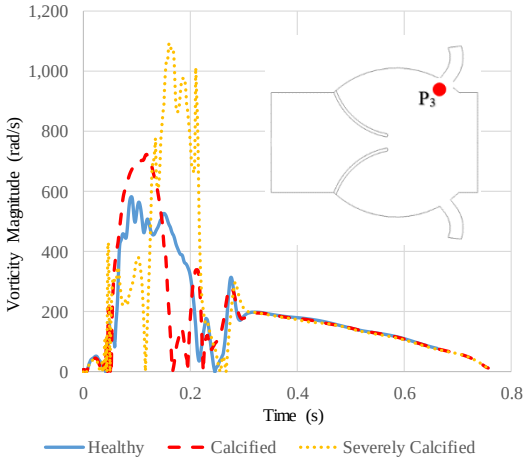

(c)

Figure 3.14 Vorticity magnitude for three different points located in sinus during cardiac cycle (a) point near leaflets (b) near wall of the sinus (c) near coronary ostia.

The vorticity magnitudes for two other points are depicted in Figure 3.14 b and c. At point P_2 (shown in Figure 3.14 b), close to the sinus wall, the peak vorticity magnitude for the severely calcified case is around 500 rad/s; it shows a significant increase in the vorticity magnitude compared to that of point P_1. Most importantly, the peak shifts towards the left so

that the maximum vorticity magnitude for point P_2 occurs at around $t = 0.09$ s. At point P_3 (shown in Figure 3.14 c), the vorticity magnitude significantly increases compared to points P_1 and P_2. For the severely calcified case, the vorticity magnitude at point P_3 is around 1000 rad/s; two times larger than that of points P_1 and P_2. According to Figure 3.14 c, the vorticity magnitude near the coronary ostia are larger than near the leaflets (shown in Figure 3.14 a) for the severely calcified case. It is implied that more energy is consumed by the main vortex near the coronary ostia because of the calcification. As a result the hemodynamic parameters inside the coronary arteries are influenced.

The AWSS at the wall of the coronary artery during the cardiac cycle are shown in Figure 3.15. As seen, the AWSS significantly increases from 0.12 Pa to 1.16 Pa at the earlier diastole along the left wall of the coronary arteries. For the right wall, the AWSS shows a significant increase from around 0.023 Pa to 0.45 Pa. It is worth mentioning, the smaller wall shear stress at the right wall of the coronary artery can be a reason for initiation of the coronary artery stenosis and atherosclerosis plaque progression.

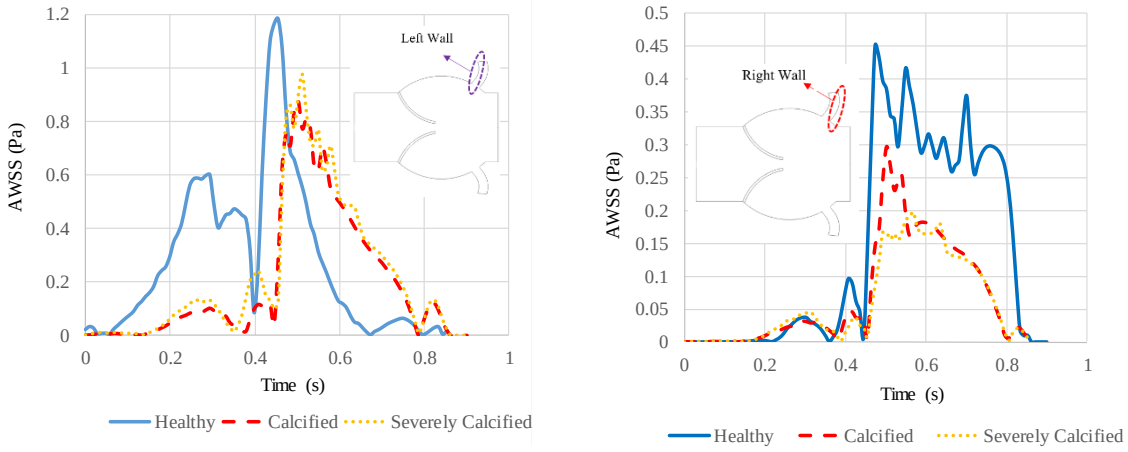

(a) (b)

Figure 3.15 Time-averaged wall shear stress on the wall of the coronary artery (a) left wall (b) right wall.

3.7 Conclusion

In this study the effect of calcification of the aortic valve leaflets on hemodynamic parameters inside the aortic root and coronary arteries was investigated. To do this, 2D models of healthy, calcified, and severely calcified aortic valves were developed in ANSYS Fluent and ANSYS Mechanical based on the echocardiography images available in the literature. Results revealed that calcification has significantly changed the hemodynamic parameters inside the aortic root and the coronary arteries, in particular:

- The transvalvular pressure gradient increases from 792 Pa (~ 6 mmHg) for a healthy aortic valve to 2885 Pa (~ 22 mmHg) for a severely calcified one.
- The aortic orifice diameter decreases from 14.2 mm for a healthy aortic valve to 8.2 mm for a severely calcified one. This leads to insufficient blood ejection during the cardiac cycle, and heart failure over time.

- The aortic valve calcification has an impact on recirculation zones within the aortic root. Results show that the structure of the vortices generated in the sinuses of the calcified aortic valve with a smaller valve orifice diameter are more complicated compared to those of a healthy case. The vortices inside the sinus cavity for the calcified valve are a combination of a strong counter-clockwise vortex with several smaller clockwise vortices; in comparison for the healthy case a dominant counter-clockwise vortex occupies the whole sinus cavity. These abnormal vortical structures lead to blood flow stagnation within the sinuses and progression of calcium deposition.
- The aortic valve calcification also has a significant impact on the wall shear stress on the fibrosa and ventricular layers of the aortic valve leaflets. This difference between the wall shear stress of the ventricular and fibrosa layers of the aortic valve can be a reason for progression of calcification.

Based on the results obtained from the coupled fluid-structure model, calcification not only changes the hemodynamic parameters inside the aortic root, but also has a significant influence on flow features inside the coronary arteries. Generally, calcification causes a significant reduction of the flow rate inside the coronary arteries. Obtained results show that the maximum velocity inside the coronary arteries decreases from 1 m/s for the healthy valve to 0.45 m/s for the severely calcified case at early diastole. Based on the results, calcification significantly decreases the wall shear stress of the coronary arteries; this reduction in the wall shear stress is a possible reason for initiation of the coronary atherosclerosis process and eventually results in coronary stenoses.

3.8 Limitations

We are dealing with a complicated model, and consequently a number of assumptions and simplifications have been employed: an idealised 2D geometry of the aortic root, sinuses, and leaflets are considered instead of 3D tricuspid leaflets since we are investigating the global dynamic behaviour of the leaflets. The arterial walls have been considered solid compared to the natural arterial walls which have a complex multilayered structure in which the Young's modulus of the walls are a function of blood pressure. The tissue of the leaflets are simplified to be linear elastic and isotropic to provide computational stability compared to real tissues which have nonlinear, anisotropic, viscoelastic and hyperplastic material properties. The varying thickness of the leaflets are not taken into account, i.e. the thickness of the leaflets is assumed to be constant, while they are naturally thicker in the line of the attachment and thinner in the belly (Mohammadi et al. 2015).

3.9 References

[1] A.H. Rapp, R.A. Lange, J.E. Cigarroa, E.C. Keeley, L.D. Hillis, Relation of pulmonary arterial diastolic and mean pulmonary arterial wedge pressures in patients with and without pulmonary hypertension, The American Journal of Cardiology, 88 (2001) 823-824.
[2] P. Kvidal, R. Bergström, L.G. Hörte, E. Ståhle, Observed and relative survival after aortic valve replacement, Journal of the American College of Cardiology, 35 (2000) 747-756.
[3] D. Garcia, P. Pibarot, C. Landry, A. Allard, B. Chayer, J. Dumesnil, L.G. Durand, Estimation of aortic valve effective orifice area by Doppler echocardiography: effects of valve inflow shape and flow rate, Journal of American Society of Echocardiography, 17 (2004) 756-765.
[4] S. Shadden, M. Astorino, J.F. Gerbeau, Computational analysis of an aortic valve jet with Lagrangian coherent structures, Chaos, 20 (2010).
[5] C.M. Otto, B. Prendergast, Aortic valve stenosis-from patients at risk to severe valve obstruction, The New England Journal of Medicine, 371 (2014) 744-756.

[6] J. Davies, K.H. Parker, D.P. Francis, A.D. Hughes, What is the role of the aorta in directing coronary blood flow, Heart, 94 (2008) 1545-1547.
[7] M.F. O'Rourke, How stiffening of the aorta and elastic arteries leads to compromised coronary flow, Heart, 94 (2008) 690-691.
[8] D. Garcia, P.G. Camici, L.-G. Durand, K. Rajappan, E. Gaillard, O.E. Rimoldi, P. Pibarot, Impairment of coronary flow reserve in aortic stenosis, Journal of Applied Physiology, 106 (2009) 113-121.
[9] C.J. Hartley, A.K. Reddy, L.H. Michael, M.L. Entman, V. Chintalagattu, A.Y. Khakoo, G.E. Taffet, Coronary flow reserve in mice: effects of age, coronary disease, and vascular loading, Conference Proceeding IEEE Engineering Medical Biological Society, (2010) 3780-3783.
[10] A. Nemes, T. Forster, I. Ungi, V. Nagy, A. Vass, A. Pálinkás, A. Varga, M. Csanády, The coronary flow velocity reserve measured by stress transoesophageal echocardiography evaluates the success of coronary interventions-results of a 5 year follow-up, Scandinavian Cardiovascular Journal, 39 (2005) 286-292.
[11] H. Maleki, Structural and fluid-structure interaction analysis of stenotic aortic valves: application to percutaneous aortic valve replacement, Thesis, (2010) Concordia University.
[12] K.S. Cunningham, A.I. Gotlieb, The role of shear stress in the pathogenesis of atherosclerosis, Laboratory Investigation, 85 (2005) 9-23.
[13] K.L. Gould, N.P. Johnson, Imaging coronary blood flow in AS: let the data talk, again, Journal of the American College of Cardiology, 67 (2016) 1423-1426.
[14] M. Michail, J.E. Davies, J.D. Cameron, K.H. Parker, A.J. Brown, Pathophysiological coronary and microcirculatory flow alterations in aortic stenosis, Nature Reviews Cardiology, 15 (2018) 420–431.
[15] I. Sathyamurthy, S. Alex, Calcific aortic valve disease: Is it another face of atherosclerosis, Indian Heart Journal, 67 (2015) 503–506.
[16] H. Hatoum, A. Yousefi, S. Lilly, P. Maureira, J. Crestanello, L. P.Dasi, An in vitro evaluation of turbulence after transcatheter aortic valve implantation, The Journal of Thoracic and Cardiovascular Surgery, 156 (2018) 1837-1848.
[17] H. Hatoum, L.P. Dasi, Spatiotemporal complexity of the aortic sinus vortex as a function of leaflet calcification, Annals of Biomedical Engineering, 47 (2019) 1116-1128.
[18] M. Bianchi, G. Marom, R.P. Ghosh, O.M. Rotman, P. Parikh, L. Gruberg, D. Bluestein, Patient-specific simulation of transcatheter aortic valve replacement: impact of deployment options on paravalvular leakage, Biomechanics and Modeling in Mechanobiology, 18 (2019) 435–451.
[19] K. Lavon, G. Marom, M. Bianchi, R. Halevi, A. Hamdan, A. Morany, E. Raanani, D. Bluestein, R. Haj-Ali, Biomechanical modeling of transcatheter aortic valve replacement in a stenotic bicuspid aortic valve: deployments and paravalvular leakage, Medical & Biological Engineering & Computing, 57 (2019) 2129-2143.
[20] A. Nemes, T. Forster, M. Csanády, Relationship between coronary flow velocity reserve and aortic stiffness, The American Journal of Physiology: Heart and Circulatory Physiology, 290 (2006) H1311.
[21] L.P. Dasi, H. Hatoum, B.L. Moore, On the significance of systolic flow waveform on aortic valve energy loss, Annals of Biomedical Engineering, 46 (2018) 2102–2111.
[22] O.M. Rotman, B. Kovarovic, M. Bianchi, M.J. Slepian, D. Bluestein, In vitro durability and stability testing of a novel polymeric transcatheter aortic valve, Biomedical Engineering, 66 (2020) 190-198.
[23] R. Gnyaneshwar, R.K. Kumar, K.R. Balakrishnan, Dynamic analysis of the aortic valve using a finite element model, The Annals of Thoracic Surgery, 73 (2002) 1122-1129.
[24] S. Smith, S. Austin, G.D. Wesson, C.A. Moore, Calculation of wall shear stress in left coronary artery bifurcation for pulsatile flow using two-dimensional computational fluid dynamics, Conference Proceeding IEEE Engineering in Medicine and Biology Society, (2006) 871–874.

[25] A. Ranga, R. Mongrain, Y. Biadilah, R. Cartier, A compliant dynamic FEA model of the aortic valve, 12th IFToMM World Congress, Besançon (France), (2007).
[26] A. Ranga, O. Bouchot, R. Mongrain, R. Mongrain, R. Mongrain, Computational simulations of the aortic valve validated by imaging data: evaluation of valvesparing techniques, Interactive Cardiovascular and Thoracic Surgery, 5 (2006) 373–378.
[27] K. Kunzelman, R. Cochran, C. Chuong, W. Ring, E. Verrier, R. Eberhart, Finite element analysis of the mitral valve, Journal of Herat Valve Diseases, 2 (1993) 326-340.
[28] J.D. Hart, G. Peters, P.J.G. Schreurs, F.P.T. Baaijens, A three-dimensional computational analysis of fluid–structure interaction in the aortic valve, Journal of Biomechanics, 36 (2003) 103-112.
[29] J.D. Hart, G. Peters, P.J.G. Schreurs, F.P.T. Baaijens, Collagen fibers reduce stresses and stabilize motion of aortic valve leaflets during systole, Journal of Biomechanics, 37 (2004) 303-311.
[30] E.J. Weinberg, M.R.K. Mofrad, A multiscale computational comparison of the bicuspid and tricuspid aortic valves in relation to calcific aortic stenosis, Journal of Biomechanics, 41 (2008) 3482-3487.
[31] S. Katayama, N. Umetani, S. Sugiura, T. Hisada, The sinus of Valsalva relieves abnormal stress on aortic valve leaflets by facilitating smooth closure, Journal of Thoracic and Cardiovascular Surgery, 136 (2008) 1528-1535.
[32] S. Nobari, R. Mongrain, R. Leask, R. Cartier, The effect of aortic wall and aortic leaflet stiffening on coronary hemodynamic: a fluid–structure interaction study, Medical & Biological Engineering & Computing, 51 (2013) 923–936.
[33] K. Cao, P. Sucosky, Aortic valve leaflet wall shear stress characterization revisited: impact of coronary flow, Journal of Computer Methods in Biomechanics and Biomedical Engineering, 20 (2017) 468-470.
[34] H.J. Kim, I.E. Vignon-Clementel, J.S. Coogan, C.A. Figueroa, K.E. Jansen, C.A. Taylor, Patient-specific modeling of blood flow and pressure in human coronary arteries, Annals of Biomedical Engineering, 38 (2010) 3195–3209.
[35] H. Mohammadi, R. Cartier, R. Mongrain, Derivation of a simplified relation for assessing aortic root pressure drop incorporating wall compliance, Medical & Biological Engineering & Computing, 53 (2015) 241–251.
[36] A. Amindari, L. Saltikb, K. Kirkkoprua, M. Yacoubc, H.C. Yalcind, Assessment of calcified aortic valve leaflet deformations and blood flow dynamics using fluid-structure interaction modeling, Informatics in Medicine Unlocked, 9 (2017) 191-199.
[37] H. Maleki, S. Shahriari, L.G. Durand, M.R. Labrosse, L. Kadem, A metric for the stiffness of calcified aortic valves using a combined computational and experimental approach, Medical & Biological Engineering & Computing, 52 (2014) 1-8.
[38] F.R. Menter, Two-equation eddy-viscosity turbulence models for engineering applications, AIAA Journal 32 (1994) 1598–1605.
[39] A.J. Pappano, W.G. Wier, Cardiovascular physiology, Mosby physiology monograph series, Elsevier, Philadelphia, (2007) 10th Edition.
[40] F.K. Benra, H.J. Dohmen, J. Pei, S. Schuster, B. Wan, A comparison one-way and two-way coupling methods for numerical analysis of fluid-structure interactions, Journal of Applied Mathematics (2011) Article ID 853560.
[41] M.A. Fernández, J.F. Gerbeau, Algorithms for fluid-structure interaction problems, Journal of Cardivascular Mathematics, 1 (2009) 307-346.
[42] D. Garcia, P. Pibarot, Louis-GillesDurand, Analytical modeling of the instantaneous pressure gradient across the aortic valve, Journal of Biomechanics, 38 (2005) 1303-1311.
[43] E.J. Keller, S.C. Malaisrie, J. Kruse, P.V. Ooij, E. Semaan, P. McCarthy, J.C. Carr, M. Markl, A.J. Barker, J.D. Collins, Restoration of physiologic hemodynamics in the ascending aorta following aortic valve replacement: a 4D flow MR study, Journal of Cardiovascular Magnetic Resonance, 18 (2016) P346.

[44] M.W. Weston, D.V. LaBorde, A.P. Yoganathan, Estimation of the shear stress on the surface of an aortic valve leaflet, Annals of Biomedical Engineering, 27 (1991) 572–579.

Chapter 4

Effect of the locations of the coronary artery ostia on aortic valve hemodynamics

In Chapter 3, the effect of the stenosis of aortic valve on the hemodynamic parameters inside the coronary arteries was investigated. It was shown that stenosis of the aortic valve not only changes the hemodynamic parameters inside the aortic root, but also impacts on the coronary artery flow and accordingly the wall shear stress on the coronary artery wall. It was also found that the variation of the wall shear stress on the coronary artery wall is one possible reason for initiation of coronary artery atherosclerosis.

Echocardiography images of the aortic valve and coronary angiographic images show that the locations of the coronary artery ostia vary among different patients. Some have coronary artery ostia initiating from a point proximal to the aortic valve, while others have coronary artery ostia distal from the aortic valve. Furthermore, clinical data shows that a considerable proportion of patients who undertook aortic valve replacement (mainly transcatheter aortic valve replacement) died after two years. The cause of this high death rate is still unknown. It is believed that it can be related to diet, the geometrical properties of the coronary arteries and aortic valve, hemodynamic variation inside the aortic root, and coronary artery obstruction generated due to the presence of a stent in transvalvular aortic valve replacement (TAVR). This chapter investigates the effect of the locations of the coronary artery ostia on the aortic valve hemodynamics in order to provide an answer to the following research question which is the second objective of this project: *whether the locations of the coronary artery ostia and shape of the sinus in different patients can affect transvalvular pressure gradient and accordingly lead to the initiation of aortic valve stenosis?*

In this chapter, fluid structure interaction models of the aortic valve leaflets considering different locations of the coronary artery ostia (proximal, middle, and distal) and different diameters of the sinus (D_{sinus} = 25, 20.8, and 17.6 mm) are developed. The transvalvular pressure gradients of aortic valves with proximal, middle and distal coronary artery ostia are calculated and compared. It is revealed that the transvalvular pressure gradient is highly dependent on the location of the coronary artery ostia. Furthermore, the effect of aortic valve stenosis on the coronary artery flow for patients with proximal, middle, and distal coronary artery ostia is studied. It is found that patients with proximal coronary ostia and severely calcified valves witness lower coronary artery flow at peak systole compared to those with distal and middle coronary artery ostia.

Details of the methodology, supporting evidence and data are presented and explained in this chapter which consists of the published journal article:

Araz. R. Kivi, Nima Sedaghatizadeh, Benjamin S. Cazzolato, Anthony C Zander, Adam J. Nelson, Ross Roberts-Thomson, Ajit Yoganathan, Maziar Arjomandi, Hemodynamics of a stenosed aortic valve: Effects of the geometry of the sinuses and the positions of the coronary ostia, International Journal of Mechanical Sciences, 188, 2020, 106015.

Statement of Authorship

Title of Paper	Hemodynamics of a stenosed aortic valve: Effects of the geometry of the sinuses and the positions of the coronary ostia
Publication Status	☑ Published ☐ Accepted for Publication ☐ Submitted for Publication ☐ Unpublished and Unsubmitted work written in manuscript style
Publication Details	Araz. R. Kivi, Nima Sedaghatizadeh, Benjamin S. Cazzolato, Anthony C Zander, Adam J. Nelson, Ross Roberts-Thomson, Ajit Yoganathan, Maziar Arjomandi, Hemodynamics of a stenosed aortic valve: Effects of the geometry of the sinuses and the positions of the coronary ostia, International Journal of Mechanical Sciences, 188, 2020, 106015.

Principal Author

Name of Principal Author (Candidate)	Araz R. Kivi		
Contribution to the Paper	Developed Ideas and Concepts • Conducted a comprehensive literature review • Developed the ideas and concepts based on the gaps of the knowledge in the field Performed the Modelling • Developed an aortic valve model in ANSYS workbench software • Developed an appropriate udf code to defined boundary conditions • Simulated the dynamic behaviour of the aortic valve leaflets • Validated the simulated model with the experimental data Interpreted Results • Extracted raw data from simulation • Post processed the data using CFD post and MATLAB • Developed a MATLAB code to extract the averaged data • Interpreted the results and compared them with the experimental results Wrote the Manuscript • Solely developed first full draft of the manuscript • Applied comments given by co-authors • Responsible for revising the manuscript after review • Acted as the corresponding author		
Overall percentage (%)	80%		
Certification:	This paper reports on original research I conducted during the period of my Higher Degree by Research candidature and is not subject to any obligations or contractual agreements with a third party that would constrain its inclusion in this thesis. I am the primary author of this paper.		
Signature		Date	29/01/2021

Co-Author Contributions

By signing the Statement of Authorship, each author certifies that:

iv. the candidate's stated contribution to the publication is accurate (as detailed above);

v. permission is granted for the candidate in include the publication in the thesis; and

vi. the sum of all co-author contributions is equal to 100% less the candidate's stated contribution.

Name of Co-Author	Nima Sedaghatizadeh		
Contribution to the Paper	Supervised the work, participated in developing ideas, and provide feedback on the manuscript.		
Signature		Date	29/01/2021

Name of Co-Author	Benjamin S. Cazzolato		
Contribution to the Paper	Supervised the work, participated in developing ideas, and evaluated the manuscript.		
Signature		Date	29/01/2021

Name of Co-Author	Anthony C Zander		
Contribution to the Paper	Supervised the work, and provide feedback on the manuscript.		
Signature		Date	16/02/2021

Name of Co-Author	Adam J Nelson		
Contribution to the Paper	Participated in developing ideas and evaluated the manuscript.		
Signature		Date	08/02/2021

Name of Co-Author	Ross Roberts-Thomson		
Contribution to the Paper	Participated in developing ideas, and provide feedback on the manuscript.		
Signature		Date	08/02/2021

Name of Co-Author	Ajit Yoganathan		
Contribution to the Paper	Evaluated the manuscript.		
Signature		Date	29/01/2021

Name of Co-Author	Maziar Arjomandi		
Contribution to the Paper	Supervised the work, participated in developing ideas, and provide feedback on the manuscript.		
Signature		Date	29/01/2021

Please cut and paste additional co-author panels here as required.

Hemodynamics of a stenosed aortic valve: effects of the geometry of the sinuses and the positions of the coronary ostia

Araz R. Kivi, Nima Sedaghatizadeh, Benjamin S. Cazzolato, Anthony C. Zander, Adam J. Nelson, Ross Roberts-Thomson, Ajit Yoganathan, Maziar Arjomandi

4.1 Abstract

Aortic valve stenosis is one of the most prevalent cardiovascular disease among adults worldwide. Stenosis of the aortic valve changes the hemodynamic parameters inside the aortic root which perpetuates aortic valve calcification and has been associated with the development of coronary artery atherosclerosis. Invasive studies have revealed that the geometry of the sinuses, as well as the locations of the coronary artery ostia, impact coronary blood flow hemodynamics, which has been associated with the development of coronary artery disease. The aim of this study is to elucidate this observed phenomenon, in which geometrical variations inside the aortic root and malfunctioning of the aortic valve because of the calcification not only affect the progression of the calcification but also lead to initiation of coronary artery atherosclerosis. A 2D fluid structure interaction model of the aortic valve was developed and simulated in ANSYS Fluent based on available echocardiography images in the literature. The model incorporates fluid structure interaction and employs the k-ω Menter's Shear Stress Transport (SST) turbulence model for the turbulent flow downstream of the leaflets. The effects of various diameters of the sinuses 25, 20.8, and 17.6 mm and positions of the coronary artery ostia (proximal, middle, and distal) on aortic root hemodynamics were investigated and parameters including transvalvular pressure gradient, valve orifice diameters, maximum jet velocity along the valve orifice area, and wall shear stresses on leaflets calculated. Results demonstrate that a severely calcified valve with the proximal coronary artery ostia witnesses a much higher transvalvular pressure gradient (approximately 10 times larger) compared to that for a healthy case. Moreover, the presence of the proximal coronary artery ostia for valves with diameters of the sinus 25 and 20.8 mm results in the reduction of the coronary blood flow and increase of the probability of coronary artery atherosclerosis.

4.2 Introduction

Stenosis of the aortic valve is the most common form of valvular heart disease among adults and frequently coexists with coronary artery disease [1]. Invasive investigations have demonstrated that the prevalence of coronary artery disease increases in the presence of aortic valve stenosis such that over half of all patients with aortic valve stenosis require simultaneous coronary bypass during aortic valve surgery [2]. Stenosis of the aortic valve occurs when calcium deposits on the aortic valve leaflets over time (shown in Figure 4.1 c). Calcium deposition changes the material properties and geometry of the leaflets and affects their functionality during the cardiac cycle which leads to heart failure over time [3-6]. Clinical studies revealed that calcification of the aortic valve not only affects the hemodynamics inside the aortic root such as the transvalvular pressure gradient, the valve orifice area, and the wall shear stress on both sides of the leaflets, but also changes the coronary blood flow hemodynamics, specifically the shear stress on the wall of the coronary arteries [7-9]. Variation of the wall shear stress on the leaflets can, in turn, intensify calcification formation on the leaflets which perpetuates stenosis over time. Furthermore, shear stress variation on the walls of the coronary arteries leads to initiation and progression of atherosclerosis and eventually

results in coronary stenosis [10-13]. The schematic view of the positions of the aortic valve, coronary arteries, and stenosis of the aortic valve and coronary arteries are shown in Figure 4.1 (a-d), respectively.

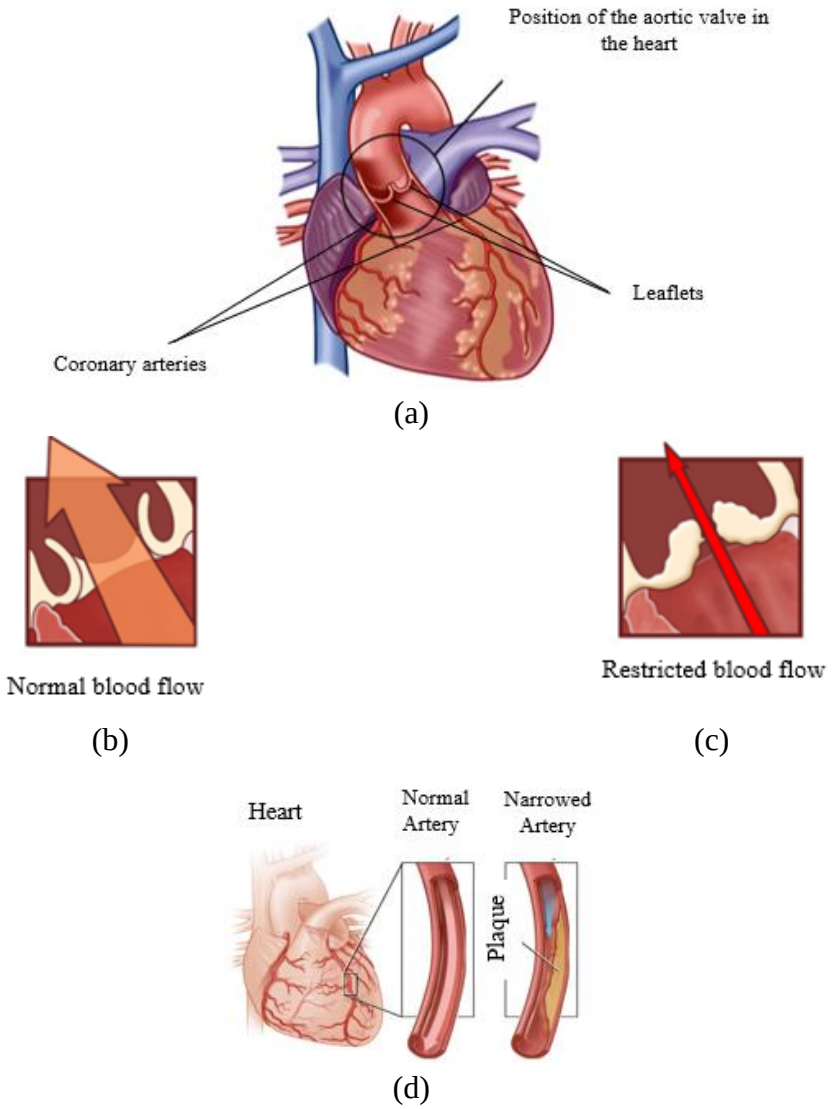

Figure 4.1 Schematic view of the (a) heart and position of the aortic valve (b) normal aortic valve with normal blood flow(c) calcified aortic valve with restricted blood flow (d) plaque progression and coronary artery stenosis [14].

Invasive investigations also demonstrated that the wall shear stress plays a significant role in the initiation of atherosclerosis within the coronary arterial wall and the progression of the calcium deposition on the leaflets. Calcification and atherosclerosis are, however, complex multifactorial processes which remain incompletely understood [9, 15-17]. It is believed that blood flow-induced shear stress affects the endothelial cells leading to endothelial dysfunction, inflammatory responses, oxidative stress which remodels the artery wall and valve structure and eventually results in progression of calcification and initiation of atherosclerosis [18-21].

During the recent decades, researchers have numerically simulated pathologies of the aortic valve and coronary artery [22-29]. Nobari et al. [23] investigated the effect of aortic valve stenosis on coronary flow hemodynamics using fluid structure interaction (FSI) modelling. They found that the coronary flow rate decreases considerably when the thickness

of the leaflets was approximately doubled. However, the presented model has ignored the tapered shape of coronary arteries. To improve the previous model, Mohammadi et al. [24] presented an FSI model of the aortic valve incorporating a tapered coronary artery wall. In the aforementioned studies the influence of leaflet stiffening due to calcification on the aortic root hemodynamics has not been examined. Following this study, Amindari et al. [22] presented a 2D FSI model of the aortic valve in which the effect of calcification of the aortic valve on the aortic root hemodynamics was studied. However, the presented model did not include the coronary artery flow nor its effect on hemodynamic variations inside the aortic root. They showed that calcification of the aortic valve leaflets leads to a significant increase in the transvalvular pressure gradient (increasing from 633 Pa for the healthy aortic valve to 2559 Pa for the severely calcified case).

In addition to numerical simulations, researchers have also performed experimental investigation of the flow behaviour inside the aortic root and coronary arteries as well as its effects on hemodynamic parameters in the presence of pathologies of the aortic valve [18, 21, 30-35]. Moore et al. [30] studied the flow behaviour inside coronary and non-coronary sinuses using particle imaging velocimetry (PIV) techniques. They showed that leaflets corresponding to coronary sinuses open 10% more compared to that of non-coronary ones. Furthermore, they demonstrated that the presence of coronary flow decreases the wall shear stress on the leaflet cusps while increasing the washout time during the cardiac cycle. The flow patterns in sinuses following transcatheter aortic valve replacement for various patients was studied by Hatoum et al. [21]. They found that washout time is strongly dependent on the valve structure and patient-specific morphologies. Furthermore, they showed that the dynamics of the sinus flow is a function of the aortic root characteristics. Another work published by the same group [18] investigated the effect of calcification of the aortic valve on hemodynamic variations inside the aortic root in the absence of coronary arteries. They found that initiation and formation of vortices in sinuses are highly sensitive to the amount of calcium deposition on the leaflets. Furthermore, the mildly calcified aortic valve experiences higher wall shear stress on the leaflets and therefore lower probability of calcium deposition compared to that of the severely calcified case. Although numerical and experimental investigations have been conducted on aortic valve pathologies during recent years, to the authors' knowledge the impact of different locations of the coronary artery ostia as well as the diameter of the sinus cavity on the hemodynamic parameters inside the aortic root and coronary arteries in the presence of calcification remains unknown.

The study presented here, was carried out to develop an understanding of the effect that the locations of the coronary artery ostia and the shape of the sinus of Valsalva on the hemodynamic characteristics of the aortic root and coronary arteries in the presence of calcification. A 2D FSI model of a healthy aortic valve was developed in ANSYS Workbench 19.1 based on the echocardiography images available in the literature. Fluid structure interaction modelling was utilised to capture the interaction between the blood flow and the leaflets. To capture the nature of the turbulence flow downstream of the leaflets, the k-ω SST turbulent model was used. The effect of calcification on the coronary artery and the aortic root hemodynamics was investigated for a range of diameters of the sinus (D_{sinus}= 25, 20.8, and 17.6 mm) and three different locations of the coronary artery ostia (proximal, middle, and distal). Results revealed that decreasing the diameter of the sinuses and changing the location of the coronary artery ostia results in significant changes in the hemodynamic parameters, not only inside the aortic root, but also within the coronary arteries.

4.3 Computational Model

A 2D FSI model of a healthy aortic valve (27 years of age) was developed in ANSYS Workbench 19.1 based on available echocardiography images in the literature [22]. The numerical model includes two different domains: structure (flexible leaflets) and fluid (blood flow) domains. The solution of the fluid part is based on the continuity and the Navier-Stokes equations as follows [36, 37]:

$$\rho\frac{\partial\overline{u_i}}{\partial t}+\rho(\frac{\partial\overline{u_i}\,\overline{u_j}}{\partial x_j})=-\frac{\partial P}{\partial x_i}+\eta\frac{\partial}{\partial x_j}(\frac{\partial u_i}{\partial x_j}+\frac{\partial u_j}{\partial x_i}-\frac{2}{3}\frac{\partial u_k}{\partial x_k}\delta_{ij}) \quad 4.1$$

in which ρ, u and P are respectively density, fluid velocity and pressure, and $\partial\overline{u_\iota}\overline{u_j}$ can be calculated based on the k-ω Menter's Shear Stress Transport (SST). The calculation for the structural component (namely mass, stiffness and damping matrices) is based on the following equation [36] which is solved using a finite element approach.

$$M.\ddot{\vec{u}}+C.\dot{\vec{u}}+K.\vec{u}=\vec{F} \quad 4.2$$

At the boundary between the fluid and solid domains, the fluid pressure and the displacement of the solid are exchanged using a two-way fluid-structure interaction modelling [38, 39]. The details of both domains are explained in the following sections.

4.3.1 Fluid domain (blood flow)

Figure 4.2 b shows the mesh of the developed model for a healthy aortic valve based on the echocardiography images shown in Figure 4.2 a. The different regions of the fluid domain including inlet, outlets (coronary and aorta), and blood flow are illustrated in Figure 4.2 c. The blood is considered as a Newtonian, isothermal, incompressible fluid with a constant viscosity and a density of 0.0035578 Pa.s and 1060 kg/m^3, respectively [24]. Although blood is inherently non-Newtonian, it has been reported that it can be considered as a Newtonian fluid in large arteries (diameter > 0.5 mm) where the Reynolds number is high and shear rate exceeds 100 s^{-1}[40-42]. The sweep method was used to generate an unstructured mesh for the fluid domain with around 10,000 prism elements (as depicted in Figure 4.2 b). As shown in Figure 4.2 b, the mesh near the artery wall and leaflets is denser in order to accurately model the boundary layers. A sensitivity analysis was carried out for both the pressure and velocity for two grid sizes (10,000 and 14,000). Based on the results, there is only 2% difference between the calculated parameters when the number of elements increases from 10,000 to 14,000. However, the computation time increased by about 40%. Therefore the 10,000 element model was considered of sufficient accuracy to be used for the remainder of the study reputed in this paper.

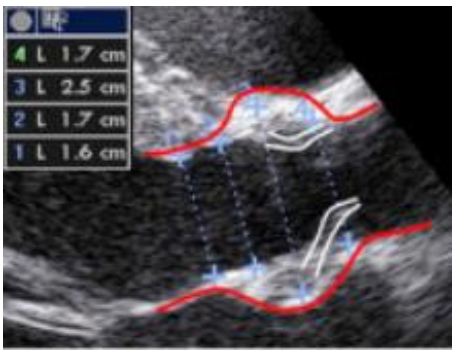

(a)

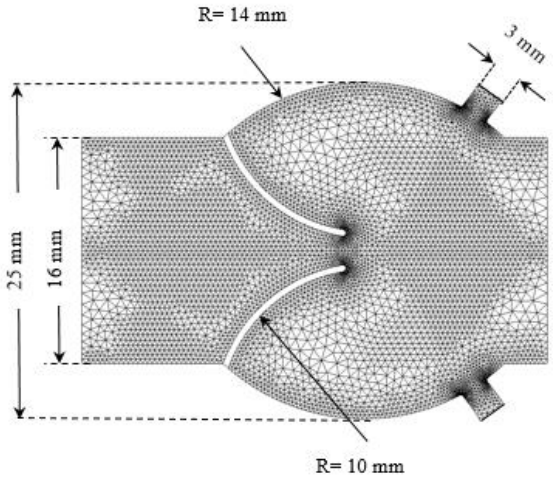

(b)

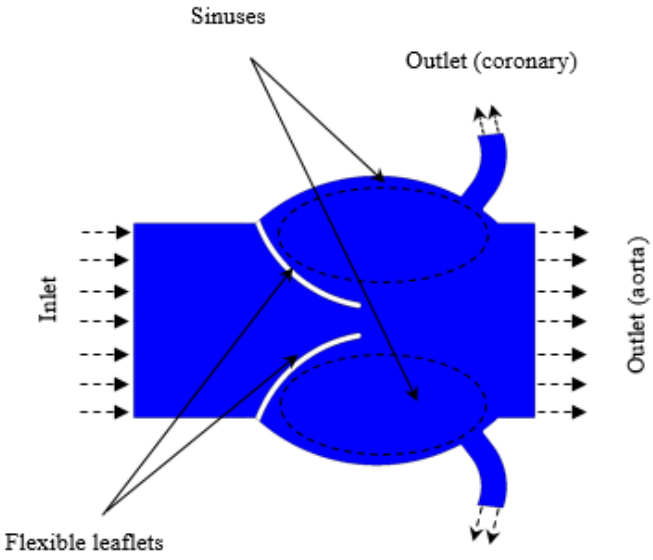

(c)

Figure 4.2 (a) Echocardiography images from a healthy aortic valve [22]; the shape of the sinuses and leaflets are traced using white and black solid lines, respectively. (b) Fluid domain mesh; denser meshes are generated near the wall and leaflets to improve the accuracy of the results (c) Healthy aortic valve with flexible leaflets, and boundary conditions; the sinuses specified by dash line, flow directions for the inlet and outlet are shown using dash-line arrows.

The computational grid was modified dynamically in order to accurately model the movement of the leaflets at every time step. The spring-based smoothing and re-meshing technique [22] was applied to remesh the fluid domain based on the instantaneous geometry of the leaflets at every time step. The *k-ω SST* turbulence model was used due to its capabilities in modelling turbulence generated by separation. Three sets of boundary conditions were defined in the fluid flow field. At the inlet (ventricular side), a time-dependent velocity profile (shown in Figure 4.3) was considered as the boundary condition. The transient velocity profile for the boundary condition at the inlet was obtained from the measured data (based on Doppler imaging) available in the literature [22]. At the coronary outlets, a transient pressure profile (based on the published data) and outflow were considered as the boundary condition (also

shown in Figure 4.3), which was obtained from clinical data of the average coronary flow [23, 43].

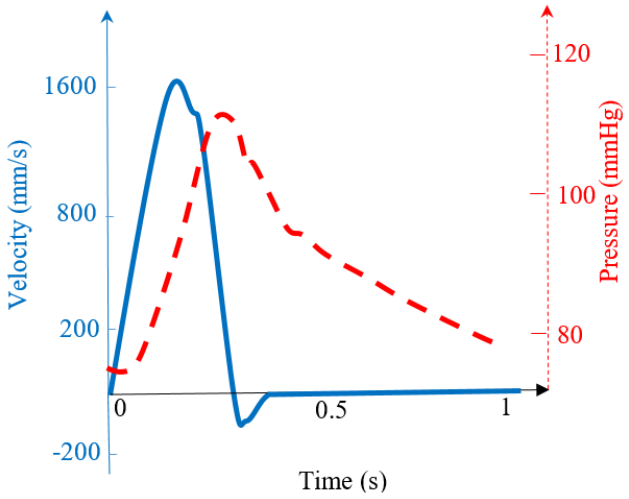

Figure 4.3 Inlet physiological velocity profile applied at the inlet plane of the model and transient pressure at coronary outlets. Based on measurements from [23].

4.3.2 Structural domain (flexible leaflets)

The structural analysis consists of two deformable leaflets which deform and move as they are exposed to blood flow. The leaflets were considered isotropic with a density, a Poisson ratio, and Young's modulus of 1060 kg/m^3, 0.3, and 2 MPa, respectively [44]. The Young's modulus of the mildly, moderately, and severely calcified cases were set to 5, 10, and 20 MPa, respectively [22, 44, 45]. To solve the equations of the dynamic motion of the leaflets, ANSYS Mechanical APDL was used based on the Newmark time integration method. The sweep method was used to generate the mesh for the leaflets using 120 tetrahedral elements. The mechanical properties of both fluid and structure domains, as well as the boundary conditions applied to the fluid domain, are presented in Table 4.1 and Table 4.2, respectively.

Table 4.1 Mechanical properties of the blood and leaflets domains used in the modelling [22, 23]

Domain	**Dynamic viscosity (Pa.s)**	**Density (kg/m^3)**	**Young's modulus (MPa)**	**Poisson's ratio**
Fluid (blood) Incompressible, Isothermal, Newtonian	0.0035578	1060	---	---
Structure (leaflets) Linear elastic, Isotropic	---	1060	2 (Healthy) 5 (Mildly Calcified) 10 (Moderately Calcified) 20 (Severely Calcified)	0.3

Table 4.2 Boundary conditions used in the modelling

	Inlet	**Outlet (coronary)**	**FSI surface**	**Walls**
Boundary conditions	Physiological velocity inlet	Physiological pressure outlet	Fluid structure interaction surface between the flexible elastic leaflets and blood flow	Solid walls for sinuses and aortic root

4.3.3 Two-way coupled FSI

In order to model the interaction between the fluid and structural domains, two methods are usually used by researchers: one-way coupling and two-way coupled methods [38]. As suggested by [36], the two-way coupled method is useful to model the interaction between the leaflets and blood flow because of the large deformation of the leaflets during the cardiac cycle. In the present study, the ANSYS coupling module was used to model the interaction between the flexible leaflets and the blood flow. To solve the continuity, Navier-Stokes, and turbulence equations for the fluid domain, the FLUENT module in ANSYS was used. In addition, to solve the equations related to deformation of the flexible leaflets, the Mechanical APDL was used in ANSYS. Then, at every time step, the data of the force and displacement were exchanged between the FLUENT and Mechanical APDL in order to capture the interaction between the structural and fluid domains.

4.4 Results

In this section, first, the model has been validated quantitatively and qualitatively against the recently published data. Then, the effect of the sinuses geometry, and position of the coronary ostia corresponding to a healthy, mildly, moderately, and severely calcified cases on hemodynamic parameters have been shown.

4.4.1 Validation

To quantitatively validate the present model, two hemodynamic parameters of the transvalvular pressure gradient (TPG) and average wall shear stress (AWSS) on the leaflets are compared against the published experimental data by Weston et al. [46] and Keller et al. [47]. The TPG_{max} and AWSS for the present study and previous experiments are reported in Table 4.3, where it can be seen that there is good agreement between the calculated parameters in this work and the experiments carried out by [46, 47].

Table 4.3 TPG_{max} and AWSS comparison between previous in-vivo experiments and current FSI modelling

	TPG_{max} (Pa)	AWSS (Pa)
Experimental results	799 [47]	3.8 [46]
Present work	791	4.5

To further validate the model, the results were qualitatively compared against recently published experimental data by Hatoum et al. [18]. Figure 4.4 provides a comparison of streamlines during systole between the present simulation and the data collected by the 2D PIV experiment. The developed model captures similar unsteady flow features in the sinuses to those observed in the PIV experiment. However, there is a small deviation observed between the experimental and current model, which can be explained by the existence of the coronary artery in the present model as well as different dimensions of the sinuses and diameter of the aortic valve.

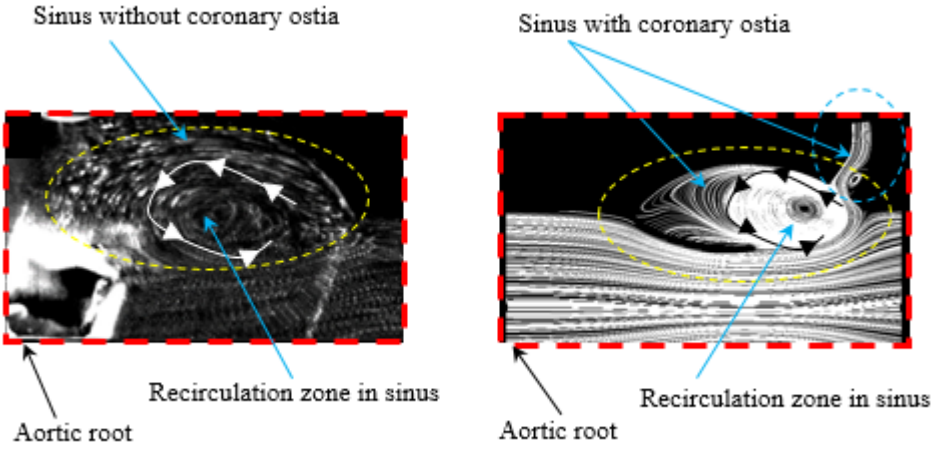

(a) (b)

Figure 4.4 Snapshot of the flow streamlines in sinuses around peak systole; a comparison of the flow streamlines in sinus between the (a) PIV experiment [18] and (b) present simulation. The radius of the sinus chamber and the diameter the aortic valve used in the aforementioned 2D PIV experiment are 19 mm and 23 mm, respectively.

4.4.2 Hemodynamic assessment

Velocity streamlines of a modelled healthy aortic valve with distal coronary ostia are depicted in Figure 4.5. As shown, the aortic valve opens during systole and allows blood flow through the aorta (shown in Figure 4.5 a-b). During the diastole phase, it closes to prevent blood from flowing back into the ventricle. During the closure period, blood flows into the coronary arteries in order to perfuse the myocardium (shown in Figure 4.5 d-e). The flow velocity in the aortic valve reaches to its peak value of 2.12 m/s, whilst the maximum velocity is 1.6 m/s at the inlet of the coronary artery; the results reveal that there is a lag between the peak velocity within the aortic valve and that of the coronary arteries. The valve orifice diameter is around 14.2 mm at mid systole (shown in Figure 4.5 b). As depicted, there are various recirculation zones in the sinuses and behind the leaflets during the cardiac cycle. At mid-systole, there are two different vorticities in the sinuses (shown with arrows in Figure 4.5 b). As illustrated in Figure 4.5 c-d, the vortices become larger from late-systole to mid-diastole, which results in a significant increase in the volume of the blood in the coronary arteries (shown in Figure 4.5 d). Due to the pressure difference between the left ventricle and the aorta, the location and the number of the vortices change during the cardiac cycle. As seen, there are four different vortices at mid-diastole: 1) A vortex near the tip of the leaflets (shown with black arrows in Figure 4.5 d), 2) A vortex attached to the wall of the sinuses (shown with dashed-circle in Figure 4.5 d), 3) A vortex attached to the belly of the leaflets (shown with red arrows in Figure 4.5 d) and 4) A vortex which is located near the base of the leaflets' ventricle side (shown with yellow arrows in Figure 4.5 d). It is observed that the presence of the vortices leads to high amplitude oscillations of the leaflets during the cardiac cycle, particularly at the diastole phases; it is implied that the vortices affect the dynamic motion of the leaflets.

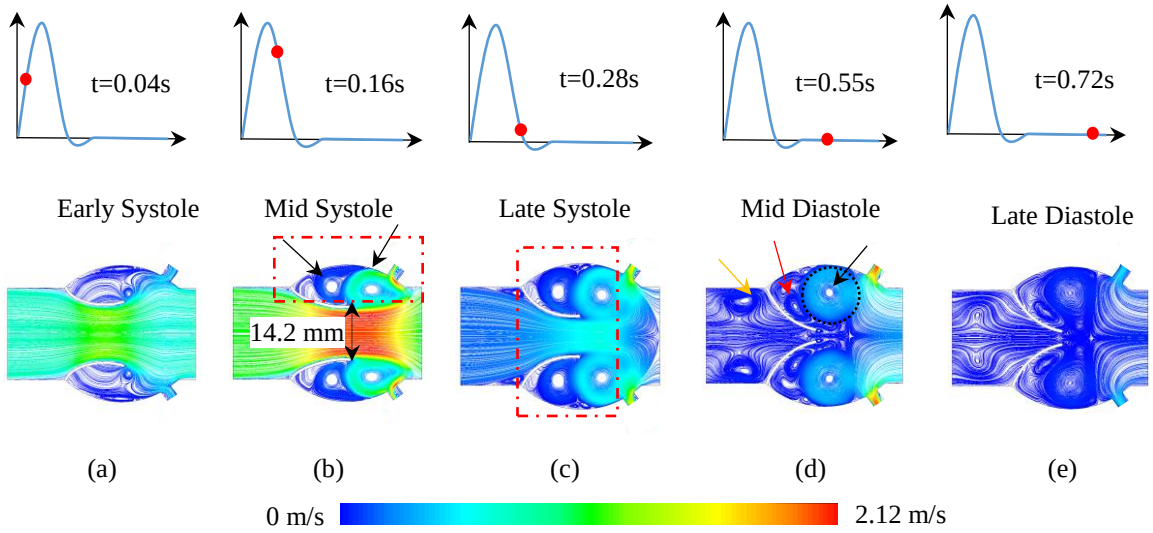

Figure 4.5 Velocity streamlines (a-e) for a healthy aortic valve during the cardiac cycle.

To investigate the effect of the location of the coronary ostia, as well as the degrees of calcification, velocity streamlines of mildly, moderately, and severely calcified aortic valves with different locations of coronary artery ostia are depicted in Figure 4.6 for the D_{sinus}= 25 mm. As shown in Figure 4.6 a-c, the maximum velocity along the aortic valve at mid systole increases from 1. 63 m/s for the mildly calcified aortic valve with distal coronary artery ostia to 2.35 m/s for the mildly calcified case with middle coronary artery ostia, and to 2.5 m/s for the mildly calcified cases with proximal coronary artery ostia. As seen, the presence of proximal coronary ostia in sinuses increases the pressure behind the leaflets and leads to about a 9% decrease in the valve orifice diameter for the mildly calcified model with distal coronary ostia when compared with the mildly calcified model with proximal coronary artery ostia.

To demonstrate the influence of the degree of calcification on the aortic root hemodynamics, velocity streamlines of moderately and severely calcified aortic valves with different locations of the coronary artery ostia are depicted in Figure 4.6 (d-f) and (g-i), separately. As shown, the velocity magnitudes of the moderately and severely calcified aortic valves with proximal coronary ostia reach 3.8 m/s and 4.6 m/s, respectively; in comparison with that of the mildly calcified case which is 2.5 m/s. This trend shows that there are approximately 52% and 84% increases in the velocity magnitude for the moderately and severely calcified cases, respectively. Furthermore, the valve orifice diameter for an aortic valve with proximal coronary artery ostia witnesses a decrease; dropping from 12.1 mm for the mildly calcified aortic valve to 10.01 mm and 9.48 mm for the moderately and severely calcified cases, respectively.

Moreover, the location of the coronary artery ostia modifies the flow features in the sinuses. As seen in Figure 4.6 (g-i), the number of vortices and their locations (shown with dashed-line in Figure 4.6 g-i) changes when the location of the coronary artery ostia is close to the left ventricle. Two additional vortices are formed in the sinuses, one near the wall of the sinus (shown with red arrows in Figure 4.6 h), and another close to the sinutubular junction (shown with black arrows in Figure 4.6 h). These vortices grow when the location of the coronary ostia is proximal to the left ventricle (comparing Figure 4.6 i-h), and affect the pressure behind the leaflets, ultimately resulting in a decrease in the valve orifice diameter. Another smaller vortex is also formed very close to the base of the leaflets (shown with yellow

arrow in Figure 4.6 g). This vortex does not allow the leaflets to move freely during the systole and can have an effect on the valve orifice diameter and the jet velocity along the aortic valve.

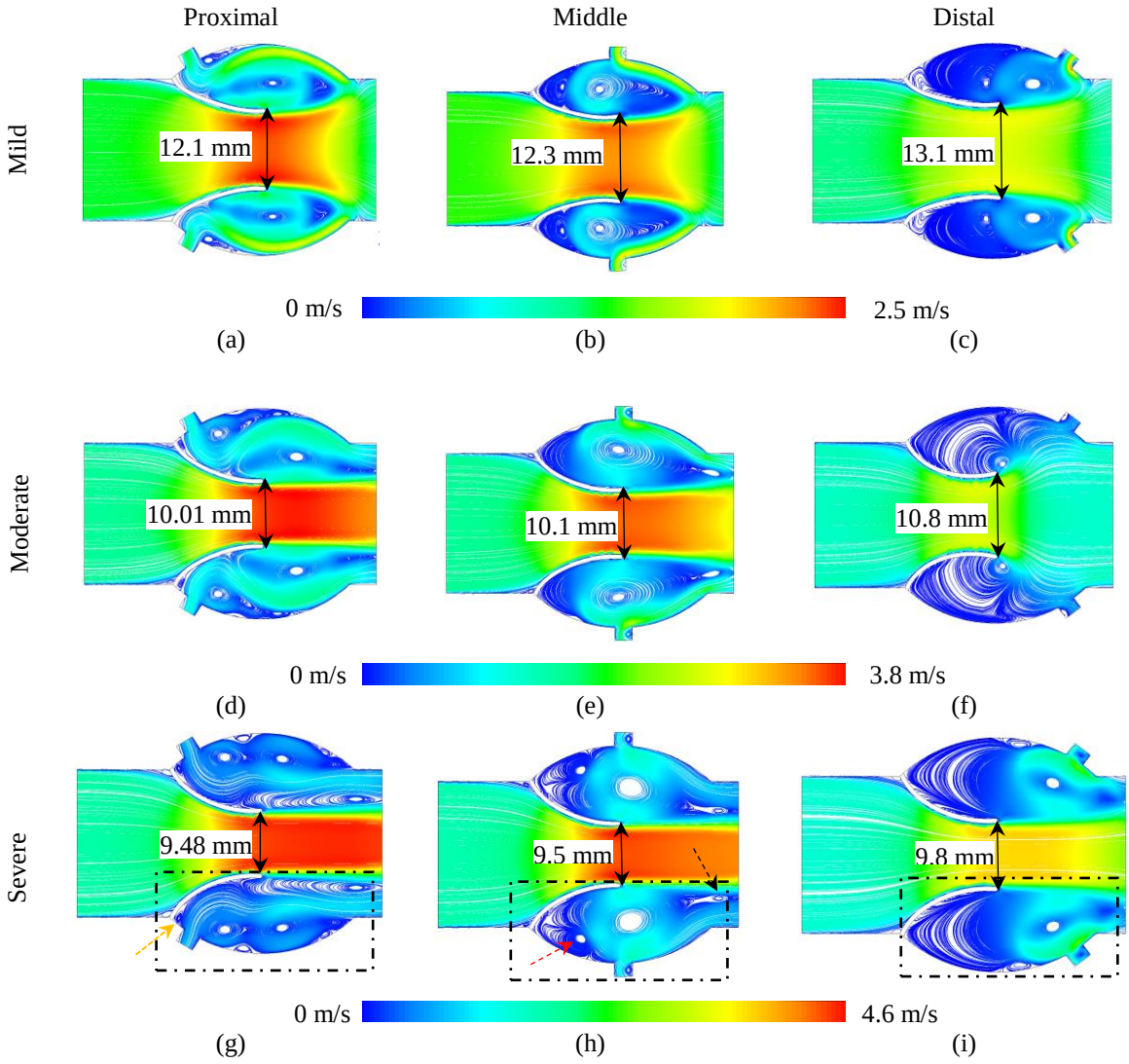

Figure 4.6 Velocity streamlines for mildly (a-c), moderately (d-f), and severely (g-h) calcified aortic valves during systolic phase with different locations of coronary ostia (proximal, middle, distal) and D_{sinus}=25 mm.

To show the effect of the shape of the sinuses on hemodynamic parameters, particularly the valve orifice diameter and the maximum jet velocity along the aortic valve, the velocity streamlines for the mildly, moderately, and severely calcified cases aortic valves are depicted in Figure 4.7 for different locations of the coronary artery ostia and D_{sinus}=23.8 mm. Comparison of Figure 4.6 and Figure 4.7 reveals that the jet velocity magnitude increases when the diameter of the sinuses decreases for all locations of the coronary artery ostia (proximal, middle, and distal). This can be explained by the pressure increase in the sinuses due to the decreased diameter of the sinuses. The increased pressure forces the leaflets and does not allow them to open properly. Ultimately, the valve orifice diameter decreases which leads to an increase in the jet velocity magnitude. The velocity magnitude increases from 4.6 m/s for the severely calcified aortic valve with proximal coronary artery ostia and D_{sinus}=25 mm to 4.81 m/s for that of with D_{sinus}=20.8 mm (an approximately 4% increase). Furthermore, the flow features inside the sinuses change, particularly for the moderately calcified aortic valve with

proximal coronary artery ostia as shown in the dash-line region in Figure 4.7 d. Four vortices are formed in the highlighted area which leads to a change in the flow features and the hemodynamic parameters inside the aortic root. The presence of the proximal coronary artery ostia leads to back flow into the sinuses. The back flow results in the formation of the vortices with different shapes and locations inside sinuses, corresponding to each of the coronary artery ostia positions.

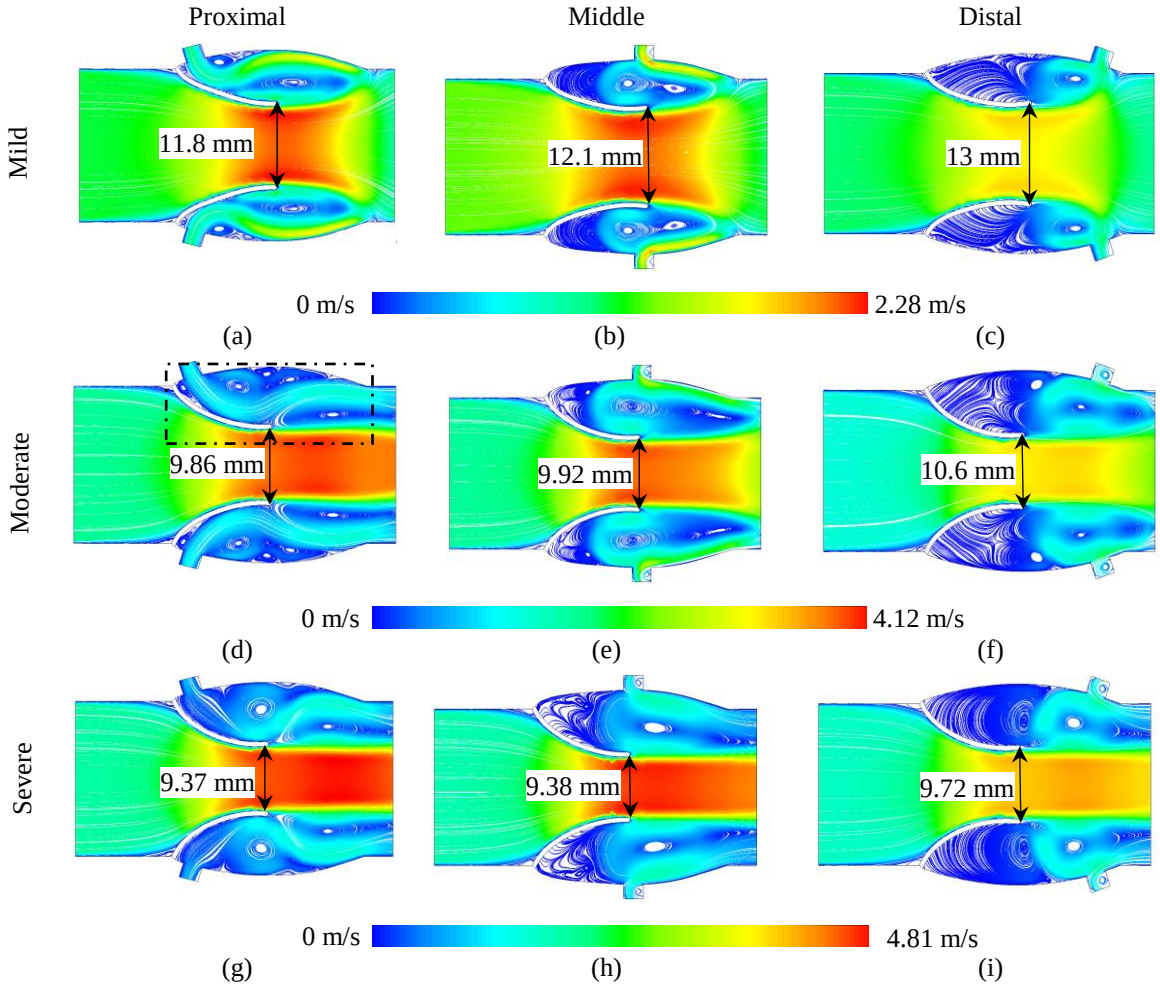

Figure 4.7 Velocity streamlines for mildly (a-c), moderately (d-f), and severely (g-h) calcified aortic valves during systolic phase with different locations of coronary ostia (proximal, middle, distal) and D_{sinus} =20.8 mm.

The effect of the diameter of the sinus on the velocity and valve orifice diameter of the mildly, moderately, and severely calcified cases are depicted in Figure 4.8 for D_{sinus} =17.6 mm. As shown, the velocity magnitude of the aortic valve with proximal coronary artery ostia and D_{sinus} =17.6 mm increases from 3.12 m/s for the mildly calcified aortic valve to 4.32 m/s for the moderately, and to 4.88 m/s for the severely calcified cases. The valve orifice diameter decreases from 11.7 mm for the mildly calcified case to 9.74 mm for the moderately, and to 9.28 for the severely calcified cases. However, the presence of the proximal coronary ostia in the sinuses forces the leaflets and does not allow them to open properly, increasing the velocity inside the coronary arteries which is able to decrease the probability of coronary artery diseases (as detailed in the Discussion section). This can be explained by more flow being pushed into the coronary artery by the leaflets as the diameter of the sinuses decreases and the coronary artery location becomes closer to the roots of the leaflets.

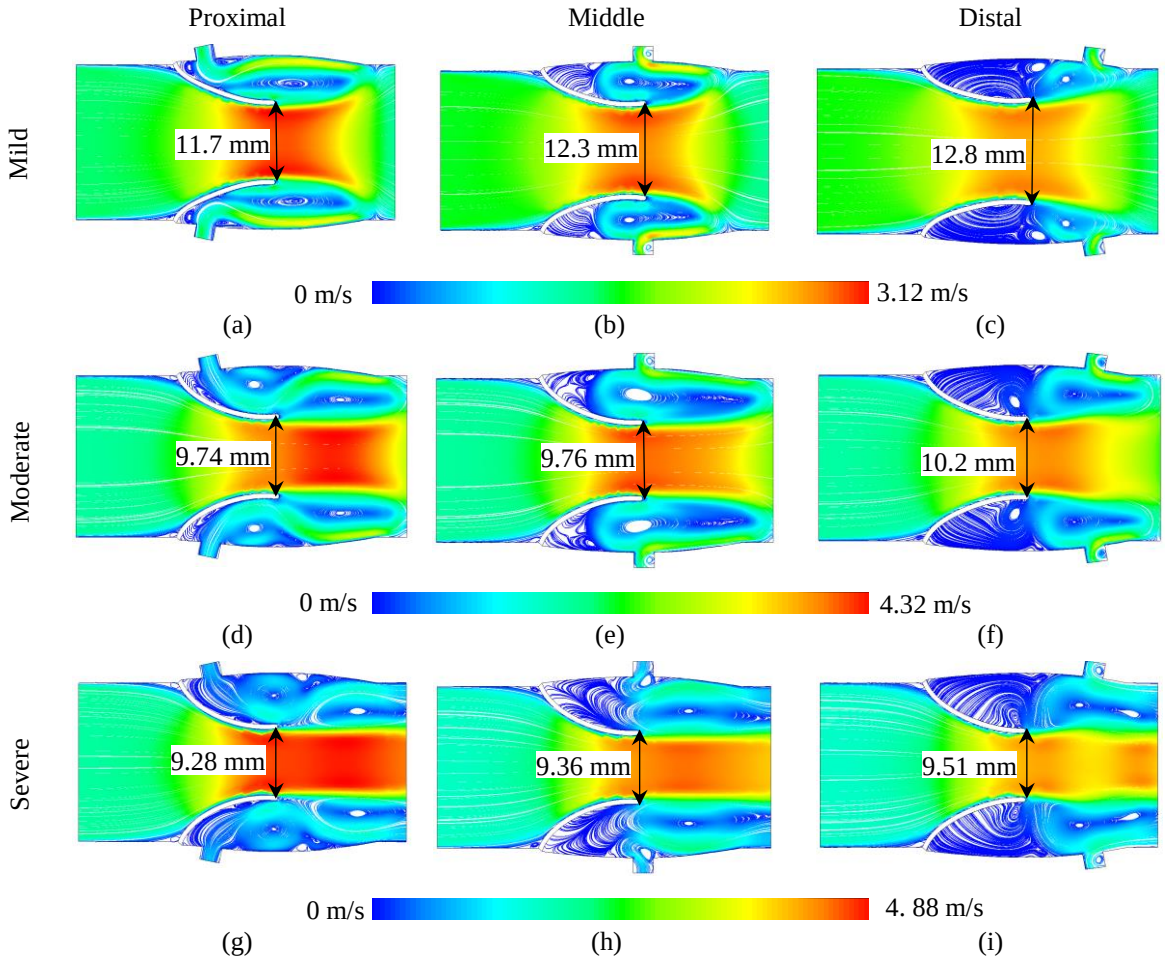

Figure 4.8 Velocity streamlines for mildly (a-c), moderately (d-f), and severely (g-h) calcified aortic valves during systolic phase with different locations of coronary ostia (proximal, middle, distal) and D_{sinus} =17.6 mm.

4.5 Discussion

The variation of the valve orifice diameter versus the velocity magnitude at a point located at the centre of aortic valve orifice for healthy, mildly, moderately, and severely calcified aortic valves with different locations of the coronary artery ostia (proximal, middle, and distal) and various diameters of the sinuses (D_{sinus}= 25, 20.8, and 17.6 mm) are illustrated in Figure 4.9. Generally, calcification decreases the valve orifice diameter and accordingly increases the velocity magnitude in the valve orifice area. Moreover, the calcified aortic valve with proximal coronary artery ostia witnesses a smaller valve orifice diameter and a higher velocity magnitude along the valve orifice; because of increased pressure behind the leaflets which forces the leaflets towards each other. Interestingly, the calcification affects the opening time of the aortic valve (as shown by comparison of the slope of the curves) such that the calcified valve has a shorter opening time compared to the healthy case (shown in Figure 4.9).

Based on the results, the location of the coronary ostia affects the stenosis process such that the aortic valve with proximal coronary ostia are more prone to become stenosed over time compared to the aortic valves with distal and middle coronary ostia. Furthermore, the diameter of the sinuses has an impact on the flow features and the hemodynamic parameters inside the sinuses. As shown in Figure 4.9, the valve orifice diameter decreases considerably when the diameter of the sinuses decreases (compare Figure 4.9 c with f and i); the lesser the diameter

of the sinuses (D_{sinus} =17.6 mm), the lesser the valve orifice diameter and the greater the jet velocity magnitude. From the aforementioned paragraphs, it can be concluded that patients with proximal coronary artery ostia and smaller diameter of the sinuses are more at risk of aortic valve stenosis and calcification formation.

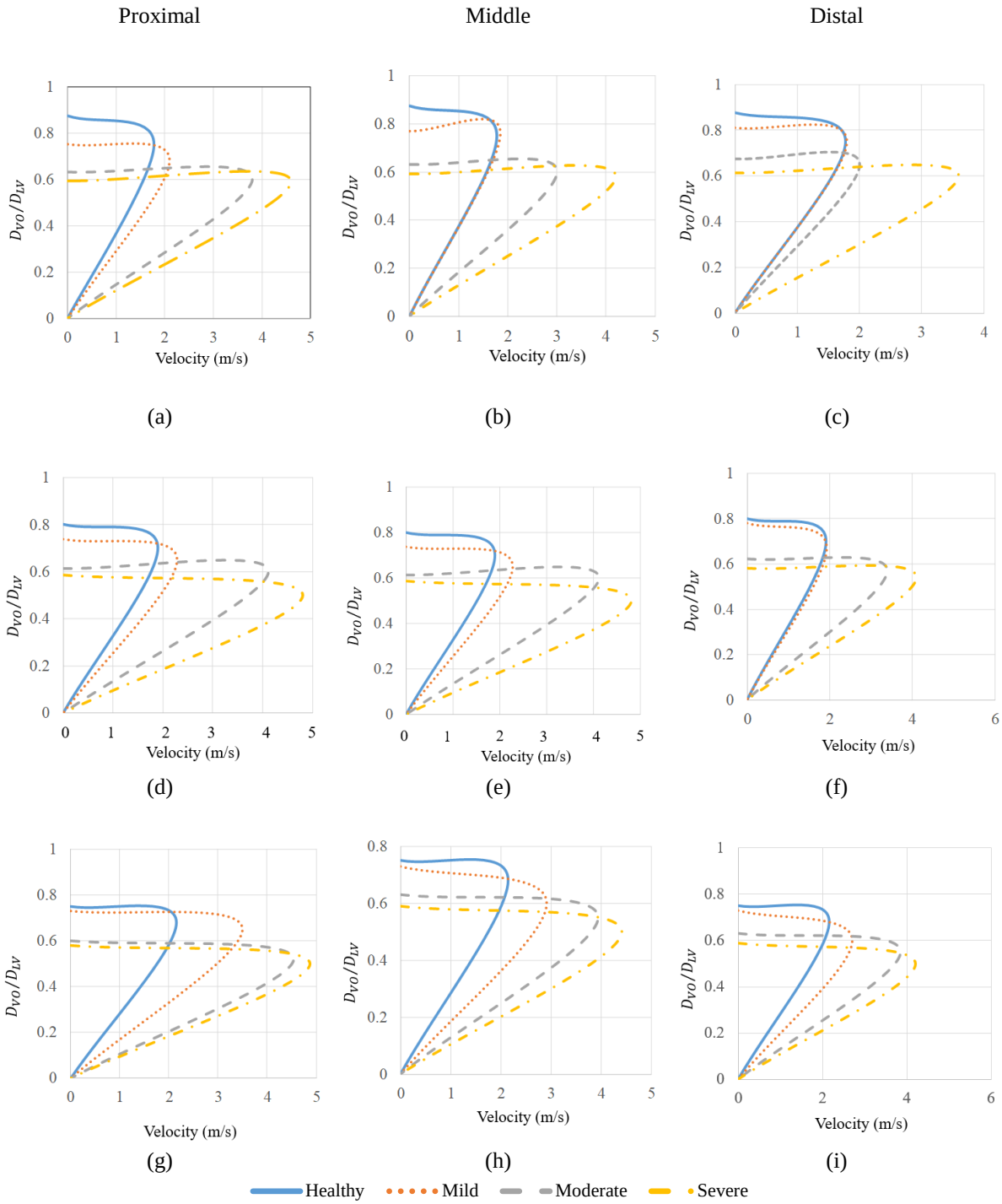

Figure 4.9 Velocity profiles corresponding to healthy, mildly, moderately, and the severely calcified aortic valves at a point located in the centre of the aortic valve orifice showing the variation of the valve orifice diameter versus velocity, (a-c) $D_{sinus}/D_{\text{Left ventricle}}$=1.5, (d-f) $D_{sinus}/D_{\text{Left ventricle}}$=1.3, (g-i) $D_{sinus}/D_{\text{Left ventricle}}$=1.1; D_{LV} and D_{VO} indicate the diameters of the left ventricle and valve orifice, respectively.

The values of transvalvular pressure gradient (TPG) of healthy, mildly, moderately, and severely calcified aortic valves with different locations of the coronary ostia (proximal, middle, and distal) and various diameters of the sinuses (D_{sinus}= 25, 20.8, and 17.6 mm) are illustrated in Figure 4.10. As shown in Figure 4.10 c, the TPG of an aortic valve with distal coronary artery ostia and D_{sinus}=25 mm increases from around 0.79 kPa for the healthy aortic valve to 10.31 kPa for the severely calcified case (an approximately 12 times increase). Moreover, the TPG is influenced by changing the diameter of the sinuses; for instance, as depicted in Figure 4.10 c, the TPG increases from approximately 10.31 kPa for the severely calcified aortic valve with D_{sinus} =25 mm to 13.41 kPa with D_{sinus} =20.8 mm, and to 14.5 kPa for D_{sinus} =17.6 mm.

Furthermore, the location of the coronary artery ostia has a considerable impact on the TPG. For instance, as shown in Figure 4.10 a and Figure 4.10 b, the TPG corresponding to the moderately calcified case with a middle coronary artery ostia and D_{sinus} =20.8 mm reaches 7.45 kPa compared to that with a distal coronary artery ostia (shown in Figure 4.10 c) which is around 6.85 kPa (an approximately 8% increase). It is worth mentioning that for the severely calcified case with a proximal coronary artery ostia and D_{sinus} =20.8 mm, as seen in Figure 4.10 a, the TPG drops surprisingly to 12.28 kPa compared to that with a distal coronary artery ostia which is around 14.5 kPa (shown in Figure 4.10 a). This is because the coronary artery ostia in this case is very close to the leaflets, therefore, blood flow can be easily pushed to the coronary arteries by the leaflets during the systole. The more blood flowing through to the coronary arteries reduces the bulk of the flow in the sinuses and subsequently allow the leaflets to open to a greater extent than the valves with middle and distal coronary artery ostia. As a result, the larger the orifice, the lesser the values of TPG become.

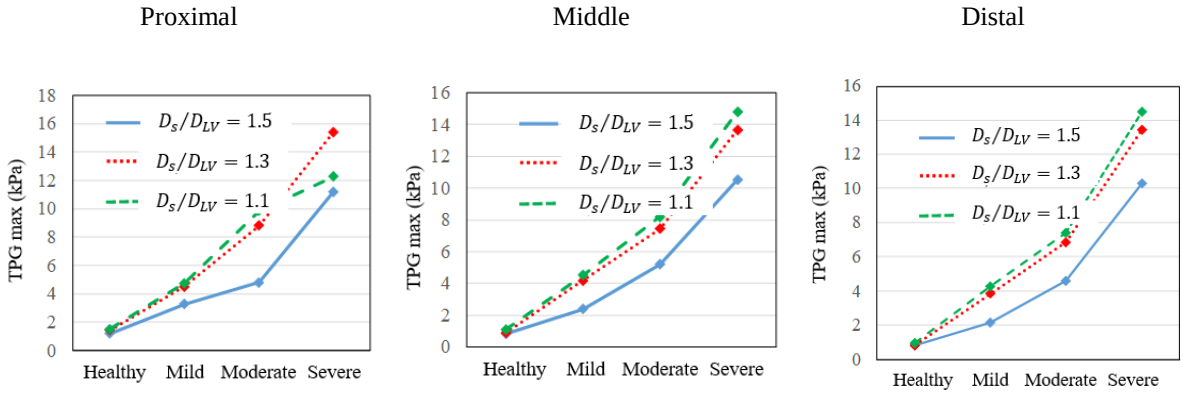

Figure 4.10 Maximum transvalvular pressure gradients (TPG_{max}) for healthy, mildly, moderately, and severely calcified aortic valves with different locations of the coronary artery ostia (proximal, middle, distal) and various diameters of the sinuses D_{sinus}= 25, 20.8, and 17.6 mm.

Calcification not only changes the hemodynamic parameters inside the aortic root but also has a considerable impact on the coronary artery hemodynamics. To demonstrate this, the velocity magnitudes at the coronary artery ostia for healthy, mildly, moderately, and severely calcified aortic valves with different locations of coronary artery ostia (proximal, middle, distal) and various diameters of the sinuses (D_{sinus}= 25, 20.8, and 17.6 mm) are illustrated in Figure 4.11. Generally, stenosis of the aortic valve decreases the velocity magnitude inside the coronary arteries (shown in Figure 4.11). Moreover, the location of the coronary artery ostia affects the velocity magnitude inside the coronary arteries; for instance, the velocity magnitude corresponding to a mildly calcified aortic valve with D_{sinus}=25 mm decrease from 1.65 m/s for the distal coronary artery ostia (shown in Figure 4.11 c) to 1.48 m/s for the middle coronary

artery ostia (shown in Figure 4.11 b), and to 0.92 m/s for the proximal coronary artery ostia (shown in Figure 4.11 a). The reduction of the coronary artery velocity due to calcification of the aortic valve accompanied with the various locations of the coronary arteries can, in turn, affect the coronary artery hemodynamics and result in initiation of coronary artery diseases and atherosclerosis plaque progression.

Furthermore, the effect of the diameter of the sinuses (D_{sinus}= 25, 20.8, and 17.6 mm) on the velocity magnitude of the coronary artery are depicted in Figure 4.11. Generally, the velocity magnitude inside the coronary artery decreases due to a decrease in diameter of the sinuses. For instance, the velocity magnitude of the coronary artery corresponding to the severely calcified case decreases from around 1 m/s for the valve with a diameter of sinuses of D_{sinus}=25 mm to 0.82 m/s for a diameter of D_{sinus}=20.8 mm Most interestingly, for the case with proximal coronary artery ostia and D_{sinus}=17.6 mm, the velocity inside the coronary artery increases compared to that with D_{sinus}=20.8 mm. As mentioned previously, this is due to the presence of the coronary artery ostia in a location closer to the leaflets. Therefore, leaflets can push the blood flow into the coronary artery and increase the velocity magnitude of the coronary artery flow.

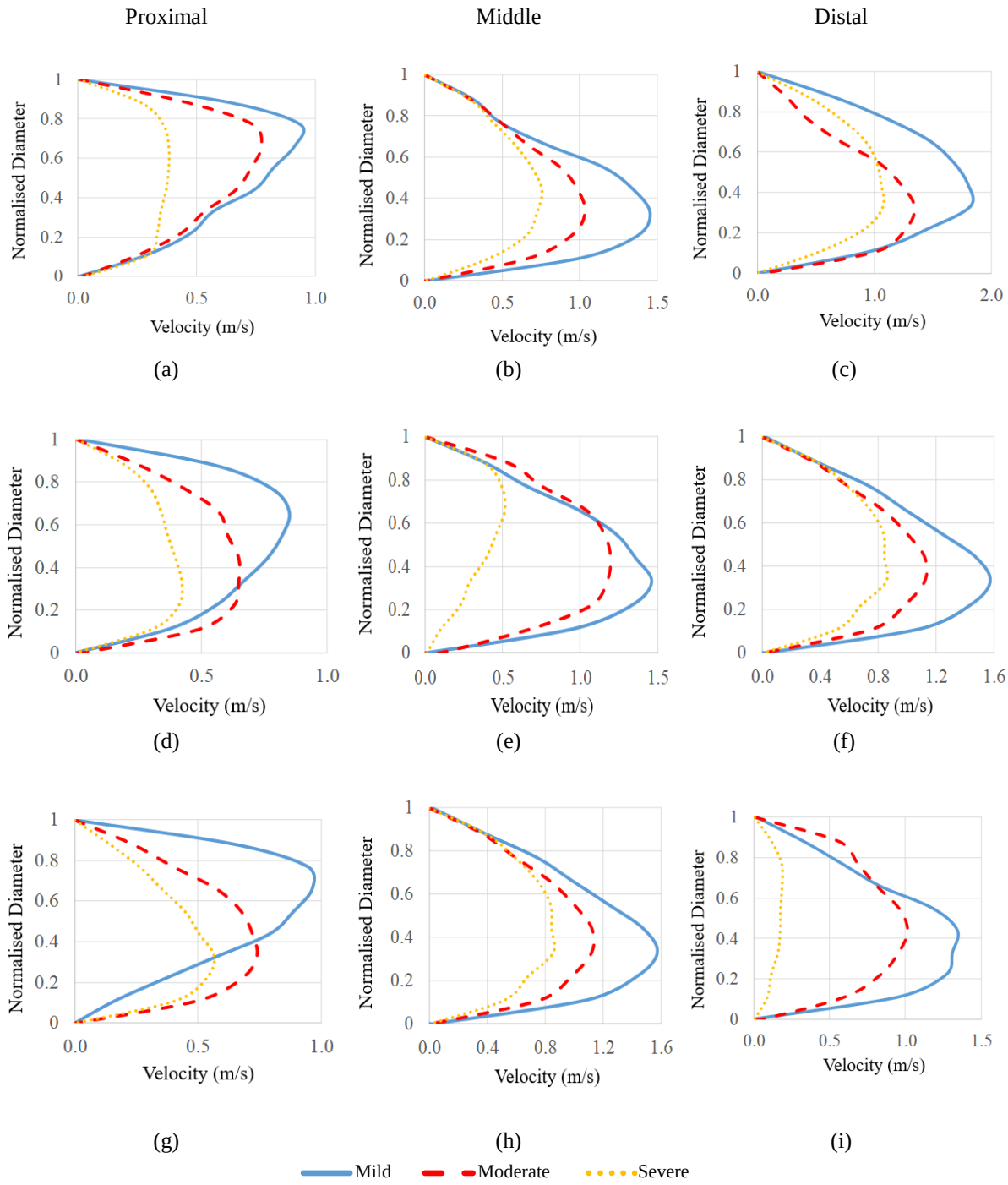

Figure 4.11 Velocity magnitudes at the coronary artery ostia at peak systole for mildly, moderately, and severely calcified aortic valves for different locations of the coronary artery ostia (proximal, middle, distal) and various diameters of the sinuses D_{sinus}= 25, 20.8, and 17.6 mm, (a-c) $D_{sinus}/D_{\text{Left ventricle}}$=1.5, (d-f) $D_{sinus}/D_{\text{Left ventricle}}$=1.3, (g-i) $D_{sinus}/D_{\text{Left ventricle}}$=1.1.

As noted previously, the main factor for initiation and progression of the calcification process has not been well identified. However, it is believed that the wall shear stress difference between the fibrosa and ventricularis layers of the aortic valve leaflets can remodel the valve structure and may play an important role in calcification of the aortic valve [18]. The average wall shear stress of the different layers of the leaflets (fibrosa and ventricularis) corresponding to healthy, mildly, moderately, and severely calcified aortic valves with different locations of the coronary artery ostia and various diameters of the sinuses are illustrated in Figure 4.12. For the ventricularis layer, calcification considerably increases the wall shear stress on the

ventricularis layers of the leaflets (shown in Fig. 13 a-c); for instance, for the valve with diameter of the sinus (D_{sinus}=25 mm) and distal coronary artery ostia (shown in Figure 4.12 c), the wall shear stress increases from around 18.2 Pa for the healthy case to 21.5 Pa for the mildly calcified, to 24.2 Pa for the moderately calcified, and to 28.2 Pa for the severely calcified cases. Furthermore, as seen in Figure 4.12 a-c, the diameter of the sinus has a significant effect on the wall shear stress on the ventricularis layers. For instance, for the severely calcified case with proximal coronary artery ostia (shown in Figure 4.12 a), the wall shear stress considerably increases from around 34.2 Pa for a calcified valve with D_{sinus}=25 mm to 52.2 Pa for D_{sinus}=20.8 mm (an approximately 52 % increase). Moreover, the location of the coronary artery ostia changes the wall shear stress on the leaflet layers. As depicted in Figure 4.12 a-c, for the severely calcified case with diameter of the sinuses D_{sinus}=17.6 mm, the wall shear stress reaches 52.2 Pa for the valve with proximal coronary artery ostia compared to that of the distal coronary artery ostia which is around 44.4 Pa (a 17% increase).

Although, calcification, on one hand, increases the wall shear stress on the ventricularis layer of the leaflets, on the other hand it decreases the wall shear stress on the fibrosa layer of the leaflets. To show this, the wall shear stress of the fibrosa layer of the aortic valve leaflets with different locations of the coronary artery ostia (proximal, middle, and distal) and various diameters of the sinuses (D_{sinus}= 25, 20.8, and 17.6 mm) are depicted in Figure 4.12 d-f. Generally, stenosis of the aortic valve reduces the wall shear stress on the fibrosa layer; for instance, the wall shear stress of the valve with distal coronary artery ostia and diameter of the sinuses (D_{sinus}=17.6 mm) drops to 0.53 Pa for the severely calcified case in comparison with that of the healthy case which is around 4.8 Pa.

Furthermore, the location of the coronary artery ostia impacts the wall shear stress of the fibrosa layer of the leaflets. As an example (seen in Figure 4.12 d-f), for the severely calcified cases with the smallest sinuses (D_{sinus}=17.6 mm), the wall shear stress decreases from 0.53 Pa for the valve with distal coronary artery ostia (shown in Figure 4.12 f) to 0.25 Pa for the proximal coronary artery ostia (shown in Figure 4.12 d); it reduces the WSS by approximately 50%.

The influence of the diameter of the sinuses on the wall shear stress on the fibrosa layer are studied in Figure 4.12 d-f. For instance, for the moderately calcified aortic valve with proximal coronary artery ostia (shown in Figure 4.12 d), the wall shear stress decreases from 1.52 Pa for the valve with D_{sinus}=25 mm to 1.43 Pa for the case with D_{sinus}=20.8 mm, and to 0.86 Pa for D_{sinus}=17.6 mm. Most interestingly, changes in the diameter of the sinuses show a significant impact on the wall shear stress of the healthy aortic valve. As depicted in Figure 4.12 d, the wall shear stress for a healthy valve deceases from 4.5 Pa for the valve with diameter of the sinus D_{sinus}=25 mm, to 3.5 Pa for D_{sinus}=17.6 mm; approximately 33% decease. It is worth mentioning that these changes in the wall shear stress of the different layers of the leaflets can, in turn, remodel the valve structure and thus impacts on the endothelium which leads to endothelial dysfunction, dysfunction of the vessel wall, inflammatory responses, and as a result initiation and progression of the calcification.

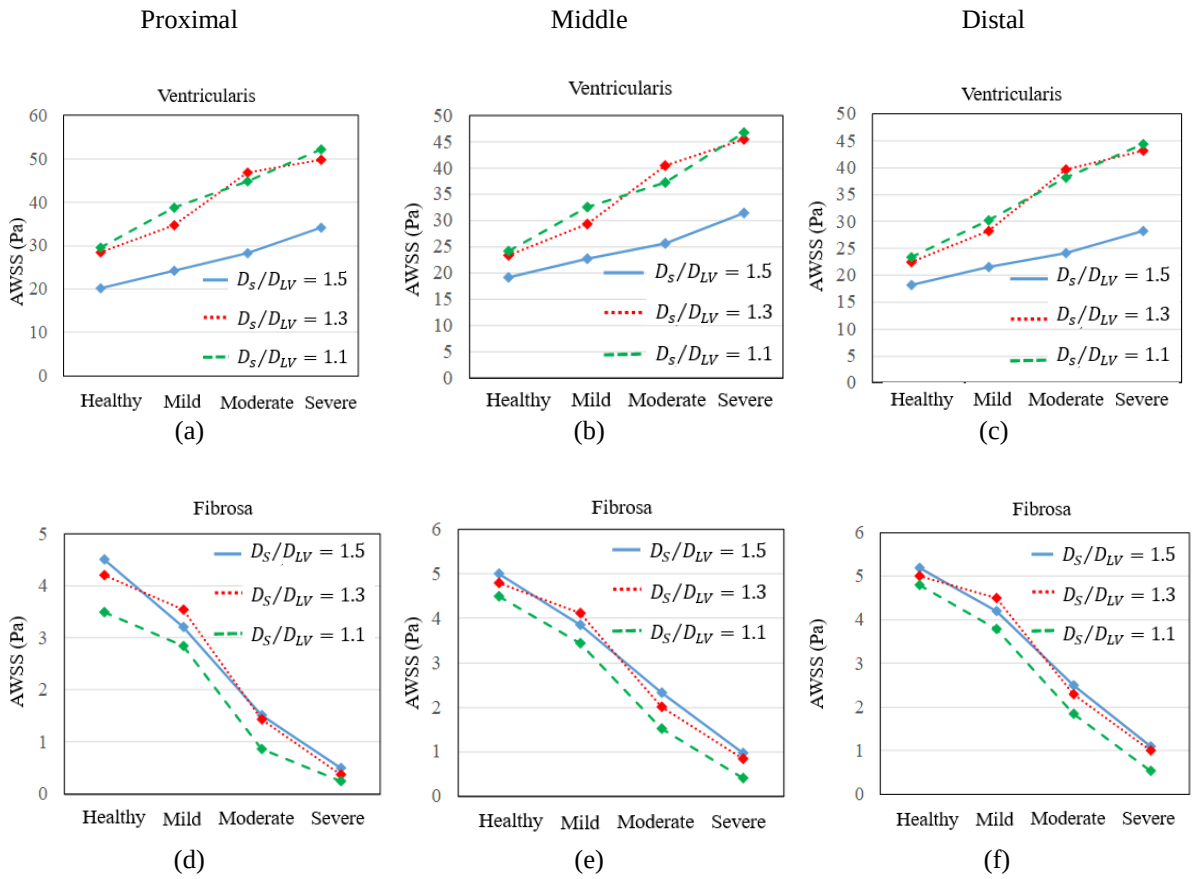

Figure 4.12 Average wall shear stresses of the ventricularis (a-c) and fibrosa (d-f) layers of the aortic valves for different location of the coronary artery ostia (proximal, middle, distal) and various diameters of the sinuses D_{sinus}= 25, 20.8, and 17.6 mm.

The effect of calcification accompanied with the locations of the coronary arteries and the diameter of the sinuses on the hemodynamics of the aortic root were investigated in the aforementioned paragraphs. In the following paragraph, the influence of the degree of valve calcification, the locations of the coronary artery ostia, and the diameter of the sinuses on the wall shear stress on the coronary artery wall are studied. To assess this, the wall shear stress of healthy, mildly, moderately, and severely calcified aortic valves with different locations of the coronary artery ostia, and various diameters of the sinuses are shown in Figure 4.13. Generally, stenosis of the aortic valve decreases the wall shear stress on the coronary artery wall; the more calcified the aortic valve, the less shear stress is imparted the on coronary arterial wall. For instance, the wall shear stress of a valve with distal coronary artery ostia and diameter of the sinuses D_{sinus}=25 mm decreases from 0.62 Pa for the healthy valve, to 0.43 Pa for the moderately calcified, and to 0.28 Pa for the severely calcified cases.

Furthermore, the influence of the locations of the coronary artery ostia on the wall shear stress at the coronary artery wall is illustrated in Figure 4.13 a-c. As seen, the wall of the coronary arteries for an aortic valve with proximal coronary artery ostia witnesses smaller wall shear stress compared to that with a distal coronary artery and a valve with a middle coronary artery ostia. For instance, the wall shear stress for a severely calcified valve with diameter of the sinuses D_{sinus}=17.6 mm decreases from 0.12 Pa for the valve with distal coronary artery ostia to 0.08 Pa for that with proximal coronary artery ostia. The influence of the diameter of the sinuses on the wall shear of the coronary artery wall are shown in Figure 4.13 a-c. Based on the results, for the severely calcified aortic valve with proximal coronary artery, for an example, the wall shear stress reduces from 0.28 Pa for the valve with diameter of the sinuses

D_{sinus}=25 mm to 0.08 Pa for Dsinus=17.6 mm. As previously mentioned, the main reason for initiation of coronary artery diseases and progression of atherosclerosis inside the coronary arteries has not been well understood, although it is believed that the wall shear stress on the wall can, in turn, accelerate this process [2]. From the aforementioned results, it can be concluded that the probability of the initiation of coronary artery diseases in an aortic valve with a proximal coronary artery and larger sinus diameter is much higher compared to either a distal coronary artery or a middle coronary artery ostia.

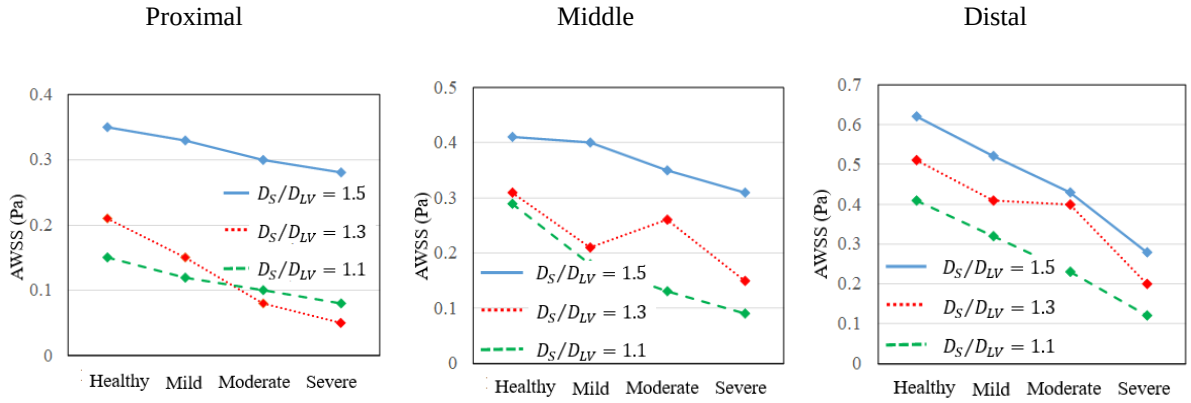

Figure 4.13 Average wall shear stresses of the coronary artery wall for valves with various diameters of the sinuses D_{sinus}= 25, 20.8, and 17.6 mm and different locations of the coronary artery ostia (proximal, middle, distal).

4.6 Conclusion

In this study, the effect of different locations of the coronary artery ostia and various diameters of the sinuses of healthy, mildly, moderately, and severely calcified aortic valve leaflets on the hemodynamic variation inside the aortic root as well as the coronary arteries was investigated. Results revealed that variation of the geometry of the sinuses and the locations of the coronary artery ostia change the hemodynamic parameters not only inside the aortic root but also within the coronary artery, in particular:

(i) The valve orifice diameter for a valve with proximal coronary artery ostia is smaller than that with distal coronary artery ostia; for instance, for a severely calcified aortic valve with a diameter of the sinus D_{sinus}=25 mm, the valve orifice diameter reduces from 9.8 mm for the valve with distal coronary artery ostia to 9.48 mm for a proximal coronary artery ostia.

(ii) The diameter of the sinuses affects the flow features within the sinuses, considerably changes the valve orifice diameter. For example, for the severely calcified valve with a distal coronary artery, the valve orifice diameter drops to 9.8 mm for the case with (D_{sinus}=17.6 mm) compared to that of with (D_{sinus}=25 mm) which is around 9.51 mm.

(iii) Similarly, the TPG is significantly affected by changing the location of the coronary artery ostia and the diameter of the sinuses. For instance, the moderately calcified aortic valve with distal coronary artery ostia and (D_{sinus}=20.8 mm) witnesses a TPG of 6.58 kPa, whilst for the case with proximal coronary artery ostia, the TPG is 8.81 kPa (an approximately 33% increase). Moreover, the TPG corresponding to a moderately calcified case with proximal coronary artery ostia increases from 4.8 kPa for the aortic valve with D_{sinus}=25 mm, to 8.81 kPa and 9.85 for those of the cases with D_{sinus}=20.8 mm and D_{sinus}=17.6 mm, respectively.

(iv) The velocity magnitude inside the coronary arteries reduces for locations of the coronary artery ostia close to the left ventricles. For instance, for the mildly calcified case with D_{sinus}=20.8 mm, the maximum velocity magnitude decreases from around 1.58 m/s for the valve with distal coronary artery ostia, to 0.84 m/s for proximal coronary artery ostia. Similarly, the velocity magnitudes inside the coronary arteries are affected by decreasing the diameter of the sinuses. For example, for a mildly calcified case with distal coronary artery ostia, the velocity magnitude within the coronary artery decreases from 1.82m/s for the valve with D_{sinus}=25 mm, to 1.4 m/s for that of with D_{sinus}=17.6 mm.

(v) The most interesting scenario observed for the velocity magnitude within the coronary arteries was for the severely calcified valve with proximal coronary arteries when decreasing the diameter of the sinuses to D_{sinus}=17.6 mm. In this case, the velocity magnitude increases to around 1 m/s, compared to D_{sinus}=20.8 mm for which it is 0.8 m/s. This is because the coronary artery ostia in this case is very close to the leaflets. Therefore, the blood flow is pushed into the coronary arteries by the movements of the leaflets. Notably, however, the presence of the proximal coronary artery ostia in the sinuses forces the leaflets and does not allow them to open appropriately; the blood flow within the coronary arteries is increased and, compared to other locations, is associated with reduced wall shear stress and thus reduced propensity for atherogenesis.

(vi) Varying the location of the coronary ostia can, in turn, affect the wall shear stresses not only on the different layers of the leaflet (ventricularis and fibrosa) but also within the coronary arteries. Generally, the wall shear stress on the ventricularis layer of the leaflet increases when the diameter of the sinuses decreases. By contrast, the WSS on the fibrosa layer of the leaflet decreases due to decreasing the diameter of the sinuses. This difference in the wall shear stress of the two layers of the leaflet may affect the endothelium and lead to the initiation and progression of the calcification process. Furthermore, the coronary arteries of an aortic valve with a smaller diameter of the sinuses witness a reduced velocity magnitude which leads to an increase in the probability of coronary artery diseases and progression of atherosclerosis.

Based on the results of this study, any observed differences in the geometry of the sinuses and the locations of the coronary artery ostia may have a significant effect on the hemodynamics of the aortic root and the coronary arteries. The change in hemodynamics can, in turn, remodel the coronary artery and the leaflet wall and lead to initiation and progression of valve calcification and coronary artery disease.

4.7 References

[1] A.H. Rapp, R.A. Lange, J.E. Cigarroa, E.C. Keeley, L.D. Hillis, Relation of pulmonary arterial diastolic and mean pulmonary arterial wedge pressures in patients with and without pulmonary hypertension, The American Journal of Cardiology, 88 (2001) 823-824.
[2] P. Kvidal, R. Bergström, L.G. Hörte, E. Ståhle, Observed and relative survival after aortic valve replacement, Journal of the American College of Cardiology, 35 (2000) 747-756.
[3] S. Stewart, E. P.Nast, F. A.Arabia, T. L.Talbot, M. Proschan, R. E.Clark, Errors in pressure gradient measurement by continuous wave Doppler ultrasound: type, size and age effects in bioprosthetic aortic valves, Journal of the American College of Cardiology, 18 (1991) 769-779.
[4] D. Garcia, P. Pibarot, C. Landry, A. Allard, B. Chayer, J. Dumesnil, L.G. Durand, Estimation of aortic valve effective orifice area by Doppler echocardiography: effects of valve inflow shape and flow rate, Journal of American Society of Echocardiography, 17 (2004) 756-765.

[5] S. Shadden, M. Astorino, J.F. Gerbeau, Computational analysis of an aortic valve jet with Lagrangian coherent structures, Chaos, 20 (2010).
[6] C.M. Otto, B. Prendergast, Aortic valve stenosis-from patients at risk to severe valve obstruction, The new england journal o f medicine, 371 (2014) 744-756.
[7] J.E. Davies, K.H. Parker, D.P. Francis, A.D. Hughes, J. Mayet, What is the role of the aorta in directing coronary blood flow, Heart, 94 (2008) 1545-1547.
[8] M.F. O'Rourke, How stiffening of the aorta and elastic arteries leads to compromised coronary flow, Heart, 94 (2008) 690-691.
[9] D. Garcia, P.G. Camici, L.G. Durand, K. Rajappan, E. Gaillard, O.E. Rimoldi, P. Pibarot, Impairment of coronary flow reserve in aortic stenosis, Journal of Applied Physiology, 106 (2009) 113-121.
[10] M. Handke, G. Heinrichs, F. Beyersdorf, M. Olschewski, C. Bode, A. Geibel, In vivo analysis of aortic valve dynamics by transesophageal 3-dimensional echocardiography with high temporal resolution, The Journal of Thoracic and Cardiovascular Surgery, 125 (2003) 1412-1419.
[11] A. Nemes, T. Forster, I. Ungi, V. Nagy, A. Vass, A. Pálinkás, A. Varga, M. Csanády, The coronary flow velocity reserve measured by stress transoesophageal echocardiography evaluates the success of coronary interventions / Results of a 5-year follow-up, Scandinavian Cardiovascular Journal, 39 (2005) 286-292.
[12] C.J. Hartley, A.K. Reddy, L.H. Michael, M.L. Entman, G.E. Taffet, Coronary flow reserve as an index of cardiac function in mice with cardiovascular abnormalities, Conference Proceeding IEEE Engineering Medical Biological Society, (2009) 1094-1097.
[13] C.J. Hartley, A.K. Reddy, L.H. Michael, M.L. Entman, V. Chintalagattu, A.Y. Khakoo, G.E. Taffet, Coronary flow reserve in mice: effects of age, coronary disease, and vascular loading, Conference Proceeding IEEE Engineering Medical Biological Society, 3780-3783 (2010).
[14] H. Maleki, Structural and fluid-structure interaction analysis of stenotic aortic valves: application to percutaneous aortic valve replacement, Conventional Thesis, Concordia University (2010).
[15] K.S. Cunningham, A.I. Gotlieb, The role of shear stress in the pathogenesis of atherosclerosis, Laboratory Investigation, 85 (2005) 9-23.
[16] K.L. Gould, N.P. Johnson, Imaging coronary blood flow in AS: let the data talk, again, Journal of the American College of Cardiology, 67 (2016) 1423-1426.
[17] M. Michail, J.E. Davies, J.D. Cameron, K.H. Parker, A.J. Brown, Pathophysiological coronary and microcirculatory flow alterations in aortic stenosis, Nature Reviews Cardiology, 15 (2018) 420–431.
[18] H. Hatoum, L.P. Dasi, Spatiotemporal complexity of the aortic sinus vortex as a function of leaflet calcification, Annals of Biomedical Engineering, 47 (2019) 1116-1128.
[19] I. Sathyamurthy, S. Alex, Calcific aortic valve disease: Is it another face of atherosclerosis, Indian Heart Journal, 67 (2015) 503–506.
[20] C.M. Otto, J. Kuusisto, D.D. Reichenbach, A.M. Gown, K.D. O'Brien, Characterization of the early lesion of 'degenerative' valvular aortic stenosis. Histological and immunohistochemical studies, Circulation, 90 (1994) 844–853.
[21] H. Hatoum, J. Dollery, S.M. Lilly, J. Crestanello, L.P. Dasi, Impact of patient-specific morphologies on sinus flow stasis in transcatheter aortic valve replacement: An in vitro study, Journal of Thoracic and Cardiovascular Surgery, 157 (2018) 540-549.
[22] A. Amindari, L. Saltik, K. Kirkkopru, M. Yacoub, H.C. Yalcind, Assessment of calcified aortic valve leaflet deformations and blood flow dynamics using fluid-structure interaction modeling, Informatics in Medicine Unlocked, 9 (2017) 191-199.
[23] S. Nobari, R. Mongrain, R. Leask, R. Cartier, The effect of aortic wall and aortic leaflet stiffening on coronary hemodynamic: a fluid–structure interaction study, Medical & Biological Engineering & Computing, 51 (2013) 923–936.

[24] H. Mohammadi, R. Cartier, R. Mongrain, Derivation of a simplified relation for assessing aortic root pressure drop incorporating wall compliance, Medical & Biological Engineering & Computing, 53 (2015) 241–251.
[25] H.J. Kim, I.E.V. Clementel, J.S. Coogan, C.A. Figueroa, K.E. Jansen, C.A. Taylor, Patient-specific modeling of blood flow and pressure in human coronary arteries, Annals of Biomedical Engineering, 38 (2010) 3195–3209.
[26] E.J. Weinberg, M.R.K. Mofrad, Transient, three-dimensional, multiscale simulations of the human aortic valve, Cardiovascular Engineering, 7 (2007) 140-155.
[27] E.J. Weinberg, M.R.K. Mofrad, A multiscale computational comparison of the bicuspid and tricuspid aortic valves in relation to calcific aortic stenosis, Journal of Biomechanics, 41 (2008) 3482-3487.
[28] M. Bianchi, G. Marom, R.P. Ghosh, O.M. Rotman, P. Parikh, L. Gruberg, D. Bluestein, Patient-specific simulation of transcatheter aortic valve replacement: impact of deployment options on paravalvular leakage, Biomechanics and Modeling in Mechanobiology, 18 (2019) 435–451.
[29] T. Fukui, K. Morinishi, Influence of vortices in the sinus of valsalva on local wall shear stress distribution, International Journal of Life Science and Medical Research, 3 (2013) 94-102.
[30] B.L. Moore, L.P. Dasi, Coronary flow impacts aortic leaflet mechanics and aortic sinus hemodynamics, Annals of Biomedical Engineering, 43 (2015) 2231-2241.
[31] H. Hatoum, B.L. Moore, L.P. Dasi, On the significance of systolic flow waveform on aortic valve energy loss, Annals of Biomedical Engineering, 46 (2018) 2102–2111.
[32] V. Sadri, I.D.M. David, C. Bloodworth, P.A. Midha, V. Raghav, A.P. Yoganathan, In vitro forward flow performance of the EDWARDS INTUITY elite rapid deployment aortic valve replacement in patient-specific anatomy, Structural Heart, 3 (2019) 63.
[33] H. Hatoum, S. Lilly, P. Maureira, J. Crestanello, L.P. Dasi, Sinus hemodynamics after transcatheter aortic valve in transcatheter aortic valve, The Annals of Thoracic Surgery, 110 (2020) 1348-1356.
[34] E.G. Butchart, J. Chambers, J.S. Borer, G. Grunkemeier, A. Yoganathan, Long-Term Durability of Transcatheter Valves: The Importance of Accurate Data, JACC: Cardiovascular Interventions, 13 (2020) 253-256.
[35] O.M. Rotman, B. Kovarovic, M. Bianchi, M.J. Slepian, D. Bluestein, In Vitro Durability and Stability Testing of a Novel Polymeric Transcatheter Aortic Valve, ASAIO Journal 66 (2020) 190-198.
[36] M.A. Fernández, J.F. Gerbeau, Algorithms for fluid-structure interaction problems, Journal of Cardivascular Mathematics, 1 (2009) 307-346.
[37] A.L. Alsabery, M.A. Sheremet, M. Ghalambaz, A.J. Chamkha, I. Hashim, Fluid-structure interaction in natural convection heat transfer in an oblique cavity with a flexible oscillating fin and partial heating, Applied Thermal Engineering 145 (2018) 80-97.
[38] F.K. Benra, H.J. Dohmen, J. Pei, S. Schuster, B. Wan, A comparison oneway and two-way coupling methods for numerical analysis of fluid-structure interactions, Journal of Applied Mathematics, 6 (2011).
[39] A.I. Alsabery, F. Selimefendigil, I. Hashim, A.J. Chamkha, M. Ghalambaz, Fluid-structure interaction analysis of entropy generation and mixed convection inside a cavity with flexible right wall and heated rotating cylinder, International Journal of Heat and Mass Transfer, 140 (2019) 331-345.
[40] M. Jahangiri, M. Saghafian, M.R. Sadeghi, Numerical simulation of non-newtonian models effect on hemodynamic factors of pulsatile blood flow in elastic stenosed artery, Journal of Mechanical Science and Technology, 31 (2017) 1003-1013.
[41] K.S. Sakariassen, L. Orning, V.T. Turitto, The impact of blood shear rate on arterial thrombus formation, Future Science OA, 1 (2015) 30-39.

[42] R.H. Haynes, Physical basis of the dependence of blood viscosity on tube radius, American Journal of Physiology, 198 (1960) 1193-1200.
[43] A.J. Pappano, W.G. Wier, Cardiovascular physiology, Mosby physiology monograph series, Elsevier, Philadelphia, 9th (2007).
[44] R. Gnyaneshwar, R.K. Kumar, K.R. Balakrishnan, Dynamic analysis of the aortic valve using a finite element model, The Annals of Thoracic Surgery, 73 (2002) 1122-1129.
[45] A. Ranga, O. Bouchot, R. Mongrain, R. Mongrain, R. Mongrain, Computational simulations of the aortic valve validated by imaging data: evaluation of valvesparing techniques, Interactive Cardiovascular and Thoracic Surgery, 5 (2006) 373–378.
[46] M.W. Weston, D.V. Laborde, A.P. Yoganathan, Estimation of the shear stress on the surface of an aortic valve leaflet, Annals of Biomedical Engineering, 27 (1991) 572-579.
[47] E.J. Keller, S.C. Malaisrie, J. Kruse, P.V. Ooij, E. Semaan, P. McCarthy, J.C. Carr, M. Markl, A.J. Barker, J.D. Collins, Restoration of physiologic hemodynamics in the ascending aorta following aortic valve replacement: a 4D flow MR study, Journal of Cardiovascular Magnetic Resonance, 18 (2016) P346.

Chapter 5

Effect of the presence of coronary artery stenosis on the sinus vortex structure

In Chapter 4, the influence of the locations of the coronary artery ostia on the hemodynamic parameters inside the aortic root and coronary artery flow was studied. It was shown that the transvalvular pressure gradient and valve orifice diameter are highly dependent on the location of the coronary artery ostia. Furthermore, the effect of the locations of the coronary artery ostia on the coronary artery hemodynamics was investigated. It was demonstrated that patients with proximal coronary artery ostia experience reduced coronary artery flow at peak systole compared to those with middle and distal coronary artery ostia.

Stenosis of the aortic valve is the most common form of valvular heart disease among adults and frequently coexists with coronary artery disease. Invasive investigations have demonstrated that the prevalence of coronary artery disease increases in the presence of aortic valve stenosis such that over half of all patients with aortic valve stenosis require simultaneous coronary bypass during aortic valve surgery. The correlation between calcific aortic valve diseases and coronary artery atherosclerosis is not well understood. It is still incompletely understood whether the presence of aortic valve stenosis initiates the coronary artery diseases or the presence of coronary artery stenosis initiates and progresses calcific aortic valve disease. This chapter is focused on providing an answer to the following research question which is the third objective of this project: *what is the correlation between coronary artery stenosis and the wall shear stress on the leaflets?*

FSI models of a healthy aortic valve with three different degrees of coronary artery stenoses are developed. The effect of the presence of coronary artery stenosis on the sinus vortex structures and most importantly the wall shear stress on the aortic valve leaflets are investigated. It is shown that the more the coronary artery becomes stenosed, the less wall shear stress experienced by the leaflets. Furthermore, the probability density functions of the wall shear stress distribution on the aortic valve leaflets for different degrees of coronary artery blockages are studied. It is shown that the leaflets of the healthy valve with a 75% stenosed coronary artery experience a lower range of wall shear stress with a higher probability of having very small wall shear stress on the leaflets. This means that a healthy valve with a 75% stenosed coronary artery is more prone to be calcified overtime.

The details of the methodology, supporting evidence and data are presented and explained in this chapter which consists of a paper format submitted to the Journal of Medical & Biological Engineering & Computing:

Araz. R. Kivi, Nima Sedaghatizadeh, Benjamin S. Cazzolato, Anthony C Zander, Adam J. Nelson, Ross Roberts-Thomson, Kelvin K. L. Wong, Maziar Arjomandi, Prediction of calcium deposition on aortic valve leaflets in the presence of coronary artery atherosclerosis, Submitted to Journal of Medical & Biological Engineering & Computing.

Statement of Authorship

Title of Paper	Prediction of calcium deposition on aortic valve leaflets in the presence of coronary artery atherosclerosis
Publication Status	☐ Published ☐ Accepted for Publication ☑ Submitted for Publication ☐ Unpublished and Unsubmitted work written in manuscript style
Publication Details	Araz. R. Kivi, Nima Sedaghatizadeh, Benjamin S. Cazzolato, Anthony C Zander, Adam J. Nelson, Ross Roberts-Thomson, Kelvin K. L. Wong, Maziar Arjomandi, Prediction of calcium deposition on aortic valve leaflets in the presence of coronary artery atherosclerosis. Submitted to the Journal of Medical & Biological Engineering & Computing.

Principal Author

Name of Principal Author (Candidate)	Araz R. Kivi		
Contribution to the Paper	Developed Ideas and Concepts • Conducted a comprehensive literature review • Developed the ideas and concepts based on the gaps of the knowledge in the field Performed the Modelling • Developed an aortic valve model in ANSYS workbench software • Developed an appropriate udf code to defined boundary conditions • Simulated the dynamic behaviour of the aortic valve leaflets • Validated the simulated model with the experimental data Interpreted Results • Extracted raw data from simulation • Post processed the data using CFD post and MATLAB • Developed a MATLAB code to extract the averaged data • Interpreted the results and compared them with the experimental results Wrote the Manuscript • Solely developed first full draft of the manuscript • Applied comments given by co-authors • Responsible for revising the manuscript after review • Acted as the corresponding author		
Overall percentage (%)	80%		
Certification:	This paper reports on original research I conducted during the period of my Higher Degree by Research candidature and is not subject to any obligations or contractual agreements with a third party that would constrain its inclusion in this thesis. I am the primary author of this paper.		
Signature		Date	29/01/2021

Co-Author Contributions

By signing the Statement of Authorship, each author certifies that:

vii. the candidate's stated contribution to the publication is accurate (as detailed above);

viii. permission is granted for the candidate in include the publication in the thesis; and

ix. the sum of all co-author contributions is equal to 100% less the candidate's stated contribution.

Name of Co-Author	Nima Sedaghatizadeh		
Contribution to the Paper	Supervised the work and provide feedback on the manuscript.		
Signature		Date	29/01/2021

Name of Co-Author	Benjamin S. Cazzolato		
Contribution to the Paper	Supervised the work and evaluated the manuscript.		
Signature		Date	29/01/2021

Name of Co-Author	Anthony C Zander		
Contribution to the Paper	Supervised the work, and provide feedback on the manuscript.		
Signature		Date	16/02/2021

Name of Co-Author	Adam J Nelson		
Contribution to the Paper	Evaluated the manuscript.		
Signature		Date	08/02/2021

Name of Co-Author	Ross Roberts-Thomson		
Contribution to the Paper	Provide feedback on the manuscript.		
Signature		Date	08/02/2021

Name of Co-Author	Kelvin K. L. Wong		
Contribution to the Paper	Provide feedback on the manuscript.		
Signature		Date	08/02/2021

Name of Co-Author	Maziar Arjomandi		
Contribution to the Paper	Supervised the work and provide feedback on the manuscript.		
Signature		Date	29/01/2021

Please cut and paste additional co-author panels here as required.

Prediction of calcium deposition on aortic valve leaflets in the presence of coronary artery atherosclerosis

Araz Rezaei Kivi, Nima Sedaghatizadeh, Benjamin Cazzolato, Anthony Zander, Adam J Nelson, Ross Roberts-Thomson, Kelvin K. L. Wong, Maziar Arjomandi

5.1 Abstract

This study aims to investigate the influence of coronary artery atherosclerosis on aortic sinus hemodynamics and calcium deposition on aortic valve leaflets as well as the prediction of the initiation and progression of calcific aortic valve disease (CAVD). A two-dimensional fluid-structure interaction model of an aortic valve leaflet with three different levels of coronary artery atherosclerosis was developed. Echocardiography images of arteries available in the literature were used for the geometrical parameters. The results show that the presence of coronary artery atherosclerosis changes the structure of the vortices inside the aortic sinus and their corresponding vorticity magnitude during the cardiac cycle. Furthermore, the results reveal that the leaflets of the aortic valve with healthy coronary arteries witness a higher shear stress during the systole compared highly stenosed coronary arteries. The higher the coronary artery stenosis the lower the shear stress ranges on the leaflets and the higher the probability of having lower shear stress on the leaflets.

5.2 Introduction

One of the most important flow features affecting hemodynamic parameters within the aortic root and coronary arteries is the formation of vortical structures inside the sinuses during the cardiac cycle [1]. Previous studies have revealed that the presence of vortices in the sinuses may have a significant effect on valve closure [2, 3] because of the pressure difference generated behind the leaflets during diastole. Bellhouse *et al*. [2] correlated the valve closure with the formation of vortex structures in the sinuses by measuring the pressure difference between the sinus cavity and the ventricle. Later, Reul *et al.* [4] showed that there is a relation between the valve closure and the transvalvular pressure gradient. Previous studies reveal that the presence of various vortex structures inside the aortic sinuses can affect not only the closing and opening of the aortic valve leaflets, but also has a significant influence on the sinus washout mechanisms and the overall performance of the aortic valve [5, 6].

The wall shear stress (WSS) on the leaflets plays an important role in the initiation and progression of calcific aortic valve disease (CAVD) [9-11] because the shear stress protects the valvular endothelial cells from oxidative, inflammatory stress, and initiation of calcification. Previous experimental [7] and numerical [8] studies show that there is a correlation between the formation of vortex structures in an aortic sinus and the WSS on leaflets. Low WSS on leaflets is potentially one of the main reasons for initiation of CAVD [7, 9], however, the calcification of aortic valve occurs via a complex mechanism which is not fully understood yet [10]. In a recent experimental study by Hatoum *et al.* [11] the effects of aortic valve stenosis on the coronary artery flow and the WSS on leaflets during systole and diastole cycles was investigated. They showed that the degrees of calcification of the aortic valve leaflets changes the vortex structures formed in the aortic sinuses and consequently the sinus washout mechanism and the wall shear stresses on leaflets. They also demonstrated that a severely

calcified aortic valve experiences lower wall shear stresses on the leaflets during both systole and diastole cycles.

Coronary artery flow plays an important role in changing the flow structures in the aortic sinuses which affects the behaviour of the aortic valve. Several researchers have developed numerical models of healthy and calcified aortic valves based on the fluid-structure interaction (FSI) method [12-14]. For example, Amindari *et al.* [14] investigated the effects of leaflet stiffening on the transvalvular pressure gradient (TPG) which is one of the main factors in diagnosing aortic valve stenosis. Using FSI they calculated the TPG for calcified and severely calcified aortic valves and also the WSS on the leaflets and compared the results with existing in-vivo data produced by doppler echocardiography [15]. They found that the leaflets of a severely calcified aortic valve witness lower shear stress values compared to that of a healthy case. In addition to the effect of coronary flow on the calcification and behaviour of aortic leaflets, the impact of calcification of aortic leaflets and sinuses on the coronary artery flow was also investigated numerically [12, 13] and experimentally [7, 11]. For example, Nobari *et el*. [13] investigated the effect of aortic valve stenosis on coronary hemodynamics using FSI modelling. They found that the coronary flow rate decreases considerably (by approximately 40%) when the thickness of the leaflets is approximately doubled. Later, the study by Mohammadi et al. [12] revealed that even the shape of the coronary artery affects the hemodynamics and behaviour of the aortic valve. Using FSI an approach, they found that a tapered shape of the coronary arteries wall decreases the WSS on coronary arteries.

While several studies have been focused on modelling the pathologies of aortic valves using different experimental and modelling techniques [16-19], the effect of coronary artery atherosclerosis on the formation and structure of vortex flow in aortic sinuses has not been investigated in detail as yet. It is expected that the blockage caused by the coronary artery stenoses changes the structure of the vorticies generated in the sinuses and accordingly leads to initiation and progression of CAVD. Thus, it is very important to elucidate this hypothesis for the formation of coronary artery stenoses resulting in the initiation and development of CAVD.

The study presented here was carried out to develop an understanding of the effect of the coronary artery atherosclerosis on the flow structures in an aortic sinus and the wall shear stresses on the aortic valve leaflets with an ultimate objective of prediction of the initiation of calcium deposition on the valve leaflets. A two-dimensional FSI model of a healthy aortic valve was developed in ANSYS Workbench 19.1. The geometry of the modelling domain and flow field parameters were selected based on echocardiography images available in the literature. FSI modelling was utilised to determine the interaction between the blood flow and aortic valve leaflets. The turbulent flow downstream of the leaflets was considered in the model using the Menter's $k\omega$ shear stress transport (SST) turbulence model [12]. The effects of the degree of stenosis inside the coronary artery (25, 50, and 75%) on the flow structure and vortex formation in the valve sinuses, and the WSS on the valve leaflets, were investigated.

5.3 Computational Model

A two-dimensional FSI model of a healthy aortic valve was developed in ANSYS Workbench 19.1. The geometry of the domain and the flow parameters were selected based on available echocardiography images of a 27-year-old subject presented in the literature [14]. The numerical model includes two different domains: structure (flexible leaflets) and fluid (blood flow) domains which include the aortic root, sinuses and coronary artery with different

degrees of stenosis. A two-way coupling FSI model was utilised to account for the interaction and momentum exchange between the fluid and solid domains. The details of the domains are explained in the following sections.

5.3.1 Fluid domain (blood flow)

The different regions of the fluid domain including inlet, outlets (coronary and aorta), and blood flow are illustrated in a. Figure 5.1 b-e shows the mesh structure in the developed model for a healthy aortic valve with either a healthy or stenosed coronary artery based on the echocardiography images shown in Figure 5.1 f. The blood is considered as a Newtonian, isothermal, incompressible fluid with a constant viscosity and a density of 0.0035578 Pa.s and 1060 kg/m^3, respectively [12]. The sweep method was used to generate an unstructured mesh for the fluid domain with approximately 10,000 prism elements. As shown in Figure 5.1 b, the mesh near the artery wall and leaflets is denser in order to accurately model the flow boundary layer. A sensitivity analysis was carried out for pressure and velocity for two grid sizes of 10,000 and 14,000. Based on the results, only a 2% difference between the calculated parameters was observed when the number of elements increased from 10,000 to 14,000, while the computation time increased by about 40% hence it was deemed that the mesh size 10,000 is an appropriate size in order to obtain accurate results.

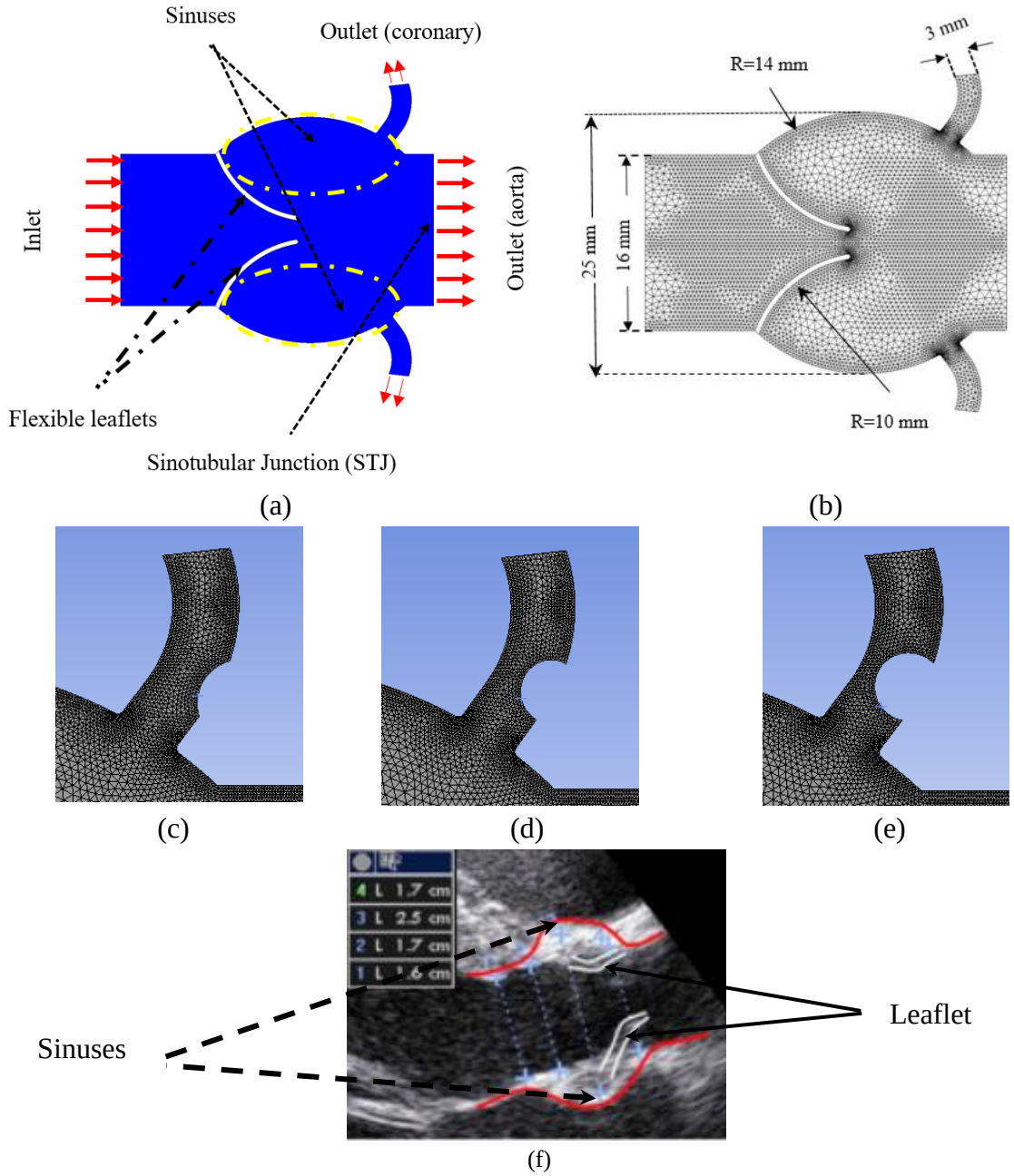

Figure 5.1 Schematic view of (a) healthy aortic valve with flexible leaflets, the sinuses are indicated by a yellow dash-line, flow directions for the inlet and outlet are shown using red arrows, (b) fluid domain mesh and boundary conditions; denser meshes are generated near the wall and leaflets to improve the accuracy of results, coronary artery mesh with different degrees of stenosis (c) 25% (d) 50% (e) 75%, and (f) echocardiography images from a healthy aortic valve [14]; the shape of the sinuses and leaflets are traced using a red and white dash-line, respectively.

The fluid domain computational grid was modified dynamically in order to accurately model the movement of the leaflets at every time step. A spring-based smoothing and re-meshing technique was applied to remesh the fluid domain at every time step based on the instantaneous geometry of the leaflets. The k-ω SST turbulence model was used due to its capability for prediction of turbulence and modelling of separated flow. Two sets of boundary conditions were applied at the inlet and outlets. At the ventricular side (inlet), a physiological velocity profile obtained from Doppler echocardiography [13] was applied as the boundary condition as shown in Figure 5.2. At the coronary artery outlets, a transient pressure profile was considered as the outlet boundary condition as also shown in Figure 5.2. This profile

obtained from the collected clinical data of the average coronary flow [20]. To extrapolate the required information from the interior domain, the outflow boundary condition was considered at the outlet of the aorta. The walls of the sinuses were assumed to be rigid. To investigate the validity of this assumption, a sensitivity analysis was carried out on the pressure and velocity components for two different models; one model with flexible leaflets and sinus walls, and another model with flexible leaflets but solid sinus walls. Results show that there is only 0.1% difference between the calculated parameters when the sinus walls change from solid to flexible while the computation time was increased by about 20%; hence it was decided to consider the model with flexible leaflets and solid sinus walls in this study.

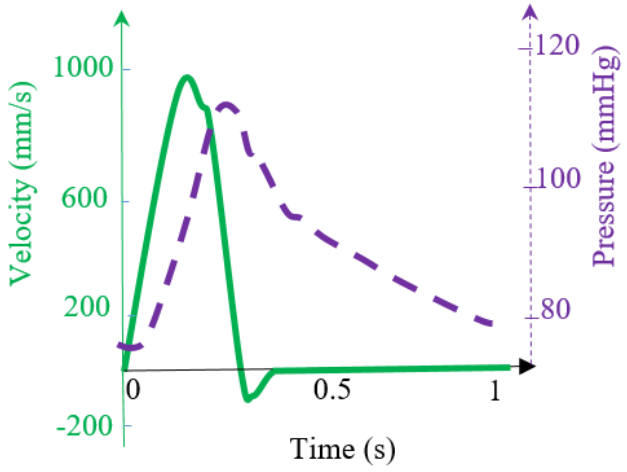

Figure 5.2 Inlet transient velocity profile applied at the inlet plane of the model (blue), and physiological pressure at coronary outlets (red). Based on measurements by [13, 14, 20].

5.3.2 Structural domain (flexible leaflets)

The structural domain of the model consists of two flexible leaflets which open during the systole to allow the blood flowing through the aorta and coronary arteries to feed the organs and heart, separately. The leaflets are assumed to be isotropic with a density of 1060 kg/m^3, Poisson's ratio of 0.3 and Young's modulus of 2 MPa [14, 21]. ANSYS Mechanical APDL was used to solve the equations of motion of the leaflets and determine the dynamic responses, stresses and strains of the leaflets based on the Newmark time integration method [14]. The mesh in the leaflets comprises 120 quadratic tetrahedral elements with a minimum of two elements through the thickness and was generated using the sweep method. To satisfy the mesh independency requirement, constant pressure was applied to the leaflets and a mesh convergence study was carried out in the steady state condition. Results show that the accuracy of the solution does not change for the models with more than 100 tetrahedral elements having a maximum skewness of 0.43. The mechanical properties of the fluid and structural domains and the boundary conditions applied to the fluid domain are presented in Table 5.1 and Table 5.2, respectively.

Table 5.1 Mechanical properties of the fluid and structural domains used in the modelling

Domain	Dynamic viscosity (Pa.s)	Density (kg/m^3)	Young's modulus (MPa)	Poisson's ratio
Fluid (blood) Incompressible, Isothermal, Newtonian	0.0035578	1060	---	---
Structure (leaflets) Linear elastic, Isotropic	---	1060	2 (healthy)	0.3

Table 5.2 Boundary conditions used in the modelling

Inlet	Outlets (coronary and aorta)	FSI surface	Walls
Transient pulsatile velocity inlet	Physiological pressure outlet Outflow in aorta Outlet	Fluid structure interaction surface between the flexible elastic leaflets and blood flow	Solid walls for sinuses and aortic root

5.3.3 Two-way coupling FSI

In order to model the interaction between the fluid and structural domains, two methods are usually used by researchers: one-way coupling and two-way coupling [22]. As suggested by [23], a two-way coupling method is useful to model the interaction between the aortic valve leaflets and blood flow due to the large deformation of the leaflets during the cardiac cycle. In the present study, the ANSYS coupling module was used to model the interaction between the flexible leaflets and the blood flow. To solve the continuity, Navier-Stokes, and turbulence equations corresponding to the fluid domain, the FLUENT module in ANSYS was used. To solve the equations related to the deformation of the flexible leaflets, Mechanical APDL was used in ANSYS. Then, at every time step, the data of the force and displacement were exchanged between the FLUENT and Mechanical APDL to capture the interaction between the structural and fluid domains.

5.4 Results and Discussion

In this section, the model is firstly validated quantitatively and qualitatively against recently published data. Then, the effects of the presence of coronary artery stenoses on the hemodynamics of the sinus structures and the WSS on the aortic valve leaflets are discussed.

5.4.1 Validation of the model

To validate the developed model, the obtained maximum transvalvular pressure gradient (TPG_{max}) and average wall shear stress (AWSS) on the leaflets were compared against the experimental data published by Keller *et al.* [15] and Yap *et al.* [24] (see Table 5.3). As can be seen, there is good agreement between the calculated TPG_{max} and AWSS in this work and the experiments carried out by Keller *et al.* [15] and Yap *et al.* [24].

Table 5.3 TPG_{max} comparison between previous in-vivo experiments and FSI modelling

	Experimental results	Present work
TPG_{max} (Pa)	799 [15]	791
AWSS on fibrosa layer (Pa)	2.12 [24]	1.82

To further validate the model, the flow features and vortex structures in the aortic sinuses were compared against the recently published experimental work by Hatoum and Dasi [11]. Figure 5.3 demonstrates a comparison of streamlines during the systole between the present simulation and PIV experiment. As shown, the developed numerical model can accurately model the flow features in the sinuses as observed in the PIV experiments by Hatoum and Dasi [11]. There is a small difference observed between the flow features due to the existence of the coronary artery in the present model and also the different dimensions of the sinuses and the diameter of the aortic valve between the experimental and numerical models. As seen, the dominant vortex in the sinus is shifted to the left due to the effect of the coronary artery in discharging the flow from the cavity.

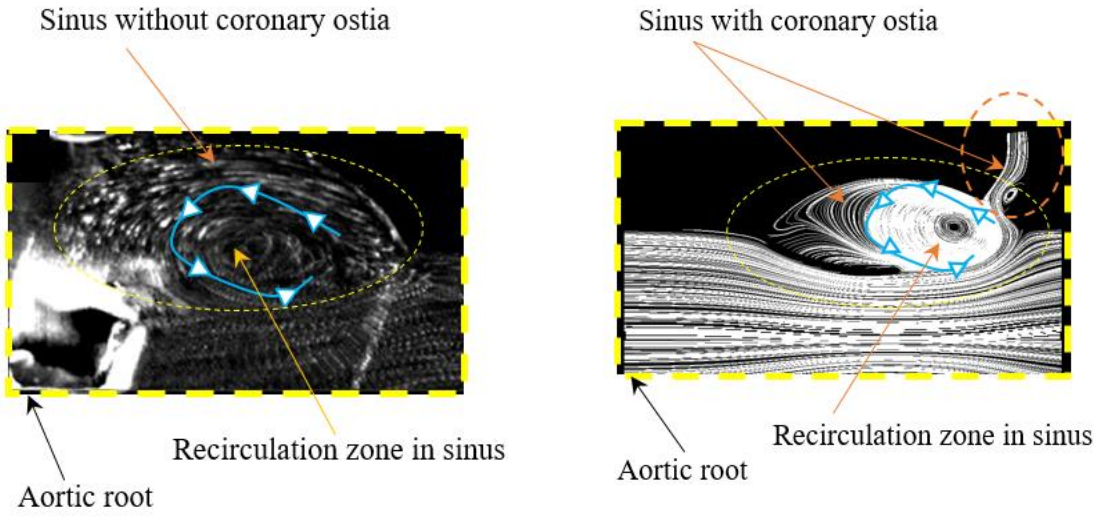

(a) (b)

Figure 5.3 Snapshot of the flow streamlines in sinuses around peak systole. A comparison of the flow streamlines in sinus between (a) the PIV experiment [11] and (b) present simulation. The vortex captured in numerical simulation matches well with the PIV experiment.

5.4.2 Hemodynamic assessment

The velocity contours for a healthy aortic valve with either healthy or stenosed coronary arteries (25, 50, and 75%) at peak systole (t=0.1s) are depicted in Figure 5.4 (a-d). As can be seen from the figure, the presence of stenosis inside the coronary arteries reduces the flow rate through the coronary arteries during the cardiac cycle which consequently results in a decrease in the valve orifice diameter. This is due to the increased pressure inside the aortic valve sinuses caused by the reduction of the flow rate in the coronary arteries. The accumulated pressure in the sinuses prevents the leaflets opening to their full extent. As illustrated in Figure 5.4 (a-d), the valve orifice diameter decreases from 14.2 mm for the healthy valve with healthy coronary arteries to 11.2 mm for the case with 75% stenosed coronary arteries. Because of this reduction in the valve orifice diameter, the flow velocity through the valve orifice increases from 1.6 m/s for the healthy valve with healthy coronary arteries to 1.82 m/s for the 75% stenosed coronary arteries. Furthermore, the reduction in valve orifice diameter results in an increase of TPG from 792 Pa for the healthy valve with a healthy coronary artery to 1765 Pa for the 75% stenosed coronary arteries. It is worth mentioning that the blocked coronary artery significantly changes the vortex structures in the aortic valve sinuses especially the number and strength of the recirculation zones within the sinuses. These changes, in turn, affect the aortic valve

hemodynamics and its performance during the cardiac cycle. The details of these changes are explained in the following paragraphs.

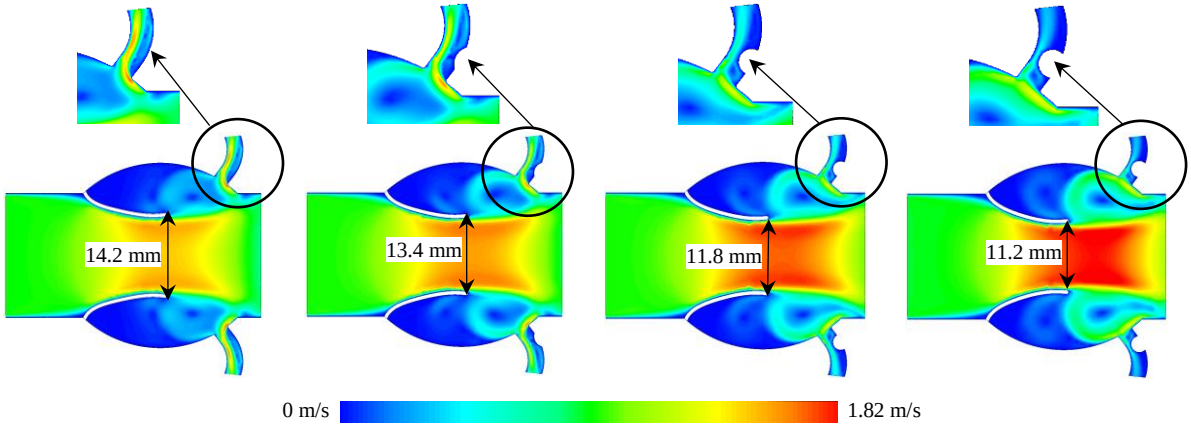

Figure 5.4 Velocity values for a healthy aortic valve with (a) healthy coronary arteries (b) 25% (c) 50% (d) 75% stenosed coronary arteries.

The presence of stenosis inside the coronary arteries affects the valve performance during the cardiac cycle. In Figure 5.5, the tip position of the leaflets vs time is illustrated. As can be seen from the figure, the maximum opening of the healthy valve with the healthy coronary arteries at peak systole is larger (7.12 mm) compared to with the 25%, 50% and 75% stenosed coronary arteries which are around 6.7 mm, 5.9 mm, and 5.6 mm, respectively. Furthermore, it is worth mentioning that the shortest opening time for the leaflets corresponds to a healthy valve with 75% stenosed coronary arteries. The opening time for the leaflets is highest for a healthy valve with healthy coronary artery, followed by a healthy valve with 25%, 50%, and 75% stenosed coronary arteries, respectively.

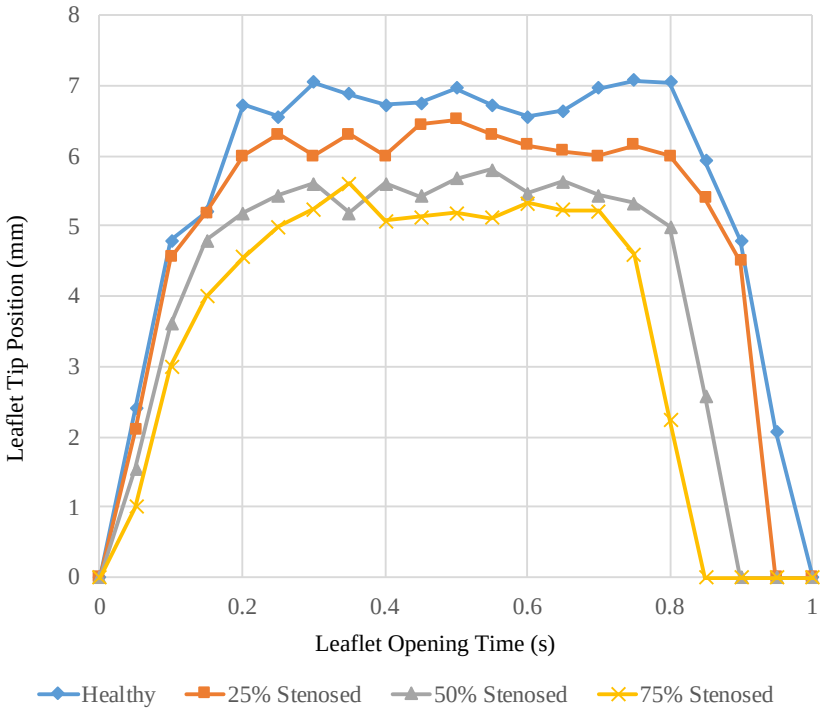

Figure 5.5 Leaflet tip position versus leaflet opening time for a healthy aortic valve with different percentage of coronary arteries stenosis.

The velocity profiles at the stenosed cross section of the coronary artery for healthy and stenosed coronary arteries at mid diastole are depicted in Figure 5.6. The peak velocity decreases from 0.42 m/s for the healthy coronary artery to around 0.36 m/s for the 25% stenosed coronary artery and 0.28 m/s for the 75% stenosed coronary artery. It is worth mentioning that the position of the maximum velocity inside the coronary artery changes when it is stenosed such that the peak velocity for the valve with a healthy coronary artery is close to the opposite wall of the coronary artery while that of the 50% stenosed coronary artery is almost at the middle of the stenosed cross section.

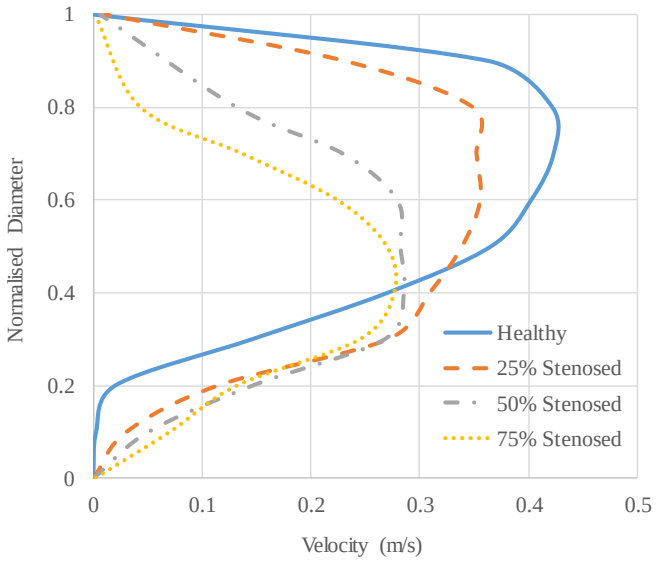

Figure 5.6 Velocity profile inside coronary artery at stenosed cross-section for healthy and stenosed coronary arteries (25, 50, 75% degrees of stenosis) at mid diastole (t=0.57s).

The circulation strength of the vortices in the sinus during the cardiac cycle for a healthy valve with healthy and stenosed coronary arteries (25, 50, and 75% blockages) is shown in Figure 5.7. As depicted in Figure 5.7 (a), the circulation strength for the healthy valve with a healthy coronary artery mainly has a predominantly positive value starting from around -0.001 m^2/s, fluctuating with a positive magnitude and reaching its maximum of around 0.015 m^2/s at t = 0.24s. This indicates the dominant vortex inside the sinus during systole is a contraclockwise (CCW) vortex that circulates inside the sinus and washes the flow out of the sinus through the aorta at the end of systole.

The effect of the presence of coronary artery stenosis on circulation inside the sinuses is illustrated in Figure 5.7 (a-d). As seen, the presence of stenosis inside coronary arteries decreases the circulation strength inside the sinus. For example, the maximum circulation magnitudes for a 25% and 50% stenosis inside the coronary arteries are 0.012 m^2/s and 0.006 m^2/s, respectively. Furthermore, the circulation magnitude corresponding to a valve with stenosed coronary arteries witnesses greater fluctuation during systole compared to those with healthy coronary arteries. The circulation magnitude for a valve with a 75% stenosed coronary arteries is shown in Figure 5.7 (d). In this case the coronary arteries witness negative and positive magnitudes of circulation strength which means that the direction of vortex circulation changes with higher frequency in comparison with the other cases investigated here. The presence of vorticies with opposite directions and higher frequency dissipates the momentum

of the flow and stagnates the flow inside the sinus. The stagnated flow in the sinuses decreases the wall shear stress on the leaflets and contributes to the initiation and progression of CAVD.

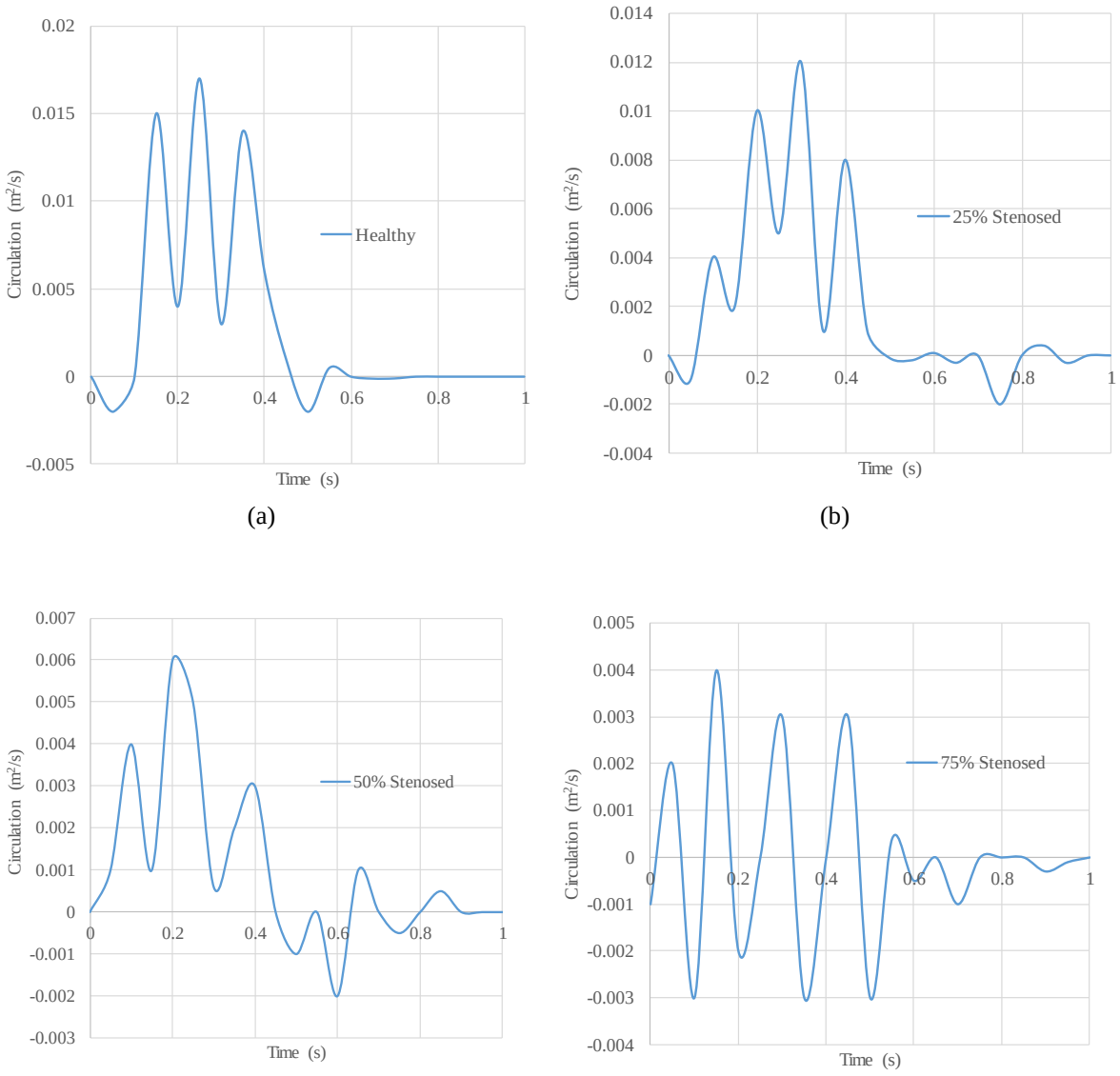

Figure 5.7 Circulation versus time inside sinus for a healthy aortic valve with (a) healthy coronary arteries (b) 25% (c) 50% (d) 75% stenosed coronary arteries.

To investigate the possibility of occurrence of CAVD, the shear stress probability density function (PDF) for a valve with healthy and stenosed coronary arteries around the leaflets region is shown in Figure 5.8 during systole and diastole. As shown, the valve with healthy coronary arteries experiences a shear stress from -1.5 to +2 Pa during the systole, and from -0.5 to +0.5 Pa during the diastole. From the figure, it is clear that a valve with stenosed coronary arteries witnesses lower ranges of shear stress compared with the one with healthy coronary arteries. The presence of stenosis inside the coronary artery decreases the shear stress on the leaflets, and increases the probability of lower shear stress on the leaflets. For example, as shown in Figure 5.8 (a and b), a valve with 75% stenosed coronary arteries witnesses a range of shear stress (changing from -0.35 to +0.35 Pa in systole, and -0.1 to +0.12 Pa in diastole) and higher probability compared with those for the valve with healthy coronary arteries which changes from -1.5 to 2 Pa and -0.5 to +0.5 Pa during systole and diastole, respectively. Based

on the results of this study, a valve with stenosis in the coronary arteries has a higher probability of having a lower values of shear stress on the leaflets. As a result, there is a higher probability of CAVD over time [7, 9].

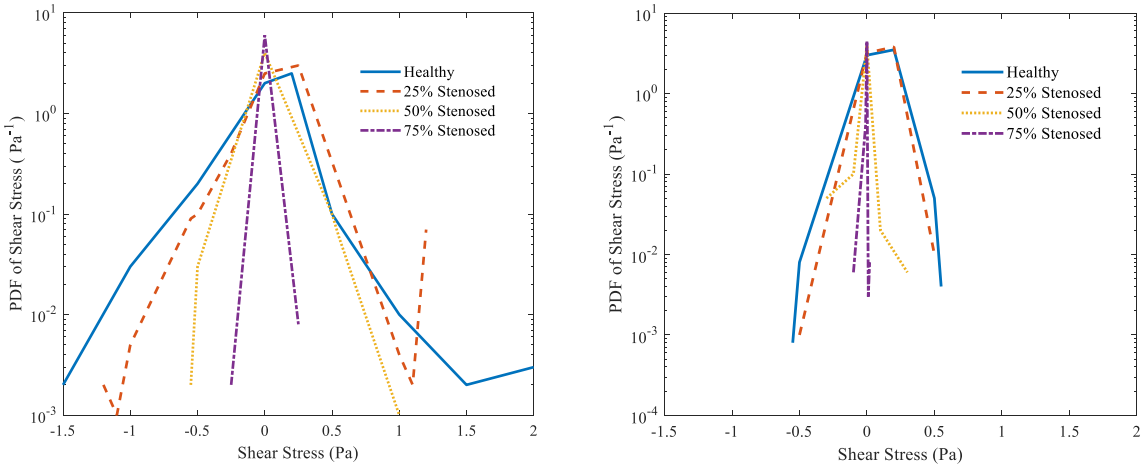

Figure 5.8 Log scale probability density function of shear stress distribution on leaflets of the healthy aortic valve for different percentage of coronary arteries atherosclerosis during cardiac cycle (a) systole (b) diastole.

5.5 Conclusion

In the present study, fluid-structure interaction modelling method was used to investigate the effects of the presence of coronary artery stenosis on the flow features and the vortex structures in aortic valve sinuses. The presence of the stenosis inside the coronary arteries not only blocks the blood flow through the coronary arteries but also significantly changes the vortex structures inside the sinuses and affects the aortic valve performance during the cardiac cycle. The most important outcomes of this study can be summarised as follows:

- The presence of stenosis inside a coronary artery reduces the coronary artery flow rate and increases the pressure inside the sinuses during systole. The accumulated pressure in the sinuses exerts forces on the leaflets and limits their angular movements during systole which results in an insufficient opening of the leaflets which can result in aortic valve stenosis over time.
- The presence of the coronary artery stenosis affects the vortex structure in the sinuses, such that a valve with a stenosed coronary artery has different vortex structures in term of their frequency and strength compared with those of a valve with a healthy coronary artery. Similarily, the circulation strength in the aortic sinuses of a stenosed coronary artery is less than that in the sinuses of a healthy coronary artery. A dominant vortex inside the sinuses of a valve with 75% stenosed coronary artery witnesses enormous fluctuations of positive and negative magnitude of circulation strength compared to the other cases examined. These fluctuations in circulation strength dissipate the momentum of the flow and stagnates the flow inside the sinuses. The stagnated flow in the sinuses decreases the values of wall shear stress on the leaflets and increases the probability of initiation and progression of CAVD.
- The wall shear stress on the leaflets for a valve with stenosed coronary arteries has a lower range compared to that for a valve with healthy coronary arteries. Moreover, the

probability density function of the shear stress corresponding to the valve with stenosed coronary arteries is higher than for healthy coronary arteries. The higher probability of lower wall shear stress on leaflets increases the probability of initiation and progression of CAVD. This means that a valve with stenosed coronary arteries is more susceptible to calcification over time.

5.6 References

[1] C. Peskin, A. Wolfe, The aortic sinus vortex, Federation Proceedings, 37 (1978) 2784-2792.
[2] B. Bellhouse, Velocity and pressure distributions in the aortic valve, Journal of Fluid Mechanics, 37 (1969) 587-600.
[3] B. Bellhouse, L. Talbot, The fluid mechanics of the aortic valve, Journal of Fluid Mechanics, 35 (1969) 721-735.
[4] H. Reul, N. Talukder, E. Mu, Fluid mechanics of the natural mitral valve, Journal of Biomechanics, 14 (1981) 361-372.
[5] R. Toninato, J. Salmon, F.M. Susin, A. Ducci, g. Burriesci, Physiological vortices in the sinuses of Valsalva: an in vitro approach for bio-prosthetic valves, Journal of Biomechanics, 49 (2016) 2635-2643.
[6] A.V. Steenhoven, P. Veenstra, R. Reneman, The effect of some hemodynamic factors on the behaviour of the aortic valve, Journal of Biomechanics, 15 (1982) 941-950.
[7] B. Moore, L.P. Dasi, Spatiotemporal complexity of the aortic sinus vortex, Experiments in Fluids 55 (2014) 1770-1778.
[8] T. Fukui, K. Morinishi, Influence of vortices in the sinus of valsalva on local wall shear stress distribution, International Journal of Life Sciences and Medical Research, 3 (2013) 94-103.
[9] L. Sun, S. Chandra, P. Sucosky, Ex vivo evidence for the contribution of hemodynamic shear stress abnormalities to the early pathogenesis of calcific bicuspid aortic valve disease, PLoS ONE, 7 (2012) 43-48.
[10] M. Thubrikar, L. Bosher, S. Nolan, The mechanism of opening of the aortic valve, Journal of Thoracic and Cardiovascular Surgery 77 (1979) 863-870.
[11] H. Hatoum, L.P. Dasi, Spatiotemporal complexity of the aortic sinus vortex as a function of leaflet calcification, Annals of Biomedical Engineering, 47 (2019) 1116-1128.
[12] H. Mohammadi, R. Cartier, R. Mongrain, Derivation of a simplified relation for assessing aortic root pressure drop incorporating wall compliance, Medical & Biological Engineering & Computing, 53 (2015) 241-251.
[13] S. Nobari, R. Mongrain, R. Leask, R. Cartier, The effect of aortic wall and aortic leaflet stiffening on coronary hemodynamic: a fluid–structure interaction study, Medical & Biological Engineering & Computing, 51 (2013) 923-936.
[14] A. Amindari, L. Saltik, K. Kirkkopru, M. Yacoub, H.C. Yalcin, Assessment of calcified aortic valve leaflet deformations and blood flow dynamics using fluid-structure interaction modeling, Informatics in Medicine Unlocked, 9 (2017) 191-199.
[15] E.J. Keller, S.C. Malaisrie, J. Kruse, P.V. Ooij, E. Semaan, P. McCarthy, J.C. Carr, A.J. Barker, J.D. Collins, Restoration of physiologic hemodynamics in the ascending aorta following aortic valve replacement: a 4D flow MR study, Journal of Cardiovascular Magnetic Resonance, 18 (2016) P346.
[16] M. Bianchi, G. Marom, R.P. Ghosh, O.M. Rotman, P. Parikh, L. Gruberg, D. Bluestein, Patient-specific simulation of transcatheter aortic valve replacement: impact of deployment options on paravalvular leakage, Biomechanics and Modeling in Mechanobiology, 18 (2019) 435-451.
[17] E.J. Weinberg, M.R.K. Mofrad, Transient, three-dimensional, multiscale simulations of the human aortic valve, Cardiovascular Engineering, 7 (2007) 140-155.

[18] E.J. Weinberg, M.R.K. Mofrad, A multiscale computational comparison of the bicuspid and tricuspid aortic valves in relation to calcific aortic stenosis, Journal of Biomechanics, 41 (2008) 3482-3487.
[19] H.J. Kim, I.E. Vignon-Clementel, J.S. Coogan, C.A. Figueroa, K.E. Jansen, C.A. Taylor, Patient-specific modeling of blood flow and pressure in human coronary arteries, Annals of Biomedical Engineering, 38 (2010) 3195-3209.
[20] A.J. Pappano, W.G. Wier, Cardiovascular physiology, Mosby physiology monograph series, Elsevier, Philadelphia: 10th Edition, (2007).
[21] A. Ranga, O. Bouchot, R. Mongrain, Computational simulations of the aortic valve validated by imaging data: evaluation of valvesparing techniques, Interactive Cardiovascular and Thoracic Surgery, 5 (2006) 373-378.
[22] F.K. Benra, H.J. Dohmen, J. Pei, S. Schuster, B. Wan, A comparison of oneway and two-way coupling methods for numerical analysis of fluid-structure interactions, Journal of Applied Mathematics, 6 (2011) 1-16.
[23] M.A. Fernández, J.F. Gerbeau, Algorithms for fluid-structure interaction problems, Journal of Cardivascular Mathematics, 1 (2009) 307-346.
[24] C.H. Yap, N. Saikrishnan, G. Tamilselvan, A.P. Yoganathan, Experimental measurement of dynamic fluid shear stress on the aortic surface of the aortic valve leaflet, Biomechanics and Modeling in Mechanobiology, 11 (2012) 171-182.

Chapter 6

Prediction of the wall shear stress distribution on aortic valve leaflets

In Chapter 5, the effect of the presence of different degrees of coronary artery stenosis on the sinus vortex structures and the wall shear stress distribution of the aortic valve leaflets were investigated. It was found that a healthy aortic valve with a 75% stenosed coronary artery is more at risk of calcification because it experiences lower range of wall shear stress on the leaflets.

Stenosis of the aortic valve and its effect on the sinus vortex structures and the wall shear stress on the leaflets is very important due to the impact the initiation and progression of calcific aortic valve disease (CAVD). Although genetic factors impact on the initiation of calcific aortic valve disease, alteration of the fluid shear stresses in the vicinity of the leaflets is believed to be one of the main factors impacting the initiation of CAVD. Whilst it is not well understood how CAVD initiates and progresses, it is believed that there is a link between the wall shear stress on the leaflets and the initiation and progression of CAVD.

The main aim of this chapter is to develop a numerical model to predict the wall shear stress distribution on the aortic valve leaflets as well as the variation of the sinus vortex structures. The model is validated against the pressure and flow rate data collected from the in-house in-vitro experiments. In this chapter, the effect of the locations of the coronary artery ostia accompanied by the presence of coronary artery stenosis on the wall shear stress distribution of the aortic valve leaflets is investigated. This study is conducted in order to find the correlation between calcific aortic valve disease and the geometrical properties of the aortic valve and coronary arteries. It is shown that an aortic valve with proximal coronary artery witnesses a lower range of wall shear stress on the leaflets with a higher probability of experiencing calcific aortic valve disease compared to those with distal and middle coronary artery ostia. Furthermore, it is shown that a valve with proximal coronary artery ostia and a 75% blocked coronary artery experiences the lowest range of wall shear stress on the leaflets with the corresponding highest probability of experiencing calcific aortic valve diseases.

The details of the methodology, supporting evidence and data are presented and explained in this chapter which consists of a paper format submitted to the Journal of Annals of Biomedical Engineering:

Araz. R. Kivi, Nima Sedaghatizadeh, Benjamin S. Cazzolato, Anthony C Zander, Adam J. Nelson, Ross Roberts-Thomson, Kelvin K. L. Wong, Maziar Arjomandi, Calcific aortic valve disease prediction based on wall shear stress distribution on the leaflets, Submitted to Journal of Annals of Biomedical Engineering.

Statement of Authorship

Title of Paper	Calcific aortic valve disease prediction based on wall shear stress distribution on the leaflets
Publication Status	☐ Published ☐ Accepted for Publication ☑ Submitted for Publication ☐ Unpublished and Unsubmitted work written in manuscript style
Publication Details	Araz. R. Kivi, Nima Sedaghatizadeh, Benjamin S. Cazzolato, Anthony C Zander, Adam J. Nelson, Ross Roberts-Thomson, Kelvin K. L. Wong, Maziar Arjomandi, Calcific aortic valve disease prediction based on wall shear stress distribution on the leaflets, Submitted to the Journal of Annals of Biomedical Engineering.

Principal Author

Name of Principal Author (Candidate)	Araz R. Kivi		
Contribution to the Paper	Developed Ideas and Concepts • Conducted a comprehensive literature review • Developed the ideas and concepts based on the gaps of the knowledge in the field Performed the Modelling • Developed an aortic valve model in ANSYS workbench software • Developed an appropriate udf code to defined boundary conditions • Simulated the dynamic behaviour of the aortic valve leaflets • Validated the simulated model with the experimental data Interpreted Results • Extracted raw data from simulation • Post processed the data using CFD post and MATLAB • Developed a MATLAB code to extract the averaged data • Interpreted the results and compared them with the experimental results Designed and fabricated a test rig • Designed and fabricated a left ventricle heart duplicator experimental test rig • Measured aortic valve flow rate and transvalvular pressure gradient • Validated the simulation with the measured experimental data Wrote the Manuscript • Solely developed first full draft of the manuscript • Applied comments given by co-authors • Responsible for revising the manuscript after review • Acted as the corresponding author •		
Overall percentage (%)	80 %		
Certification:	This paper reports on original research I conducted during the period of my Higher Degree by Research candidature and is not subject to any obligations or contractual agreements with a third party that would constrain its inclusion in this thesis. I am the primary author of this paper.		
Signature		Date	29/01/2021

Co-Author Contributions

By signing the Statement of Authorship, each author certifies that:

x. the candidate's stated contribution to the publication is accurate (as detailed above);

xi. permission is granted for the candidate in include the publication in the thesis; and

xii. the sum of all co-author contributions is equal to 100% less the candidate's stated contribution.

Name of Co-Author	Nima Sedaghatizadeh		
Contribution to the Paper	Supervised the work and provide feedback on the manuscript.		
Signature		Date	29/01/2021

Name of Co-Author	Benjamin S. Cazzolato		
Contribution to the Paper	Supervised the work and evaluated the manuscript.		
Signature		Date	29/01/2021

Name of Co-Author	Anthony C Zander		
Contribution to the Paper	Supervised the work, and provide feedback on the manuscript.		
Signature		Date	16/02/2021

Name of Co-Author	Adam J Nelson		
Contribution to the Paper	Evaluated the manuscript.		
Signature		Date	08/02/2021

Name of Co-Author	Ross Roberts-Thomson		
Contribution to the Paper	Provide feedback on the manuscript.		
Signature		Date	08/02/2021

Name of Co-Author	Kelvin K. L. Wong		
Contribution to the Paper	Provide feedback on the manuscript.		
Signature		Date	08/02/2021

Name of Co-Author	Maziar Arjomandi		
Contribution to the Paper	Supervised the work and provide feedback on the manuscript.		
Signature		Date	29/01/2021

Please cut and paste additional co-author panels here as required.

Calcific aortic valve disease prediction based on wall shear stress distribution on the leaflets

Araz R. Kivi, Nima Sedaghatizadeh, Benjamin S. Cazzolato, Anthony C. Zander, Adam J. Nelson, Ross Roberts-Thomson, Kelvin K. L. Wong, Maziar Arjomandi

6.1 Abstract

The aim of this study is to investigate the influence of leaflets stiffening, the positions of coronary artery ostia, and the presence of the stenosed coronary arteries on aortic sinus hemodynamics and wall shear stress on aortic valve leaflets as well as the prediction of the initiation and progression of calcific aortic valve disease (CAVD). A two-dimensional fluid-structure interaction (FSI) model of a healthy, a calcified, and a severely calcified aortic valve leaflets was developed based on echocardiography images available in the literature. The effect of the presence of three different degrees of coronary artery atherosclerosis and positions of the coronary artery ostia on sinus flow patterns and hemodynamics was investigated. The results show that the calcification of an aortic valve affects sinus vortex structures and accordingly wall shear stress on aortic valve leaflets. Furthermore, the results reveal that wall shear stress on aortic valve leaflets is highly affected by the positions of the coronary artery ostia, and different degrees of the stenosis of the coronary arteries. For example, the severely calcified aortic valve with proximal coronary artery ostia and 75% stenosed coronary arteries witnesses a lowest ranges of the wall shear stresses on the leaflets compared with other models. It is also shown that the severely calcified leaflets with proximal coronary ostia and 75 % stenosed coronary arteries experiences higher probability of having smaller wall shear stresses on the leaflets. This means that this model has a higher probability of the progression of stenosis overtime.

6.2 Introduction

The formation of the vortical structures inside the sinus of Valsalva is one of the most important flow features which affect hemodynamic parameters in the aortic root [1-3] and coronary arteries [4-10]. It was shown that the existence of aortic sinus vortices play an important role in the valve closure [4, 10]. In different studies the effects of the aortic sinus vortex on sinus washout mechanism [11, 12] and overall performance of the aortic valve [4, 13] have been investigated. For example, Toninato *et al.* [4] carried out an in-vitro experiment with different bioprosthetic valves and investigated vortical structures downstream of the valves in the presence and absence of the sinuses. They showed that the formation of the vortices in the sinuses of a bioprosthetic valve affects the ejection and closing phases. Hatoum *et al.* [11] evaluated the influence of the depth and angle of the transcatheter aortic valve (TAV) positioning on sinus vortices, transvalvular pressure gradient (TPG), leakage fraction (LF) and sinus washout mechanism. They showed that the flow pattern in sinuses is highly affected by the depth and rotation of the TAV which then impacts TPG, LF, and sinus washout mechanism. A similar study was carried out by the same group [12] in which they demonstrated the effect of sinus vortex structure on transcatheter aortic valve replacement (TAVR) operation and likelihood of leaflets thrombosis downstream of TAVR because of the poor sinus washout mechanisms.

The coronary artery flow has an impact on sinus vortex topologies and hemodynamics [9, 10, 12]. Recently, Moore *et al*. [10] studied the effects of the presence of the coronary artery flow on aortic leaflets mechanics and sinus hemodynamics. They showed that a leaflet corresponding to a coronary sinus opens 10% more than that of with non-coronary sinuses.

Furthermore, they also demonstrated that the presence of coronary flow increases flow velocity near the leaflets base and pushes the vorticities deeper into the sinus which affects wall shear stress on the leaflets. Several numerical studies also have investigated the effects of the presence of the coronary flow on sinus hemodynamics [14-16]. For example, Wald *et al*. [14] studied the influences of aortic stenosis (AV) and TAV implementation on coronary blood flow during diastole phases. They showed that the AS increases the jet velocity along the valve and as a result the vortex in sinus corresponding to a valve with sever degree of stenosis moves towards downstream of leaflets and affects coronary artery flow. They elucidated the clinically observed phenomenon that AV and coronary artery flow are interdependent [16].

Leaflets stiffening plays a crucial role in initiation and progression of CAVD because of its effect on sinus vortex structures and wall shear stress on the leaflets [17-20]. However, it is not well understood yet how CAVD initiates and progresses, it is believed that lower shear stress on leaflets significantly impacts CAVD [17, 19, 21, 22]. Recently, Hatoum *et al.* [11] showed the effect of TAV rotation on shear stress patterns on the leaflets. They also investigated the effect of the presence and absence of coronary arteries on shear stress distribution on leaflets. They demonstrated that the leaflets of the bioprosthetic aortic valve with coronary artery ostia witness higher ranges of wall shear stress compared to that of without coronary artery ostia. Later, another study [23] have been carried out by the same research group in which they have investigated the effect of leaflets stiffening on wall shear stress on the leaflets. They visualised the aortic sinus vortex structures corresponding to the valves with different degrees of calcification and evaluated their association with CAVD. They showed that the severely calcified aortic valve experiences lower magnitudes of wall shear stress on the leaflets compared to moderately and mildly calcified cases.

However previous studies have investigated the effect of the leaflet stiffening on sinus vortex structures and valve opening and closing period, there is a gap of knowledge regarding the influence of the positions of the coronary artery ostia and the presence of different degrees of coronary artery stenosis accompanied with leaflet stiffening on sinus vortex structures and accordingly probability density function of wall shear stress distribution on leaflets. Thus, in this article, the effect of leaflets stiffening, different degrees of coronary artery stenosis, and different positions of the coronary artery ostia, on wall shear stress distribution on leaflets is reported. The aim of this study is to elucidate how the geometrical variations (leaflet stiffening and different positions of the coronary artery ostia) and the presence of the different degrees of the coronary artery stenosis can change sinus vortex structures and what are their potential relationship with CAVD. A two-dimensional FSI model of a healthy, a calcified and a severely calcified aortic valve was developed in ANSYS Workbench 19.1. The geometry of the domain and flow field parameters were extracted from the echocardiography images available in the literature. FSI modelling was utilised to determine the interaction between the blood flow and aortic valve leaflets. The $k-\omega$ turbulence model was used to compute the turbulent flow field downstream of the leaflets. The effects of the leaflet stiffening considering coronary artery atherosclerosis on the vortical structures inside the sinus were studied. The probability density function (PDF) of wall shear stresses on the leaflets corresponding to a healthy, a calcified, and a severely calcified aortic valve with taking into account the different degrees of coronary artery stenosis and positions of the coronary artery ostia were calculated and compared.

6.3 Computational Model

Commercial ANSYS software was utilised to simulate a two-dimensional fluid structure interaction model of an aortic valve with healthy leaflets. A 2D echocardiography image from a 27 years old subject with healthy valve available in the literature [24] was used to generate

the geometry of a two-dimensional FSI model. The simulated model includes two main domains: structural domain and fluid domain including sinuses, coronary arteries with different degrees of stenosis, and aortic root. A two-way system coupling technique was used to simulate the interaction between the structural and fluid domains. The details of both domains are explained in the following sections.

6.3.1 Fluid domain (blood flow)

The different parts of the fluid domain including inlet, blood flow, outlets (aorta and coronary) are shown in Figure 6.1 a. The structure of the mesh corresponding to a healthy aortic valve with healthy and stenosed coronary arteries are shown in Figure 6.1 b-e. The model is extracted from the echocardiography available in the literature which is shown in Figure 6.1 f. The blood flow is assumed as an isothermal, Newtonian, and incompressible fluid with a density and viscosity of 1060 kg/m^3 and 0.0035578 Pa.s, respectively [25]. To generate unstructured mesh for the fluid domain, the sweep method was utilised with around 10,000 prism elements. As it is seen in Figure 6.1 b, to accurately model the flow in the vicinity of the walls of the leaflets, a denser mesh is generated near the leaflets and the wall of the arteries. In order to verify the results, the mesh independency study was conducted for pressure and velocity considering two different mesh size of 10,000 and 14,000. The results show that the calculated parameters change only 2% while the computational time increases by 40%. Thus, it was assumed that 10,000 elements in the domain produces a sufficient resolution to obtain more accurate results.

In order to accurately model the dynamical movement of the aortic valve leaflets, the mesh of the computational domain was modified at every time step. To re-mesh the fluid domain at every time step, spring-based smoothing and re-meshing techniques were utilised. The k-ω SST turbulence model was utilised to accurately model the separated flow in the vicinity of the leaflets. A physiological velocity profile (shown in Figure 6.2) extracted from the Doppler echocardiography technique [16] was applied as a boundary condition at the inlet of the fluid domain. At the outlet of the coronary arteries, a transient pressure profile (shown in Figure 6.2) was considered as a boundary condition. These data were collected from the averaged clinical data available in the literature [26]. At the outlet of the aorta, the outflow boundary condition was applied to extrapolate the required information from the fluid domain. The walls of the sinuses were considered to be rigid. In order to validate this simplification, a sensitivity study was conducted on the pressure and velocity components for two different models: one model with elastic sinus walls and leaflets, and another model with solid sinus wall but elastic leaflets. Results demonstrate that the calculated parameters change only 0.1% while the computational time increases by 20%. Therefore, the model with elastic leaflets and solid sinus wall was studied in the current study.

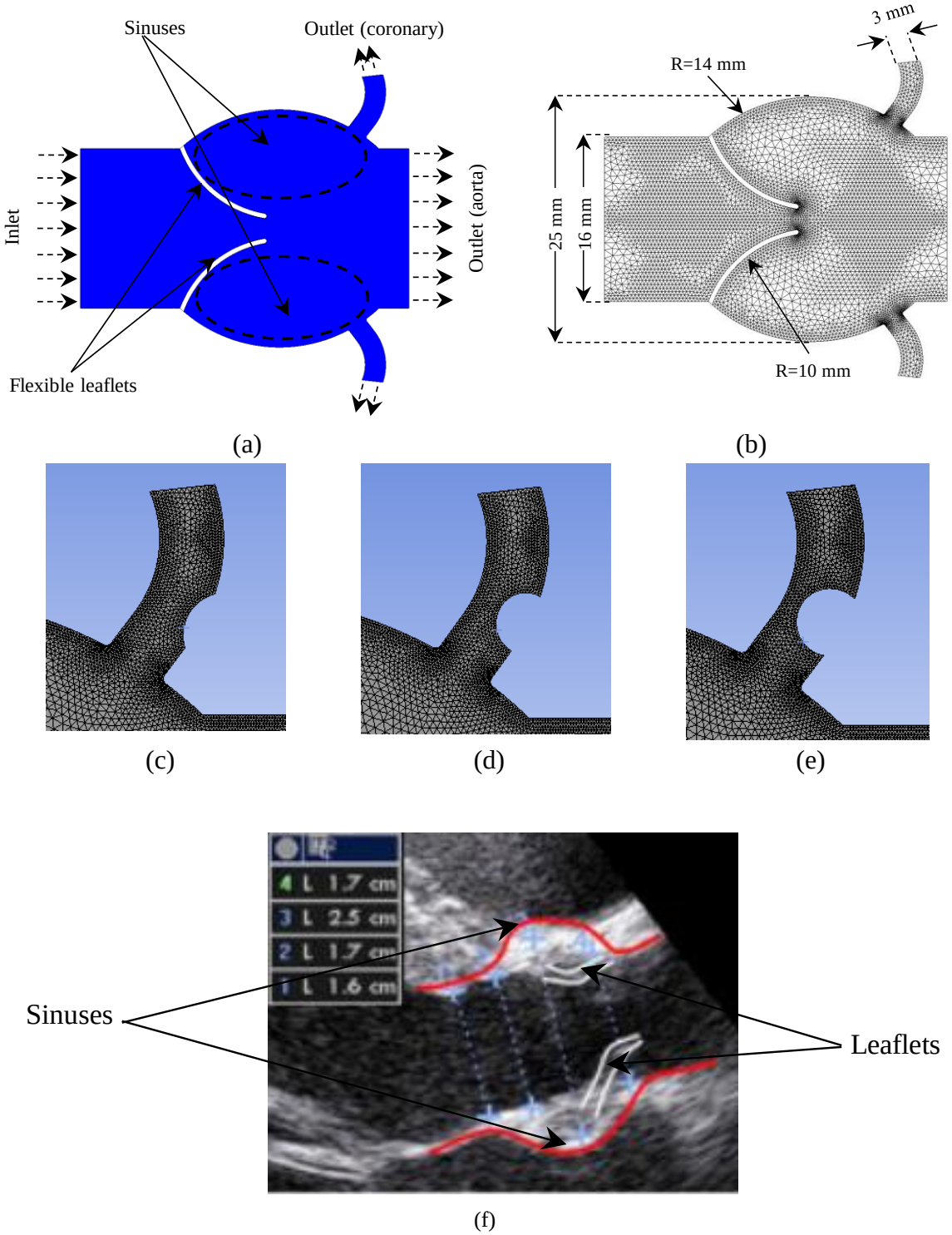

Figure 6.1 A schematic of (a) healthy aortic valve with flexible leaflets. The sinuses are marked by a black dash-line, flow directions for the inlet and outlet are shown using black arrows, (b) fluid domain mesh structure and boundary conditions. A denser meshes structures is used near the wall and leaflets to improve the accuracy of results. Coronary artery mesh structure with different degrees of stenosis (c) 25% (d) 50% (e) 75%, and (f) echocardiography images from a healthy aortic valve [24]; the shape of the sinuses and leaflets are traced using a red and white dash-line, respectively.

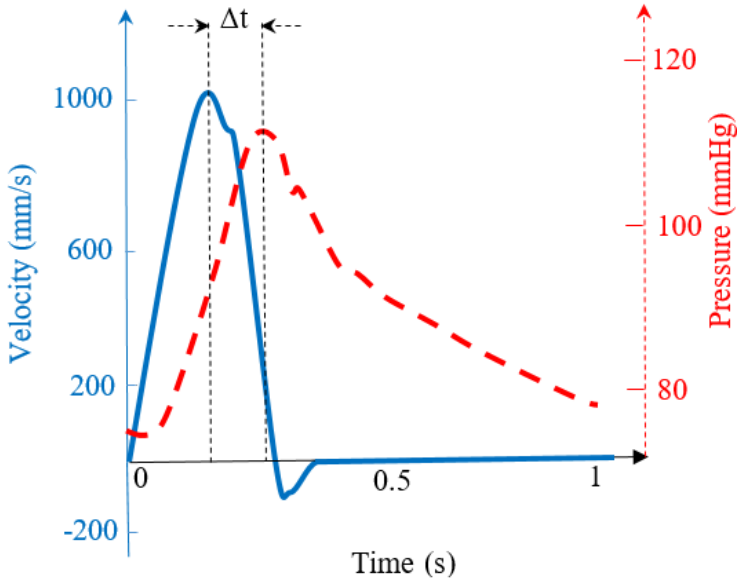

Figure 6.2 Inlet transient velocity profile applied at the inlet plane of the model (blue), and physiological pressure at coronary outlets (red). Based on measurements by [16, 24, 26].

6.3.2 Structural domain (deformable leaflets)

The structural domain includes two deformable leaflets which can move during the systole phase because of the force applied by the fluid domain. The structural part of a healthy valve was considered as isotropic material with Young's modulus, density and Poisson's ratio of 2MPa, 1060 kg/m^3, and 0.3, respectively [24, 27, 28]. In the current study, it was assumed that the calcium deposits uniformly along the leaflets which changes the Young's modulus of the leaflets to 10MPa (calcified case) and 20MPa (severely calcified case) [24]. The structural part was solved using Mechanical APDL module of the ANSYS. Leaflets were meshed based on the sweep method with approximately 120 quadratic tetrahedral element having at least two elements through the thickness of the leaflets. A mesh convergence study was conducted by applying constant pressure along the leaflets. Results revealed that the mesh independency is achieved by considering 100 tetrahedral elements along the leaflets with maximum skewness of 0.43. The mechanical characteristics of structural and fluid domains accompanied with applied boundary conditions are presented in Table 6.1 and Table 6.2, respectively.

Table 6.1 Mechanical properties of the fluid and structural domains used in the modelling

Domain	**Dynamic viscosity (Pa.s)**	**Density (kg/m^3)**	**Young's modulus (MPa)**	**Poisson's ratio**
Fluid (blood) Incompressible, Isothermal, Newtonian	0.0035578	1060	---	---
Structure (leaflets) Linear elastic, Isotropic	---	1060	2 (healthy) 10 (calcified) 20 (severely calcified)	0.3

Table 6.2 Boundary conditions used in the modelling

Inlet	Outlets (coronary and aorta)	FSI surface	Walls
Transient pulsatile velocity inlet	Physiological pressure outlet Outflow in aorta Outlet	Fluid structure interaction surface between the flexible elastic leaflets and blood flow	Solid walls for sinuses and aortic root

6.3.3 Two-way coupling FSI

To model the interaction between the structural and fluid domains, two techniques are typically utilised: one is known as one-way coupling and another one is two-way coupling [29]. Due to the large deformation of the leaflets [30], the two-way coupling is frequently used by researchers to simulate the interaction between the structural (flexible leaflets) and fluid domains (blood flow). The system coupling module of the commercial software ANSYS was utilised in the current work in order to simulate the interaction between the structural (flexible leaflets) and fluid (blood flow) domains. FLUENT module in ANSYS was used to solve the Navier-Stokes, and turbulence equations within the fluid domain. Mechanical APDL was utilised to solve the deformation equation corresponding to the structural (flexible leaflets) domain. System coupling module of the ANSYS was used to exchange the displacement and force data between the structural and fluid domain at every time step.

6.4 Experimental setup

Data obtained from the in-vitro experiment was used to validate the developed computational model. Figure 6.3 a and b show the experimental test rig which includes (1) a controllable in–house piston pump which is able to produce physiological aortic flow profile, (2) and (4) pressure sensors (OMEGA PX319 silicon pressure sensor) to measure the pressure before and after the bioprosthetic valve in order to calculate the transvalvular pressure gradient, (3) a 21mm Edwards Intuity (Edwards Lifesciences, Irvine, California) bioprosthetic aortic valve mounted inside a silicon-based sinus chamber, (5) a flow sensor (OPTIBATCH 4011C) used to measure the physiological aortic flow rate, (6) a compliance chamber used to add resistance to the aortic flow and create appropriate backflow during the diastole, (7) a resistance valve, (8) a fluid reservoir, (9) a computer, power supply and DAQ card (NI USB-6211). Figure 6.3 c shows the test section including the silicon-based sinus model and the mounted bioprosthetic aortic valve (shown in Figure 6.3 d).

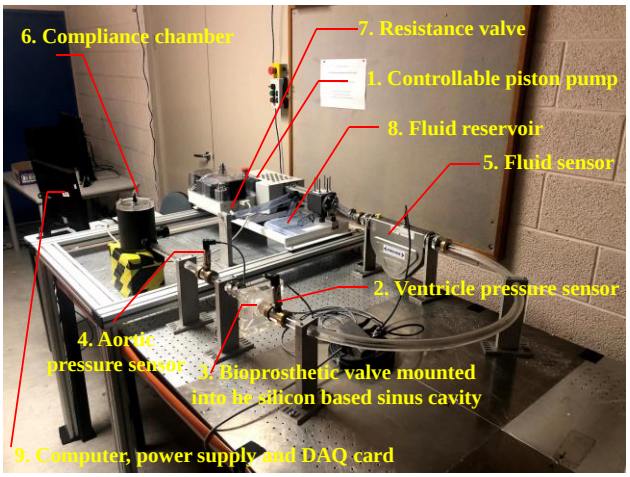

(a)

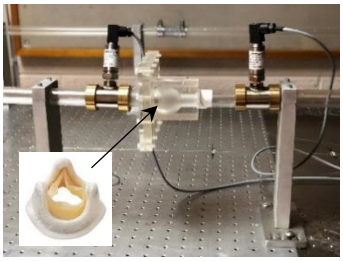

(b)

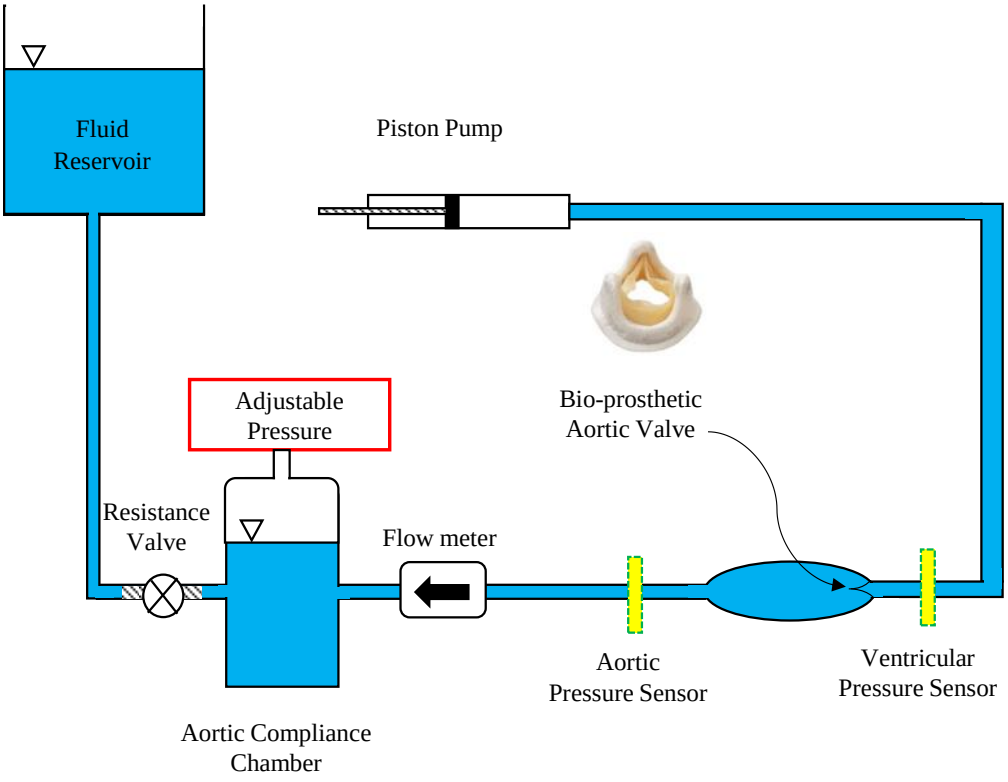

(c)

Figure 6.3 (a) experimental test setup: (1) in-house controllable piston-pump, (2) ventricle pressure sensor, (3) bioprosthetic aortic valve mounted inside silicon-based sinus chamber, (4) aortic pressure sensor, (5) flow sensor, (6) compliance chamber, (7) resistance valve, (8) fluid reservoir, (9) computer, power supply and DAQ card, (b) test section with a 21 mm bioprosthetic Edwards Intuity aortic valve (Edwards Lifesciences, Irvine, California) [31] mounted inside silicon based sinus chamber, (c) Schematic of the test setup.

To mimic the viscosity and density of the blood, the working fluid was chosen a mixture of 40% glycerine and 60% distilled water by mass fraction based on the literature [32-34]. Mach#3 software was used to control the in-house built piston-pump to produce the physiological flow rate profile through the aortic valve. The pressures before and after the valve were measured using two pressure sensors (OMEGA PX319 silicon pressure sensor with

accuracy of 0.04%) to ensure physiological conditions. Flow and pressure measurements were recorded in LabVIEW at least for 50 cycles. The aortic flow rate was measured using flow meter (OPTIBATCH 4011C with accuracy of 0.15%) and compared to that of extracted from the computational model. As it can be seen in Figure 6.4, there is a good agreement between the aortic flow rate profile between the experimental and computational models. The averaged TPG corresponding to a bioprosthetic valve used in the experiment is measured (658.32) and compared with that of the computational model (633 Pa). It is worth mentioning that, there is only 4% differences between the TPG measured in experiment and calculated TPG in FSI simulation. The pressure and flow rate measurements reported in this study are the average data of the eight measurements, and the maximum measurements error were reported as 0.15%.

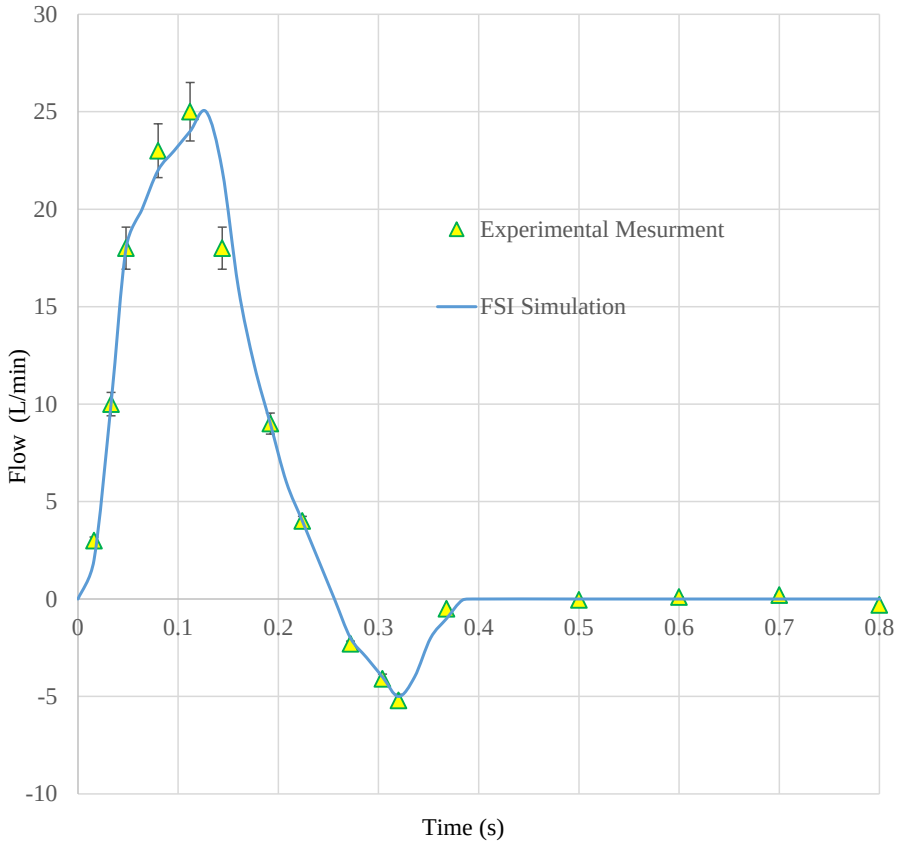

Figure 6.4 Aortic valve flow waveform comparison between the experimental and computational models.

6.5 Results and discussions

Velocity streamline at peak systole (t=0.1s) for a healthy aortic valve with healthy coronary arteries, a calcified aortic valve with 25% stenosed coronary arteries, and severely calcified aortic valve with 75% stenosed coronary arteries are depicted in Figure 6.5 (a-c), respectively. As it can be seen, the valve orifice diameter decreases from 14.2 mm (shown in Figure 6.5 a) for the healthy valve with healthy coronary arteries to 10.4 mm (shown in Figure 6.5 b) for the calcified valve with 25% stenosed coronary arteries, and to 8.11mm (shown in Figure 6.5 c) for the severely calcified valve with 75% stenosed coronary arteries. It is worth mentioning that valve orifice diameter corresponding to severely calcified case with healthy coronary arteries is approximately 9.6 mm which is 18 % larger than that of with a healthy valve with 75% stenosed coronary arteries. It means that the more the valve becomes stiff and the coronary arteries get blocked, the less is the valve orifice diameter. Furthermore, the leaflets

stiffening accompanied by coronary artery stenoses increases the jet velocity in the aortic valve. As can be seen, the maximum jet velocity at peak systole increases from 1.65 m/s for the healthy valve with healthy coronary arteries to 2.34 m/s for the calcified valve with 25% stenosed coronary arteries, and to 2.51 m/s for the severely calcified case with 75% stenosed coronary arteries. By contrast, leaflets stiffening accompanied by coronary artery stenosis decreases coronary artery flow velocity. As shown in Figure 6.5 (a-c), the velocity inside coronary arteries at peak systole decreases from 0.64 m/s for the healthy valve with healthy coronary arteries to 0.45 m/s for the calcified valve with 25% stenosed coronary arteries, and 0.23 m/s for the severely calcified case with 75% stenosed coronary arteries.

Leaflets stiffening and coronary artery stenosis affect the sinus vortex structures and coronary flow features. As depicted in Figure 6.5 a, recirculation zone corresponding to the healthy valve with healthy coronary arteries (shown with RZ_1) at peak systole has two main vortices occupying aortic valve sinuses. These vortices are smaller compared to those corresponding to the sinuses of the severely calcified valve with 75% stenosed coronary arteries (shown with RZ_2 in Figure 6.5 c). Furthermore, the bigger vortices generated in the sinuses of the severely calcified valve with 75% stenosed coronary arteries are closer to coronary artery ostia compared to those of with the sinuses of the healthy valve with healthy coronary arteries. The increase in the size of the vortices can prevent blood flowing into the coronary arteries at peak systole and change the flow structures inside the coronary arteries.

The presence of stenosis inside coronary arteries can, in turn, affect the flow features in coronary arteries. As can be seen, there is a large vortex near the right wall of the coronary arteries corresponding to a healthy valve with healthy coronary arteries (shown with R_1 in Figure 6.5 a). As the coronary arteries get blocked, the number of vortices increases. As depicted, there are two main vortices inside the coronary arteries before and after the stenosis (shown in with R_2 and R_3 in Figure 6.5 b). It is worth mentioning that the more the coronary arteries become blocked, the bigger vortices generated before and after the coronary stenosis (shown with R_4 and R_5 in Figure 6.5 c).

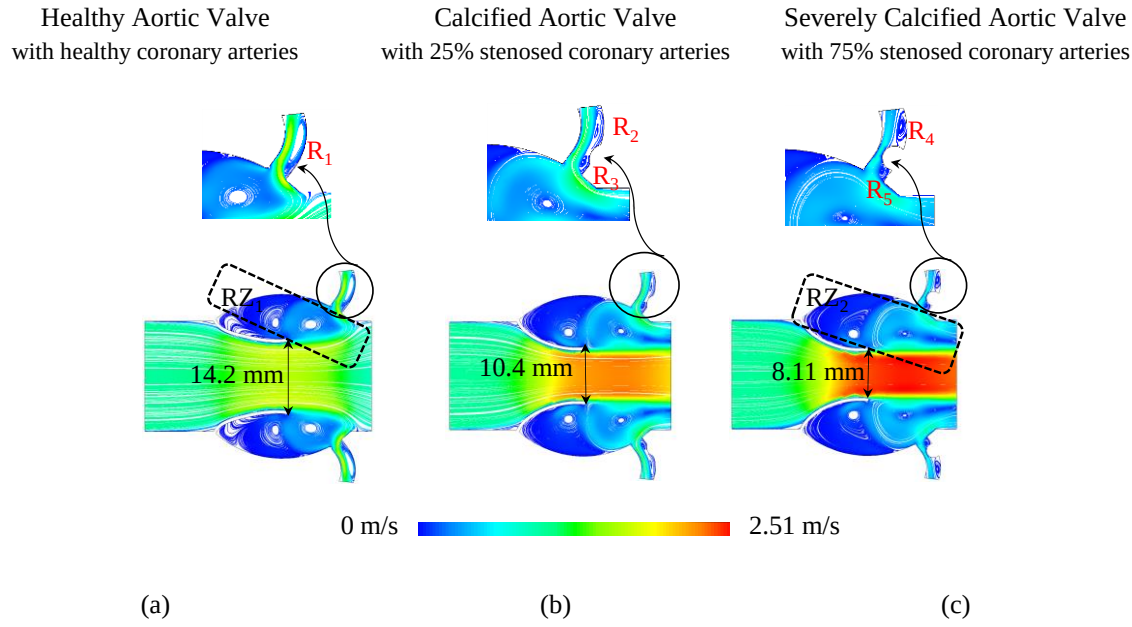

Figure 6.5 Velocity streamlines for (a) a healthy aortic valve with healthy coronary artery, (b) a calcified valve with 25% stenosed coronary artery, and (c) a severely calcified valve with 75% stenosed coronary artery.

To illustrate the effects of the leaflet stiffening and the position of the coronary artery ostia on sinus vortex structures, the circulation versus time for the healthy, calcified, and severely calcified aortic valve with a healthy distal, middle and proximal coronary artery ostia are depicted in Figure 6.6 a-c. Generally, leaflets stiffening significantly changes the vortex structures inside the sinus cavity. As it can be seen in Figure 6.6 a, a dominant counter clockwise (CCW) vortex corresponding to a healthy valve with a healthy distal coronary artery ostia has a peak at approximately +0.016 m^2/s (shown with P_1 in Figure 6.6 a), whilst the dominant vortex corresponding to a severely calcified case with healthy distal coronary artery ostia is a clockwise (CW) vortex with the strength of +0.008 m^2/s. It is due to a larger sinus cavity for the severely calcified valve in comparison with a healthy valve which affects the number of CW and CCW vortices inside the sinus cavity. It means that the severely calcified aortic valve witnesses a large number of CW vortices generated near the leaflets impacting the dominant vortex's strength and structure.

The effects of the position of the coronary artery ostia on sinus vortex structures are illustrated in Figure 6.6 a-c. As shown, peak circulation strength decreases from approximately +0.016 m^2/s (shown with P_1 in Figure 6.6 a) for a healthy valve with distal coronary artery ostia, to +0.006 m^2/s (shown with P_3 in Figure 6.6 a) for that of with proximal coronary artery ostia. For the severely calcified valve, the peak decreases from approximately -0.01 m^2/s (shown with P_2 in Figure 6.6 a) for the severely calcified case with distal coronary artery ostia to -0.002 (shown with P_4 in Figure 6.6 c) for that of with proximal coronary artery ostia. It means that as the coronary artery ostia becomes closer to the base of the leaflet, the circulation strength reduces. It is also worth mentioning that a valve with a middle coronary artery ostia witnesses a larger recirculation strength during the diastole phase (shown with Z_B in Figure 6.6 b) compared to that of corresponding to a valve with a proximal and a distal coronary artery ostia (shown with Z_A and Z_C in Figure 6.6 a and c).

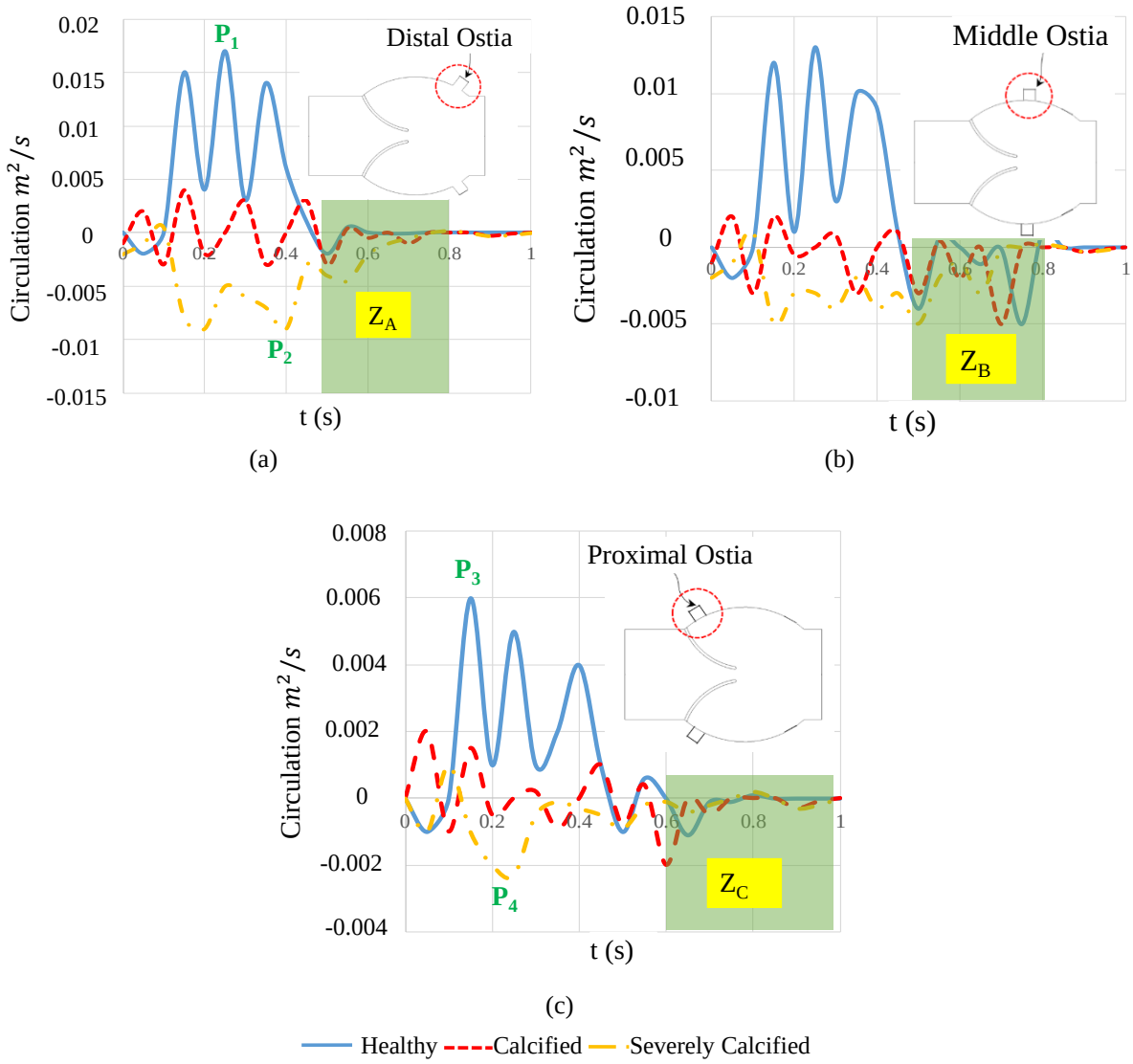

Figure 6.6 Circulation versus time inside sinus cavity for healthy, calcified, and severely calcified aortic valves with a healthy (a) distal, (b) middle, and (c) proximal coronary arteries.

The probability density function (PDF) of shear stress distribution on leaflets during systole and diastole for the healthy, calcified, and severely calcified aortic valve with a healthy distal, middle, and proximal coronary artery ostia is illustrated in Figure 6.7. Generally, as shown in Figure 6.7 a and b (see orange shaded rectangular), a severely calcified valve experiences lower ranges of shear stress during systole (- 0.5 to + 0.5 Pa), and diastole (-0.1 to + 0.2 Pa) on the leaflets with a higher probability of having lower shear stresses compared to those of with healthy valve which are (systole: -1.5 to + 2 Pa, and diastole: -0.55 to + 0.55 Pa). Furthermore, Figure 6.7 shows that the more the coronary artery ostia moves towards the leaflets base, the less is the range of the wall shear stress on the leaflets, and the higher is the probability of having lower shear stress on the leaflets. For example, shear stress ranges corresponding to a healthy valve with distal, middle, and proximal coronary artery ostia during the systole are shown in Figure 6.7 c and e (orange and green shaded rectangular). As can be seen, the leaflets of the healthy valve with a distal coronary artery ostia have ranges around (-1.5 to + 2 Pa), whilst that of corresponding to a healthy valve with middle and proximal coronary artery ostia are (-1.2 to + 1.2 Pa) and (-0.6 to +0.6 Pa), respectively. This means that a healthy valve with a proximal coronary artery ostia is more prone to calcification because of having a high probability of lower ranges of shear stress on the leaflets.

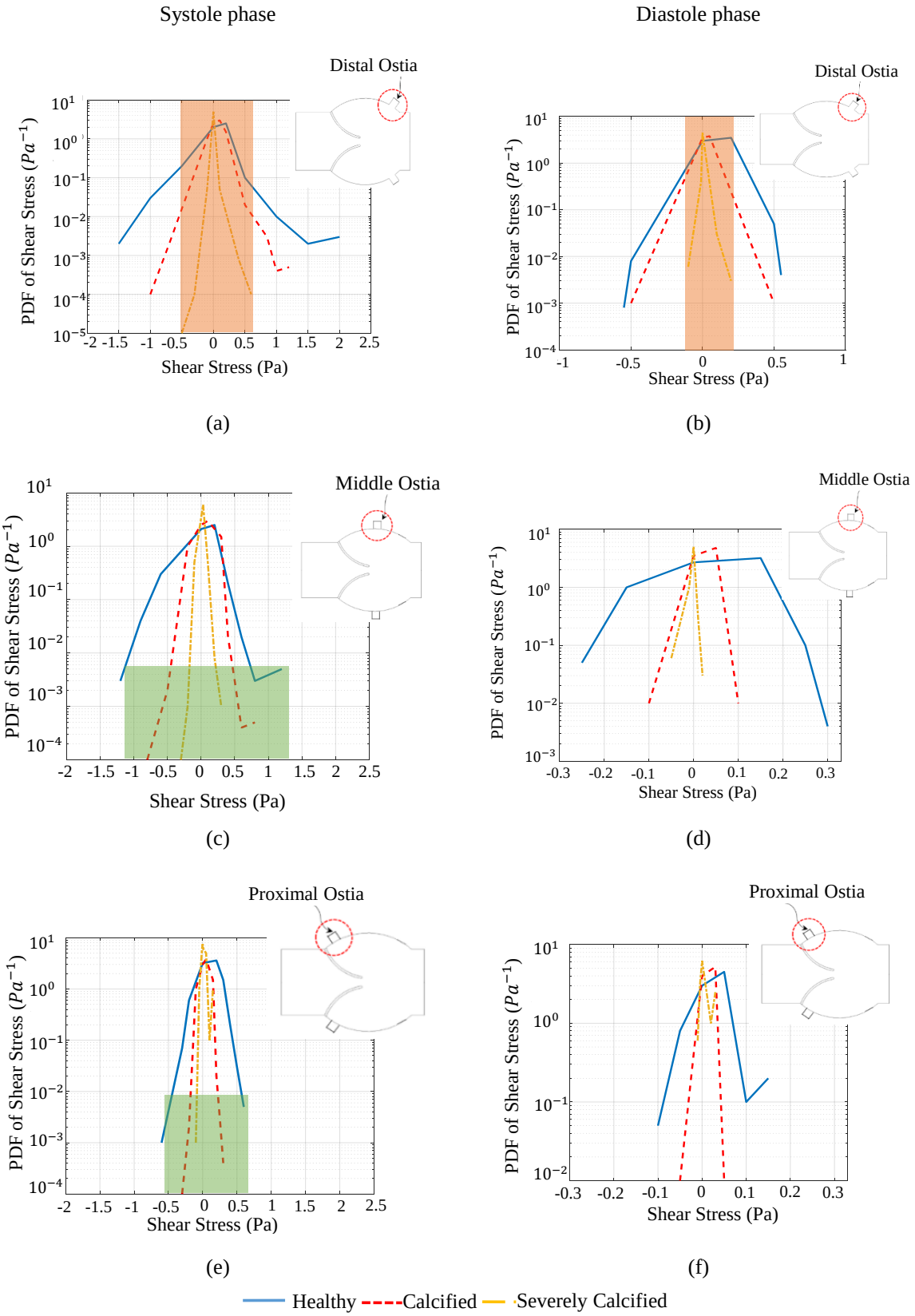

Figure 6.7 Log scale probability density function of shear stress distribution on leaflets during systole and diastole for healthy, calcified, and severely calcified aortic valve with a healthy (a, b) distal, (c, d) middle, and (e, f) proximal coronary arteries.

The effects of the different degrees of coronary artery stenoses accompanied by leaflets stiffening on sinus vortex structures are demonstrated in Figure 6.8 a-c. As can be seen, the presence of a coronary artery stenosis accompanied by intensified circulation strength in the sinus cavity. For example, the circulation strength corresponding to a healthy valve with a 25%

stenosed coronary artery has a peak around 0.012 m^2/s (shown with P_5 in Figure 6.8 a) compared with that of related to a healthy valve with healthy coronary arteries which was approximately 0.016 m^2/s (shown with P_1 in Figure 6.6 a). Similarly, for the severely calcified valve, the circulation strength peak corresponding to a valve with 75% stenosed coronary artery (shown with P_6 in Figure 6.8 c) is -0.025 m^2/s, while that of with the valve with healthy coronary arteries was around -0.002 m^2/s (shown with P_4 in Figure 6.6 c).

Furthermore, the most interesting result is that the circulation variation in sinus cavity corresponding to a calcified aortic valve with 50% and 75% coronary artery stenosis fluctuates with almost negative magnitudes (as shown in Figure 6.8 b and c), While, this behaviour corresponding to a calcified valve with the healthy coronary artery (shown in Figure 6.6 b and c) is different as it fluctuates around the horizontal axis with positive and negative magnitudes. It can be concluded that a dominant vortex in sinus cavity for the calcified valve with 50 and 75% stenosed coronary arteries is a CW vortex with negative magnitude during the cardiac cycle, while that of related to a valve with heathy coronary arteries is a combination of CW and CCW vortices converting to each other over the cardiac cycle.

It is also worth mentioning that the presence of higher degrees of stenosis (75% stenosis) inside the coronary arteries creates a recirculation during the diastole (shown with orange shaded rectangular in Figure 6.8 c) compared with that with 25% stenosis (shown with orange shaded rectangular in Figure 6.8 a) which is almost zero. This circulation strength can affect shear stress on leaflets during the diastole.

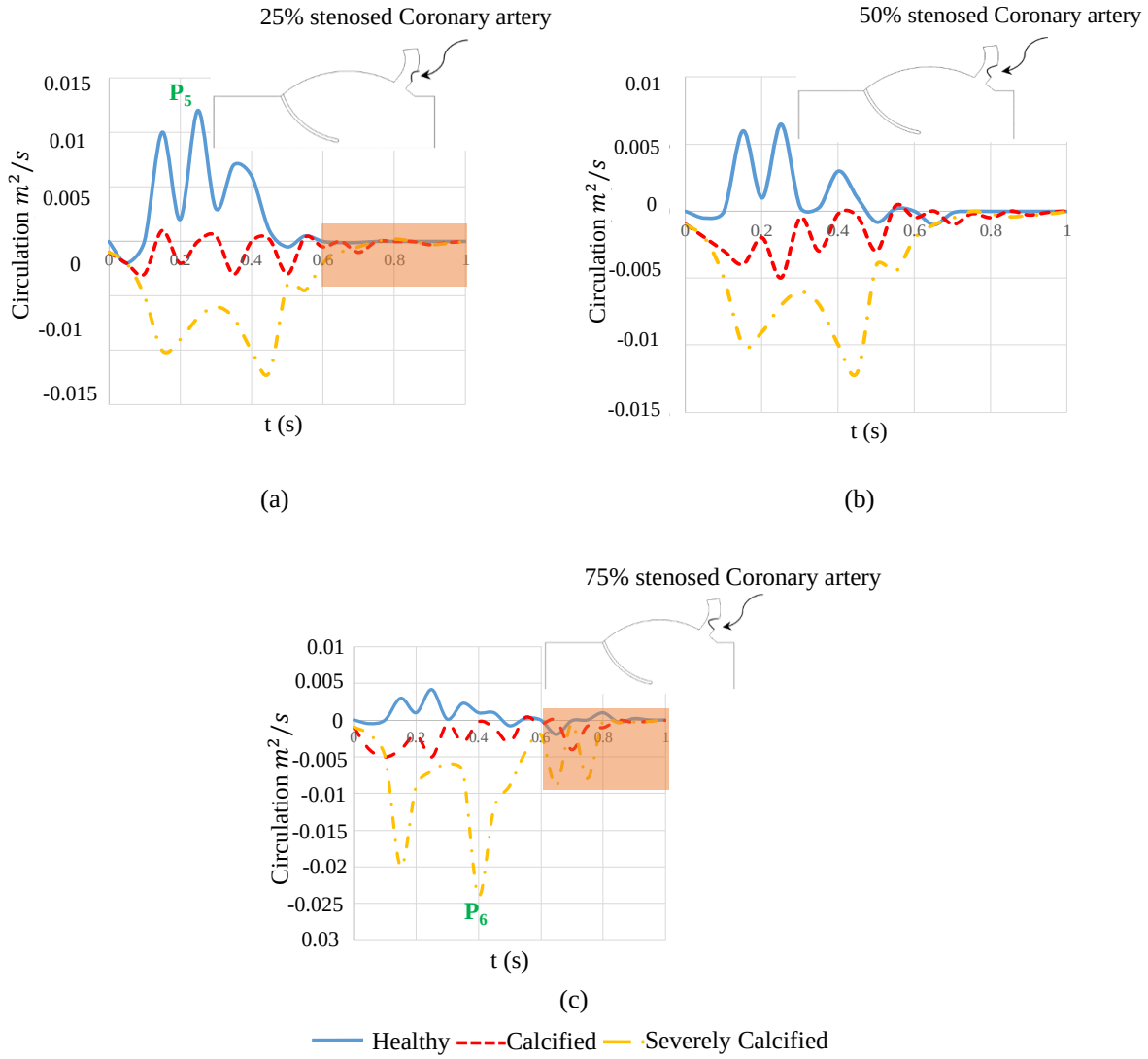

Figure 6.8 Circulation versus time inside sinus cavity for healthy, calcified, and severely calcified aortic valves with (a) 25%, (b) 50%, and (c) 75% stenosed coronary arteries.

The effects of the position of the coronary artery ostia (distal, middle, and proximal) for the healthy, calcified, and severely calcified valves with severe coronary stenosis (75% degrees of stenosis) on shear stress on the leaflets during systole and diastole are illustrated in Figure 6.9. Generally, the more the coronary artery ostia moves towards the leaflets' base, the less is the shear stress ranges on the leaflets, and the higher is the probability of the generation of smaller shear stress. For example, as can be seen in Figure 6.9, a healthy valve with a proximal stenosed coronary artery experiences lower ranges of shear stresses on the leaflets during the systole (-0.3 to +0.35 Pa), and diastole (-0.05 to +0.1 Pa) compared with a healthy valve with a middle and a distal coronary artery ostia which witness shear stress ranging from (systole: -1 to +1Pa and diastole: -0.15 to +0.15 Pa) and (systole: -1.2 to +1.2 Pa, and diastole: -0.25 to +0.25 Pa), respectively.

Furthermore, a severely calcified valve with a 75% stenosed proximal coronary artery has the lowest ranges of the shear stress among the other kind of severely calcified valves. As it is clear from Figure 6.9 a and d, the shear stress ranges corresponding to a severely calcified valve with a proximal 75% stenosed coronary artery during systole and diastole are around (-0.02 to + 0.05 Pa) and (-0.002 to + 0.01 Pa), respectively. Whilst, a severely calcified aortic

valve with a middle and a distal 75% stenosed coronary arteries confront higher shear stress ranging from (-0.2 to + 0.2 Pa; -1 to + 0.25Pa) for the systole and (-0.01 to + 0.02 Pa; -0.05 to + 0.02 Pa) for the diastole. It is worth mentioning that shear stress ranges corresponding to any kind of valves (healthy, calcified, and severely calcified) with healthy coronary arteries are higher than those of with 75% stenosed coronary arteries (comparing Figure 6.9 with Figure 6.7). It means that stenosis inside coronary arteries decreases shear stress on the leaflets and increases the probability of having lower shear stress ranges on the leaflets. The lower shear stress on the leaflets increases the progression of aortic valve calcification.

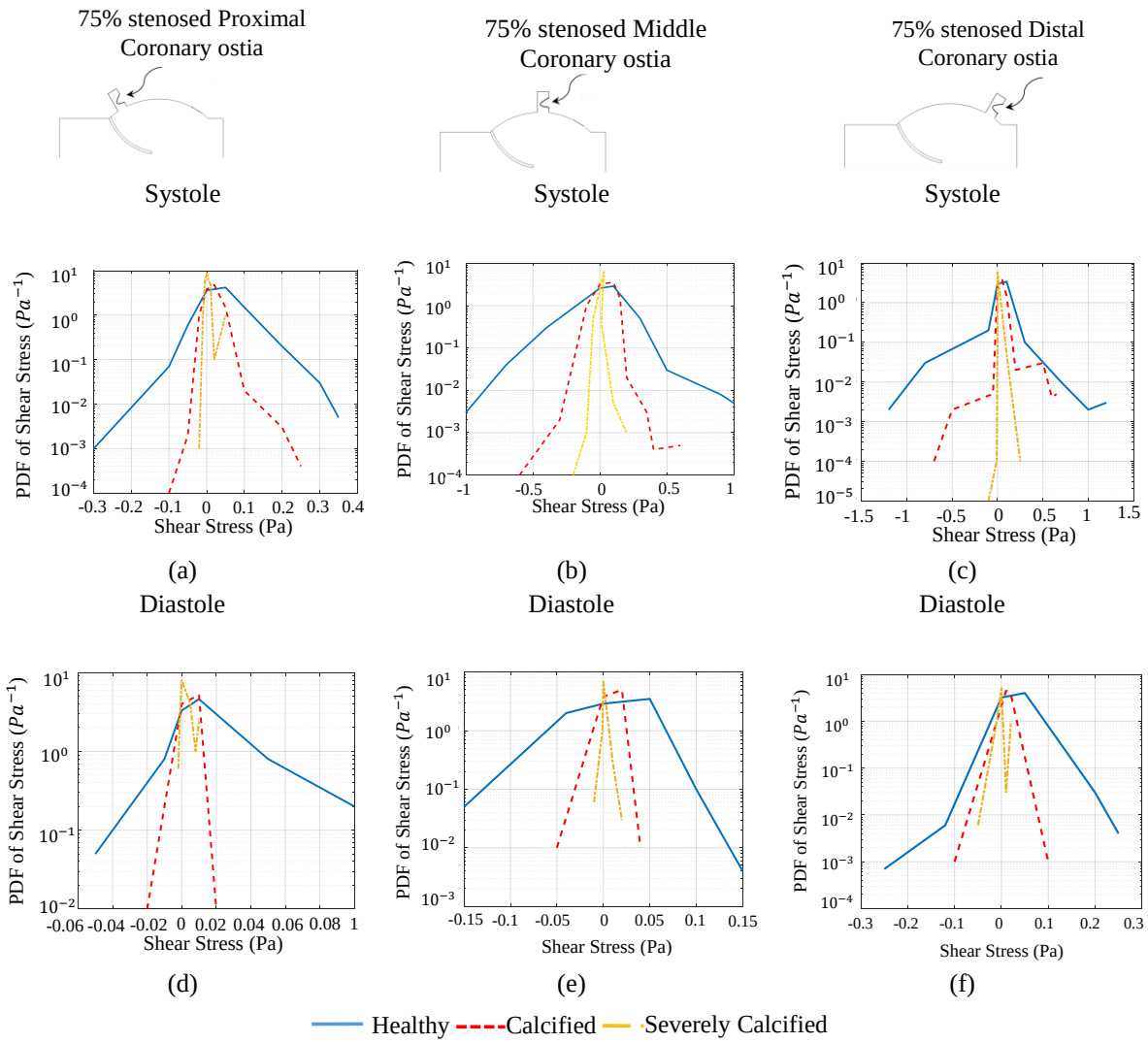

Figure 6.9 Log scale probability density function of shear stress distribution on leaflets during systole and diastole for healthy, calcified, and severely calcified aortic valve with a 75% (a, d) proximal, (b, e) middle, and (e, f) distal coronary arteries.

6.6 Conclusion

In the present study, fluid structure interaction modelling was used to investigate the effects of the leaflets stiffening, the positions of the coronary artery ostia and stenosis inside coronary artery on flow features, the sinus vortex structures, and shear stress on the aortic valve leaflets. The presence of the coronary artery stenosis accompanied with leaflets stiffening significantly impact flow features inside the sinuses and changes shear stress on the leaflets which eventually affects the aortic valve performance. The most important outcomes of this study can be summarised as follows:

- Leaflets stiffening affects not only valve orifice diameter, jet velocity along the valve but also significantly changes sinus vortex structures and accordingly shear stress on the leaflets; the more the valve becomes calcified, the less is the shear stress ranges and the higher is the probability of having lower sheas stress on the leaflets.
- The positions of the coronary artery ostia impacts on sinus vortex structures and sheas stress on the leaflets. The more the valve moves towards leaflets base, the less is the shears stress ranges on the leaflets. For example, a healthy valve with healthy proximal coronary artery ostia witnesses lower ranges of shear stress with higher probability of corresponding shear stress. It means that a healthy valve with proximal coronary artery ostia are more prone to get calcified over times compared to those of with distal and middle coronary artery ostia.
- The presence of stenosis inside coronary arteries accompanied with leaflets stiffening intensify flow features inside sinuses and decreases shear stress ranges on the leaflets. For example, a severely calcified aortic valve with 75% stenosed proximal coronary arteries experiences the lowest ranges of shear stress on the leaflets with highest probability of corresponding shear stress and accordingly highest probability of progression of CAVD.

6.7 References

[1] L.P. Dasi, H.A. Simon, P. Socosky, A. P. Yoganathan, Fluid mechanics of artificial heart valves, Clinical and Experimental Pharmacology and Physiology, 36 (2009) 225-237.
[2] N. Saikrishnan, C. H. Yap, N.C. Milligan, N.V. Vasilyev, A.P. Yoganathan, In vitro characterization of bicuspid aortic valve hemodynamics using particle image velocimetry, Annals of Biomedical Engineering, 40 (2012) 1760-1775.
[3] A. Ducci, S. Tzamtzis, M.J. Mullen, G. Burriesci, Hemodynamics in the Valsalva sinuses after transcatheter aortic valve implantation (TAVI), The Journal of Heart Valve Disease, 22 (2013) 688-696.
[4] R. Toninato, J. Salmon, F. M. Susin, A. Ducci, G. Burriesci, Physiological vortices in the sinuses of Valsalva: an in vitro approach for bio-prosthetic valves, Journal of Biomechanics, 49 (2016) 2635-2643.
[5] H. L. Leo, H. Simon, J. Carberry, S. C. Lee, A.P. Yoganathan, A comparison of flow field structures of two tri-leaflet polymeric heart valves, Annals of Biomedical Engineering, 33 (2005) 429-443.
[6] H. L. Leo, L. P. Dasi, J. Carberry, H. Simon, A. P. Yoganathan, Fluid dynamic assessment of three polymeric heart valves using particle image velocimetry, Annals of Biomedical Engineering, 34 (2006) 936-952.
[7] D.A. Rubenstein, W. Yin, M.D. Frame, Biofluid Mechanics: an Introduction to Fluid Mechanics, Macrocirculation, and Microcirculation, Elsevier, Amsterdam (2012).
[8] C.G. Caro, T.J. Pedley, R.C. Schroter, W.A. Seed, The Mechanics of Circulation (2nd ed.), Cambridge University Press, New York (2012).
[9] H. Hatoum, B. L. Moore, P. Maureira, J. Dollery, J. A. Crestanello, L. P. Dasi, Aortic sinus flow stasis likely in valve-in-valve transcatheter aortic valve implantation, The Journal of Thoracic and Cardiovascular Surgery, 154 (2017) 32-43.
[10] B. L. Moore, L. P. Dasi, Coronary flow impacts aortic leaflet mechanics and aortic sinus hemodynamics, Annals of Biomedical Engineering, 43 (2015) 2231-2241.
[11] H. Hatoum, J. Dollery, S. M. Lilly, A. Crestanello, L. P. Dasi, Implantation depth and rotational orientation effect on valve-in-valve hemodynamics and sinus flow, The Annals of Thoracic Surgery, 106 (2018) 70-78.
[12] H. Hatoum, J. Dollery, S. M. Lilly, J. Crestanello, L. P. Dasi, Impact of patient-specific morphologies on sinus flow stasis in transcatheter aortic valve replacement: an in vitro study, The Journal of Thoracic and Cardiovascular Surgery, 157 (2018) 540-549.

[13] H. Hatoum, B. L. Moore, L.P. Dasi., On the significance of systolic flow waveform on aortic valve energy loss, Annals of Biomedical Engineering, 46 (2018) 2102-2111.
[14] S. Wald, A. Liberzon, I. Avrahami, A numerical study of the hemodynamic effect of the aortic valve on coronary flow, Biomechanics and Modeling in Mechanobiology, 17 (2018) 319-338.
[15] M. Bianchi, G. Marom, R. P. Ghosh, O. M. Rotman, P. Parikh, L. Gruberg, D. Bluestein, Patient-specific simulation of transcatheter aortic valve replacement: impact of deployment options on paravalvular leakage, Biomechanics and Modeling in Mechanobiology, 18 (2019) 435-451.
[16] S. Nobari, R Mongrain, R Leask, R Cartier, The Effect of Aortic Wall and Aortic Leaflet Stiffening on Coronary Hemodynamic: A Fluid-Structure Interaction Study, Medical & Biological Engineering & Computing, 51 (2013) 923-936.
[17] J. Lincoln, V. Garg, Etiology of valvular heart disease, Circulation, 78 (2014) 1801-1807.
[18] D. A. Towler, Molecular and cellular aspects of calcific aortic valve disease, Circulation Research, 113 (2013) 198-208.
[19] B. Moore, L. P. Dasi, Spatiotemporal complexity of the aortic sinus vortex, 2014, 55 (2014) 1770-1778.
[20] M. Thubrikar, L. Bosher, S. Nolan, The mechanism of opening of the aortic valve, The Journal of Thoracic and Cardiovascular Surgery, 77 (1979) 863-870.
[21] T. E. David, J. Ivanov, Is degenerative calcification of the native aortic valve similar to calcification of bioprosthetic heart valves, The Journal of Thoracic and Cardiovascular Surgery, 126 (2003) 939-941.
[22] C. M. Otto, J. Kuusisto, D. D. Reichenbach, A. M. Gown, K. D. O'brien, Characterization of the early lesion of 'degenerative' valvular aortic stenosis. Histological and immunohistochemical studies, Circulation, 90 (1994) 844-853.
[23] H. Hatoum, L. P. Dasi, Spatiotemporal complexity of the aortic sinus vortex as a function of leaflet calcification, Annals of Biomedical Engineering, 47 (2019) 1116-1128.
[24] A. Amindari, L. Saltik, K. Kirkkopru, M. Yacoub, H.C. Yalcin, Assessment of calcified aortic valve leaflet deformations and blood flow dynamics using fluid-structure interaction modeling, Informatics in Medicine Unlocked, 9 (2017) 191-199.
[25] H. Mohammadi, R. Cartier, R. Mongrain, Derivation of a simplified relation for assessing aortic root pressure drop incorporating wall compliance, Medical & Biological Engineering & Computing, 53 (2015) 241-251.
[26] A.J. Pappano, W.G. Wier, Cardiovascular physiology, Mosby physiology monograph series, Elsevier, Philadelphia: 10th Edition (2007).
[27] R. Gnyaneshwar, R. K. Kumar, K.R. Balakrishnan, Dynamic analysis of the aortic valve using a finite element model, The Annals of Thoracic Surgery, 73 (2002) 1122-1129.
[28] A. Ranga, O. Bouchot, R. Mongrain, Computational simulations of the aortic valve validated by imaging data: evaluation of valvesparing techniques, Interactive Cardiovascular and Thoracic Surgery, 5 (2007) 373-378.
[29] F.K. Benra, H.J. Dohmen, J. Pei, S. Schuster, B. Wan, A comparison of oneway and two-way coupling methods for numerical analysis of fluid-structure interactions, Journal of Applied Mathematics, 6 (2011) 1-16.
[30] M. A. Fernández, J. F. Gerbeau, Algorithms for fluid-structure interaction problems, Journal of Cardivascular Mathematics, 1 (2009) 307-346.
[31] S. E. Jahren, P. P. Heinisch, J. Wirz, B. M. Winkler, T. Carrel, D. Obrist, Hemodynamic Performance of Edwards Intuity Valve in a Compliant Aortic Root Model, Conf Proc IEEE Eng Med Biol Soc, 33 (2015) 8-15.
[32] V. Deplano, Y. Knapp, E. Bertrand, E. Gaillard, Flow behaviour in an asymmetric compliant experimental model for abdominal aortic aneurysm, Journal of Biomechanics, 40 (2007) 2406-2413.

[33] J. Charonko, S. Karri, J. Schmieg, S. Prabhu, P. Vlachos, In vitro, timeresolved PIV comparison of the effect of stent design on wall shear stress, Annals of Biomedical Engineering, 37 (37) 1310-1321.
[34] D. Tanné, E. Bertrand, L. Kadem, P. Pibarot, R. Rieu, Assessment of left heart and pulmonary circulation flow dynamics by a new pulsed mock circulatory system, Experiments in Fluids, 48 (2010) 837-850.

Chapter 7

Conclusions and future work

The work presented in this thesis investigated a number of phenomena related to the dynamical motion of aortic valve leaflets, the hemodynamic variation within the aortic root, sinuses, and coronary arteries as well as the generation of sinus vortex structures. More specifically, this thesis has developed a numerical model to predict the variation of the hemodynamic parameters and find the correlation between the hemodynamic variation inside the sinus cavity and the initiation of calcific aortic valve diseases. The effect of the geometrical parameters on the hemodynamic variation inside the sinus cavity and the coronary arteries has also been studied. During the course of this research, numerical studies and in-vitro experiments were conducted to develop a better understanding of the correlation between the aortic valve hemodynamics and initiation and progression of aortic valve and coronary artery diseases.

7.1 Significance of present work

In spite of a vast number of studies in the field of cardiovascular fluid mechanics and numerical simulation of the dynamical motion of the aortic valve, the correlation between the variation of the hemodynamic parameters within the sinus cavity and the initiation of calcific aortic valve disease is still a subject of discussion. Much research into modelling of the aortic valve has been focused on simulation of the dynamical motion of the aortic valve leaflets using different numerical methods (such as finite element analysis, computational fluid dynamics, and fluid structure interaction) and considering different material properties of the aortic valve leaflets. However, in-vitro studies have shown a strong relation between calcification of the aortic valve and the valve orifice area. Therefore, there is a need to develop a numerical model which is able to calculate the hemodynamic variations inside the sinus cavity and coronary arteries in order to predict a correlation between the hemodynamic variations such as vorticity magnitude inside the sinus cavity, the wall shear stress on the leaflets and initiation of calcific aortic valve diseases. The main achievements and significance of this thesis can be summarised as:

- A numerical fluid structure interaction model of the dynamical motion of the aortic valve leaflets considering coronary arteries was developed using the system coupling module of ANSYS-Fluent software. The influence of stenosis of the aortic valve on the hemodynamic variations inside the aortic root, sinus cavity, and coronary arteries was investigated. It was found that stenosis of the aortic valve not only affects the hemodynamic parameters inside the aortic root such as transvalvular pressure gradient, and valve orifice diameter, but also significantly changes the coronary artery flow rate and accordingly, the wall shear stress on the coronary artery wall. These changes in the hemodynamic parameters inside the coronary artery weakens the wall of the coronary arteries and results in initiation of coronary artery atherosclerosis.
- The effect of the locations of the coronary artery ostia (distal, middle, and proximal) on the hemodynamic parameters within the aortic root was investigated. It was shown that transvalvular pressure gradient and valve orifice dimeter are highly dependent on the locations of the coronary artery ostia. For

instance, a healthy valve with a proximal coronary artery has a smaller valve orifice diameter compared to that with a distal coronary artery. Furthermore, the effect of the different locations of the coronary artery ostia on the aortic valve hemodynamics in the presence of aortic valve stenosis was also investigated. It was shown that a stenosed aortic valve with a proximal coronary artery has the smallest valve orifice diameter and is therefore more prone to calcification over time.

- It is believed that aortic valve and coronary artery stenoses are interdependent. This is why the presence of coronary artery stenosis on the sinus vortex structures was investigated in this study. It was shown that the sinus cavity of a healthy valve with healthy coronary arteries experiences greater levels of flow vorticity compared a healthy valve with stenosed coronary arteries. This means that the blood flow in the sinus cavity of a healthy valve with healthy coronary arteries, is guided in such a way that any accumulation are washed out of the sinus cavity more efficiently than for the sinus cavity of a healthy valve with stenosed coronary arteries. Furthermore, it was found that the leaflets of a healthy valve with a stenosed coronary artery experiences less wall shear stress compared to a healthy valve with healthy coronary arteries. This means that the leaflets of a healthy valve with stenosed coronary arteries is more prone to calcification over time.
- A validated numerical FSI model of the aortic valve was developed which is able to predict the distribution of the wall shear on the leaflets for both healthy and stenosed valves. It was found that a severely calcified valve witnesses a lower range of wall shear stress on the leaflets with higher probability of having lower wall shear stress on the leaflets. Furthermore, the probability density function of the wall shear stress on the leaflets for valves with proximal, middle, and distal coronary artery ostia were investigated. It was found that a severely calcified valve with proximal coronary ostia experiences the least wall shear stress on the leaflets with highest probability of having smallest wall shear stress.
- It is worth mentioning that the results provided in the current thesis has elucidated clinical observations whether the geometrical properties such as the locations of the coronary artery ostia, coronary artery stenosis are correlated with the initiation/progression of the aortic valve calcification.

7.2 Future work

The 2D FSI model of the aortic valve leaflets developed in this study is able to predict the wall shear stress distribution on the leaflets and the hemodynamic variation inside the aortic root and coronary arteries. This high fidelity model can be used by other researchers with the following suggested topics for future research:

- The present model can be extended to 3D simulation of the aortic valve leaflets considering the coronary arteries. The extended model could then be used to predict the wall shear stress on the left and right coronary cusps (RCC & LCC) as well as the non-coronary cusp (NCC). Furthermore, the sinus vortex structures corresponding to each sinus (i.e. left, right and non-coronary sinuses) can be analysed and correlations with the wall shear stress on the leaflets can be compared.
- As the leaflets of the aortic valve have nonlinear hyperelastic and viscoelastic material properties, the effect of the hyperelasticity and viscoelasticity of the

leaflets on the wall shear stress on the leaflets can be modelled. This was not explored in this thesis.

- There are a number of congenital diseases associated with the aortic valve such as abnormality of the leaflets (bicuspid aortic valve) which can be modelled. The effect of the abovementioned abnormality on the hemodynamic parameters inside the aortic root can be investigated.
- The influence of the aortic stiffness on the performance of the aortic valve, aortic valve closure and ejection times, sinus washout time can be investigated. This would address a current gap in the knowledge regarding the effect of the aortic stiffness on the sinus vortex structure and its correlation with calcific aortic valve diseases.
- The effect of aortic valve stenosis on the flow rate and the hemodynamic parameters inside both ascending and descending aorta can be studied. The influence of coarctation of the aorta on the sinus flow patterns, the wall shear stress distribution on the aortic valve leaflets, flow rate profile inside the coronary artery, and the wall shear stress on the walls of the coronary arteries is still unknown.
- The correlation between calcification of the aortic valve and the aortic stiffness, as well as, the flow rate in the ascending and descending aorta is not well understood. It is still unknown whether the aortic stiffness changes the wall shear stress distribution on the aortic valve leaflets as well as the hemodynamics of the coronary artery.

Appendix A: Calcification effects on hemodynamics of the aortic valve

Fluid structure interaction analysis of a calcified aortic valve

A. R. Kivi, N. Sedaghatizadeh, M. Arjomandi, A. Zander, B. Cazzolato

School of Mechanical Engineering, the University of Adelaide, Adelaide, SA, 5005

A fluid structure interaction model of the aortic valve leaflet is developed in order to study the effect of the leaflets stiffening on transvalvular pressure gradient and valve orifice diameter. The influence of the thickness of the leaflets because of the calcification on aortic valve hemodynamic is studied. It is found that the thicker is the aortic valve leaflets, the less is the valve orifice diameter, and the higher is the transvalvular pressure gradient.

The details of the methodology, supporting evidence and data are presented and explained in the following section. This chapter consists of the published conference paper:

Paper accepted in AFMC conference: A. R. Kivi, N. Sedaghatizadeh, M. Arjomandi, A. Zander, B. Cazzolato, Fluid structure interaction (FSI) analysis of a calcified aortic valve, 21st Australasian Fluid Mechanics Conference, 2018 Adelaide, Australia.

Statement of Authorship

Title of Paper	Fluid structure interaction (FSI) analysis of a calcified aortic valve
Publication Status	☑ Published ☐ Accepted for Publication ☐ Submitted for Publication ☐ Unpublished and Unsubmitted work written in manuscript style
Publication Details	A. R. Kivi, N. Sedaghatizadeh, M. Arjomandi, A. Zander, B. Cazzolato, Fluid structure interaction (FSI) analysis of a calcified aortic valve, 21st Australasian Fluid Mechanics Conference, 2018 Adelaide, Australia.

Principal Author

Name of Principal Author (Candidate)	Araz R. Kivi		
Contribution to the Paper	Developed Ideas and Concepts • Conducted a comprehensive literature review • Developed the ideas and concepts based on the gaps of the knowledge in the field Performed the Modelling • Developed an aortic valve model in ANSYS workbench software • Developed an appropriate udf code to defined boundary conditions • Simulated the dynamic behaviour of the aortic valve leaflets • Validated the simulated model with the experimental data Interpreted Results • Extracted raw data from simulation • Post processed the data using CFD post and MATLAB • Developed a MATLAB code to extract the averaged data • Interpreted the results and compared them with the experimental results Wrote the Manuscript • Solely developed first full draft of the manuscript • Applied comments given by co-authors • Responsible for revising the manuscript after review • Acted as the corresponding author		
Overall percentage (%)			
Certification:	This paper reports on original research I conducted during the period of my Higher Degree by Research candidature and is not subject to any obligations or contractual agreements with a third party that would constrain its inclusion in this thesis. I am the primary author of this paper.		
Signature		Date	29/01/2021

Co-Author Contributions

By signing the Statement of Authorship, each author certifies that:

xiii. the candidate's stated contribution to the publication is accurate (as detailed above);

xiv. permission is granted for the candidate in include the publication in the thesis; and

xv. the sum of all co-author contributions is equal to 100% less the candidate's stated contribution.

Name of Co-Author	Nima Sedaghatizadeh		
Contribution to the Paper	Supervised the work and provide feedback on the manuscript.		
Signature		Date	29/01/2021

Name of Co-Author	Maziar Arjomandi		
Contribution to the Paper	Supervised the work and provide feedback on the manuscript.		
Signature		Date	29/01/2021

Name of Co-Author	Benjamin S. Cazzolato		
Contribution to the Paper	Supervised the work and evaluated the manuscript.		
Signature		Date	29/01/2021

Name of Co-Author	Anthony C Zander		
Contribution to the Paper	Supervised the work, and provide feedback on the manuscript.		
Signature		Date	08/02/2021

Please cut and paste additional co-author panels here as required

Abstract

Aortic valve stenosis is one of the most common cardiovascular diseases. The stenotic aortic valve is formed by calcium deposition on the fibrosa layer of the aortic-valve leaflets. In general, a stenotic valve cannot operate properly leading to additional pressure on the heart and consequently its failure over time. The calcified aortic valve affects the flow pattern in the aortic root, the wall shear stress on the valve leaflets and hemodynamic parameters such as the transvalvular pressure gradient, and the valve orifice area. A stenotic aortic valve is usually detected by measuring the hemodynamic parameters using echocardiography, which has associated with substantial errors due to its nature. Computational fluid dynamics is an alternative technique to calculate the hemodynamic parameters and accordingly help cardiologists to predict the aortic valve stenosis. To do this, the computational fluid dynamic models of the aortic valve are generated using medical images from the patients. These models are able to provide detailed information from the fluid flow parameters and also precise data from the hemodynamic parameters. These precise calculations enable engineers to detect the aortic-valve stenosis. To date, computational fluid dynamic models have not taken into account the interaction between the fluid and structural domains. Fluid structure interaction modelling methodology has been used to obtain more accurate results by considering the interaction between the flowing blood and deformable aortic-valve leaflets. The aim of this paper is to investigate the effect of calcification of the aortic-valve leaflets on the flow pattern and hemodynamic parameters such as transvalvular pressure gradient and valve orifice area based on fluid structure interaction modelling methodology using ANSYS. The geometry has been developed in ANSYS Workbench based on echocardiography images available in the literature. A pulsatile inlet velocity extracted from Doppler velocity measurement data in the literature has been used as an inlet boundary condition. For modelling the turbulent flow downstream of the leaflets, the k-ω SST turbulence model was used. For comparison, both healthy and calcified aortic valves were modelled and analysed. Results show that the transvalvular pressure gradient increases from 769 Pa for the healthy aortic valve to 2356 Pa for the calcified one. Furthermore, there is a significant decrease in the valve orifice diameter, from 13.5 mm for the healthy aortic valve leaflets to 9.21 mm for the calcified one. It was also shown that the wall shear stress on fibrosa and ventricular layers of the leaflets are significantly changed as a result of change in the thickness and material properties of the leaflets. Averaged wall shear stress on the ventricular surface increases from 16.3 Pa for the healthy case to 23.8 Pa for the calcified aortic valve. For the fibrosa surface, it decreases from 3.42 Pa for the healthy leaflets to 1.53 Pa for the calcified one.

Introduction

The aortic valve is a unidirectional valve located between the left ventricle and aorta. It opens during the ventricular systole allowing the oxygenated blood to be pumped from the heart to pass through the aortic valve and enter the aorta. At the ventricular diastole, when the valve closes it prevents blood from flowing back to the heart. The calcification of the aortic-valve leaflets is one the most prevalent diseases particularly among adults over 65 years old [2]. The calcification prevents the aortic valve leaflets from opening and closing appropriately, resulting in aortic valve stenosis. The stenotic aortic valve increases the velocity of the blood in the valve orifice and results in an increased transvalvular pressure gradient and accordingly higher heart attack risk [1].

Doppler echocardiography is the most common diagnostic method for detection of aortic valve stenosis via measuring the jet velocity, effective orifice area (EOA) and transvalvular

pressure gradient (TPG). However, determining the TPG and EOA via echocardiography has associated significant errors due to the assumed constant axial velocity along the jet orifice area [2]. Computational fluid dynamic (CFD) models generated from medical images are an alternative, and can provide detailed information on the fluid flow parameters. Using this information enables engineers to calculate the hemodynamic parameters such as TPG and valve orifice area (VOA) and accordingly diagnose aortic valve stenosis. Various studies have investigated the blood flow pattern and determined the hemodynamic forces on the valve leaflets during the systolic phase [4-5]. The effect of fluid flow on dynamical motion of the leaflets has also received attention, recently. A 3D aortic valve model has been presented by Weinberg et al. [4]. They have investigated the influence of the calcification on the dynamical motion of the aortic-valve leaflet using LS-Dyna. According to their results, there is a relation between the valve calcification and aging. Halevi et al. [5] studied the effect of calcification on valve orifice area via CFD. They used individual patient MRI images to generate 3D models of the aortic valve. They utilised ABAQUS to analyse the dynamical motion of the leaflets. They showed that the valve orifice area decreases with calcium deposits present on the leaflets. The effect of leaflet movement on the fluid flow has been neglected in these studies.

To investigate the complex dynamic motion of the aortic valve leaflets, taking into account the interaction between the blood flow and the movement of the leaflets, the fluid structure interaction (FSI) approach was applied by De Hart et al [6]. In a more recent study by Halevi et al. [7], the influence of calcification on the hemodynamics of the aortic valve using 3D FSI models was reported. They used ABAQUS for modelling the structural part and Flow Vision for simulating the fluid part. Fedele et al. [3] implemented an analytical FSI modelling approach using moving resistive immersed implicit surfaces. The same FSI approach was used to investigate the aortic valve dynamics. In another work, Vahidkhah et al. [8] investigated the formation of blood stasis on prosthetic aortic valves using a 3D FSI mathematical model. As an alternative approach to mathematical modelling, Amindari et al. [9] utilised ANSYS for modelling a 2D aortic valve. They demonstrated the effect of calcification on TPG and VOA due to changing material properties of the valve leaflets.

In this study, the effect of calcification on the hemodynamic parameters of the aortic valve has been investigated taking into account both changes in the thickness and material properties of the leaflets. Using echocardiography images available in the literature [9], a 2D model of the aortic valve has been generated in ANSYS Workbench 18.2. ANSYS FLUENT and ANSYS MECHANICAL APDL were selected to solve the fluid and structural part, respectively. The System Coupling FSI Module in ANSYS Workbench was used to link the fluid and structure fields. The combined effect of the changes in the thickness and material properties of the aortic valve leaflets due to the calcium deposition on the hemodynamic parameters has been investigated.

Numerical Modelling

Figure A. 1 shows a two-dimensional model of the aortic valve, aortic root, sinuses, and leaflets implemented in ANSYS Workbench 18.2 from echocardiography images available in the literature [9]. To apply FSI in the simulation, the model is divided into three sections: fluid domain, structure domain, and FSI surfaces. In the fluid domain (Figure A. 1) the blood is assumed incompressible and Newtonian with a constant density and viscosity of 1060 kg/m^3 and 0.0035578 J/s, respectively [9-10]. A velocity inlet boundary condition is defined at the inlet of the aortic valve. The velocity inlet has a pulsatile profile as measured by LaDisa et al. [10] using Doppler technique (Figure A. 2). The outlet boundary condition is considered as a

pressure outlet. An unstructured mesh was used in the fluid domain based on sweep method, with 9952 prism elements and maximum skewness of 0.52 (as shown in Figure A. 3).

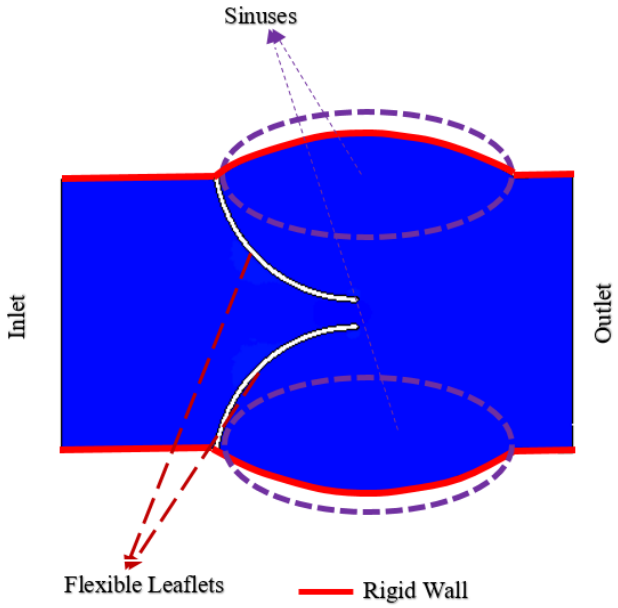

Figure A. 1 Schematic view of the aortic root with flexible leaflets, inlet, outlet and sinuses, and aortic wall.

The material properties of the leaflets are assumed to be isotropic and elastic with a density of l050 kg/m^3 and a Young modulus of E=2 MPa for the healthy aortic valve leaflets and E=10 MPa for the calcified one [11-12]. The Poisson's ratio of the leaflet is assumed as 0.3 [9]. For the structure domain a total of 120 tetrahedral elements with a maximum skewness of 0.43 are used. The blood forces the leaflets to move inside the fluid domain. The surfaces between the blood and leaflets are hence defined as fluid structure interaction surfaces.

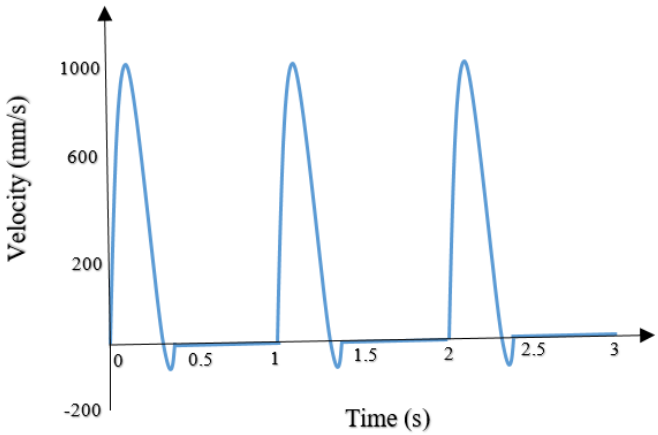

Figure A. 2 Inlet transient velocity profile applied to the inlet surface of the model (only a single cycle is considered in this paper)

Due to the application of the pulsatile velocity profile at the inlet of the aortic valve it is expected to exhibit turbulent flow downstream of the leaflets at peak systole at the maximum Reynolds number of around 4766. Hence, to obtain reliable results taking into account the separation and circulatory flow behind the leaflets, the k-ω SST turbulence model was utilised.

Due to the limitation of the 1-way uncoupled approach in FSI simulation of highly coupled fluid and structure domains, in particular when it is applied to flexible biological tissues [13], a 2-way coupled implicit approach is used to analyse the fluid structure interaction simulation of the aortic-valve leaflets.

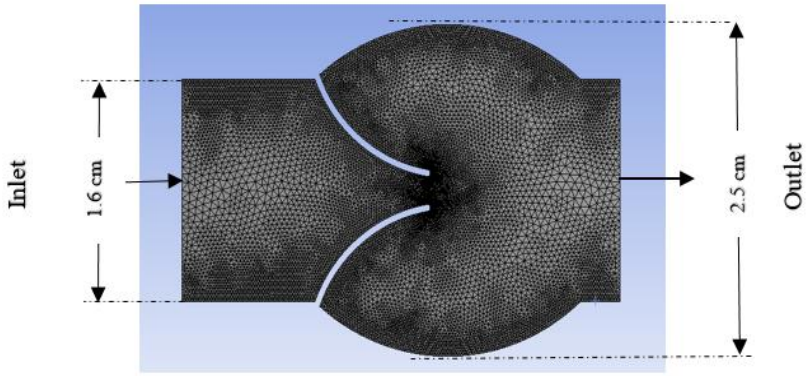

Figure A. 3 Schematic view of the fluid domain mesh and accompanying boundary conditions

Validation of the Model

To validate the model, the maximum jet velocity, transvalvular pressure gradient, and valve orifice area at peak systole of healthy and calcified leaflets are compared with the published data of Amindari et al. [9].

Table A. 1 Maximum jet velocity, valve orifice area, transvalvular pressure gradient for healthy and calcified models

Aortic valve	TPG (Pa)	VOA (mm)	MJV (m/s)
Healthy (thickness=0.6mm, E=2 MPa)	769 (633[9])	13.5 (14[9])	1.59 (1.57[9])
Calcified (thickness=1mm, E=2MPa)	1854	10.8	1.92
Calcified (thickness=1mm, E=10MPa)	2356	9.21	2.32

Results and Discussion

The velocity contours for a healthy aortic valve during the systolic phase are shown in Figure A. 4. As shown in Figure A. 4, for the healthy aortic valve, the velocity reaches the maximum velocity jet flow (V=1.59 m/s) at the valve orifice during the systole. Near the ventricularis surface of the aortic valve leaflets at peak systole, the velocity profile is significantly increased (shown with arrows in Figure 5) while inside the jet orifice area the velocity contours do not change significantly. As a result, the velocity gradient near the ventricularis surface causes the high wall shear stress (WSS) on these surfaces. The WSS difference between the ventricularis and fibrosa layers of leaflets is one of the main reason for calcification of the aortic valve leaflets [9].

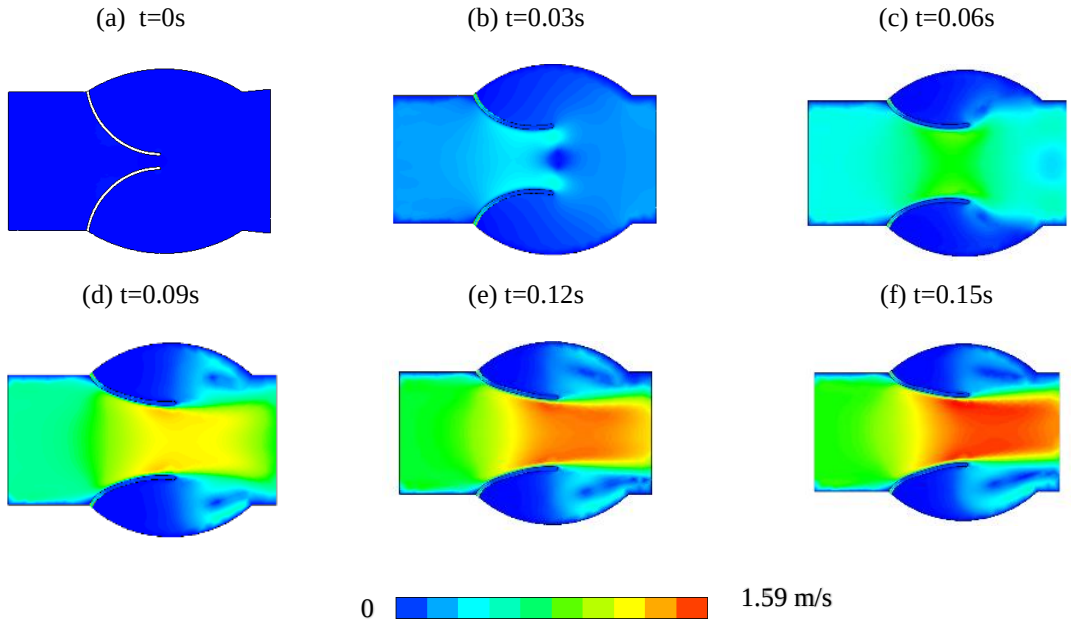

Figure A. 4 Velocity contours of the healthy aortic valve during cardiac cycle.

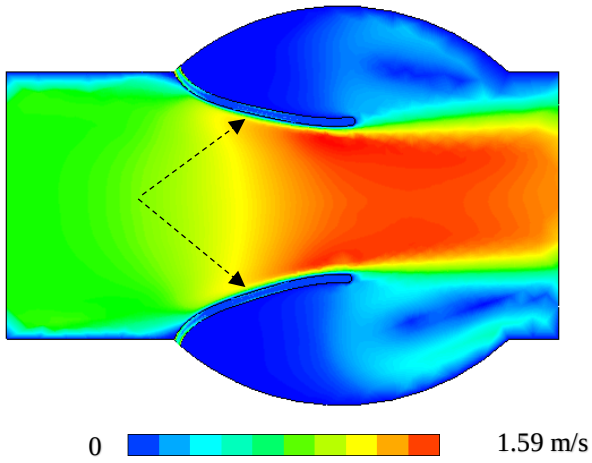

Figure A. 5 Velocity contour of the healthy aortic valve at t= 0.15s; arrows show a significant increase in the velocity near ventricularies layer.

The velocity streamlines of the healthy aortic valve with Young's modulus E=2MPa is depicted in Figure A. 6 during the cardiac cycle. The vortices are created behind the sinuses because of the flow separation at the tip of the leaflets. As seen, the vortices move from behind the sinuses at peak systole toward the end of sinuses at the end of systole and grow during the systolic phase. It is worth mentioning that the shape and location of the vortices are affected by the opening angle of the leaflets and the parameters of the flow during the cardiac cycle.

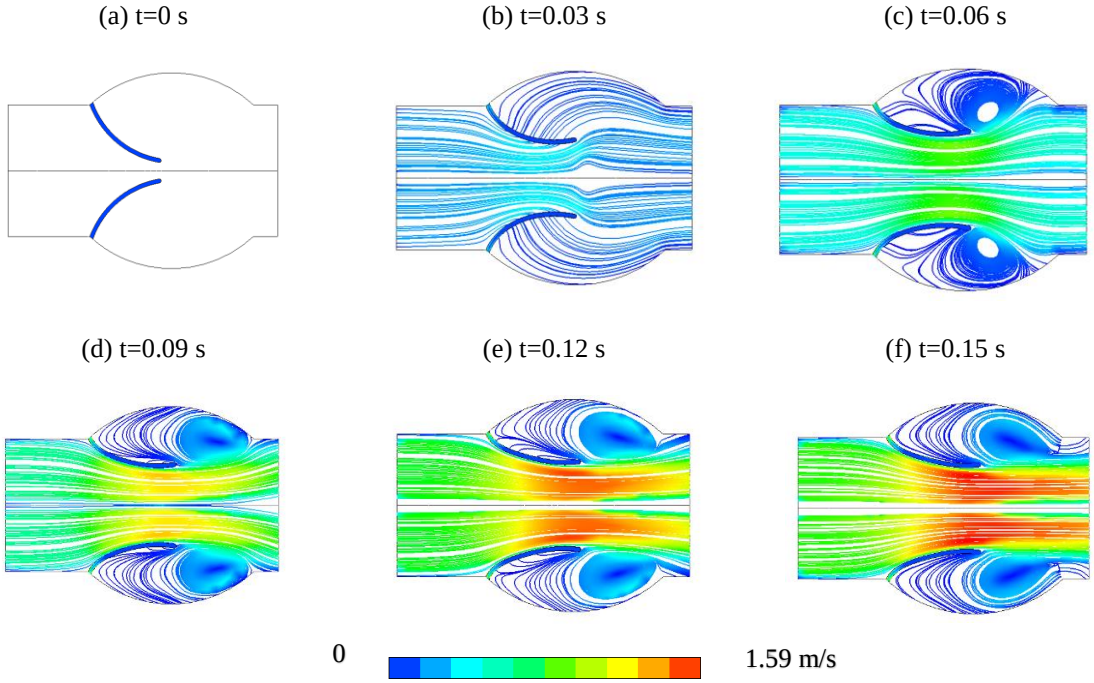

Figure A. 6 Velocity streamlines of the model of the healthy aortic valve during systole phase

Figure A. 7 shows the velocity streamlines of the model during the diastole phases. As seen, the vortices become larger downstream of the leaflets (shown with black arrows) and start disappearing during the diastole phases. It is worth mentioning that the flexible leaflets start oscillating during the diastole phases because of the pressure difference between the left ventricle and aorta. At the same time, because of the oscillation of the leaflets, two other vortices are created and become larger on the rear of the sinuses (shown with red arrows). At the end of diastole at t= 0.27 and t= 0.35, two different vortices, one with smaller size behind the leaflets (in ventricularis surfaces) and another with larger size (near the outlet) are created, respectively (shown with blue arrows).

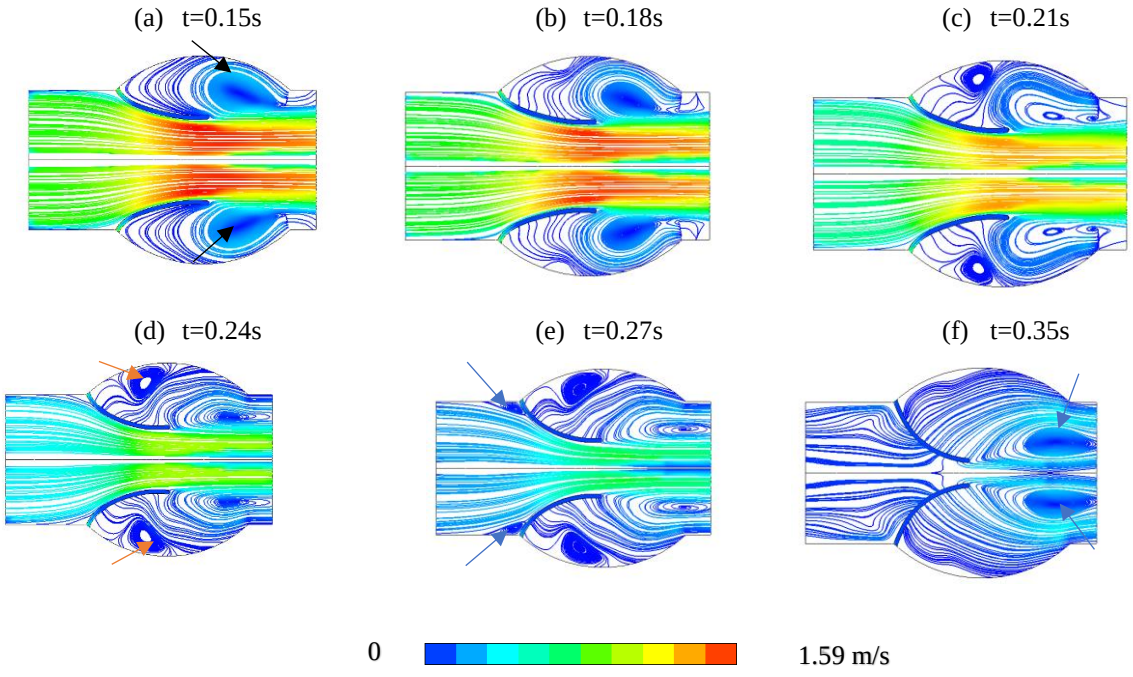

Figure A. 7 Velocity streamlines of the model during diastole phase.

Figure A. 8 depicts the velocity streamlines for healthy (Figure A. 8 a) and calcified (Figure A. 8 b and Figure A. 8 c) aortic valve leaflets. As explained, because of calcium deposition on the leaflets over time, they thicken and stiffen. The effect of the calcification on the valve orifice diameter is represented in Figure A. 8 (b) and (c). As seen, the thickened leaflets (Figure A. 8 (b)) have smaller valve orifice diameter (10.8 mm) in comparison with the healthy one 13.5 mm. Calcium deposition not only changes the thickness of the aortic valve leaflets, but also increases the elastic modulus of the leaflets. For the calcified aortic valve with higher thickness and Youngs modulus (thickness=1mm, E=10MPa), the valve orifice diameter is the smallest one at 9.21 mm. It is worth noting that the shape, location, and strength of the vortices for the calcified leaflets differ to the healthy one.

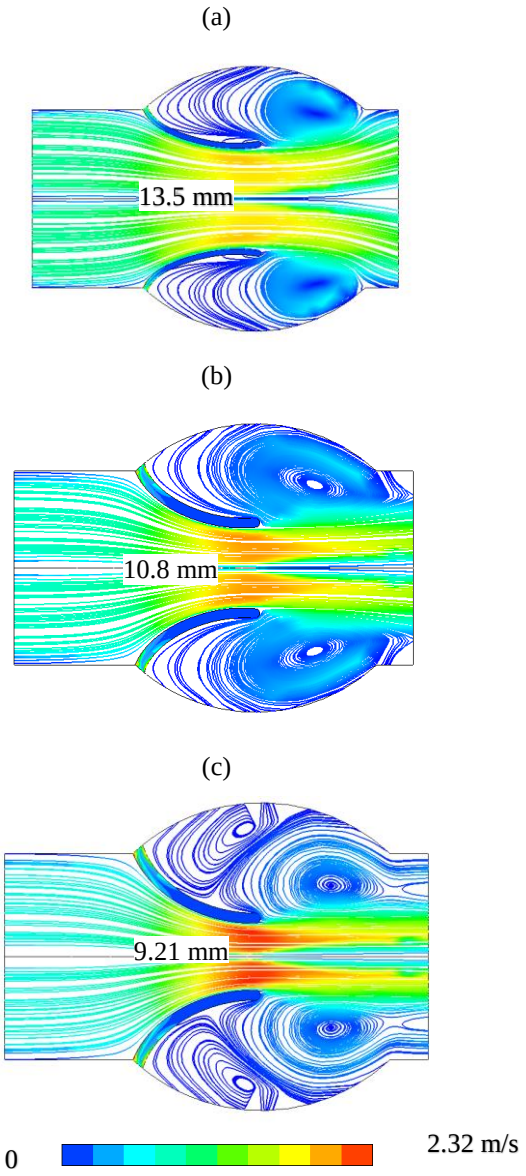

Figure A. 8 Velocity streamlines at peak systole for **(a)** healthy (E=2MPa, thickness=0.6mm), **(b)** calcified (E=2MPa, thickness= 1mm), **(c)** (E=10MPa, thikness=1mm).

As shown in Figure A. 8, the size of the vortices for the calcified aortic valve are bigger than those of the healthy one. The fluid flow for the healthy aortic valve near the annulus and behind the sinuses are stronger than calcified ones. This shows that calcification changes the shape of the flow behind the sinuses particularly along the base of the leaflets. Furthermore, the calcification changes the transvalvular pressure gradient. As shown in Figure A. 9, the TPG

for the healthy valve is around 769 Pa, while for the calcified aortic valve with higher thickness is around 1854 Pa, and for the stiffened one is 2356 Pa, respectively.

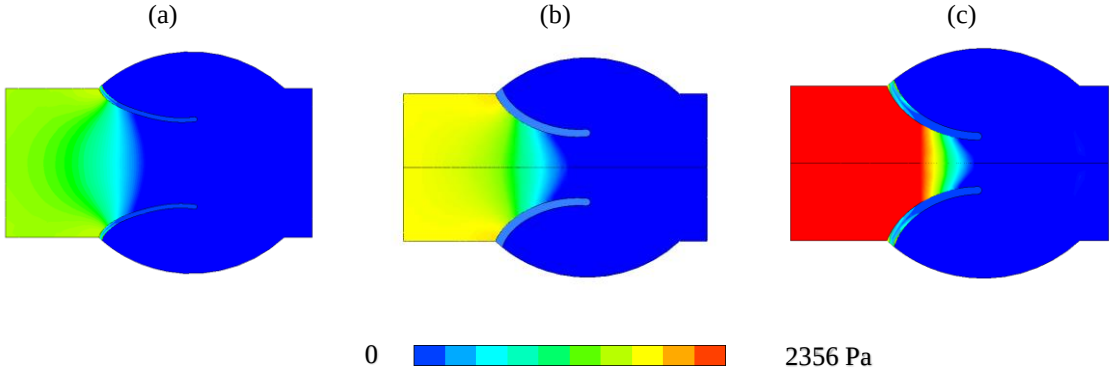

Figure A. 9 Pressure contours of the healthy and calcified models of the aortic valve at peak systole.

Conclusion

In this study the influence of calcification of the aortic-valve leaflets on the hemodynamic parameters such as TPG, VOA, and flow pattern have been investigated via FSI simulation. The velocity contours and streamlines for healthy and calcified aortic valves have been demonstrated during cardiac cycle. Streamlines show that the wall shear stresses are higher near the ventricularis surface of the aortic valve at peak systole; the differentiation between the WSS of ventricularis and fibrosa layers is one the main reason for calcium deposition. Moreover, the circulatory flow is created behind the sinuses because of the complex geometry and flow separation on the leaflet tips. The generated vortices in the upper sinuses rotate clock wise whilst the one in the lower sinuses rotates in the opposite direction. Simulation results reveal that valve orifice area decreases from 13.5 mm (opening ratio of 84%) for the healthy valve to 9.21 mm (opening ratio of 48%) for the calcified one because of the calcification. The TPG at the peak systole increases from 769 Pa for the healthy aortic valve to 2356 Pa for the calcified one. Furthermore, the size and location of the vortices have changed in the calcified aortic valve. The size of the vortices of the calcified valve are observed to be bigger compared to the healthy one.

References

[1]. Otto, C.M., Prendergast, B., Aortic-valve Stenosis-from Patients at Risk to Severe Valve Obstruction, The New England Journal of Medicine, **371** (8), 2014, 744-756.

[2]. Stewart, S.F., Nast, E.P., Arabia, F.A., Talbot, T. L., Proschan, M., Clark, R.E., Errors in Pressure Gradient Measurement in Bioprosthetic Aortic Valves, Journal of the American College of Cardiology, **18** (3), 769-779.

[3]. Fedele, M., Faggiano, E., Dede, L., Quarteroni, A., A Patient-Specific Aortic Valve Model on Moving Resistive Immersed Implicit Surfaces, Journal of Biomechanics and Modelling in Mechanobiology, **16** (5), 2017, 1779-1803.

[3]. Weinberg, E.J., Schoen, F.J., Mofrad, M.R.K., A Computational Model of Aging and Calcification in the Aortic Heart Valve, Plos One, **4** (6), 2009, 59-6.

[4]. Halevi, R., Hamdan, A., Marom, G., Mega, M., Raanani, E., Haj-Ali, R., Progressive Aortic Valve Calcification: Three-Dimensional Visualization and Biomechanical Analysis. Journal of Biomechanics, **48** (3), 2015, 489-497.

[5]. De Hart, J., Peters, G.W., Schreurs, P.J., Baaiiens, F.P, A Two-Dimensional Fluid-Structure Interaction Model of the Aortic Valve, Journal of Biomechanics, **33** (9), 2000, 1079-1088.
[6]. Halevi, R., Hamdan, A., Marom, G., Lavon, K., Ben-Zekry, S., Raanani, E., Bluestein, D., Haj-Ali, R., Fluid Structure Interaction Modelling of Calcific Aortic Valve Disease Using Patient-Specific Three-Dimensional Calcification Scans, Journal of Medical & Biological Engineering & Computing, **54** (11), 2016, 1683-1694.
[7]. Vahidkhah, K., Azadani, A.N., Supra-Annular Valve-in-Valve Implantation Reduced Blood Stasis on the Transcatheter Aortic Valve Leaflets, Journal of Biomechanics, **58**, 2017, 114-122.
[8]. Amindari, A., Saltik, L., Kirkkopru, K., Yacoub, M., Yalcin, H.C., Assessment of Calcified Aortic Valve Leaflet Deformation and Blood Flow Dynamics Using Fluid Structure Interaction Modeling, Informatics in Medicine Unlocked, **9**, 2017, 191-199.
[9]. LaDisa, J.F., Alberto Figueroa, C., Vignon-Clementel I.E., Kim, H.J., Xiao, N., Ellwein, L.M., Chan, F.P., Feinstein, J.A., Taylor, C.A., Computational Simulations for Aortic Coarctation: Representative Results from a Sampling of Patients. Journal of Biomechanical Engineering, **133**, 2011, 091008.

[10].Ranga, A., Mongrain, R., Bidadilah, Y., Cartieer, R., A Compliant Dynamic FEA Model of the Aortic Valve, In 12th IFTOMM World Congress, 2007.
[11]. Gnyaneshwar, R., Kumar R.K., Balakrishnan, K.R., Dynamic Analysis of the Aortic Valve Using a Finite Element Model, The Annals of Thoracic Surgery, **73** (4), 2002, 1122-1129.
[12]. Benra, F.K., Dohmen, H.J., Pei. J., Schuster, S., Wan, B., A Comparison of One-Way and Two-Way Coupling Methods for Numerical Analysis of Fluid-Structure Interaction. Journal of Applied Mathematics, 2011:16.

Appendix B: Wall shear stress distribution on the aortic valve leaflets and its correlation with aortic valve calcification

Calcification Effect on the Wall Shear Stress Distribution of the Aortic Valve Leaflets

A. R. Kivi[1], N. Sedaghatizadeh[1], B. Cazzolato[1], A. Zander[1], R. Roberts-Thomson[2, 4], A. Nelson[2, 3, 4], M. Arjomandi[1]

[1]School of Mechanical Engineering, University of Adelaide, Adelaide, South Australia 5005, Australia
[2]South Australian Health and Medical Research Institute, Adelaide, Australia
[3]Duke Clinical Research Institute, Durham, NC, USA
[4]Royal Adelaide Hospital, Adelaide, Australia

A fluid structure interaction model of the aortic valve leaflet is developed in order to study the effect of calcification accompanied with the different diameter of the sinuses on wall shear stress of the aortic valve leaflets as well as sinus flow patterns. The model is validated against the experimental data collected from the in-house in-vitro experimental test. The transvalvular pressure gradient and aortic flow rate obtained from the simulation are compared with that of extracted from the experimental measurements. The results show that a severely calcified valve with smallest sinus dimeter ratio witnesses higher trasnvalvular pressure gradient. Furthermore, wall shear stress on the leaflets of a valve with smaller sinus diameter ratio, is lower compared to that of with bigger sinus diameter ratio.

The details of the methodology, supporting evidence and data are presented and explained in the following section. This chapter consists of the published conference paper:

Paper accepted in AFMC conference: A. R. Kivi, N. Sedaghatizadeh, B. Cazzolato, A. Zander, R. Roberts-Thomson, Adam Nelson, M. Arjomandi, Fluid structure interaction (FSI) analysis of a calcified aortic valve, 22nd Australasian Fluid Mechanics Conference, 2020 Brisbane, Australia.

Statement of Authorship

Title of Paper	Calcification effect on the wall shear stress distribution of the aortic valve leaflets
Publication Status	☑ Published ☐ Accepted for Publication ☐ Submitted for Publication ☐ Unpublished and Unsubmitted work written in manuscript style
Publication Details	

Principal Author

Name of Principal Author (Candidate)	Araz R. Kivi		
Contribution to the Paper	Developed Ideas and Concepts • Conducted a comprehensive literature review • Developed the ideas and concepts based on the gaps of the knowledge in the field Performed the Modelling • Developed an aortic valve model in ANSYS workbench software • Developed an appropriate udf code to defined boundary conditions • Simulated the dynamic behaviour of the aortic valve leaflets • Validated the simulated model with the experimental data Interpreted Results • Extracted raw data from simulation • Post processed the data using CFD post and MATLAB • Developed a MATLAB code to extract the averaged data • Interpreted the results and compared them with the experimental results Wrote the Manuscript • Solely developed first full draft of the manuscript • Applied comments given by co-authors • Responsible for revising the manuscript after review • Acted as the corresponding author		
Overall percentage (%)			
Certification:	This paper reports on original research I conducted during the period of my Higher Degree by Research candidature and is not subject to any obligations or contractual agreements with a third party that would constrain its inclusion in this thesis. I am the primary author of this paper.		
Signature		Date	29/01/2021

Co-Author Contributions

By signing the Statement of Authorship, each author certifies that:

xvi. the candidate's stated contribution to the publication is accurate (as detailed above);

xvii. permission is granted for the candidate in include the publication in the thesis; and

xviii. the sum of all co-author contributions is equal to 100% less the candidate's stated contribution.

Name of Co-Author	Nima Sedaghatizadeh		
Contribution to the Paper	Supervised the work and provide feedback on the manuscript.		
Signature		Date	29/01/2021

Name of Co-Author	Benjamin S. Cazzolato		
Contribution to the Paper	Supervised the work and evaluated the manuscript.		
Signature		Date	29/01/2021

Name of Co-Author	Anthony C Zander		
Contribution to the Paper	Supervised the work, and provide feedback on the manuscript.		
Signature		Date	16/02/2021

Name of Co-Author	Ross Roberts-Thomson		
Contribution to the Paper	Provide feedback on the manuscript.		
Signature		Date	08/02/2021

Name of Co-Author	Adam J Nelson		
Contribution to the Paper	Evaluated the manuscript.		
Signature		Date	08/02/2021

Name of Co-Author	Maziar Arjomandi		
Contribution to the Paper	Supervised the work and provide feedback on the manuscript.		
Signature		Date	29/01/2021

Please cut and paste additional co-author panels here as required

Abstract

Wall shear stress on the aortic valve leaflets has been the main factor for the initiation and progression of calcific aortic valve disease (CAVD). This study aims to investigate the effects of leaflets stiffening and sinus diameter on sinus vortex structures, wall shear stress distribution on aortic valve leaflets as well as its correlation with CAVD. A two-dimensional fluid-structure interaction (FSI) model of healthy aortic valve leaflets was developed based on echocardiography images available in the literature. The turbulent flow downstream of the leaflets was considered in the model using $k-\omega$ turbulent model. Results show that leaflets stiffening not only affects hemodynamic parameters within the aortic root such as transvalvular pressure gradient (TPG), jet velocity along with the valve, and valve orifice diameter but also has a significant effect on sinus vortex structures and wall shear stress distribution on the leaflets. The results demonstrate that severely calcified aortic valve witnesses lower ranges of shear stress on the leaflets during the systole and diastole (ranging from -0.5 to + 0.5 Pa for the systole and -0.1 to + 0.2 Pa for the diastole) with higher probability compared to those of with healthy valve which ranges from -1.5 to +2 Pa and -0.55 to + 0.55 Pa during the systole and diastole, respectively. It is also showed that wall shear stress on the leaflets is highly dependent on the diameter of the sinuses.

Introduction

The vortical structures formed inside sinus is one of the most important flow features which affects aortic valve hemodynamic and its performance [1]. It is now confirmed that sinus vortical structures affect the opening and closing mechanism of the aortic valve leaflets [2]. It is also showed that the presence of vortical structures inside sinus has an impact on sinus washout mechanism [3] and the overall performance of the aortic valve [4, 9]. The experimental study carried out by Toninato *et al*. [2] on the effects of sinuses, showed that vortices generated downstream of the leaflets for the aortic valve model in the presence of sinuses enhances ejection and closing time compared to that of with the model without the sinuses. Recently, Hatoum *et al*. [5] also showed that the influence of sinus flow pattern on transcatheter aortic valve replacement (TAVR) operation and the likelihood of leaflets thrombosis occurred after TAVR due to the poor washout mechanisms.

Coronary artery flow also has an impact on sinus vortex structures [6], wall shear stress on the leaflets [7], and sinus washout mechanism [8]. Recently, Moore *et al*. [10] carried out an experiment showing that the leaflets corresponding to the coronary sinus open 10% more than that of associated with the non-coronary sinus leaflet. Wald et al. [11] studied that the effect of the aortic valve stenosis on coronary artery flow. They showed that aortic valve stenosis affects sinus vortex structures and accordingly has an impact on coronary artery flow. They demonstrated that aortic valve with a severe degree of stenosis witnesses lower coronary blood flow compared to that of with healthy valve.

Stenosis of the aortic valve has an impact on aortic valve hemodynamic and plays an important role in the initiation and progression of CAVD [12]. Although it is believed that lower shear stress on the leaflets has an impact on the initiation and progression of the calcification, it is not yet well understood how CAVD initiates and progresses [9]. For example, Hatoum *et al*. [13] investigated the effects of the presence and absence of coronary arteries on wall shear stress distribution on the leaflets. They demonstrated that the leaflets of the

bioprosthetic valve with coronary artery ostia experience higher ranges of wall shear stress compared to that of in the absence of coronary artery ostia.

In the present study, the influences of leaflets stiffening and sinus diameter on hemodynamic parameters within the aortic root, sinus vortex structures and the probability distributions of the wall shear stress on the leaflets were studied. A two-dimensional FSI model of a healthy aortic valve was developed using ANSYS Workbench 19.2 based on echocardiography images available in the literature. The turbulent flow downstream of the leaflets was considered using $k-\omega$ turbulent model. An in-vitro experimental campaign was designed to validate the presented computational model. The probability distribution of wall shear stress on aortic valve leaflets corresponding to a healthy, calcified, and severely calcified aortic valve with taking in to account different diameters of the sinus were calculated and compared.

Numerical Modelling

A 2.5D FSI model of a healthy aortic valve was developed in ANSYS workbench 19.2. The geometry of the domain and flow parameters were selected based on the available echocardiography images of a 27-year-old subject (shown in Figure B. 1 c) presented in the literature [8]. The numerical model includes two different domains: structure (flexible leaflets) and fluid (blood flow) domains. A two-way coupling FSI model was utilised to account for the interaction and momentum exchange between the fluid and solid domains. The different regions of the fluid domain including inlet, outlet (coronary and aorta), and blood flow are illustrated in Figure B. 1 a. Figure B. 1 b shows the mesh structure in the developed model for a healthy valve based on the echocardiography images shown in Figure B. 1 c.

The blood is considered as a Newtonian, isothermal, incompressible fluid with a constant viscosity and a density of 0.0035578 Pa.s and 1060 kg/m^3, respectively [7]. The sweep method was used to generate an unstructured mesh for the fluid domain along the thickness with approximately 10,000 prism elements. As shown in Figure B. 1 b, a finer mesh is adapted near the leaflets to accurately model the flow highly affected by these surfaces. A sensitivity analysis was carried out for pressure and velocity for two grid sizes of 10,000 and 14,000. Based on the results, only a 2% difference between the calculated parameters was observed when the number of elements increased from 10,000 to 14,000, while the computation time increased by about 40%. Hence, it was deemed that the mesh size 10,000 is sufficient to obtain accurate results. Generally, the size of the elements throughout the domain were reduced with the focus on refining the mesh in the areas where the gradient is the largest such near the leaflets' wall and entrance of coronary arteries. For both elements size, $k-\omega$ SST turbulence model was used to model the turbulent flow downstream of the leaflets in which criteria for near wall treatment were addressed.

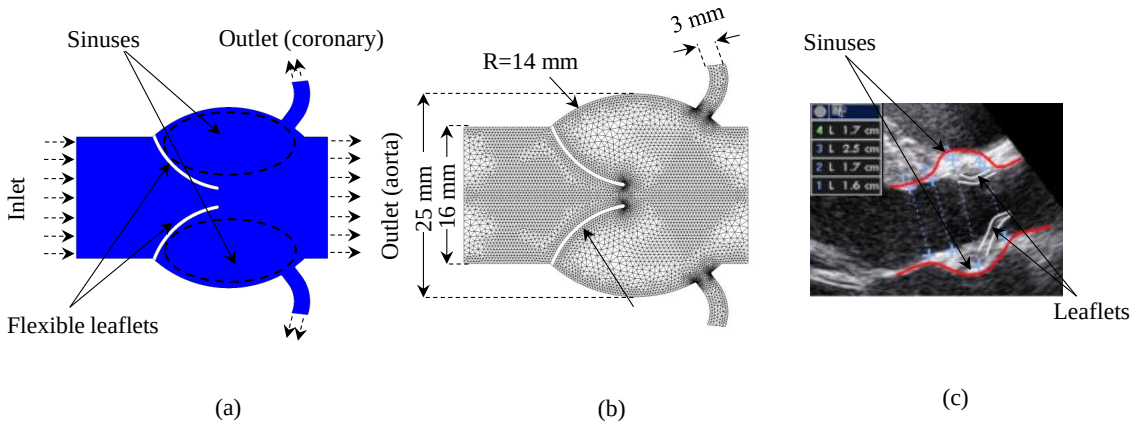

Figure B. 1 Schematic view of (a) healthy aortic valve with flexible leaflets, sinuses, and flow directions for the inlet and outlets (b) fluid domain mesh with dimensions of the aortic root (c) echocardiography images from a healthy aortic valve [8].

Two sets of boundary conditions were applied at the inlet and outlets. At the ventricular side (inlet), a physiological velocity profile obtained from Doppler echocardiography [8] was applied as the boundary condition. At the coronary artery outlets, a transient pressure profile was considered as the outlet boundary condition. This boundary conditions profile obtained from the collected clinical data of the average coronary flow [7]. To extrapolate the required information from the interior domain, the outflow boundary condition was considered at the outlet of the aorta. The walls of the sinuses were assumed to be rigid. To investigate the validity of this assumption, a sensitivity analysis was carried out on the pressure and velocity components for two different models; one model with flexible leaflets and sinus walls, and another model with flexible leaflets but solid sinus walls. Results show that there is only 0.1% difference between the calculated parameters when the sinus walls change from solid to flexible while the computation time was increased by about 20%; hence it was decided to consider the model with flexible leaflets and solid sinus walls in this study.

The structural domain of the model consists of two flexible leaflets which move as they are exposed to blood flow. The leaflets are assumed to be isotropic with a density of 1060 kg/m3, Poisson's ratio of 0.3 and Young's modulus of 2 MPa [6]. It is considered that calcium is uniformly distributed on the leaflet layers. The Young's modulus for the calcified and severely calcified cases are set to be 10 MPa, and 20 MPa, respectively [8]. ANSYS Mechanical APDL was used to solve the equations of the motion of the leaflets and find the dynamic responses, stresses and strains of the leaflets based on the Newmark time integration method. The mesh used for the leaflets was generated using the sweep method comprising 120 quadratic tetrahedral elements with a minimum of two elements through the thickness. To satisfy the mesh independency requirement, constant pressure was applied to the leaflets and a mesh convergence study was carried out at steady state. Results show that the accuracy of the solution does not change for the models with more than 100 tetrahedral elements and with a maximum skewness of 0.43. In the present study, the ANSYS coupling module was used to model the interaction between the flexible leaflets and the blood flow.

Experimental Setup

An in-vitro experimental campaign was designed to validate the presented computational model. Figure B. 2 shows the experimental test rig containing (1) a controllable in–house piston pump which can produce physiological aortic flow profile, (2) and (4) a pressure sensor (OMEGA PX319 silicon pressure sensor) to measure the pressure before and after the bioprosthetic valve to calculate the transvalvular pressure gradient, (3) a 21mm Edwards Intuity (Edwards Lifesciences, Irvine, California) bioprosthetic aortic valve mounted inside a silicon based sinus chamber, (5) a flow meter (OPTIBATCH 4011C) which is used to measure the physiological aortic flow rate, (6) a compliance chamber used to add resistance to the aortic flow and create appropriate backflow during the diastole, (7) resistance valve, (8) fluid reservoir, (9) computer, power supply and DAQ card (NI USB-6211).

Figure B. 2 Experimental test setup: (1) in-house controllable piston-pump, (2) ventricle pressure sensor, (3) bioprosthetic aortic valve mounted inside silicon based sinus chamber, (4) aortic pressure sensor, (5) flow sensor, (6) compliance chamber, (7) resistance valve, (8) fluid reservoir, (9) computer, power supply and DAQ card.

Figure B. 3 a shows the schematic view of the experimental test rig including all the parts. Figure B. 3 b shows the test section including pressure sensors (measuring left ventricle and aorta pressures) and a bioprosthetic aortic valve mounted into the silicon based sinus chamber. The working fluid is a mixture of 40% glycerine and 60% distilled water by mass fraction based on the literature [12, 13] which was used to mimic the viscosity and density of the blood. Mach3 software was used to control the in-house controllable piston-pump in order to reach the physiological flow rate profile. The pressures before and after the valve were measured using two pressure sensors (OMEGA PX319 silicon pressure sensor) to ensure physiological conditions. Flow and pressure measurements were recorded in LabVIEW at least for 50 cycles. The measured aortic flow rate is compared to that of extracted from the computational model. As can be seen in Figure B. 4, there is a good agreement between the computed and measured

aortic flow rate. The TPG corresponding to a bioprosthetic valve used in the experiment is measured (658.32) and compared with that of computed by the model (633 Pa). It is worth mentioning that there is only a 4% difference between the TPG measured in experiment and calculated TPG in FSI simulation.

(a)

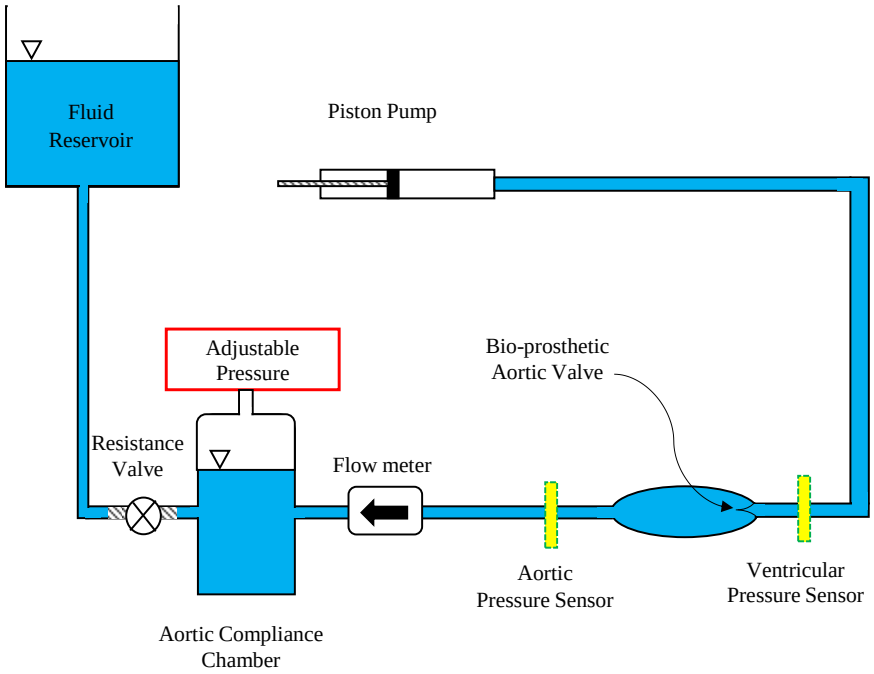

(b)

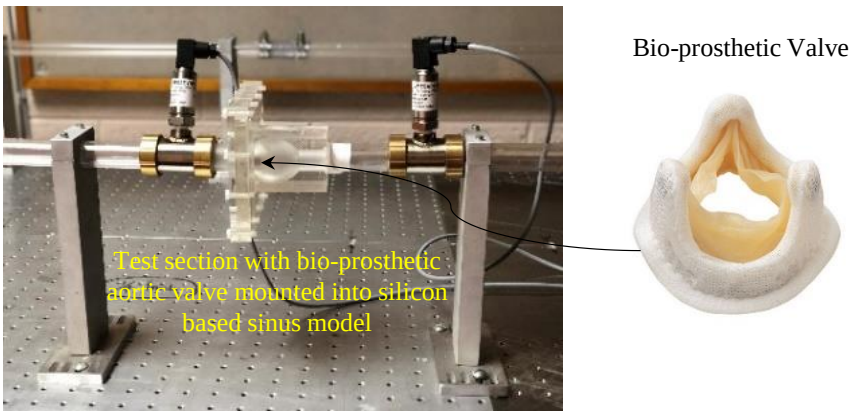

Figure B. 3 (a) Schematic view of the experimental test rig (b) test section including two pressure sensors and a bioprosthetic aortic valve mounted into silicon based sinus chamber.

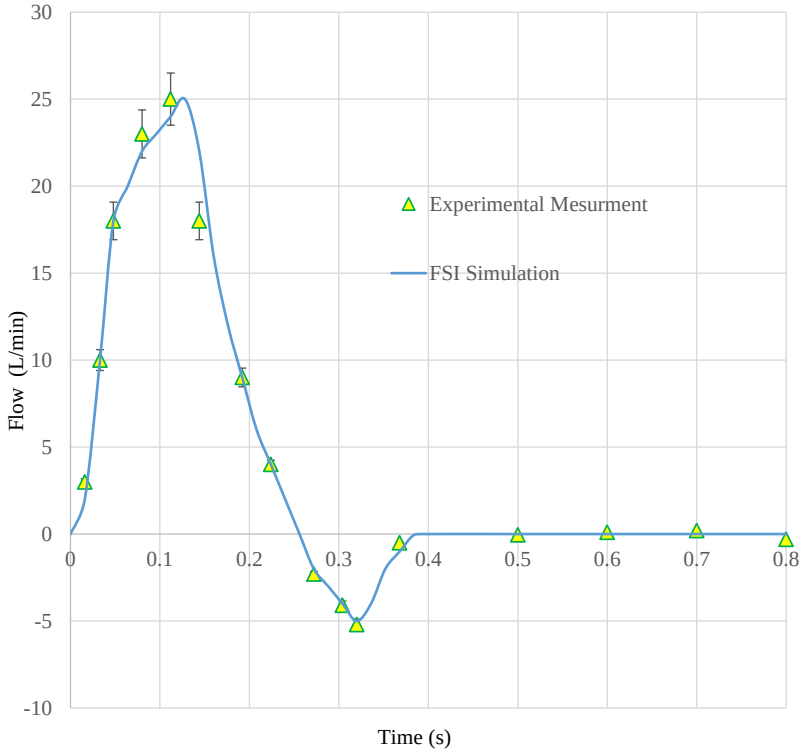

Figure B. 4 Flow rate profile along the aortic valve corresponding to FSI simulation (solid line) and experimental measurement (solid triangles).

Results and Discussion

Figure B. 5 shows velocity streamlines for a heathy aortic valve during the cardiac cycle. As shown, the valve opens during systole and allows blood flow through the aorta (shown in Figure B. 5 a-c). During the diastole phase, it closes to prevent blood from flowing back into the left ventricle. During the closure period, blood flows into the coronary arteries in order to perfuse the myocardium (shown in Figure B. 5 d and e). The jet velocity along the aortic valve reaches to its maximum, 1.65 m/s at peak systole (t=0.1s). While the maximum velocity inside coronary arteries is around 1 m/s during diastole. As shown in Figure B. 5 b, the valve orifice diameter is around 14.2 mm at mid systole. At mid systole, two main vortices generated inside sinuses (shown in Figure B. 5 b with solid-line arrows); one is near the coronary artery ostia and another is very close to the leaflets. These vortices grow in size during the diastole due to an increase in the cavity area (shown in Figure B. 5 d with dash-line arrows).

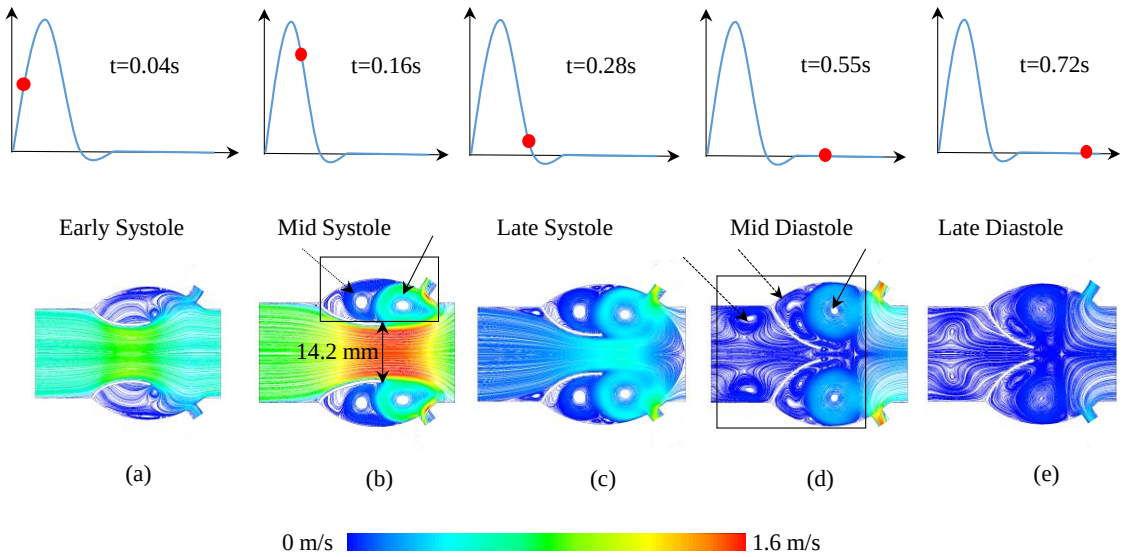

Figure B. 5 Velocity streamline (a-e) for a healthy aortic valve during the cardiac cycle.

The effects of leaflets stiffening on the valve orifice diameter are depicted in Figure B. 6 a-c. As shown, the valve orifice diameter decreases from 14.2 mm for the healthy aortic valve to 9.6 mm for the severely calcified case. By contrast, the jet velocity increases from 1.6 m/s for the healthy aortic valve to around 2.4 m/s for the severely calcified case. It is worth to mention that leaflets stiffening not only affect hemodynamic parameters inside the aortic root but also significantly changes sinus vortices. As can be seen in Figure B. 6, there are two main vortices inside sinuses of the healthy aortic valve (shown in Figure B. 6 a). While, for the calcified aortic valve, three main vortices occupy sinus cavity (shown in Figure B. 6 b); one is near the coronary artery ostia, another one is very close to leaflets tip, and a very small vortex is formed close to the base of the leaflet. For the severely calcified case, two small vortices near the leaflets become one bigger vortex (shown in Figure B. 6 c). These vortices are shifted toward leaflets tip and pressurising leaflets from opening and results in a decrease in valve orifice diameter. It is also worth to mention that different sinus vortex structures and cavity sizes associated with calcified and severely calcified aortic valve affect coronary artery blood flow. The coronary artery blood flow velocity decreases from 1 m/s for the healthy aortic valve to around 0.45 m/s for the severely calcified one (shown in Figure B. 6 a-c).

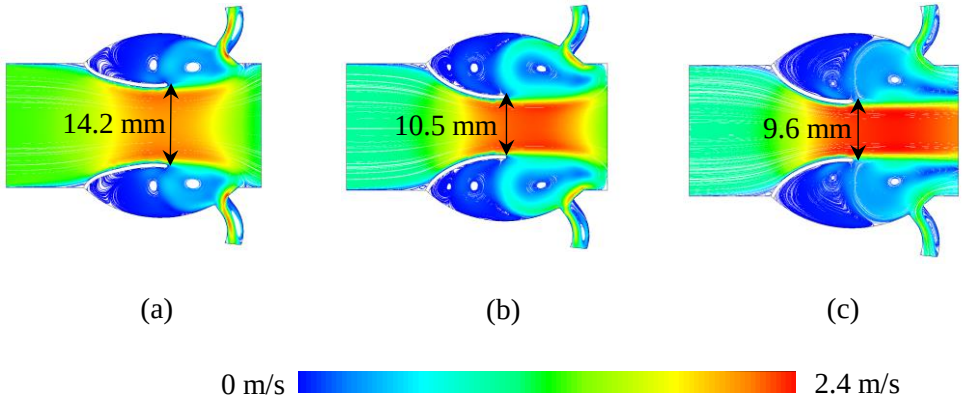

Figure B. 6 Velocity streamline for (a) healthy (b) calcified and (c) severely calcified aortic valve at peak systole.

The effect of sinus diameter accompanied by leaflets stiffening on TPG are depicted in Figure B. 7. As can be seen, decreasing the diameter of the sinus increases the TPG. For example, a healthy valve with 25 mm sinus diameter witnesses lower TPG (0.79 kPa) compared to that of with 17.6 mm sinus diameter which has a TPG around 0.96 kPa. Furthermore, leaflets stiffening significantly intensify increasing in TPG due to a decrease in sinus diameter. For example, TPG corresponds to severely calcified aortic valve with 25 mm sinus diameter is around 10.31 kPa, while that of with 17.6 mm sinus diameter is 14.5 kPa. These differences in the TPG of the severely calcified valve with smaller and bigger sinus diameter is approximately 5 times more than that of which is experienced by a healthy valve with smaller and bigger sinus diameter.

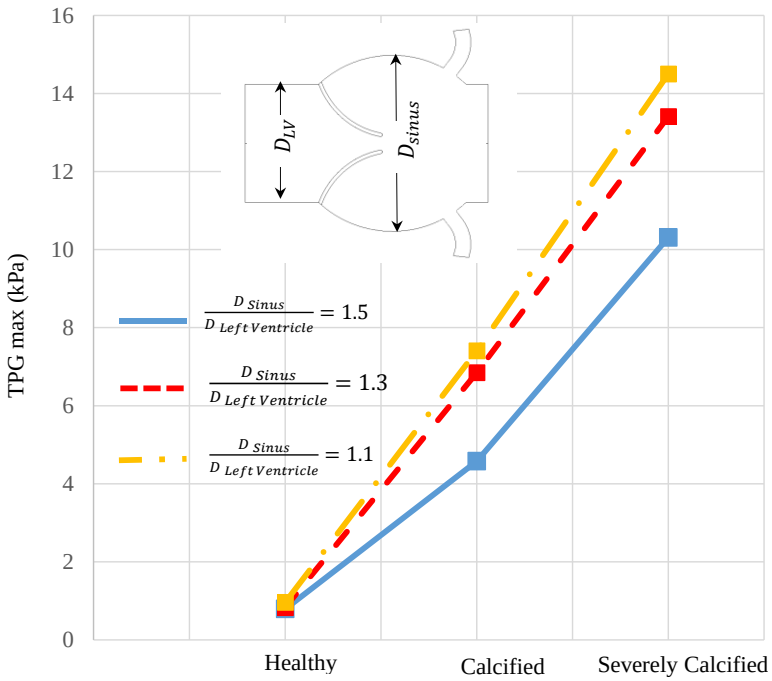

Figure B. 7 Maximum transvalvular pressure gradient (TPGmax) for a healthy, calcified, and severely calcified aortic valve with a various diameter of the sinuses D_{Sinus}=*25, 20.8, and 17.6 mm*

The circulation strength inside the sinus cavity corresponding to a healthy, calcified, and severely calcified aortic valve during the cardiac cycle is shown in Figure B. 8. As can be seen, a dominant vortex inside sinus cavity for a healthy aortic valve is a CCW vortex with maximum strength value of approximately 0.015 m^2/s at early diastole. Whilst, for the severely calcified case, a dominant vortex is a CW vortex with a negative value of -0.01 m^2/s. These changes in the value and direction of the dominant vortex can be explained by the presence of several small CW vortices around the leaflets tip, base and sinus cavity of the severely calcified aortic valve. Results show that sinus cavity of the severely calcified aortic valve witnesses lots of small CW vortices which changes sinus vortex structures by dissipating the energy of the main vortices.

The probability distributions of the wall shear stress on leaflets of a healthy, calcified and severely calcified aortic valve for different diameter of sinuses are shown in Figure B. 9. As seen in Figure B. 9 a, a severely calcified aortic valve with D_{sinus}=25 mm witnesses lower ranges of wall shear stress on the leaflets during the systole (ranging from -0.5 to +0.55 Pa) compared to that of with healthy case which is around -1.5 to 2 Pa. Furthermore, the less the diameter of the sinuses, the lower is the wall shear stress distribution on the leaflets and the higher is the probability of having lower shear stress on the leaflets.

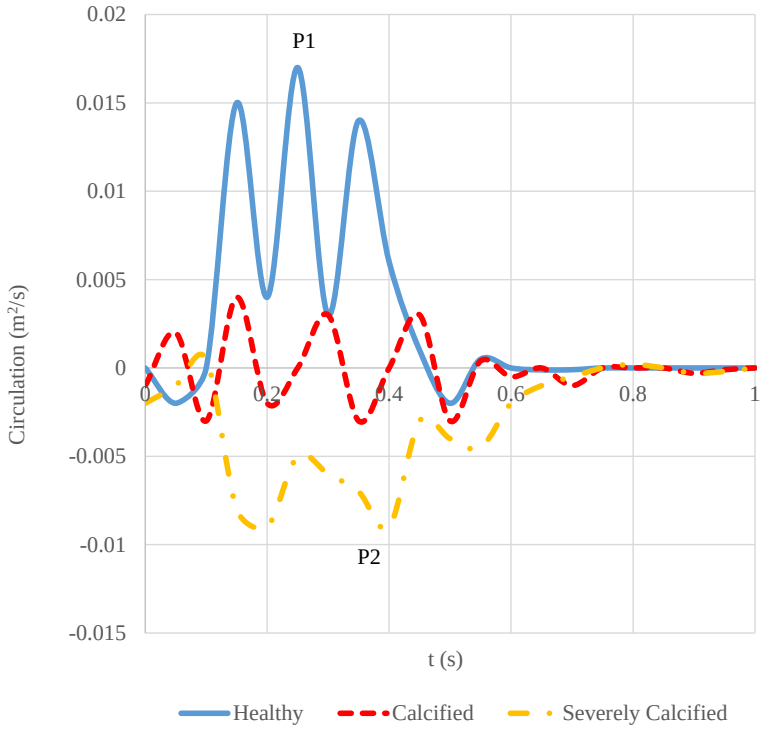

Figure B. 8 Circulation versus time inside the sinus cavity for a healthy, calcified, and severely calcified aortic valve.

(a)

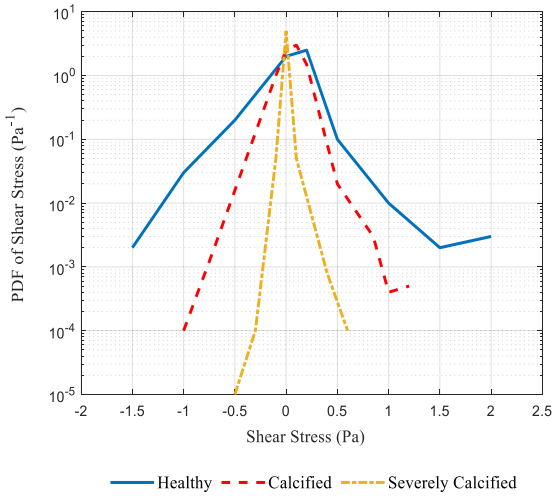

(b)

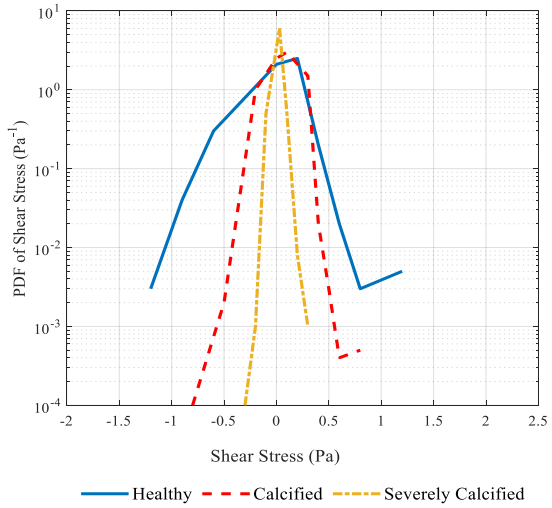

(c)

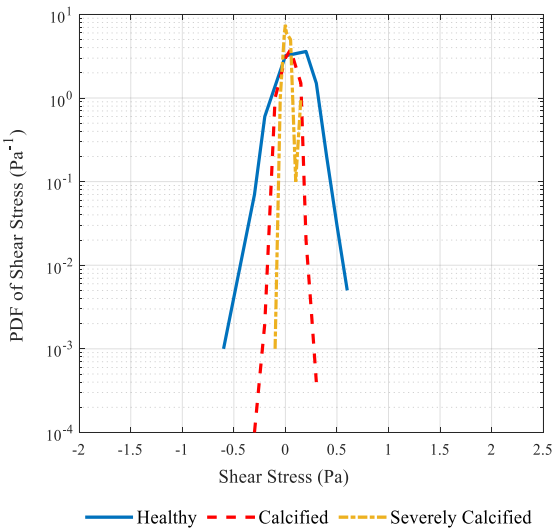

Figure B. 9 Log scale probability density function of wall shear stress distribution on leaflets during systole for healthy, calcified, and severely calcified aortic valve with a various diameter of the sinuses (a) D_{sinus}=25 mm (b) D_{sinus}=20.8 mm, and (c) 17.6 mm.

Conclusion

In this study, the effects of leaflets stiffening and sinus diameter on aortic valve hemodynamic, wall shear stress distribution on leaflets, and its association with CAVD are investigated. The results show that a healthy valve with smaller sinus diameter experiences more TPG compared to that of with larger sinus diameter and are more prone to be calcified. Furthermore, a severely calcified aortic valve witnesses lower ranges of wall shear stress and a higher probability of having smaller shear stress on the leaflets. It means that a severely calcified aortic valve is in the risk of getting stenosed over time.

References

[1] Fukui, T., Morinishi, K. (2013). Influence of vortices in the sinus of Valsalva on local wall shear stress distribution. International Journal of Life Sciences and Medical Research, 3, 94-103.

[2] Toninato, R., Salmon, J., Susin, F.M., Ducci, A., Burriesci, G. (2016). Physiological vortices in the sinuses of Valsalva: an in vitro approach for bio-prosthetic valves. Journal of Biomechanics, 49, 2635-2643.

[3] Moore, B., Dasi, L.P. (2014). Spatiotemporal complexity of the aortic sinus vortex. Experiments in Fluids, 55, 1770-1778.

[4] Bianchi, M., Marom, G., Ghosh R.P., Rotman, O.M., Parikh, P., Gruberg, L., Bluestein, D. (2019). Patient-specific simulation of transcatheter aortic valve replacement: impact of deployment options on paravalvular leakage. Biomechanics and modelling in mechanobiology, 18, 435-451.

[5] Hatoum, H., Dollery, J., Lilly, S.M., Crestanello, J., Dasi, L.P. (2018). Impact of patient morphologies on sinus flow stasis in transcatheter aortic valve replacement: an in-vitro study. Journal of Thoracic and Cardiovascular Surgery, 157, 540-549.

[6] Mohammadi, M., Cartier, R., Mongrain, R. (2015). Derivation of a simplified relation for assessing aortic root pressure drop incorporating wall compliance. Medical & Biological Engineering & Computing, 53, 241-251.

[7] Nobari, S., Mongrain, R., Leask, R., Cartier, R. (2013). The effect of aortic wall and aortic leaflet stiffening on coronary hemodynamic: a fluid-structure interaction study. Medical & Biological Engineering & Computing, 51, 923-936.

[8] Amindar, A., Saltik, L., Kirkkopru, K., Yacoub, M., Yalcin, H.C. (2017). Assessment of calcified aortic valve leaflet deformations and blood flow dynamics using fluid-structure interaction modelling. Informatics in Medicine Unlocked, 9, 191-199.

[9] Sun, L., Chandra, S., Sucosky, P. (2012). Ex vivo evidence for the contribution of hemodynamic shear stress abnormalities to the early pathogenesis of calcific bicuspid aortic valve disease. PLoS ONE, 7, 43-48.

[10] Moore, B.L., Dasi, L.P. (2015). Coronary flow impacts aortic leaflet mechanics and aortic sinus hemodynamic. Annals of Biomedical Engineering, 43, 2231-2241.

[11] Wald, S., Liberzon, A., Avrahami, I. (2018). A numerical study of the hemodynamic effect of the aortic valve on coronary flow. Biomechanics and modelling in mechanobiology, 17, 319-338.

[12] Hatoum, H., Dasi, L.P. (2019). Spatiotemporal complexity of the aortic sinus vortex as a function of leaflet calcification. Annals of Biomedical Engineering, 47, 1116-1128.
[13] Hatoum, H., Dasi, L.P. (2018). Sinus hemodynamics in representative stenotic native bicuspid and tricuspid aortic valves: an in-vitro study. Fluids, 3, 56.